PHYTOPATHOLOGIA MEDITERRANEA

Plant health and food safety
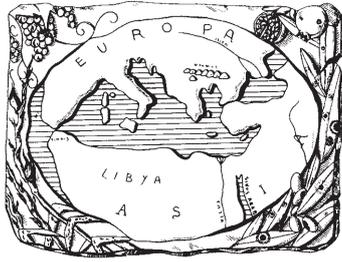
The international journal of the
Mediterranean Phytopathological Union

FUP
FIRENZE
UNIVERSITY
PRESS

PHYTOPATHOLOGIA MEDITERRANEA

Plant health and food safety

Phytopathologia Mediterranea is an international journal edited by the Mediterranean Phytopathological Union. The journal's mission is the promotion of plant health for Mediterranean climate and regions, safe food production, and the transfer of knowledge on diseases and their sustainable management.

The journal deals with all areas of plant pathology, including epidemiology, disease control, biochemical and physiological aspects, and utilization of molecular technologies. All types of plant pathogens are covered, including fungi, nematodes, protozoa, bacteria, phytoplasmas, viruses, and viroids. Papers on mycotoxins, biological and integrated management of plant diseases, and the use of natural substances in disease and weed control are also strongly encouraged. The journal focuses on phytopathology and closely related fields in the Mediterranean agro-ecological regions. The journal includes three issues each year, publishing Reviews, Original research papers, Short notes, New or unusual disease reports, News and opinion, Current topics, Commentaries, and Letters to the Editor.

PHYTOPATHOLOGIA MEDITERRANEA

The international journal of the Mediterranean Phytopathological Union

OPEN ACCESS

Research Papers

Isolation, characterization and genomic analysis of a novel lytic bacteriophage infecting *Agrobacterium tumefaciens*

Miloud SABRI[1,#], Kaoutar EL HANDI[1,#], Orges CARA[1,2], Angelo DE STRADIS[3], Toufic ELBEAINO[1,4,*]

[1] International Centre for Advanced Mediterranean Agronomic Studies (CIHEAM of Bari), Via Ceglie 9, 70010 Valenzano (Ba), Italy
[2] Department of Soil, Plant and Food Sciences, University of Bari Aldo Moro, Bari, Italy
[3] National Research Council of Italy (CNR), Institute for Sustainable Plant Protection (IPSP), University of Bari, Via Amendola 165/A, 70126 Bari, Italy
[4] National Research Council of Italy (CNR), Institute for Sustainable Plant Protection (IPSP), Piazzale Enrico Fermi, 1- 80055 Portici (NA), Italy
* Corresponding author: elbeaino@iamb.it
# These authors share first authorship.

Summary. *Agrobacterium tumefaciens* causes crown gall, and economic losses in important crops, including apple, pear, peach, and almond. Difficulties controlling this disease with conventional pesticides require alternative antibacterial agents. A novel lytic bacteriophage, *Agrobacterium* phage PAT1 (PAT1), with high lysis potential against *A. tumefaciens*, was isolated from wastewater. Interaction between PAT1 and *A. tumefaciens* cells was investigated using transmission electron microscopy. PAT1 adsorbed, infected, and replicated on *A. tumefaciens* in ≤30 min. Turbidity assays showed that PAT1 [Multiplicity of Infection (MOI) = 1] inhibited *A. tumefaciens* growth by 82% for 48 hours. PAT1 was resistant to broad ranges of pH (4 to 10) and temperatures (4 to 60°C). Bioinformatics analyses of the PAT1 genomic sequence showed that the bacteriophage was closely related to *Atuphduovirus* (*Autographiviridae*) phages. The PAT1 genome size was 45,040 base pairs with a G+C content of 54.5%, consisting of 54 coding sequences (CDS), of which the functions of 23 CDS were predicted, including an endolysin gene which could be used as an antimicrobial against *A. tumefaciens*. No lysogenic mediated genes or genes encoding virulence factors, antibiotic resistance, or toxins were detected in PAT1 genome. The bacteriophage showed potential as a biocontrol agent against *A. tumefaciens* infections, expanding the limited catalogue of lytic *A. tumefaciens* phages, although efficacy for control of crown gall *in planta* remains to be evaluated.

Keywords. Plant pathogenic bacteria, crown gall, phage therapy, biocontrol.

INTRODUCTION

Agrobacterium tumefaciens is a Gram-negative, non-spore-forming, motile, rod-shaped plant pathogenic bacterium that causes crown gall many

plant species (Etminani *et al.*, 2022). Crown gall compromises commercialization of plants in more than 60 families, including dicotyledonous plants, ornamentals brambles, and pome fruit, stone fruit, and nut trees (Lee *et al.*, 2009; Choi *et al.*, 2019; Etminani *et al.*, 2022). *Agrobacterium tumefaciens* is commonly found in the rhizospheres of many plants, where it survives on root exudates (Eckardt, 2006). The bacterium infects host plants through wounds roots, stems and crowns, which often occur in orchards during pruning and in nurseries through transplanting and grafting (Eckardt, 2006; Etminani *et al.*, 2022). The pathogen then becomes pathogenic by transforming plants with a fragment of the tumor-inducing (Ti) plasmid, a transfer-DNA (T-DNA) which induces abnormal proliferation of host plant cells via synthesis of phytohormones, leading to the formation of tumours (galls) (Kawaguchi *et al.*, 2019; Thompson *et al.*, 2020). Galls usually develop at plant crowns but can also occur above ground on secondary or lateral roots and main stems. These tumours restrict water and nutrient flow causing yield losses and, in severe cases, plant death (Eckardt, 2006; Asghari *et al.*, 2020).

There are no synthetic chemical treatments for controlling crown gall. Eco-friendly management of this disease using biocontrol agents, such as the non-pathogenic *Agrobacterium radiobacter* isolate K84 and its genetically modified isolate K1026, have been shown to be effective in several locations (Penyalver *et al.*, 2000). However, K84 and K1026 are ineffective against some strains of *A. tumefaciens*; thereby limiting their ability to provide broad-spectrum control (Vicedo *et al.*, 1993). Therefore, there is a requirement to identify new effective biocontrol agents against *A. tumefaciens*.

Virulent (lytic) bacteriophages, which are viruses that specifically infect and lyse bacteria, are potential options for field scale biological control. These bacteriophages are ubiquitous, recognized as safe agents, and are potent antibacterial agents in agriculture (Svircev *et al.*, 2018; Álvarez *et al.*, 2019; Sabri *et al.*, 2022). Lytic phages have advantageous characteristics, including ease of discovery, high host bacterium specificity, self-replicating nature, harmlessness to eukaryotes, low environmental impacts, low cost and simplicity for preparation, high efficiency at low multiplicity of infection (MOI). Their post-application levels increase reducing bacterial host survival, in contrast with antimicrobial compounds (Loc-Carrillo and Abedon, 2011; Sabri *et al.*, 2024).

Seven lytic phages have been reported to infect this bacterial plant pathogen. These are: 7-7-1 (Kropinski *et al.*, 2012), Atu_ph02 and Atu_ph03 (Attai *et al.*, 2017), Atu_ph07—a jumbo phage (Attai *et al.*, 2018),

Atu_ph04 and Atu_ph08 (Attai and Brown, 2019), and Milano (Nittolo *et al.*, 2019). The present study isolated and characterized a novel lytic phage of *A. tumefaciens*, named *Agrobacterium* phage PAT1 (PAT1), which demonstrated *in vitro* antibacterial efficacy against *A. tumefaciens*.

MATERIALS AND METHODS

Bacterial strains and culture conditions

Bacteria listed in Table 1 were grown either at 28°C in liquid yeast extract peptone glucose broth (YPG) (5.0 g L^{-1} yeast extract, 5.0 g L^{-1} peptone, 10.0 g L^{-1} glucose) or on yeast extract peptone glucose agar (YPGA, YPG supplemented with 1.5% agar).

Bacteriophage isolation, purification, and titration

The phage described in the present study was isolated from a sewage water sample collected in April 2023 at the untreated influx point of the wastewater processing station in Bari (south of Italy; Latitude: 41.1081° N, Longitude: 16.2606° E). One L of sewage water was passed through a 75 × 100 mm Grade 1 filter paper (Whatman) to remove large particles, and the filtered through a 0.22 μm filter (Merck) to remove cellular debris. The resulting filtrate was centrifuged at 109,000 (Rotor J50.2 Ti, Beckmann Coulter) for 1 h at 4°C to pellet phage particles. The pellet was resuspended in 2 mL of phage buffer [100 mM Tris-HCl (pH 7.6); 10 mM MgCl$_2$; 100 mM NaCl; and 10 mM MgSO$_4$) and stored at 4°C. For phage enrichment, *A. tumefaciens* strain CFBP 5770 was grown at 28°C on YPG agar for 24 h and transferred to 2 mL of YPG broth at optical density at 600 nm (OD 600) of 0.1, to which 100 μL of pre-treated sample were added. The culture enrichment was incubated at 28°C for 24 h. Phage was purified from filtrate using the double agar overlay method (Kropinski *et al.*, 2009). A single clear plaque-forming unit was transferred into 1 mL of phage buffer and this process was repeated three times to ensure isolation of a single phage. To obtain high phage titre, 1 mL of *A. tumefaciens* strain CFBP 5770 culture at OD 600 of 0.2 was inoculated into 500 mL of YPG broth, 1 mL of purified phage was added, and the mix was incubated for up to 24 h at 28°C. Amplified phages were filtered through 0.22 μm filters, concentrated by high-speed centrifugation (108,800 g for 1 h), resuspended in 2 mL of phage buffer, and stored at 4°C for further analysis. The phage titre was determined through a double-layer assay.

Table 1. Bacterial isolates used for determining the host range of PAT1.

Species	Isolate[a]	Host plant	Origin
Xanthomonas campestris pv. *campestris*	CFBP 1710	*Brassica oleracea* var. *botrytis*	France
Xanthomonas albilineans	CFBP 1943	-	Burkina Faso
Erwinia amylovora	PGL Z1 [b]	*Pyrus communis*	Italy
Pseudomonas syringae pv. *syringae*	CFBP 311	*Pyrus communis*	France
Dickeya chrysanthemi biovar *chrysanthemi*	CFBP 1346	*Chrysanthemum maximum*	Italy
Pseudomonas savastanoi pv. *savastanoi*	CFBP 5050	*Olea europaea*	Portugal
Agrobacterium larrymoorei	CFBP 5473	*Ficus benjamina*	USA
Agrobacterium rubi	CFBP 5521	*Rubus* sp.	Germany
Agrobacterium tumefaciens	CFBP 5770	*Prunus persica*	Australia
Agrobacterium tumefaciens	YD 5156-2018	*Prunus domestica*	Greece
Agrobacterium tumefaciens	YD 5660-2007	*Prunus dulcis*	Greece
Agrobacterium tumefaciens	BPIC 139	*Vitis vinifera*	Greece
Agrobacterium tumefaciens	BPIC 284	*Prunus dulcis*	Greece
Agrobacterium tumefaciens	BPIC 310	*Pyrus amygdaliformis*	Greece
Agrobacterium vitis	CFBP 2738	*Vitis vinifera*	Greece
Agrobacterium vitis	BPIC 1009	*Vitis vinifera*	Greece

[a] CFBP: French Collection of Phytopathogenic Bacteria, Angers, France. YD: Collection of bacterial strains isolated in diagnostic work of the bacteriology laboratory, Benaki Phytopathological Institute. BPIC: Benaki Phytopathological Institute collections.
[b] Collection of CIHEAM-IAM, Bari, Italy.

Spot assays of phage lytic activity

Lytic activity of PAT1 against *A. tumefaciens* was assessed using a spot assay as follows: 200 µL of *A. tumefaciens* strain CFBP 5770 suspension (10^8 CFU mL^{-1}) were mixed with soft agar (YPG supplemented with 0.7% agar), which was poured into a petri plates (6 mL per plate) and allowed to dry. Drops (10 µL each) of phage solution containing 108, 107, 106, 105, or 104 PFU mL^{-1} were spotted onto the surfaces of the plates. The spots were dried at room temperature and the plates then cultured for 24 h at 28°C.

Transmission Electron Microscopy (TEM)

To assess the morphological and lytic properties of the purified phage PAT1, a culture of *A. tumefaciens* strain CFBP 5770 was challenged with PAT1 (MOI = 1) for 1 h at room temperature. Representative images of the phage and bacterium cells were taken at 10-, 30-, or 60-min intervals post-infection (pi) using a transmission election microscope (FEI MORGAGNI 282D) using the dip method. Carbon-coated copper/rhodium grids underwent 2 min. incubation with either the phage alone or with phage-treated cells, followed by rinsing with 200 µL of distilled water. Negative staining was obtained by immersing the grids in 200 µL of a 0.5 % w/v UA-Zero EM stain solution (Agar-Scientific Ltd).

The samples were viewed at microscope accelerating voltage of 80 kV.

DNA extraction, whole-genome sequencing, and bioinformatic analysis of PAT1

Genomic DNA of PAT1 was extracted from a high-titre stock of phage particles at ~10^{10} PFU mL^{-1} using a DNeasy Plant Extraction kit, following the manufacturer's protocol (Qiagen). The extracted DNA was quantified using a NanoDrop™ One/OneC Microvolume UV-Vis Spectrophotometer (ThermoFisher Scientific). Subsequently, 500 ng of purified genomic DNA was sent for Illumina sequencing (2 × 150 bp paired-end mode) (Eurofins Genomics). The reads were quality checked and trimmed using BBDuk Trimmer 1.0 and *de novo* assembled using the Tadpole tool with different k-mers (Geneious Prime 2024.0.7). The nucleotide sequence similarity of the obtained phage with those reported in GenBank was calculated based on a complete nucleotide alignment of the genomic sequences of most PAT1-related phages using Geneious. The functions of ORFs were annotated with Geneious, using the complete genomic sequences of the phages most closely related at the molecular level to PAT1, i.e., *Agrobacterium* phage Atu_ph02 (accession number NC_047845) and *Agrobacterium* phage Atu_ph03 (accession number NC_047846); and the HHpred and HHblits of the Bioinformatics

toolkit (https://toolkit.tuebingen.mpg.de/tools/hhpred). A search for tRNA genes in the genome of PAT1 was performed using Prokka 1.14.0 (https://Kbase.us).

The predictions of antibiotic resistance genes, acquired virulence genes, and toxin-encoding genes were assessed using, respectively, resFinder 4.5.0, Virulence-Finder 2.0.5 and ToxFinder 1.0 softwares, in the CGE tool (http://www.genomicepidemiology.org/). The complete genome sequence of PAT1 was deposited at GenBank and a circular map of the genome and phylogenetic tree were constructed using g ViPTree (Nishimura *et al.*, 2017).

Optimal multiplicity of infection (MOI) of phage PAT1

To investigate the phage's ability to inhibit growth of *A. tumefaciens* in liquid medium, a "killing assay" was carried out; thus phage PAT1 and host bacterial strain CFBP 5770 were mixed at MOIs of 1, 0.1, 0.01, 0.001, or 0.0001. Each mixture was then inoculated into 2 mL of YPG broth and incubated at 28°C for 48 h. During incubation, four optical density (OD) measurements (at 0 min, 6 h, 24 h, and 48 h) and at OD600 were taken using a NanoDrop™ One/OneC Microvolume UV-Vis Spectrophotometer.

Host range analysis

The host range of PAT1 was assessed using the phage sensitivity spot test described above. Bacterial strains listed in Table 1 were cultured at 28°C on YPGA plates for up to 2 d. The cultures were then each suspended in sterile distilled water, and 200 µL of bacterial suspension (OD600 = 0.2) were mixed with 6 mL volumes of YPG soft agar, which were then poured into Petri plates, and allowed to dry. Drops (10 µL each) of phage solution at 10^8, 10^7, 10^6, 10^5, or 10^4 PFU mL^{-1} were spotted onto the surfaces of the plates, which were then dried at room temperature. The plates were then incubated for up to 2 d at 28°C. Presence of clear zones was recorded for the respective strains, indicating strain susceptibility to PAT1.

Temperature and pH effects on PAT1

Temperature effects on PAT1 were assessed by incubating 100 µL of phage suspensions (~10^7 PFU mL^{-1}) for 1 h, at 4, 28, 40, 50, 60, or 70°C. Following incubation, serial dilutions were made with phage buffer, and phage titres were determined using the double agar overlay method. To assess pH effects, phage suspensions (100 µL) were each to 900 µL of sterile-filtered YPG that was pH-adjusted using 1 M NaOH or 1 M HCl. The inoculated cultures were then incubated at 28°C for 1 h. Subsequently, serial dilutions were made with phage buffer, and phage titres were determined using the double agar overlay method.

RESULTS

Spot assays

PAT1 produced clear lysis zones on the *A. tumefaciens* lawns (Figure 1) at all assessed titres, demonstrating the lysis potential of PAT1 against the bacterium.

Morphological and lytic properties of PAT1

PAT1 produced clear plaques, ranging from 2 to 5 mm diam. on lawn cultures of the *A. tumefaciens* strain CFBP 5770 (Figure 2A). TEM analysis showed that PAT1 had morphological features typical of a podovirus morphotype C1, with icosahedral and Head-tail geometries. The capsid diameter was approx. 60 (± 3) nm (length/width ratio = 1), and the non-contractile tails were 10 (± 2) nm in length (Figure 2B). TEM was also used to explore at the ultrastructural level the virulence of PAT1 against *A. tumefaciens*. Micrographs showed adsorption
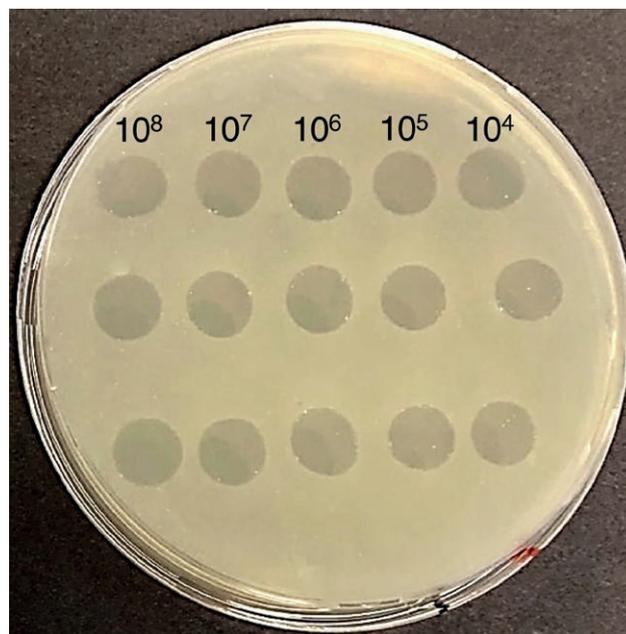
Figure 1. A YPGA plate showing antibacterial activity against *Agrobacterium tumefaciens* of PAT1 at different titres (10^8 to 10^4 PFU mL^{-1}, in triplicates).
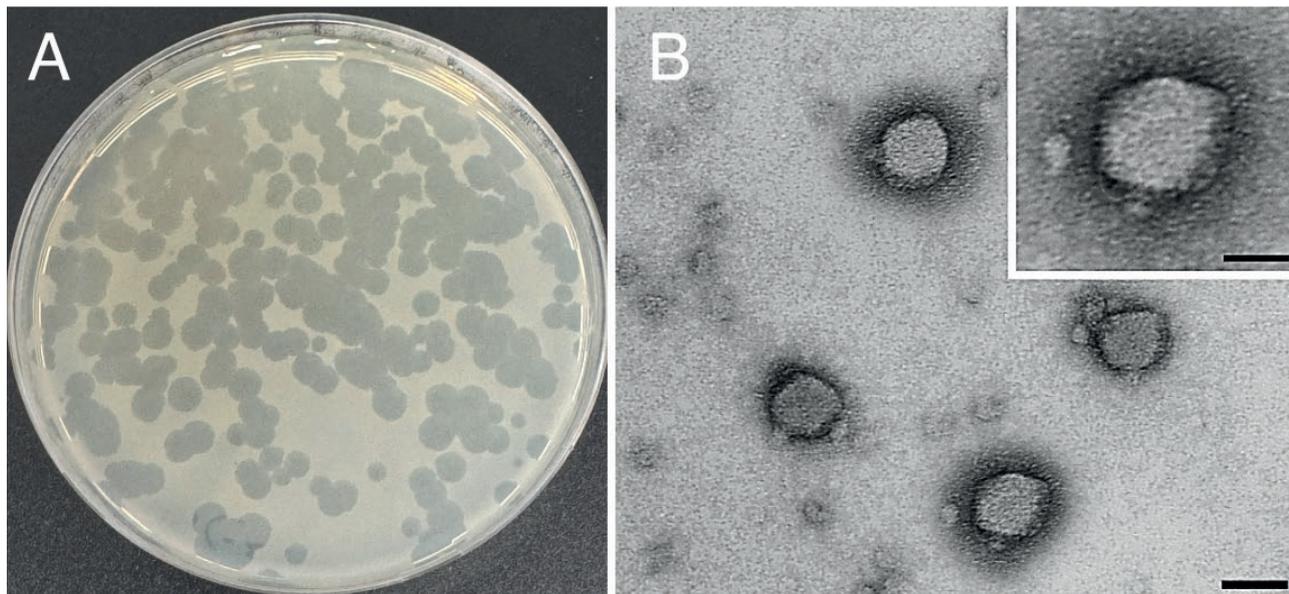
Figure 2. (A) Plaques caused by PAT1 on an *Agrobacterium tumefaciens* double layer agar plate. (B) Transmission electron microscope image of PAT1 showing a particle each with an icosahedral capsid and a very short non-contractile tail. Scale bars: 50 nm and 25 nm (inset).

of PAT1 on cell surfaces of *A. tumefaciens* at 10 min pi (Figure 3B), while the lysed cells of *A. tumefaciens* and release of progeny virions from infected bacteria were visualized at 30 min pi (Figure 3, C and D). These observations demonstrated the ability of PAT1 to adsorb, replicate and kill *A. tumefaciens* in less than 30 min for a complete infection cycle, and indicate that the infection cycle was lytic.

Temperature and pH effects on phage PAT1, and host range

The thermal and pH effects on PAT1 were estimated by measuring variations in survival rates as functions of the numbers of plaque-forming units (PFU). The phage was generally stable at temperatures from 4°C to 60°C, while it had approx. tenfold less infectivity at 60°C, and incubation at 70°C for 1 h killed the phage (Figure 4 A). PAT1 also had stable infectivity across the assessed pH range of 4 to 10 (Figure 4 B).

Host range analysis of PAT1 carried out for 16 bacterial strains (Table 1) showed that strains CFBP 5770 and BPIC 284 of *A. tumefaciens* were equally susceptible to PAT1, with the phage producing clear lysis zones at the different tested titres (data not shown). However, PAT1 was inactive against other *A. tumefaciens* strains, and the plant pathogenic bacteria examined, indicating that this phage is likely to be specific to strains of *A. tumefaciens*.

Bacteriolytic effects of PAT1 on growth of Agrobacterium tumefaciens

The ability of PAT1 to restrict the growth of *A. tumefaciens* strain CFBP 5770 was determined at different MOIs (1, 0.1, 0.01, 0.001, and 0.0001). All MOIs were effective, and the phage restricted growth of *A. tumefaciens* for 24 h (Figure 5). However, after 24 h, PAT1-infected bacteria displayed increased ODs, indicating emergence of phage-resistant mutants. Additionally, bacteria treated with the greatest MOI (1) showed slower increase in OD readings after 24 h (Figure 5), so MOI = 1 was determined as optimal MOI for PAT1. Despite the resistance development, PAT1 (MOI = 1) gave considerable antibacterial activity against *A. tumefaciens* growth, achieving an 82% reduction in bacterial growth at 48 h pi. At the end of the experiments, PAT1-resistant mutants were isolated on YPGA agar plates, and resistance to PAT1 was confirmed by spot assay. These results show that PAT1 possesses effective inhibitory potency against *A. tumefaciens*, indicating its potential for controlling crown gall.

Genomic and phylogenetic analyses of PAT1

The whole genome sequencing and *de novo* assembly of PAT1 revealed a double-stranded DNA genome of length of 45,040 base pairs, with a G + C content of
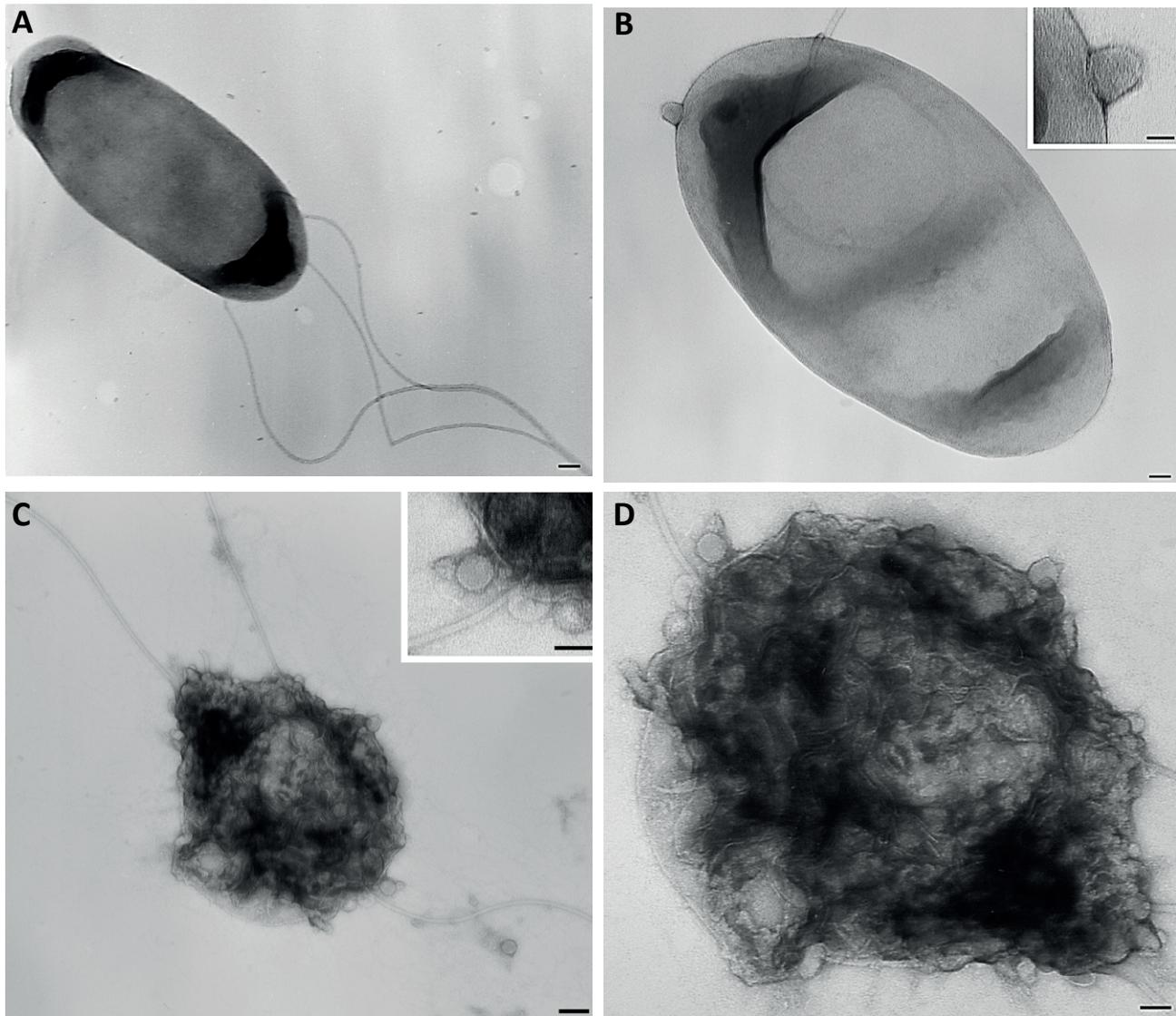
Figure 3. Transmission electron micrographs of *Agrobacterium tumefaciens* cells challenged with PAT1. A. untreated *tumefaciens* cell, used as control. B. PAT1 attachment on an *A. tumefaciens* cell surface (inset shows the point of phage penetration). C and D. Lysis of PAT1-treated *A. tumefaciens* cells with release of phage progeny (inset in C). Scale bars: A and C, 100 nm; B and D 50 nm; insets, B = 25 nm and C = 50 nm.

54.5%. This is less than that of *A. tumefaciens* (average 58.5%) (Deschamps *et al.*, 2016). The complete genome of PAT1 consisted of 54 coding sequences (CDSs), of which 31 (57.4%) encode for hypothetical proteins. The functions of 23 CDSs (42.6%) were predicted. These 23 CDs encode proteins involved with DNA replication and regulation, DNA packaging and structural proteins, and cell lysis, as highlighted on the genomic map (Figure 6). Prokka and Geneious analyses showed no tRNA encoding genes were present in the genome of PAT1. CGE analysis showed that the PAT1 genome did not contain any known genes associated with antibiotic resistance,

lysogenicity, toxins, or other virulence factors. These results indicate that PAT1 is suitable for use as a biocontrol agent.

Genome sequence analysis also showed that PAT1 shared maximum nucleotide similarities of 78.7% with Agrobacterium phage Atu_ph02 (accession number NC_047845) and 78.5% with Agrobacterium phage Atu_ph03 (accession number NC_047846) (Figure 7). Both phages are members of *Atuphduovirus* (*Autographiviridae*) and are known to infect *A. tumefaciens*. Based on the demarcation criteria of the "International Committee on Taxonomy of Viruses" (ICTV) for classification

(A)

(B)

Figure 4. Histograms showing results of thermal and pH stability tests of PAT1. (A) Phage titre after being treated with different temperatures for 60 min. (B) Phage infectivity after incubation at different pHs for 60 min. Phage titres were determined using the double agar overlay method. Error bars indicate standard deviations of means, from three replicates.

Figure 5. Growth curves for *Agrobacterium tumefaciens* treated with PAT1 at different MOIs. Mean optical densities of the bacterium cultures are shown for untreated bacteria or after different MOI treatments, up to 48 h pi. The bars indicate standard errors of the means for three replicates.

of new bacteriophages species (sequence similarity ≤ 95%), PAT1 is a putative new species, and is accordingly named Agrobacterium phage PAT1.

The compete genome sequence of PAT1 was deposited in GenBank under the accession number PQ082932. The proteomic tree of the PAT1 genome sequence, along with its close homologues and outliers based on genome-wide sequence similarities computed by tBLASTx, allocated PAT1 in a clade with Agrobacterium phage Atu_ph02 and Agrobacterium phage Atu_ph03, in *Atuphduovirus* in *Autographiviridae* (Figure 8). Therefore, PAT1 is considered as a tentative novel member of *Atuphduovirus*.

Figure 6. Genomic map of PAT1, representing 54 coding sequences encoded by the genome. Hypothetical proteins are displayed in grey, and predicted proteins are indicated with assigned functions highlighted with different colours.

DISCUSSION

Phages are currently regarded as efficient biocontrol agents, due to their characteristics of high selectivity in targeting specific bacteria without disrupting beneficial microbiota, hence maintaining environmental balance (Federici *et al.*, 2021). Additionally, phages self-replicate at infection sites, minimizing the need for repeated applications and ensuring sustained antibacterial activity (Xu *et al.*, 2022). Unlike other biocontrol agents, where development of resistance is often irreversible, bacteriophages have the unique ability to adapt and evolve alongside bacterial populations, by developing novel mechanisms to counteract this resistance to ensure sustained efficacy of biocontrol applications (Borges, 2021). However,

Figure 7. Genomic alignment of PAT1 with its close homologues. The coloured vertical blocks between the genomes indicate levels of nucleotide similarity. The genome alignment was generated using ViPTree.

the scarcity of effective lytic phages against *A. tumefaciens* underscores a critical gap in the biocontrol arsenal (Attai and Brown, 2019). Addressing this deficiency is important, as *A. tumefaciens* poses threats to agricultural productivity. The present study has described isolation and characterization of a novel and potent lytic phage, designated phage PAT1, thereby increasing the pool of *A. tumefaciens* phages, and providing a potentially eco-friendly solution for managing this plant pathogen.

Wastewater treatment stations normally collect sewage from many sources, such as farms, hospitals, industry, and elsewhere. These stations could be sources of a diverse range of bacterial communities, making them ideal habitats for bacteriophage isolation. In this context, a lytic phage against *A. tumefaciens*, named Agrobacterium phage PAT1, was isolated and characterized from the untreated influx point at the wastewater processing station of Bari, Italy. TEM analysis showed that PAT1 had morphological characteristics like those of podoviruses in *Caudoviricetes*, while genomic and phylogenetic analyses further identified PAT1 as a novel species within *Atuphduovirus* (*Autographiviridae*). In assessing the suitability of PAT1 as a biocontrol agent, prediction of genes functions in the PAT1 genome showed the absence of known genes associated with antibiotic resistance, lysogenicity, toxins or other virulence factors.

PAT1 was found to maintain stability of activity over a wide range of pH (4 to 10) and temperature (4°C to 60°C). Host range analysis showed that PAT1 is host-specific, with the ability to lyse only two strains of *A. tumefa-*

ciens out of six examined. PAT1 was also inactive against other bacterial species tested, indicating that PAT1 is likely to be specific to strains of *A. tumefaciens*. This host range is comparable to that of previously described *A. tumefaciens*-infecting phages (i.e., Agrobacterium tumefaciens phages Atu_ph04 and Atu_ph08), which were shown to be unable to infect A. tumefaciens strains (Attai and Brown, 2019). The narrow host range can be advantageous in PAT1 applications, as the phage potentially cannot infect non-target beneficial bacteria, likely to provide precise disease control. However, the high specificity of PAT1 for limited strains of *A. tumefaciens* can hinder its effectiveness for use in biocontrol of crown gall disease.

To address this shortcoming, phage engineering could host ranges of bacteriophages (Jia *et al.*, 2023). Gene editing techniques such as the CRISPR-Cas system can replace or modify receptor binding proteins (RBPs) to allow phages to recognize new hosts, thereby augmenting spectra of strains targeted by engineered phages (Jia *et al.*, 2023; Gencay *et al.*, 2024). It is also possible to strategically change the host range of bacteriophages, using advanced high-throughput methods such as transposon sequencing and iCRISPR technology, to identify specific bacteriophage receptor recognition genes, and then introducing modifications or performing gene swapping through in-host recombinations or out-of-host syntheses (Jia *et al.*, 2023).

The lytic activity of PAT1 against *A. tumefaciens* was examined through a series of assays and microscopy analyses. The results of TEM analysis demonstrated
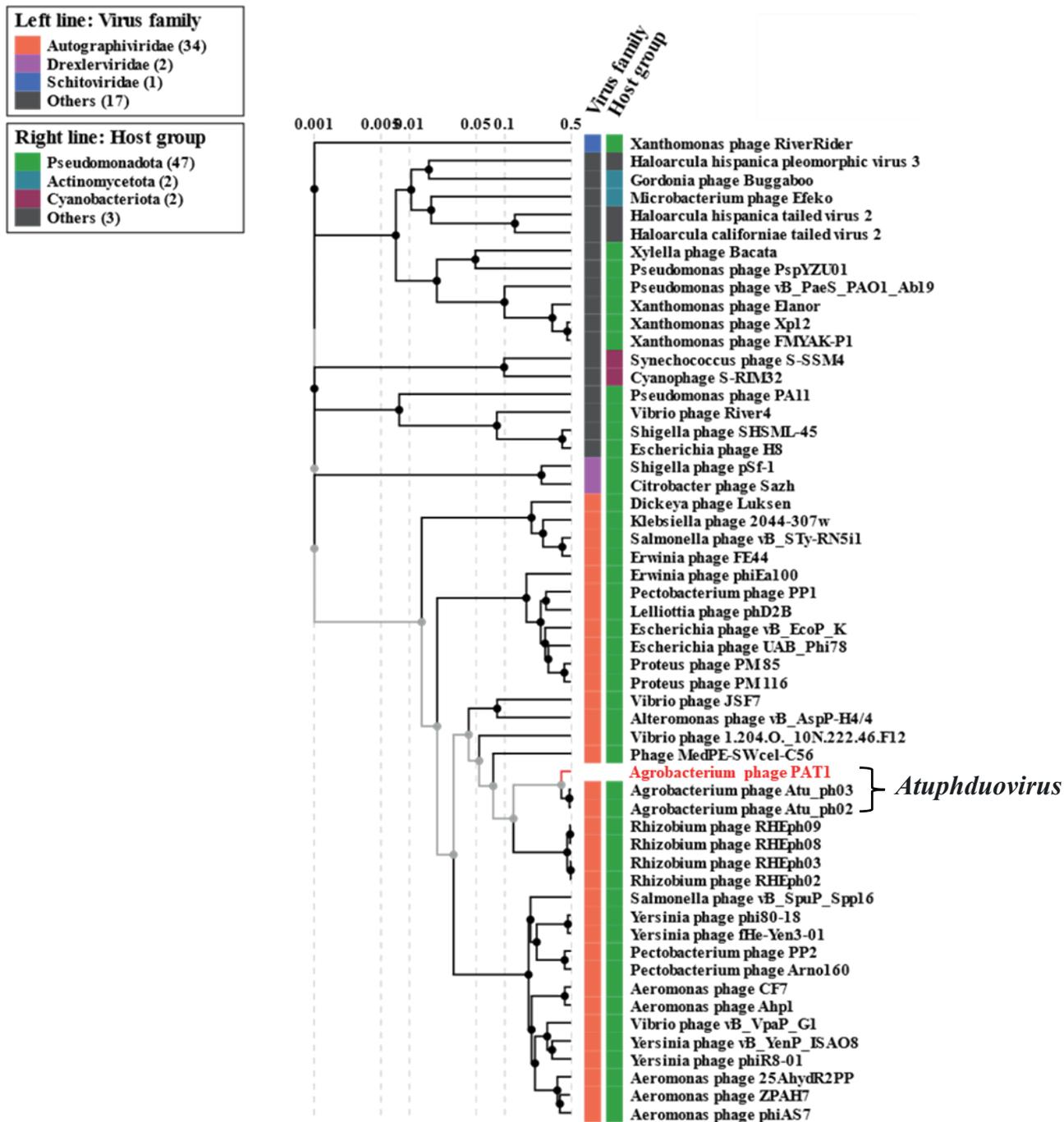
Figure 8. Proteomic tree of PAT1, generated by ViPTree based on genome-wide sequence similarities computed by tBLASTx, showing the allocation of PAT1 among species belonging to *Atuphduovirus* (*Autographiviridae*).

the ability of PAT1 to complete its lytic life cycle in *A. tumefaciens* cells within 30 min. Results from the MOI assays showed that PAT1 inhibited growth of *A. tumefaciens* for 24 h, with the greatest MOI giving the greatest reductions. However, incubation to 48 h resulted in increased ODs, both in control and phage treated samples, which reflect emergence of phage-resistant mutants. At this time stage, however, growth of *A. tumefaciens* treated with PAT1 (MOI = 1) was still reduced by 82% compared to untreated bacteria.

Phage resistance in bacteria is mediated through several adaptive mechanisms, including alterations in surface receptor structures that prevent phage adsorption, bacterial capsule modifications, and activation of intrinsic bacterial defense systems such as CRISPR-Cas (Egido et al., 2022). These resistance mechanisms have been detected observed across several bacterial species (Hyman and Abedon, 2010). To deal with this resistance, previous studies demonstrated that combinations of phages with other antimicrobial compounds (i.e., bacteriocins, antimicrobial peptides, antagonistic bacteria) leverages specific targeting abilities of phages and the mechanisms of other antimicrobial agents, leading to enhanced bacterial control reactions and reduced risks of resistance development (Knezevic and Aleksic Sabo, 2019). Therefore, employing PAT1 in conjunction with other antimicrobial compounds may increase efficiency of anti-bacterial activity, preserving the therapeutic potential of PAT1 and reducing the risk of resistance development. Furthermore, bacteriophage-derived endolysins, which are recognized as powerful and broad-spectrum bactericidal agents that can rapidly and precisely hydrolyze bacterial cell walls, are potential alternatives to antibiotics (Wong et al., 2022; Liu et al., 2023; Khan et al., 2024). These phage-encoded enzymes exert bactericidal activity both individually, and synergistically when combined with other antibacterials, thereby enhancing their efficacy (Fischetti, 2018). For example, the combination of the phage endolysin SAL200 with SOC anti-staphylococcal antibiotics gave synergistic effects *in vitro* and *in vivo* on *Staphylococcus aureus* infections (Kim et al., 2018). Endolysins have also been employed successfully against plant pathogenic bacteria, indicating their promise in sustainable agriculture (Vu and Oh, 2020; Nazir et al., 2023). In the present study, genomic analysis revealed the presence of an endolysin within the PAT1 genome, which could also be exploited against *A. tumefaciens*. This highlights the possible use of endolysin from PAT1, alone or in conjunction with other antimicrobials, to develop an integrated and effective biocontrol strategy against crown gall.

Phage PAT1 is a new biological agent in the list of phages that have been reported to specifically target *Agrobacterium* spp., particularly those responsible for plant diseases. On a practical level, these phages have shown potential for applications in agriculture. For example, the OLIVR1 phage has been successfully used to disinfect hydroponic greenhouse nutrient solutions from *A. rhizogenes*, the pathogen responsible for hairy roots in greenhouse-grown plants (Fortuna et al., 2023). The research in the present study was limited to the identification and characterization of PAT1, as an initial step towards evaluating its lysis potential and suitability for combating *A. tumefaciens*. The results obtained position PAT1 as a promising candidate for further evaluation in combating *A. tumefaciens* infections, both in greenhouse and in the field horticulture and agriculture.

CONCLUSIONS

The bacteriophage characterized in this study has several advantageous properties, including high stability over wide pH and temperature ranges, absence of toxins, lysogenicity or antibiotic resistance genes, a rapid infections cycle, presence of two endolysins genes, and good lysis potential against *A. tumefaciens*. These attributes indicate that PAT1 has potential for controlling crown gall, or as a component of integrated management of this disease. However, further investigations are required to explore the *in-planta* efficacy of PAT1, and its combination with other antibacterial agents.

AUTHOR CONTRIBUTIONS

M.S. and K.E.H.; writing (original draft), visualization, validation, software, methodology, investigation, formal analysis, data curation, and conceptualization: O.C.; software, investigation, and formal analysis; A.D.S.; writing (review and editing), methodology, investigation, conceptualization, and validation: T.E.; writing (review and editing), visualization, supervision, validation, software, methodology, formal analysis, data curation, conceptualization, resources, project administration, and funding acquisition. All the authors have read and agreed to the published version of the manuscript.

LITERATURE CITED

Álvarez B., López M.M., Biosca E.G., 2019. Biocontrol of the major plant pathogen *Ralstonia solanacearum* in

irrigation water and host plants by novel waterborne lytic bacteriophages. *Frontiers in Microbiology* 10, https://doi.org/10.3389/fmicb.2019.02813.

Asghari S., Harighi B., Ashengroph M., Clement C., Aziz A., Esmaeel Q., Ait Barka E., 2020. Induction of systemic resistance to Agrobacterium tumefaciens by endophytic bacteria in grapevine. *Plant Pathology* 69: 827–837. https://doi.org/10.1111/ppa.13175.

Attai H., Brown P.J.B., 2019. Isolation and characterization T4- and T7-Like phages that infect the bacterial plant pathogen Agrobacterium tumefaciens. *Viruses* 11: 528. https://doi.org/10.3390/v11060528.

Attai H., Boon M., Phillips K., Noben J.-P., Lavigne R., Brown P.J.B., 2018. Larger than life: Isolation and genomic characterization of a Jumbo phage that infects the bacterial plant pathogen, *Agrobacterium tumefaciens*. *Frontiers in Microbiology* 9: 1861. https://doi.org/10.3389/fmicb.2018.01861.

Attai H., Rimbey J., Smith G.P., Brown P.J.B., 2017. Expression of a peptidoglycan hydrolase from lytic bacteriophages Atu_ph02 and Atu_ph03 triggers lysis of *Agrobacterium tumefaciens*. *Applied and Environmental Microbiology*, 83: e01498-17. https://doi.org/10.1128/AEM.01498-17.

Borges A.L., 2021. How to train your bacteriophage. *Proceedings of the National Academy of Sciences*, 118: e2109434118. https://doi.org/10.1073/pnas.2109434118.

Choi O., Bae J., Kang B., Lee Y., Kim S., Fuqua C., Kim J., 2019. Simple and economical biosensors for distinguishing *Agrobacterium*-mediated plant galls from nematode-mediated root knots. *Scientific Reports, Nature Publishing Group* 9: 17961. https://doi.org/10.1038/s41598-019-54568-2.

Deschamps S., Mudge J., Cameron C., Ramaraj T., Anand A., Fengler K., Hayes K., Liaca V., Jones T.J., May G., 2016. Characterization, correction and de novo assembly of an Oxford Nanopore genomic dataset from *Agrobacterium tumefaciens*. *Scientific Reports, Nature Publishing Group* 6: 28625. https://doi.org/10.1038/srep28625.

Eckardt N.A., 2006. A genomic analysis of tumor development and source-sink relationships in *Agrobacterium*-induced crown gall disease in *Arabidopsis*. *The Plant Cell* 18: 3350–3352. https://doi.org/10.1105/tpc.107.050294.

Egido J.E., Costa A.R., Aparicio-Maldonado C., Haas P.J., Brouns S.J.J., 2022. Mechanisms and clinical importance of bacteriophage resistance. *FEMS Microbiology Reviews* 46: fuab048. https://doi.org/10.1093/femsre/fuab048.

Etminani F., Harighi B., Mozafari A.A., 2022. Effect of volatile compounds produced by endophytic bacteria on virulence traits of grapevine crown gall pathogen, Agrobacterium tumefaciens. *Scientific Reports*, Nature Publishing Group 12: 10510. https://doi.org/10.1038/s41598-022-14864-w.

Federici S., Nobs S.P., Elinav E., 2021. Phages and their potential to modulate the microbiome and immunity. *Cellular & Molecular Immunology* 18: 889–904. https://doi.org/10.1038/s41423-020-00532-4.

Fischetti V.A., 2018. Development of phage lysins as novel therapeutics: A historical perspective. *Viruses* 10: 310. https://doi.org/10.3390/v10060310.

Fortuna K.J., Holtappels D., Venneman J., Baeyen S., Vallino M., Verwilt P., Rediers H., De Coninck B., Maes M., Van Varenbergh J, Lavigne R., Wagemans J., 2023. Back to therRoots: Agrobacterium-specific phages show potential to disinfect nutrient solution from hydroponic greenhouses. *Applied and Environmental Microbiology* 89: e00215-23. https://doi.org/10.1128/aem.00215-23.

Gencay Y.E., Jasinskytė D., Robert C., Semsey S., Martínez V., *et al.*, Sommer M.O.A., 2024. Engineered phage with antibacterial CRISPR–Cas selectively reduce E. coli burden in mice. *Nature Biotechnology* 42: 265–274. https://doi.org/10.1038/s41587-023-01759-y.

Hyman P., Abedon S.T., 2010. Bacteriophage host range and bacterial resistance. *Advances in Applied Microbiology* 70: 217–248. https://doi.org/10.1016/S0065-2164(10)70007-1.

Jia H.-J., Jia P.-P., Yin S., Bu L.-K., Yang G., Pei D.-S., 2023. Engineering bacteriophages for enhanced host range and efficacy: insights from bacteriophage-bacteria interactions. *Frontiers in Microbiology* 14. https://doi.org/10.3389/fmicb.2023.1172635.

Kawaguchi A., Nita M., Ishii T., Watanabe M., Noutoshi Y., 2019. Biological control agent *Rhizobium* (=*Agrobacterium*) vitis strain ARK-1 suppresses expression of the essential and non-essential vir genes of tumorigenic R. vitis. *BMC Research Notes* 12: 1. https://doi.org/10.1186/s13104-018-4038-6.

Khan F.M., Rasheed F., Yang Y., Liu B., Zhang R., 2024. Endolysins: a new antimicrobial agent against antimicrobial resistance. Strategies and opportunities in overcoming the challenges of endolysins against Gram-negative bacteria. *Frontiers in Pharmacology* 15. https://doi.org/10.3389/fphar.2024.1385261.

Kim N.-H., Park W.B., Cho J.E., Choi Y.J., Choi S.J., *et al.*, Kim H.B., 2018. Effects of phage endolysin SAL200 combined with antibiotics on Staphylococcus aureus infection. *Antimicrobial Agents and Chemotherapy* 62: 10.1128/aac.00731-18. https://doi.org/10.1128/aac.00731-18.

Knezevic P., Aleksic Sabo V., 2019. Combining bacteriophages with other antibacterial agents to combat bac-

teria. (A. Górski, R. Międzybrodzki and J. Borysowski, ed.), *Cham, Springer International Publishing*, 257–293. https://doi.org/10.1007/978-3-030-26736-0_10.

Kropinski A.M., Van den Bossche A., Lavigne R., Noben J.-P., Babinger P., Schmitt R., 2012. Genome and proteome analysis of 7-7-1, a flagellotropic phage infecting Agrobacterium sp H13-3. *Virology Journal* 9: 102. https://doi.org/10.1186/1743-422X-9-102.

Kropinski A.M., Mazzocco A., Waddell T.E., Lingohr E., Johnson R.P., 2009. Enumeration of bacteriophages by double agar overlay plaque assay. *Methods in Molecular Biology* 501: 69–76. https://doi.org/10.1007/978-1-60327-164-6_7.

Lee C.-W., Efetova M., Engelmann J.C., Kramell R., Wasternack C., et a.,Deeken R., 2009. *Agrobacterium tumefaciens* promotes tumor induction by modulating pathogen defense in *Arabidopsis thaliana*. *The Plant Cell* 21: 2948–2962. https://doi.org/10.1105/tpc.108.064576.

Liu B., Guo Q., Li Z., Guo X., Liu X., 2023. Bacteriophage endolysin: A powerful weapon to control bacterial biofilms. *The Protein Journal* 42: 463–476. https://doi.org/10.1007/s10930-023-10139-z.

Loc-Carrillo C., Abedon S.T., 2011. Pros and cons of phage therapy. *Bacteriophage* 1: 111–114. https://doi.org/10.4161/bact.1.2.14590.

Nazir A., Xu X., Liu Y., Chen Y., 2023. Phage endolysins: advances in the world of food safety. *Cells* 12: 2169. https://doi.org/10.3390/cells12172169.

Nishimura Y., Yoshida T., Kuronishi M., Uehara H., Ogata H., Goto S., 2017. ViPTree: the viral proteomic tree server. *Bioinformatics* 33: 2379–2380. https://doi.org/10.1093/bioinformatics/btx157.

Nittolo T., Ravindran A., Gonzalez C.F., Ramsey J., 2019. Complete genome sequence of *Agrobacterium tumefaciens* Myophage Milano. *Microbiology Resource Announcements* 8: e00587-19. https://doi.org/10.1128/MRA.00587-19.

Penyalver R., Vicedo B., López M.M., 2000. Use of the genetically engineered *Agrobacterium* strain K1026 for biological control of crown gall. *European Journal of Plant Pathology* 106: 801–810. DOI : 10.1023/A:1008785813757.

Sabri M., El Handi K., Valentini F., De Stradis A., Achbani E.H., *et al.*, Elbeaino T., 2022. Identification and characterization of Erwinia Phage IT22: A new bacteriophage-based biocontrol against *Erwinia amylovora*. *Viruses* 14: 2455. https://doi.org/10.3390/v14112455.

Sabri M., El Handi K., Cara O., De Stradis A., Valentini F., Elbeaino T., 2024. Xylella phage MATE 2: a novel bacteriophage with potent lytic activity against *Xylella fastidiosa* subsp. *pauca*. *Frontiers in Microbiology* 15. https://doi.org/10.3389/fmicb.2024.1412650.

Svircev A., Roach D., Castle A., 2018. Framing the future with bacteriophages in agriculture. *Viruses* 10: 218. https://doi.org/10.3390/v10050218.

Thompson M.G., Moore W.M., Hummel N.F.C., Pearson A.N., Barnum C.R., *et al.*, Shih P.M., 2020. Agrobacterium tumefaciens: A bacterium primed for synthetic biology. *BioDesign Research* 8189219. https://doi.org/10.34133/2020/8189219.

Vicedo B., Peñalver R., Asins M.J., López M.M., 1993. Biological control of i, colonization, and pAgK84 transfer with i K84 and the tra- mutant strain K1026. *Applied and Environmental Microbiology* 59: 309–315.

Vu N.T., Oh C.-S., 2020. Bacteriophage usage for bacterial disease management and diagnosis in plants. *The Plant Pathology Journal* 36: 204–217. https://doi.org/10.5423/PPJ.RW.04.2020.0074.

Wong K.Y., Megat Mazhar Khair M.H., Song A.A.-L., Masarudin M.J., Chong C.M., *et al.*, Teo M.Y.M., 2022. Endolysins against Streptococci as an antibiotic alternative. *Frontiers in Microbiology* 13: https://doi.org/10.3389/fmicb.2022.935145.

Xu H.-M., Xu W.-M., Zhang L., 2022. Current status of phage therapy against infectious diseases and potential application beyond infectious diseases. *International Journal of Clinical Practice* 2022: 4913146. https://doi.org/10.1155/2022/4913146.

ORCID:
DG: 0000-0001-9261-8104
NH: 0000-0001-5436-5994
SN: 0000-0002-6202-4791
KEH: 0000-0001-6732-2627
TE: 0000-0003-2211-7907

Research Papers

Detection and characterization of *Xylella fastidiosa* in Iran: first report in alfalfa (*Medicago sativa*)

Davood GHANBARI[1,2], Nader HASANZADEH[1,*], Mariam GHAYEB ZAMHARIR[2], Shaghayegh NASR[3], Kaoutar EL HANDI[4], Toufic ELBEAINO[4,5,*]

[1] Department of Plant Protection, Faculty of Agricultural Science and Food Industries, Science and Research Branch, Islamic Azad University, Tehran, Iran
[2] Plant Diseases Department, Agricultural Research, Education and Extension Organization (AREEO), Iranian Research Institute of Plant Protection, PO Box 19395-1454, Tehran, Iran
[3] Microorganism Bank, Iranian Biological Resources Center (IBRC), Tehran, Iran
[4] Istituto Agronomico Mediterraneo di Bari (CIHEAM-IAMB), Via Ceglie 9, 70100 Valenzano (BA), Italy
[5] Institute for Sustainable Plant Protection of the National Research Council (IPSP-CNR), Piazzale Enrico Fermi 1 – 80055 Portici (NA), Italy
*Corresponding authors. E-mail: hasanzadehr@yahoo.com; elbeaino@iamb.it

Summary. Bacterial pathogens, especially *Xylella fastidiosa* (*Xf*), are significant threats to agricultural productivity, affecting economically important crops. The recent detection of *Xf* in Europe and the Middle East, including Iran, has emphasized the urgency for comprehensive surveillance to assess and understand the genetic diversity and distribution of this pathogen. A comprehensive survey from 2019 to 2022 was carried out in Iran to investigate *Xf* occurrence. A total of 403 samples were collected from alfalfa, almond, citrus, cherry, grapevine, olive, and pistachio plantations. Using serological (DAS-ELISA) and molecular (PCR) techniques, *Xf* was detected in nine samples from grapevine, five from almond, and 18 from alfalfa, and these include the first records *Xf* infections in alfalfa in Iran. Multiprimer-PCR assays carried out on *Xf*-infected plants, using ALM1/ALM2, *XF*2542-L/*XF*2542-R, and *XF*1968-L/*XF*1968-R primers for subspecies and strain differentiation, showed that the isolates from almond were *Xf* subsp. *multiplex*, and those from alfalfa were *Xf* subsp. *fastidiosa*. The *Xf* subsp. *multiplex* infecting almonds belonged to *Xf* genotype II. Pathogenicity tests carried out using *Xf* subsp. *multiplex* and *fastidiosa* isolates showed that the pathogen caused symptoms on *Nicotiana benthamiana* plants within 20 d post-inoculation. This study emphasizes the requirement for continuous monitoring, to mitigate the impacts of *Xf* on Iranian agriculture, and to prevent widespread outbreaks of this pathogen in multiple crop types.

Keywords. Detection, isolation, pathogenicity test, symptomatology.

INTRODUCTION

Plant diseases, particularly those caused by bacterial pathogens, continue to pose significant challenges to agricultural productivity (Nazarov

et al., 2020). Among these pathogens, *Xylella fastidiosa* (*Xf*) is an important vascular pathogen, affecting a wide range of economically important crops including grapevine, olive, citrus, coffee, and stone fruits, as well as numerous ornamental and forest species (Loureiro *et al.*, 2023). The pathogen is primarily vectored by sap-feeding insects, including sharpshooters and spittlebugs (Avosani *et al.*, 2024). Originating in South America, *Xf* has been responsible for several important plant diseases, including Pierce's disease (PD), olive quick decline syndrome (OQDS), almond leaf scorch (ALS), and citrus variegated chlorosis (CVC) (Picciotti *et al.*, 2023). Recent emergence of *Xf* in Europe has raised concerns regarding the presence of multiple genotypes of the pathogen, and the vulnerability of diverse plant species to infections. Detection of the pathogen in the Middle East and western Asia has underscored requirements for comprehensive investigations and surveillance to understand its distribution, genetic diversity, and potential impacts on agriculture in these regions (Loureiro *et al.*, 2023).

The first report on the presence of *Xf* in the Middle East and western Asia was in 2014 in Iran, where the pathogen was reported from symptomatic grapevines, almond and pistachio trees, with identification based on graft transmission, isolation on culture media, pathogenicity tests, and positive reactions in DAS-ELISA and PCR assays specific for the bacterium (Amanifar *et al.*, 2014; 2016).

In Iran, *Xf* was found in commercial almond orchards in Chaharmahal va Bakhtiari, West Azerbaijan and Semnan provinces (Amanifar *et al.*, 2014). At the same time, in the Razavi-Khorassan province, a severe apricot decline syndrome was observed, which had been previously associated with phytoplasmas, but some plants also tested positive for *Xf* (Karimishahri *et al.*, 2016). According to Amanifar *et al.* (2019), there are two subspecies of *Xf* in Iran, determined after gene sequencing and observations of differences in biological and morphological characteristics of bacterial colonies. These were subsp. *fastidiosa* isolated from grapes, and subsp. *multiplex* isolated from pistachios and almonds (Amanifar *et al.*, 2016; 2014). *Xylella fastidiosa* can increase host range through horizontal gene transfer (HGT), enabling the bacterium to acquire genetic material from other organisms, potentially including genes associated with infection of new host plants (D'Attoma *et al.*, 2020; Pierry *et al.*, 2020, Woods *et al.*, 2020). Genetic variation can also occur within *Xf* populations, from mutations and recombination, which give rise to variants with altered characteristics, potentially enhancing their ability to infect increased host ranges. These mechanisms, together with selective environmental pressures, can result in adaptation and expansion of *Xf* host range (O'Leary and Burbank, 2023).

Instances of leaf scorch and dieback symptoms, like those caused by *Xf* on several crop, have been reported in numerous alfalfa fields across regions of Iran.

Upon confirmation of the bacterium's presence within this country, it became important that routine surveillance efforts were initiated, aiming to mitigate occurrence and dissemination of *Xf* in previously unaffected areas, while also monitoring spread of the pathogen. Despite these observations, no investigations on the possible presence of *Xf* in these crops had been carried out. Therefore, the objective of the present study was to conduct an extensive survey to evaluate the presence of *Xf* in almond, grape, citrus, and alfalfa plants across different regions of Iran, to update knowledge of the distribution of *Xf* in this country.

MATERIALS AND METHODS

Study areas and collection of samples

A systematic sampling campaign was carried out in crops of different Iranian regions over the summer seasons from 2019 to 2022, in the regions of Qazvin, Isfahan, Chaharmahal Bakhtiari, Gilan, Zanjan, Tehran, and the central regions of Hormozgan and Kerman. In total, 403 samples were collected from different crop types, including alfalfa, almonds, cherry, citrus, grapevine, olive, and pistachio, showing symptoms recalling those caused by *Xf* (Figure 1). Each sample, which consisted of 4 to 6 cuttings/trees (up to 20 cm each), was kept in a closed plastic bag, labelled with relevant information (date, location, presence/absence of symptoms) (Table 1), and then kept in a cooling box during transport, brought to the laboratory and was conserved at 4°C before being analysed.

Serological detection (DAS-ELISA)

All samples underwent the double-antibody sandwich-enzyme linked immunosorbent assays (DAS-ELISA), using a polyclonal antibody kit (Agritest, Bari, Italy), according to the manufacturer's instructions. ELISA plates were coated with anti *Xf*-IgG and incubated at 37°C for 4 h. After washing, samples were loaded and incubated overnight at 4°C. Alkaline-phosphatase conjugated-anti *Xf*-IgG was added, and incubated at 37°C for 4 h. Absorbance was measured using a Multiskan FC microplate reader (ThermoFisher Scientific) at 405 nm. Positive reactions were identified if absorbance was three times greater than controls after 120 min.

Figure 1. Grapevine (a), alfalfa (b), and almond (c) plants infected with *Xylella fastidiosa* and showing symptoms of marginal leaf scorch, wilting of foliage, and withering of branches.

Table 1. Hosts, locations, sampling dates, and numbers of samples collected, for plants showing disease symptoms.

Host	Sampling province	Sampling date	Number of samples
Alfalfa	Chaharmahal va Bakhtiari	September 2021	3
		September 2022	6
	Isfahan	September 2021	3
		September 2022	6
Almond	Alborz	September 2022	12
	Chaharmahal va Bakhtiari	August\September 2021	11
		September 2022	35
	Isfahan	August\September 2021	8
		September 2022	54
Cherry	Isfahan	September 2022	15
Citrus	Hormozgan, Gilan kerman	September 2020	40
Grapevine	Alborz	August\September 2021	3
	Qazvin	August\September 2019	50
		September 2020	32
		August 2021	41
		August 2022	53
Olive	Gilan, Zanjan	December 2021	17
Pistachio	Tehran, Markazi	September 2021	14
		Total	403

Molecular detection (PCR)

DNA extraction was carried out using CTAB buffer (Hendson *et al.*, 2001). For each sample 1 mL of homogenized extract was placed in a 2 mL microcentrifuge tube and heated at 65°C for 30 min, followed by centrifugation at 16,000× g for 5 min. Subsequently, 1 mL of the supernatant was carefully transferred into a fresh 2 mL capacity micro-centrifuge tube, and 1 mL of chloroform-isoamyl-alcohol (24:1) was added, mixed thoroughly, and centrifuged at 16,000× g for 10 min. Supernatant (700 μL) was then transferred to a 1.5 mL microcentrifuge tube, and approx. 0.7 volume of cold 2-propanol (490 μL) was added. After gentle mixing twice by inversion, the tubes were incubated at –20°C for 20 min. Subsequent centrifugation at 16,000× g for 20 min allowed for recovery of a pellet from each tube, which was washed with 1 mL of 70% ethanol and centrifuged again at 16,000× g for 10 min. The sample was then vacuum dried, and the pellet was resuspended in 100 μL of DNase/RNase-free water.

PCR assays were carried out using *Xf*-specific primers, *i.e.*, RST31 (5'-GCGTTAATTTTCGAAGTGATTC-GA-3') and RST33 (5'-CACCATTCGTATCCCGGTG-3') (Minsavage *et al.*, 1994). PCR reactions were carried out in 20 μL final volumes each containing 4 μL of Bioline buffer [(5 mM dNTPs and 15 mM MgCl$_2$), 0.5 μL (10 pmoL μL^{-1}) of each primer, 0.2 μL Taq DNA polymerase (Lifetechnologies), 3 μL of total DNA template]. The cycle program used was 95°C for 5 min, followed by 40 cycles each at 95°C for 30 sec, 55°C for 1 min, and 72°C for 1 min, and a final extension at 72°C for 5 min. The assays were electrophoresed on 1.2% TBE agarose gel and were visualized under UV light after staining with GelRed dye (Biotium).

Biological detection (isolation)

Upon the confirmation of *Xf* DNA presence through one of the diagnostic techniques, isolations of *Xf* were carried out from positive almond and alfalfa plant samples. These were achieved through direct printing of twigs on buffered charcoal yeast extract (BCYE) agar plates (Wells *et al.*, 1981). Twigs of length 8 to-10 cm were surface sterilized with 2% sodium hypochlorite for 2 min, were then rinsed in 70% ethanol for 2 min

followed by three rinses with sterile water. Each twig was then cut in half and pressed at one end with a plier, while the other end was gently pressed onto BCYE plates to make imprints. The plates were then closed and sealed with parafilm, incubated at 28°C for 4 weeks and regularly checked for the appearance of *Xf*-like colonies, which typically appeared as small, circular, and whitish yellow in colour.

Pathogenicity tests

The virulence potential of newly isolated *Xf* strains was assessed using a pathogenicity test. This involved *Xf* inoculations into stems of *Nicotiana benthamiana* plants, which are widely used as an experimental host for *Xf* (Lopes *et al.*, 2000). One-month-old *N. benthamiana* plants were each inoculated with 50 µL of *Xf* suspension (OD_{600} = 0.32) prepared in phosphate buffered saline (PBS; pH 7.4, 0.01 M), using a 0.1 mL capacity insulin syringe. The plants were then maintained in a controlled environment at 28°C for 2 months and were visually inspected for development of characteristic symptoms of *Xf* (*i.e.*, leaf scorch). The presence of *Xf* in the symptomatic *N. benthamiana* plants was confirmed through PCR assays using the RST31/33 primers.

Multiprimer-PCR specific detection of Xylella fastidiosa *subspecies*

The colonies presumed to be *Xf* were purified on BCYE plates, and the isolates were then subjected to PCR assays to verify their *Xf* nature, using *Xf*-specific primers RST31/RST33 as described above. Subsequently, all newly identified *Xf* strains, *i.e.*, those found in infected plants and those identified from plates, were subjected to a multiprimer-PCR assays, using ALM1/ALM2, *XF*2542-L/ *XF*2542-R, and *XF*1968-L/*XF*1968-R primers to differentiate the strains into the three *Xf* subsp., *fastidiosa*, *multiplex*, or *sandyi* (Hernandez-Martinez *et al.*, 2006).

RESULTS

Serological and molecular detection of Xylella fastidiosa

The ELISA assay results yielded insights into the presence of *Xf* within the tested samples. Among the 176 grapevine samples tested, nine samples from Qazvin and Takistan provinces were positive for *Xf* infections. Of the 123 almond and 18 alfalfa samples tested, five from each plant type were found to be infected, with all the host plants originating from the provinces of Isfahan, Chaharmahal va Bakhtiari. These results were then verified through PCR assays using the *Xf*-specific RST31/RST33 primers, which confirmed the presence of *Xf* in all ELISA-positive samples, and its absence in the samples gave negative reactions (Figure 2). All the assessed olive, citrus, cherry and pistachio samples were found to be negative for *Xf*, based both on the ELISA and PCR assays.

Isolation of Xylella fastidiosa *from infected samples*

All almond and alfalfa samples that tested positive for *Xf* in ELISA and PCR assays were utilized for isolation of bacteria, using the printing method (Table 2). Two *Xf* isolates from alfalfa and one from almond were recovered on BCYE plates (Figure 3). All isolated bacterial colonies were further confirmed as *Xf* by PCR, using RST31/RST33 primers, and each isolate was triple-cloned before being stored in PBS supplemented with glycerol (50%) and maintained at -80°C.
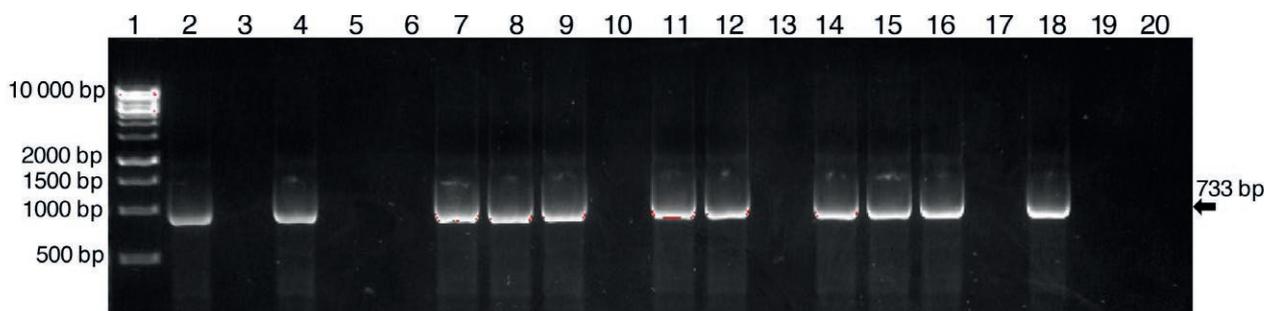
Figure 2. Agarose gel electrophoresis showing PCR amplified products using RST31/RST33 primers (733 bp). Representative samples from grapevine (lanes 2 and 4), alfalfa (lanes 7 to 9), and almond (lanes 11, 12, 14, 15 and 16), producing the expected amplicon, indicate presence of *Xf*. Lanes 3, 5, 6, 10, 13, 17 and 19 are for plant samples that tested negative. Lane 18 is for gDNA of *Xf* used as the positive control reaction. Lane 20 is for the negative control reaction. Lane 1 is the 1 Kbp DNA ladder.

Figure 3. BYCE media plates (4 weeks after preparation) showing bacterial colonies of *Xylella fastidiosa* isolated from plants of alfalfa (Q7A and Q257B) or almond (Q8B), infected with *Xylella fastidiosa*.

Table 2. Host plant species and geographical origins of the *Xylella fastidiosa* isolates obtained in this study.

Host plant	Region	Isolates	ELISA	PCR	Culture on BCYE
Alfalfa	Isfahan	Q7A	+	+	+
	Isfahan	Q23H	+	+	-
	Chaharmahal\Bakhtiari	Q58Z	+	+	-
	Chaharmahal\Bakhtiari	Q257B	+	+	+
	Chaharmahal\Bakhtiari	Q125P	+	+	-
Almond	Isfahan	Q55X	+	+	-
	Isfahan	Q57S	+	+	-
	Isfahan	Q25P	+	+	-
	Chaharmahal\Bakhtiari	Q47F	+	+	-
	Chaharmahal\Bakhtiari	Q8B	+	+	+

Figure 4. Agarose gel electrophoresis showing multiprimer-PCR amplified products. Amplification was achieved using ALM1/ALM2, *XF*2542-L/*XF*2542-R, and *XF*1968-L/*XF*1968-R primer pairs, with samples from almond (lanes 2 to 6) indicating infections by *Xanthomonas fastidiosa* subsp. multiplex, and samples from alfalfa (lanes 7 to 11) indicating infections by -*Xf* subsp. *Xf* subsp. *fastidiosa*. Lane 1: 1 Kbp DNA ladder.

Multiprimer-PCR assays

To differentiate the subsp. of the *Xf*-infected isolates from almond and alfalfa plants, a multiprimer-PCR assay was carried out, using the methods of Hernandez-Martinez *et al*. (2006). PCRs were with primers XF1968-L and XF1968-R amplifying a 638 bp fragment from oleander leaf scorch (OLS) strains but not from Pierces' Disease (PD) strains or almond leaf scorch (ALS) strains that belong to *Xf* subsp. *fastidiosa*. PCR with primers XF2542-L and XF2542-R amplify a 412 bp fragment from PD strains, but not from OLS strains. PCR with primers ALM1 and ALM2 produces a fragment of 521 bp from strains isolated from almond that belong to *Xf* subsp. *multiplex*.

The multiprimer-PCR results showed that when the *Xf* isolates from almond were tested, three bands of 412, 521, and 638 bp were obtained; whereas *Xf* alfalfa isolates uniquely yielded a 412 bp band (Figure 4), indi-

demonstrating that they belonged to genotype II of *Xf*, in contrast to the genotype I isolates, which produce only two bands in the PCR.

Pathogenicity tests

The pathogenicity tests showed that all isolates caused symptoms on *N. benthamiana* plants. At 20 days post inoculation (dpi), the *Xf*-infected tobacco plants had leaf margin and interveinal chloroses, and then scorch symptoms at 4 to 6 weeks after inoculation (Figure 5).

DISCUSSION AND CONCLUSIONS

Early detection of *Xf* infections is essential for effective management of this harmful plant pathogen. Emergence of *Xf* in new areas and failure to contain its spread in previously affected regions have become severe international problems (El Handi *et al*., 2022). To date, sev-
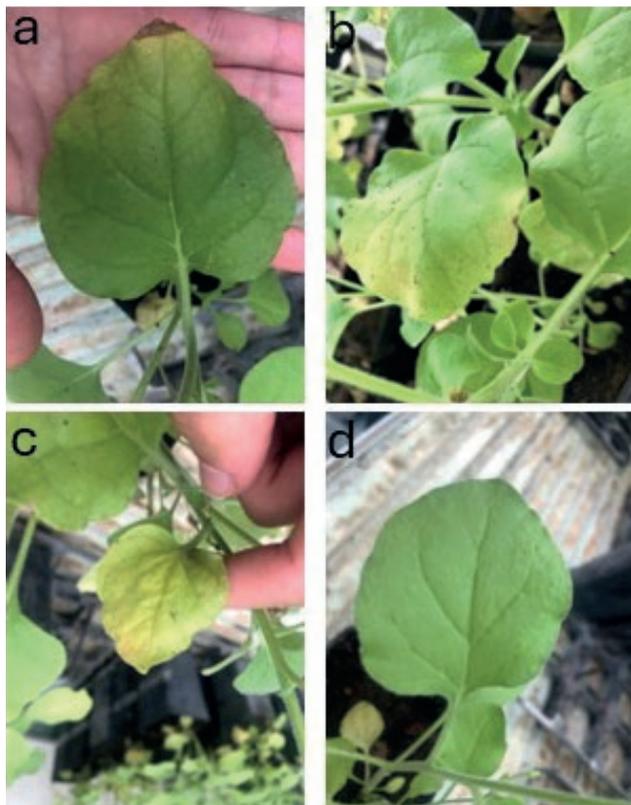
Figure 5. *Nicotiana benthamiana* plants inoculated with different isolates of *Xylella fastidiosa* sub sp. *alfalfa* [(a) isolates Q7A and (b) 257B)], and isolates from almond [(c) isolate Q8B], showing typical symptoms of *Xf* infections, including scorch of leaf margins, wilting of foliage, and withering of branches. (d) *N. benthamiana* plants inoculated with sterile water and showing no symptoms.

eral *Xf* subspecies have been isolated and identified from a wide variety of host plants (Loureiro *et al.*, 2023). The broad distribution of this pathogen from the American continent to different parts of the world demonstrates its adaptability to various environmental conditions. As a result, the spectrum of host species vulnerable to this potentially serious pathogen continues to increase (Castro *et al.*, 2021).

In Iran, the detection of new *Xf* subspecies could lead to important disease outbreaks, resulting in considerable socio-economic and agricultural challenges impacting local economies. To prevent these scenarios, it is important to monitor and counter the spread of *Xf*, and to accurately map its distribution, by identifying infested zones and developing effective control strategies to contain the pathogen (El Handi *et al.*, 2022). This proactive approach is essential for limiting emergence of *Xf*, thereby safeguarding agricultural sustainability and economic stability. The present research extends previous

studies conducted in Iran (Amanifar *et al.*, 2019; 2016), aiming to update and monitor the presence of *Xf* in different Iranian regions and different host species. This study, which assessed 403 plant samples from several crop types and carried out during 4 consecutive years, detected, for the first time, *Xf* in alfalfa as a new host in this country. The results showed incidence ALS and PD in particular orchards, which occasionally resulted in withering symptoms on affected trees. Almond trees, as well vineyards Takestan City, in the Qazvin province, are noteworthy examples. Takestan City has the largest vineyards in Iran. Furthermore, isolation of *Xf* from alfalfa and almond hosts is a first record of this pathogen in Iran.

The results of multiprimer-PCR analyses of *Xf* isolates from alfalfa and almond in Iran, but not on those from grapevine which were previously characterized by Amanifar *et al.* (2016), demonstrated the presence of *Xf* belonging to subsp. *fastidiosa*, which was associated with alfalfa leaf scorch symptoms. The same method for identification of subspecies and strains was utilized by Hernandez-Martinez *et al.* (2006) for the differentiation of strains of *Xf* infecting grape, almond, and oleander. Similarly, in the present study, *Xf* subsp. multiplex isolates from almond were genotype II of *Xf*. Normally, strains of the *Xf* subsp. *multiplex* are less fastidious, can easily grow on artificial media, and produce mild ALS and PD symptoms (Almeida and Purcell, 2003). Isolation of *Xf* on artificial culture media, together with the results obtained from the pathogenicity test on *N. benthamiana*, are important for characterization of *Xf* strains in different hosts and crop varieties in Iran. The presence of *Xf* was observed in alfalfa fields located near almond trees affected by *Xf* infections.

At field scales, proximity between alfalfa fields and grapevine and almond plantations suggests a potential mechanism of leafhopper transfer between these plantations. Therefore, it is important that intensive insect surveys are carried out to identify potential vectors of *Xf* within and outside affected areas.

In conclusion, the swift detection of novel subspecies of *Xf* in Iran is important for effective outbreak management and mitigation of the diseases caused by this pathogen. The severe OQDS outbreaks in Italy demonstrate the necessity for proactive surveillance and rapid reaction strategies for managing these diseases in Iran. Implementing strict quarantine measures, deploying targeted control strategies, and encouraging collaboration among researchers, policymakers, and agricultural stakeholders, are all important components of proactive prevention of introduction and spread of new *Xf* subspecies in this country.

AUTHOR CONTRIBUTIONS

D.G: writing of original draft, visualization, validation, methodology, formal analysis, and validation. N.H: writing, review and editing, visualization, supervision, resources, and administration. M.G.Z: investigation, visualization, and methodology. S.N: investigation, visualization, and methodology. K.E.H.: visualization, methodology, analysis, review, and editing. T.E: methodology, review and editing, visualization, supervision, resources, and funding acquisition. All authors read, revised, and approved the final manuscript.

LITERATURE CITED

Almeida R.P.P., Purcell, A.H., 2003. Biological traits *of Xylella fastidiosa* strains from grapes and almonds. *Applied Environmental Microbiology* 69: 7447–7452.

Amanifar N., Babaei G., Mohammadi A.H., 2019. *Xylella fastidiosa* causes leaf scorch of pistachio (*Pistacia vera*) in Iran. *Phytopathologia Mediterranea* 58(2): 369–378.

Amanifar N., Taghavi M., Salehi M., 2016. *Xylella fastidiosa* from almond in Iran: overwinter recovery and effects of antibiotics. *Phytopathologia Mediterranea* 55(3): 337-345.

Amanifar N., Taghavi M., Izadpanah K., Babaei G., 2014. Isolation and pathogenicity of *Xylella fastidiosa* from grapevine and almond in Iran. *Phytopathologia Mediterranea* 53(2): 318–327.

Avosani S., Nieri R., Mazzoni V., Anfora G., Hamouche Z., Zippari C., Cornara D., 2024. Intruding into a conversation: How behavioral manipulation could support management of *Xylella fastidiosa* and its insect vectors. *Journal of Pest Science* 97(1): 17–33.

Castro C., Di Salvo B., Roper M.C., 2021. *Xylella fastidiosa*: A reemerging plant pathogen that threatens crops globally. *PLoS Pathogens* 17(9): e1009813.

D'Attoma G., Morelli M., De La Fuente L., Cobine P.A., Saponari M., de Souza A.A., Saldarelli P., 2020. Phenotypic characterization and transformation attempts reveal peculiar traits of *Xylella fastidiosa* subspecies *pauca* strain De Donno. *Microorganisms* 8(11): 1832.

El Handi K., Sabri M., Valentini F., De Stradis A., Achbani E.H., Hafidi M., El Moujabber M., Elbeaino T., 2022. Exploring active peptides with antimicrobial activity. In Planta against *Xylella fastidiosa*. *Biology* 11: 1685. https://doi.org/10.3390/biology11111685.

Hendson M., Purcell A.H., Chen D., Smart C., Guilhabert M., Kirkpatrick B., 2001. Genetic diversity of Pierce's disease strain and other pathotypes of *Xylella fastidiosa*. *Applied and Environmental Microbiology* 67: 895–903.

Hernandez-Martinez R., Costa H.S., Dumenyo C.K., Cooksey D.A., 2006. Differentiation of Strains of *Xylella fastidiosa* Infecting Grape, Almonds, and Oleander Using a Multiprimer PCR Assay. *Plant Disease* 90: 1382–1388. https://doi.org/10.1094/PD-90-1382.

Karimishahri M.R., Paltrinieri S., Sajadinejad M., Contaldo N., Bertaccini A. 2016. Molecular detection of prokaryotes in apricot showing decline and leaf scorch symptoms in Iran. *Phytopathogenic Mollicutes* 6(1): 33. https://doi.org/10.5958/2249-4677.2016.00006.2.

Lopes S.A., Ribeiro D.M., Roberto P.G., França S.C., Santos J.M., 2000. Nicotiana tabacum as an experimental host for the study of plant-*Xylella fastidiosa* interactions. *Plant Disease* 84: 827–830. https://doi.org/10.1094/PDIS.2000.84.8.827.

Loureiro T., Mesquita M.M., Dapkevicius M.D.L.E., Serra L., Martins Â., Cortez I., Poeta P., 2023. *Xylella fastidiosa*: A glimpse of the Portuguese situation. *Microbiology Research* 14(4): 1568–1588.

Minsavage G.V., Thompson C.M., Hopkins D.L., Leite M.V.B.C., Stall R.E., 1994. Development of a polymerase chain reaction protocol for detection of Xylella fastidiosa in plant tissue. *Phytopathology* 84: 456–461.

Nazarov P.A., Baleev D.N., Ivanova M.I., Sokolova L.M., Karakozova M.V., 2020. Infectious plant diseases: Aetiology, current status, problems and prospects in plant protection. *Acta Naturae* 12(3): 46.

O'Leary M.L., Burbank L.P., 2023. Natural recombination among Type I restriction-modification systems creates diverse genomic methylation patterns among *Xylella fastidiosa* strains. *Applied and Environmental Microbiology* 89(1): e01873-22.

Picciotti U., Araujo Dalbon V., Ciancio A., Colagiero M., Cozzi G., De Bellis L., Porcelli F., 2023. "Ectomosphere": Insects and microorganism interactions. *Microorganisms* 11(2): 440.

Pierry P.M., Uceda-Campos G., Feitosa-Junior O.R., Martins-Junior J., de Santana W.O., Coletta-Filho H.D., da-Silva A.M., 2020. Genetic diversity of *Xylella fastidiosa* plasmids assessed by comparative genomics. *Tropical Plant Pathology* 45: 342-360.

Wells J.M., Raju B.C., Nyland G., Lowe S.K., 1981. Medium for isolation and growth of bacteria associated with plum leaf scald and phony peach diseases. *Applied and Environmental Microbiology* 42: 357–363.

Woods L.C., Gorrell R.J., Taylor F., Connallon T., Kwok T., McDonald M.J., 2020. Horizontal gene transfer potentiates adaptation by reducing selective constraints on the spread of genetic variation. *Proceedings of the National Academy of Sciences* 117(43): 26868–26875.

ORCID:
MC: 0000-0003-2170-9521
MM: 0000-0001-5491-5562
CV: 0000-0001-6317-0734
KÇ: 0000-0002-4381-4149
FM: 0000-0002-7480-922X
SC: 0000-0002-1353-4373
MG: 0000-0002-8495-7971

Research Papers

Estimated costs of plum pox virus and management of sharka, the disease it causes

Mariano CAMBRA[1,*], Mónica MADARIAGA[2], Christina VARVERI[3], Kadriye ÇAĞLAYAN[4], Ali Ferhan MORCA[5], Sergei CHIRKOV[6], Miroslav GLASA[7,8]

[1] *Instituto Valenciano de Investigaciones Agrarias (IVIA), Virology and Immunology, Plant Protection and Biotechnology Centre, 46113 Moncada-Valencia, Spain. Currently retired*
[2] *Instituto de Investigaciones Agropecuarias INIA-La Platina, 11610 Santiago, Chile*
[3] *Benaki Phytopathological Institute, Laboratory of Virology, Scientific Directorate of Phytopathology, 14561 Kifissia, Greece*
[4] *Mustafa Kemal University, Plant Protection Department, 31034 Antakya-Hatay, Türkiye*
[5] *Directorate of Plant Protection Central Research Institute, Gayret Mah, Fatih Sultan Mehmet Bulv, 06172, Yenimahalle, Ankara, Türkiye*
[6] *Dept. of Virology, Faculty of Biology, Lomonosov Moscow State University, Moscow 119234, Russia*
[7] *Institute of Virology, Biomedical Research Center of Slovak Academy of Sciences, Bratislava, Slovakia*
[8] *Faculty of Natural Sciences, Institute of Biology and Biotechnology, University of Ss. Cyril and Methodius, Trnava, Slovakia*
*Corresponding author. E-mail: mcambra@mcambra.es

Summary. The disease "sharka", caused by *Potyvirus plumpoxi* (plum pox virus), is the most harmful viral disease affecting stone fruits. The virus spreads over long distances through illegal and insufficiently controlled exchange of infected propagative plant material. Once established in an area, the virus spreads locally through vegetative propagation of infected plant material, and naturally through aphid-vectors. Previously considered a European problem, sharka has now been reported in 54 *Prunus*-growing countries in all continents except Oceania, although the disease has been eradicated from the United States of America. The economic cost of the disease in the 28 years from 1995 to 2023 is estimated to be €2.4 × 10⁹, equivalent to approx. 0.17% of the stone fruit industry's value. This includes more than over €2 × 10⁹ in direct fruit losses, €1.4 million from international rejection of symptomatic fruit, and over €100 million in eradication and disease limitation costs. Indirect costs include €137 million, mainly associated with ELISA analyses, and approx. €130 million in costs related to research and science networks. Cumulative global losses from the sharka pandemic since the decade 1910/20 probably surpass €13 × 10⁹. These outlays exclude indirect trade costs, economic losses, genetic erosion of traditional cultivars, and the costs of developing new cultivars tolerant or resistant to plum pox virus. The decline in these costs compared to the previously evaluated €10 billion from the 1970s to 2006 is analyzed. Four case studies (for Spain, Turkey, Chile, and Greece) illustrate different sharka scenarios and management strategies.

Keywords. PPV, direct costs, indirect costs, losses, ELISA tests, eradication, subsidies, quarantine, RNQP.

Plant pathogens causing crop diseases are threats to global food security (Strange and Scott, 2005; Savary *et al.*, 2019), and economic losses caused by plant viruses are important (Jones and Naidu, 2019). However, there have been few studies on economic losses caused by viruses in temperate stone-fruit trees (e.g., Paulus and Ullstrup, 1978; Németh, 1994; Tresh *et al.*, 1994; Waterworth and Hadidi, 1998; Matthews and Hull, 2002; Cambra *et al.*, 2006a; Hadidi and Barba, 2011; Rao and Reddy, 2020), while there has been more research evaluating economic losses caused by phytophagous arthropods, fungi (especially those causing foliar damage), or oomycetes (e.g., Culliney, 2014; Simões *et al.*, 2023). Few attempts have been made to establish stone fruit yield, quality, and economic losses caused by the plant viruses.

Diseases can decrease plant productivity and production of marketable fruit. Losses caused by virus diseases depend on many factors, such as prevalence or incidence of infections, severity of diseases, virulence and host range of prevalent strains/variants of virus pathogens, host cultivar susceptibility, duration of infections, and fluctuating prices for crop products. Plant health is closely linked to international trade because invasive pests and pathogens can be introduced through the movement of plants and plant products across borders and continents, disrupting trade and causing economic losses. Direct assessment of the costs of prevention, management, and decrease in crop losses is complex and often imprecise (Oerke *et al.*, 1994; Savary *et al.,* 2019), primarily due to uncertainties surrounding the proportions of non-marketable crop products. This depends on factors such as intended uses of produce, whether for export or local consumption, and the availability of published information and data.

Plum pox ("sharka") is caused by plum pox virus-PPV, and is the most harmful disease of stone fruits. Several authors have reviewed the impacts of this disease on European stone fruit production, especially of apricot and European plum (e.g. Németh (1994), Kegler and Hartmann (1998), Nemchinov *et al.* (1998), Capote *et al.* (2006) and Sochor *et al.* (2012). A broad estimate of the international costs associated with plum pox management, excluding indirect trade losses, has been estimated to exceed €10 × 10^9 (Cambra *et al.*, 2006a) during the 1970s to 2006, since the beginning of the sharka pandemic until the 1970s. Additionally, limited technical resources and a lack of experience in managing the disease led to considerable social and political implications during the early decades of the spread of the disease. The costs associated with the disease involve direct losses in stone fruit production, commercialization, eradication, compensatory measures, and lost revenue, along with indirect costs including those for preventive measures such as quarantine, surveys, inspections, control of nurseries, diagnostics, management measures, and the impacts on foreign and domestic trade (Cambra *et al.*, 2006a; Barba *et al.*, 2011). As well this disease cause losses in national biodiversity and genetic erosion, particularly affecting traditional and well-adapted *Prunus* species cultivated in areas where sharka is endemic, that are very susceptible to PPV.

The plum pox virus and sharka disease: an overview

Plum pox virus (*Potyviridae*, *Potyvirus plumpoxi*), the causal agent of sharka, is to date the only potyvirus known to infect temperate fruit trees. PPV is a well-characterized virus (Sochor *et al.*, 2012; García *et al.*, 2014; Rimbaud *et al.*, 2015; García *et al.*, 2024), and is considered one of the top ten viral pathogens (Scholthof *et al.*, 2011) of high scientific and biotechnological relevance. PPV diversity is currently structured into ten monophyletic strains, that in the chronological order of discovery, are: Dideron (D), Marcus (M), El Amar (EA), Cherry (C), Recombinant (Rec), Türkiye (T), Winona (W), Ancestor M (An), Cherry Russian (CR), and Cherry Volga (CV) (EPPO, 2023). The different strains have specific genome sequences, and may vary in their spectra of natural hosts, symptomatology, pathogenicity, epidemiology, aphid transmissibility, and geographical distributions with some restricted to particular regions. Some degree of within-strain variation has also been observed.

Three predominant strains have broad geographical distributions. These are PPV-D, PPV-M, and PPV-Rec (García *et al.*, 2014). PPV-D is widespread in Europe, and is the cause of most PPV outbreaks in North and South America and Asia. This virus is found in all *Prunus* species except cherry. PPV-M has been reported mainly in Central and Southern Europe and Japan, and affects all *Prunus* species except cherry and causes rapid epidemics in different peach cultivars. PPV-M generally causes more severe symptoms than PPV-D. PPV-Rec has a similar epidemiology to PPV-D, but is less adapted to peach, and has been reported mainly in several European countries. PPV-EA has only been reported in Egypt, in several *Prunus* species except cherry and almond. PPV-C is widespread in Russia, common in Moldova, and has occasionally been reported in Belarus, Croatia, Hungary, Germany and Italy restricted to sour (*P. cerasus*) and sweet (*P. avium*) cherries. PPV-T is common in Türkiye, found in several *Prunus* species except for cherry and almond. PPV-W has been reported in Eastern Euro-

pean countries and Canada, in several *Prunus* species except for cherry and almond. PPV-An is found in Eastern Albania in several *Prunus* species except for cherry and almond. PPV-CR and PPV-CV are cherry adapted strains that were discovered in Russia on sour cherry (Glasa *et al.*, 2013; Jelkmann *et al.*, 2018; Oishi *et al.*, 2018; EPPO, 2023; García *et al.*, 2024).

The geographic distribution of PPV is increasing. Since sharka was first reported in Bulgaria in 1917-1918 on *Prunus domestica* by Atanasoff (1932), and in 1993 in apricot trees (Németh, 1994), the virus is now officially present in most of continental Europe, with endemic status in many central and Southern European countries. The virus has progressively spread to many countries (currently 54) in nearly all continents. Reported incidence of emerging and re-emerging PPV is increasing in new areas where *Prunus* stone fruit industries are important (García *et al.*, 2024). Mexico is the most recent country of reported PPV (Loera-Muro *et al.*, 2017). As the virus is efficiently transmitted through grafting and other vegetative propagation methods, the primary pathway for PPV spread over long distances is illegal trafficking and insufficiently controlled exchange of infected, symptomless, propagative plant materials (Cambra *et al.*, 2006a; EPPO, 2024). Once PPV has become established in an orchard, vector aphids naturally spread the virus locally, through a nonpersistent stylet-borne inoculum mechanism.

PPV is the only stone fruit virus transmitted by aphids over short distances within and between orchards. The feasibility of experimental PPV transmission from infected fruit has also been reported (Labonne and Quiot, 2001; Gildow *et al.*, 2004), but PPV is a nonpersistent virus, which is acquired by insect vectors and inoculated during short periods, without any latent period. This putative transmission method has had economic repercussions, evidenced by batches of infected fruits from Chile being rejected in Brazil due to virus detection (Rezende *et al.*, 2016). Madariaga *et al.* (2024) compared relative accumulation of PPV load between freshly harvested infected fruit and fruit subjected to cold storage, simulating transit conditions to export markets over two consecutive seasons. Their study showed reduction in viral RNA in fruit exposed to cold storage compared to freshly harvested fruit. The known aphid species colonizing or visiting *Prunus* spp. and described as PPV-vectors include 29 species (Labonne *et al.* 1995; Kimura *et al.*, 2016; Cambra and Vidal, 2017).

A statistical model for PPV prediction in *Prunus* nursery blocks using vector and virus incidence data is available (Vidal *et al.*, 2020). Sharka epidemiology and PPV dissemination have been addressed by Gottwald *et al.* (2013), Rimbaud *et al.* (2015), and Gutiérrez-Jara *et*

al. (2023). The woody host list (EPPO-Global Database, 2020; Chirkov *et al.*, 2022) includes cultivated, wild, and ornamental *Prunus* species and hybrids, among them *Prunus fruticose,* the latest species described as a PPV host, as well of non-rosaceous woody plants such as *Spiraea* sp. and *Tilia* spp. (García et al. 2024).

PPV infections cause the most detrimental diseases of stone fruit trees, as these can severely reduce fruit quality and induce premature fruit drop in some cultivars, especially in *P. domestica* (Figure 1, a and b). Symptoms of sharka may appear on host leaves, shoots, bark, petals, fruit, and fruit stones (Damsteegt, 2008; García *et al.*, 2014; Rodoni *et al.*, 2020). Because PPV is easily transmitted by aphids and by vegetative multiplication, production of PPV-free plants is difficult. Specific
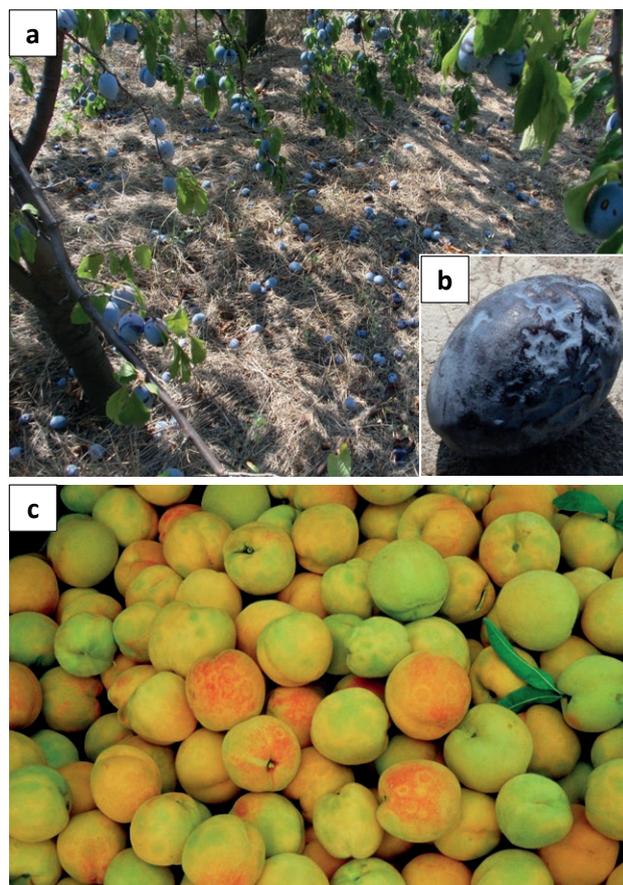
Figure 1. Typical symptoms induced by plum pox virus (PPV): (a) on a highly susceptible plum cultivar showing premature fruit drop; (b), symptoms on a fruit from the same cultivar; (c) 'Catherine' peach fruit discarded in a packinghouse, showing sharka symptoms. Photograph credits: a and b, Dr M. Glasa; c, Dr M.A. Cambra, (Centro de Protección Vegetal y Certificación, DGA, Montañana-Zaragoza, Spain. Photograph c is part of the photograph gallery accessible to members of GEDDI-Spanish Society of Phytopathology (SEF).

regulatory and control strategies need to be implemented to curb the disease in nurseries, requiring considerable effort by nurserymen and frequent inspections. Foliar treatments with horticultural mineral oil as a physical barrier have been shown to reduce natural PPV infections in nursery blocks (Vidal *et al.*, 2010). The disease does not kill infected trees; but if they are not removed from orchards, they become reservoirs of PPV (Cambra *et al.*, 2006a; EPPO PRA, 2012).

The presence of PPV in a country creates difficulties for export of certified planting material and for fruit. Visual inspections cannot guarantee the sanitary status of individual plants, so the use of analytical methods may be necessary for accurate diagnoses (Rimbaud *et al.*, 2015). A range of diagnostic tools are used for detecting PPV. Diagnosis is currently based on integrated approaches, which include biological indexing and serological and molecular amplification assays (EPPO, 2024). Despite the development of many sensitive nucleic-acid-based techniques, the ELISA technique remains the most common for PPV detection (Cambra *et al.*, 2011; Rimbaud *et al.*, 2015). Several PPV detection kits are available, based on specific monoclonal or polyclonal antibodies, and the ELISA method is appropriate for large-scale testing and has low per sample cost.

Serological tests have been, and continue to be, key for PPV management (detection and diagnosis), despite the poor assessment of these methods provided by the most recent EPPO (2023) standard for PPV diagnosis, compared to previous EPPO standards and IPPC-FAO (2018). This is likely due to the lack of experience in serological methods of teams that carry out the EPPO validations. Currently, the technique of choice for nucleic acid-based PPV detection is reverse transcription quantitative real-time PCR (RT-qPCR), with loop-mediated isothermal amplification (LAMP) being another option. Protocols are available for direct use of plant crude extracts or immobilized tissue-prints of plant or squashed vector samples feasible as PCR targets, instead of purified RNA (Capote *et al.*, 2009). This opens the possibility of large-scale use RT-qPCR. Biological, serological and molecular amplification methods for PPV detection and identification have been summarized by Rimbaud *et al.* (2015) and IPPC-FAO (2018), and a number of novel molecular amplification methods are referenced in EPPO (2023).

Research and innovation in plant breeding (including search for cultivars resistant or tolerant to PPV, and pathogen-derived resistance in transgenic *Prunus* species), pest control, and orchard management all contribute to the continued advancement of stone fruit production, which is threatened by PPV. The economic costs of these innovations, representing an indirect cost associated with sharka, has been partially assessed as research in the present paper. An example is the PPV-resistant, genetically engineered *P. domestica* cultivar HoneySweet (Ravelonandro *et al.*, 2013; Scorza *et al.*, 2016), which was deregulated in 2007 in United States of America (USA) (Scorza *et al.*, 2007).

Recognition of plum pox virus as a pest by plant protection organizations

PPV was included in the EPPO A2 list (version 2023-09) of quarantine pests recommended for regulation in the EPPO countries since 2000. However, according to European Union (EU) legislation in 2019, the virus was reclassified as a regulated non-quarantine pest (RNQP), defined as 'a non-quarantine pest whose presence in plants for planting affects the intended use of those plants with an economically unacceptable impact and which is therefore regulated within the EU territory´ (EU regulation 2016/2031). This transcendental decision was primarily made due to PPV being already present and widespread across most EU countries, with difficulty or impossibility of PPV eradication from several areas (Pedrelli *et al.*, 2024). Therefore, pest infestation may be tolerated (as plants for planting which infected above a given threshold would result in unacceptable economic impact). Consequently, farmers are compelled to directly manage PPV in EU countries, although private management of diseases such as sharka is generally inefficient (Martinez *et al.*, 2024). The concept of RNQP has been implemented in the EU Plant Health Law (EU Regulation 2016/2031), specifically for professional operators. Currently, PPV is also of regulatory interest to other Regional Plant Protection Organizations which recommend their member countries to regulate PPV as a quarantine pest locally present in their region (A2 list). These organizations include: i) APPPC-Asia and Pacific Plant Protection Commission, which includes 25 member countries; ii) the COSAVE-Comité de Sanidad Vegetal of Cono Sur, including Argentina, Bolivia, Brazil, Chile, Paraguay, Peru, and Uruguay; iii), the -North American Plant Protection Organization (NAPPO); and iv) the -Inter-African Phytosanitary Council (IAPSC), which declares PPV as absent (list A1) in African countries except Egypt, Morocco, and Tunisia. In these organizations, except for the EU, quarantine measures (exclusion, eradication, containment) aim to prevent unacceptable economic, environmental, and social impacts resulting from the introduction and spread of named pests (in this case PPV). These measures are mandatory and imply direct and indirect dis-

ease management-associated costs. Furthermore, some countries have regulated or prohibited the importation of PPV-susceptible planting material from countries where PPV is declared, or which have adopted strict regulations regarding the conditions of plant production in the exporting countries (Rimbaud *et al.*, 2015). NAPPO and COSAVE member countries implement phytosanitary controls at entry, or indexing of imported plant material confined in post-entry quarantine facilities (e.g., NAPPO, 2009). Similarly, this system was implemented in countries free of PPV, such as Australia (Rodoni *et al.*, 2006) and New Zealand (Lebas *et al.*, 2006). This strategy and its legal framework entail significant costs associated with preventing the entry of PPV, which are not evaluated in the present study.

Relevance of stone fruit industries in countries where PPV has been detected

Prunus stone fruit trees (excluding almond) are important in food production. In 2019, stone fruit production totaled approx. 49 million t, and was cultivated across approx. 5 million ha (FAOSTAT, 2023). The average estimated value of stone fruit production for 1995 to 2023 is approx. €51 × 10⁹ per year. This estimate is based on generalized assumptions about production volumes, market prices, and growth rates over time, according to FAOSTAT data. This value includes production of: common and Japanese apricots, peaches (clingstone, freestone, semi-freestone, yellow fleshed, white fleshed, donut or flat, nectarines, blood peaches), European, Japanese, and green plums (*Prunus cerasifera*), and sour and sweet cherries. Additionally, almonds (production of 3.2 million t in 2019) are cultivated across numerous countries where sharka is spreading. The significant economic value of stone fruit trees includes direct revenue generated from fruit sales as well as income generated along supply chains, including farming, processing, distribution, and retail. These fruit products also offer nutritional benefits and are part of different cultural traditions.

PPV has been detected in the main stone fruit-producing countries, except in Australia, New Zealand and the Republic of South Africa. China is the greatest producer of stone fruits (Huang *et al.*, 2008; Guillesky, 2018), and PPV infections have potential to cause major economic damage to the stone-fruit industry in that country (Xing *et al.*, 2017). Nevertheless, despite the presence of sharka, countries such as Italy, Spain, and the USA remain prominent producers of stone fruit and almonds, making substantial contributions to global production (FAOSTAT, 2023). Chile (Retamales, 2011) and Argentina have also emerged as key players in the

Southern hemisphere, exporting substantial volumes of stone fruit to international markets during their respective growing seasons. Türkiye is an important country for apricot, cherry, peach and plum production (Bolat *et al.*, 2017; TURKSTAT 2023), and significant are Iran (Ghahremani *et al.* 2023) and Greece (Huang *et al.*, 2008; OPEKEPE, 2023) as peach producers.

Overall, the period from 1995 to 2023 has seen important increase in world cultivation and production of stone fruit varieties, which has been driven by technological, economic, and environmental factors. The stone fruit industry generates significant value and provides income for growers, processors, distributors, exporters, and retailers.

MATERIAL AND METHODS

Direct losses and cost estimation

The estimated direct costs associated with sharka management primarily include those related to production losses: premature fruit drop and rejection of symptomatic fruit in packinghouses, usually expressed as percentages. Losses due to the rejection of symptomatic fruit batches during export have been assessed only in sporadic reported cases. Estimated costs due to the eradication of productive field trees or plant blocks in nurseries have also been evaluated, although direct losses from unmarketable planting material if PPV is detected are not included due to the lack of available data. The value of subsidies, or compensation and loss of income costs, based on official data from countries actively managing sharka, have been included when available.

Production of each species is primarily estimated using agricultural production data available from FAOSTAT (2023), and adjusted to estimate costs in Spain with data from the Spanish Ministry of Agriculture, Fisheries and Food (MAPA, 2021) and official information from local Plant Protection Services. Production information was retrieved mainly for the top ten producer countries of each crop, and the production averages were calculated for the period 1995–2023, during which a significant increase in cultivation occurred. Production was also adjusted in some cases with more local statistical data, including ISTAT (2023) for Italy, TURKSTAT (2023) for Türkiye, and OPEKEPE (2023) for Greece. Direct losses were calculated based on the estimated percentage of unmarketable fruit for specific crops. The estimates were based on information about PPV strains present in each country and the reported extent of the disease (Damsteegt, 2008; Loera-Muro *et al.*, 2017; Zhou *et al.*, 2021; EPPO, 2024; Pedrelli *et al.*,

2024). To estimate percentage losses, typical losses were estimated for each stone fruit species, along with information obtained from packinghouses, local experts, and evaluations by the present study authors. Despite the considerable variability from year to year, the estimated losses were considered fixed across all seasons and for each year during the evaluated period, for fresh, dried, or canned fruits. However, cool springs tend to generate more disease symptoms, due to the coinciding development of fruit with increased viral titer compared to warmer springs. Sometimes, in early cultivars, fruit is more affected than for later cultivars. However, this was not considered in the present study, due to the complexity of determining which years were more favorable for symptom expression in each production area. In Spain, monetary value was mainly calculated based on the average prices for fresh fruit during 2010 to 2020, according to data provided by MAPA (2021). These values were (for 100 kg bulk pallets): for peaches, 1.3 € kg^{-1}; for plums, 0.90 € kg^{-1}; and for apricots, 0.59 € kg^{-1}. The reference prices, based on export values of quality fresh stone fruit, reflects Spain's position as a major exporter (EC, 2022). For estimating global losses (excluding Spain), retail prices perceived by farmers in local markets were used, as well as prices for bulk exported fruit. These values ranged from a minimum to a reference price ex-packaging station (EU, 2023) for: peaches, 0.4–1.3 € kg^{-1}; plums, 0.25–1.0 € kg^{-1}; apricots, 0.15–1.3 € kg^{-1}; and cherries, 0.2–1.7 € kg^{-1}. To calculate the value of losses, the lowest value was used, even if it fell below the estimated production cost price of peaches for Spanish farmers, which is approx. 0.4 € kg^{-1} (CREDA, 2023). The retail price used for fresh apricots from some areas (including Beijing, China) was 0.5 € kg^{-1}. A comprehensive overview of current prices, markets, and trade is available in various publications (e.g., Mulderij, 2018).

Direct economic losses due to rejection of fruit with sharka symptoms were evaluated according to the documented case of Chile Brazil border in the 2016–2017 season, which is the only reported international case. However, sporadic reports fruit showing sharka symptoms in supermarkets have appeared in local newspapers and online commercial documents reports, but these have not led to significant consequences. The economic feasibility of eradication or disease removal efforts was evaluated based on data from the literature.

The losses of biodiversity and genetic heritage due to sharka, primarily affecting traditional European plum and apricot cultivars, is mentioned but has not been evaluated. This situation occurs particularly in European countries where the sharka is endemic, and resilience is achieved through the use of tolerant cultivars.

Estimations of indirect losses.

Indirect costs include those for disease preventive measures, including pre- and post-quarantine facilities, surveys (at a reference cost of €35 ha^{-1}), inspections, prevention measures, special facilities in nurseries, nursery control, and selection in packing houses to remove symptomatic fruit. Additionally, sampling and diagnostics, development of specific laws, policies for compensation to affected growers, research and development investments, and the impacts on foreign and domestic trade should be estimated. Among indirect costs, those with available data for calculation have been evaluated. The most readily available are costs associated with disease detection and diagnosis, and for research grants. Costs for surveys and inspections have been partially estimated for some countries.

ELISA serological tests are important for management of PPV. Numbers of ELISA tests performed annually were estimated, by consulting the main international companies that market PPV kits for screening, universal detection, or for identifying PPV isolates (mainly PPV-D, PPV-M and PPV-C). The international companies that collaborated by providing data were: AMR Lab, Spain, currently integrated into Plant Print Diagnostics; Agdia, USA (https://www.agdia.com); Agritest, Italy (https://agritest.it); Bioreba, Switzerland (https://www.bioreba.ch/bioreba.aspx/t_new); Plant Print Diagnostics, Spain, (including former AMR Lab and Real-Durviz kits, https://plantprint.net); and Prime Diagnostics, The Netherlands (https://primediagnostics.com).

The pandemic condition of sharka and the perceived importance of the associated socio-economic losses have led to research focused on basic molecular aspects of PPV and its potential as a biotechnological tool (García *et al.,* 2014; García *et al.* 2024). These studies began in Europe and have expanded to other regions where PPV was detected. In parallel, programmes were initiated aiming to introduce resistance to PPV into elite cultivars of apricot, European plum, and peach, and to develop strategies to reduce virus spread and virulence, such as transgenic protection, immunomodulation, RNA silencing, and Spray-Induced Gene Silencing (SIGS) (Cirili *et al.*, 2016; De Mori *et al.*, 2020; García *et al.*, 2024). This research activity has required significant financial investment, which is challenging to quantify, as it has been accompanied by numerous field trials, such as the genetically engineered plum cultivar HoneySweet (Scorza *et al.*, 2016). The amounts invested in research have been obtained from data available from the main funding agencies for research projects in the countries that are most active in this field.

RESULTS AND DISCUSSION

Direct losses and cost evaluation

The general data are summarized in Table 1. Direct economic losses due to the rejection of fruit with symptoms at country borders have likely occurred in several countries, but the most recent documented cases, related to Chile, have occurred at the Brazilian border. Rejections occurred in the 2016-2017 season, for 525,440 t of nectarines (31.2% of the rejected fruit), and plums (68.8% of the rejected fruits), with associated cost of €1.4 million (Chilean customs). These costs included export expenses, the value of product, and legal and regulatory fees. However, some costs were not accounted for, including reputation damage, opportunity costs if the rejected shipments were part of larger sales plans, lost potential revenue and market expansion opportunities due to the inability to sell fruit to Brazilian markets, and remediation costs if corrective actions were required to meet Brazilian import regulations. However, after multiple negotiations, it was accepted that stone fruit infected by PPV-D did not pose risks of spreading the virus, and PPV is no longer regulated in Chilean exports.

Eradication or disease removal was a goal during the early years of the sharka epidemic, but this was technically challenging due to the lack of serological methods and large-scale kits with high specificity antibodies for testing large numbers of plants (Cambra *et al.*, 2011). Currently, eradication of PPV is feasible if there is commitment to protecting the stone fruit industry, along with political will, support from farmers, appropriate subsidies, and supportive laws. The cost-benefit ratio of eradication is favourable. The direct costs of eradication can be evaluated for some countries that have attempted this with total success (USA), partial success (Canada), or failure after years of attempts (Spain). In countries where initial outbreaks of PPV were discovered with low prevalence in geographically restricted areas, eradication programmes could be undertaken without compromising the stone fruit industries. Canada and USA are good examples of how stringent procedures lead to successful reduction of inoculum (in Canada), at least in some

Table 1. Estimated world direct (A) and indirect (B) economic costs [million euros (€)] associated with management of plum pox virus and sharka in Prunus fruit crops during the period 1995 to 2023.

			A. Direct costs		
	Virus strain	Region/Country	Cost (million €)[a]		
			Partial	Subtotal	Total
Prunus fruit types					
Apricot	PPV-D[b]		389.76		
	PPV-M[c]		175.64		
				565.40	
Plum		Europe	910		
		China	37.52		
		Third group[d]	1.11		
		Fourth group[e]	0.12		
				948.75	
Peach			*511.56*	*511.56*	
Cherry			*na[f]*	*na*	
					2,025.71
Border rejections		Brazil/Chile	1.4	***1.4***	
Eradication and disease removal		USA	30.3		
		Canada	50		
		Spain	13.5		
		Other countries[g]	6.2		
				100	
					2,127.11

(Continued)

Table 1. (Continued).

	Test type	Region/Country	Cost (million €)[a]		
			Partial	Subtotal	Total
B. Indirect costs					
Pathogen detection and diagnoses	Serological tests		120		
	Molecular amplification tests and sequencing		17		
				137	
Research		EU	27.7		
		Russia	0.36		
		Chile	0.94		
		USA	90		
		Other	11		
				130	
					267
TOTAL (A+B)					**2,394.11**

[a] Estimated million euro amounts are expressed in nominal values (without adjustment for inflation). When data were available in US dollars, the conversion to euros was made using the 2023 exchange rate.
[b] Estimated for Argentina, China, Cyprus, Canada, Croatia, Egypt, France, Germany, India, Iran, Israel, Italy, Japan, Jordan, Kazakhstan, Mexico, Pakistan, Portugal, Russia, Spain, Syria, Türkiye, Tunisia, Uzbekistan, and Ukraine.
[c] Estimated for Albania, Bulgaria, Bosnia and Herzegovina, Greece, Moldova, North Macedonia, Poland, Romania, Serbia, Slovakia, and Slovenia.
[d] Estimated for Chile, India, Iran, Serbia, Russia, Türkiye, Ukraine, and Uzbekistan.
[e] Estimated for Argentina, Armenia, Bosnia and Herzegovina, Israel, Kazakhstan, Mexico, Moldova, North Macedonia, Syria, and Turkmenistan.
[f] na, not analyzed.
[g] Estimated for Argentina, China, Chile, France, Italy, Japan, Lithuania, Portugal, the Netherlands, and Türkiye.

states, or eradication of the pathogen (in the USA) (Rimbaud *et al.*, 2015).

In the USA, PPV was first detected in Pennsylvania in 1999 (Levy *et al.* 2000), and later in Michigan and New York State in 2006 (Snover-Clift *et al.*, 2007). To prevent further spread of sharka, which threatened the country's stone fruit industry, valued at approximately €5,355 million (US\$ 6.3 billion), the USDA quickly issued an emergency declaration providing much-needed funding and support for eradication of PPV across the country. Within 10 years, PPV eradication was achieved in Pennsylvania (Welliver *et al.*, 2014) and later in other areas of USA (USDA, 2019). This was confirmed by the NAPPO, after three consecutive years of stone fruit field surveys with no further PPV detections. Costs associated with eradication in the USA amounted to approx. €30.3 million (Welliver *et al.*, 2014), which included analysis of 1.9 million samples using ELISA, removal and destruction of 750 ha of stone fruit plants (approx. 188,000 trees), and compensation for lost fruit production, among other expenses.

In Canada, PPV was detected in Ontario and Nova Scotia in 2000 (Thompson *et al.*, 2001). An eradication programme was then initiated, with intensive surveys that led to the removal of 264,000 trees in 6 years, following analyses of over 2.6 million samples using ELISA (Thompson, 2006). Despite a total expenditure of approx. €50 million until 2010 (including the analyses of 3 million trees using ELISA, and indemnities), the programme was terminated in 2011 without fully eradicating the pathogen. However, the programme achieved a significant reduction in inoculum and other disease management benefits (Gottwald *et al.*, 2013).

In the important stone fruit industry of Spain, detection of PPV-D in 1984 raised significant concerns due to potentially severe damage, mainly in apricot trees, which suffered losses estimated at 5% by 1998. This prompted a voluntary eradication programme, resulting in the uprooting of more than 2.3 million trees from 1989 to 1998, at a total cost of over €63 million, including tree removal and indemnities (Cambra *et al.*, 2006b). During the period 1995 to 2023, approx. €3 million was spent on subsidies for uprooting PPV-D infected trees. PPV-M was first detected in Spain in 2002 in the Autonomous Community of Aragón near the border with Catalonia, and the pathogen was subsequently eradicated (Capote *et al.*, 2010). Over the next 8 years,

there were no further detections of PPV-M in commercial stone fruit orchards in the area, suggesting successful eradication. However, in 2016, several new foci of PPV-M were again detected in Catalonia and neighboring Aragón in the northeast of the Iberian Peninsula. The costs associated with a renewed tree removal programme were about €10.5 million, including analysis of approx. 1 million samples using ELISA.

The direct costs associated with eradication efforts in the USA, Canada, and Spain totaled €93.8 million from 1995 to 2023. This total should be supplemented with costs incurred in other countries, particularly in Northwestern Europe, where local eradication programmes have been implemented or are ongoing, such as Switzerland, Denmark and Sweden, despite their respectively low stone fruit production (Capote *et al.*, 2006; Rimbaud *et al.*, 2015). Additionally, expenditure on efforts to reduce inoculum or limit disease spread, mainly in Argentina, China, Chile, France, Italy, Japan, Lithuania, Portugal, the Netherlands, and Türkiye, evaluated at €6.2 million, should be included in the total costs. As an example, in Türkiye, approx. €60,000 were paid to producers for tree removal during 2019-2023. Given the difficulties with international cost evaluation, an estimate of the direct costs associated with eradication and disease control in all areas where susceptible fruit trees are grown likely surpassed €100 million from 1995 to 2023.

Evaluation of indirect costs

General data are summarized in Table 1. According to information received from the leading diagnostic companies that market kits based on PPV-specific monoclonal (MAb) or polyclonal (PAb) antibodies, approx. 20.5 million serological analyses were performed using ELISA between 1995 and 2023. Of these, 5 million tests were conducted using the CP broad spectrum PPV-specific monoclonal antibody 5B/IVIA-PPD (MAb) (Candresse *et al.*, 2011), and more than 15 million tests were conducted with PAbs or a cocktail of MAb-PAbs. Additionally, other companies or research institutes have probably marketed or conducted approx. 4 million tests, particularly in Europe, China (Guo *et al.*, 2023) and Japan (Oishi *et al.*, 2018). During the period in which various eradication programmes were implemented in Canada, the USA, and Spain, the total number of ELISA tests performed would reach approx. 24 million. This averages to more than 857,000 tests done annually. The costs of these serological tests, including sample collection, are estimated at approx. €120 million. In addition, expenses associated with molecular amplification techniques (each test estimated at €15, including sample collection), and high-throughput sequencing technologies (each test current cost of €550, including bioinformatic analysis) should also be included. For example, in Russia, where molecular amplification techniques have been widely used since 2010, approx. 10,000 RT-PCR assays have been conducted to confirm PPV infections, determine the PPV strains, sequence the 3'-terminal (Cter-NIb-CP-3'-UTR) genome regions, and validate HTS results. Approx. 50 full-length PPV genomes were determined using a high-throughput sequencing approach, and 3,000 PCR products were sequenced bidirectionally by the Sanger method using the facilities at Evrogen (Moscow, Russia). The total Russian expenses are estimated to be €240,000, excluding ELISA (approx. 2,500 tests performed). It is estimated that the total world annual cost of molecular amplification and sequencing probably exceeded €600,000 during the analyzed period, totalling approx. €17 million. This brings the total world costs for detection, diagnoses, and characterization of PPV to greater than €137 million (Table 1).

Costs linked to investments in research projects and development of PPV-resistant plants have primarily been applied in Europe, with subsequent efforts extending to other countries as PPV detection increased. Among European projects, notable initiatives funded by the European Union (EU) during the period 1995-2023 include SharCo (2008–2012), "Containment of sharka virus in view of EU-expansion, FP7-KBBE-Specific Programme 'Cooperation': Food, Agriculture and Biotechnology (https://cordis.europa.eu/project/id/204429/reporting/fr), and the EU project MARS (2013–2015), "Marker Assisted Resistance to Sharka", which focused on the production of sharka-resistant stone fruit cultivars (https://cordis.europa.eu/project/id/613654). These projects have received approx. €5.4 million, along with other smaller research projects and networks (€3.3 million), totaling approx. €8.7 million. In addition to these, there have been national and bilateral funding initiatives, primarily in France, Italy, Poland, Romania, and Spain (approx. €15 million), as well as contributions from other EU member countries (approx. €4 million). In total, these efforts in the EU have amounted to approx. €27.7 million (from 1995 to 2023).

In Russia, PPV investigations were financially supported by the Russian Foundation for Basic Research (RFBR), the Russian Science Foundation (RSF), and the Ministry of Science and Higher Education of the Russian Federation. Since 2010, the total amount of all grants has been approx. €360,000.

The Government of Chile, through institutions such as National Research and Development Agency (ANID), the

Agricultural and Livestock Service (SAG), and the Agrarian Innovation Foundation (FIA), has allocated funds totalling €940,000 primarily for epidemiological studies.

Funds invested in research projects in the USA through the United States Department of Agriculture (USDA), the Agricultural Research Service (ARS), the National Institute of Food and Agriculture (NIFA), and the Animal and Plant Health Inspection Service (APHIS), from the time of the initial sharka outbreak and response (1999 to 2003), through ongoing disease management and research (2004 to 2019), to the final eradication declaration in 2019, are estimated at approx. €90 million. This includes some specific funding and support for eradication of PPV across the country and bilateral actions with other countries.

Funds invested by other leading stone fruit producer countries for PPV research and management are difficult to quantify, owing to lack of specific and detailed public financial records. Argentina, Brazil, India, Japan, and other countries, are also investing in PPV research, estimated at about €11 million. Consequently, estimated total funds devoted to this research likely exceeded €130 million from 1995 to 2023 (Table 1).

An indirect indicator of the costs associated with scientific and technical research is the number of resulting articles and patents published by the end of June 2024, which totalled 16,200 (retrieved from Google Scholar using the keywords 'sharka disease,' 'plum pox virus,' and 'Plum pox potyvirus').

Case study for Spain

According to FAO (2024) and Batlle *et al.* (2018), Spain is a leading stone fruit producer, with production having significant socioeconomic impacts. Sharka was detected in Spain in 1984, and the direct losses due to fruit rejection of Prunus stone fruit are here assessed.

Peaches and nectarines (*Prunus persica*) are the primary stone fruit grown in Spain, with the country ranking as the second or third largest producer, after China and alternating with Italy. Peach cultivation in Spain accounts for 54.2% (about 80,000 ha) of the prunus industry´s total surface area, generating an average national production of approx. 870,720 t of fruit, and with a clear trend for increased cultivated surface area and production, reaching about 2.5 million t in 2016/17. Non-marketable peach fruit due to sharka symptoms are currently estimated at 0.5% of the total produced. This results in annual estimated losses of approx. 4,354 t year^{-1}. Over the evaluated 28 year (1995 to 2023), this total loss of fruit is valued at approx. €158,500 at the average price of €1.30 kg^{-1}. Losses of fresh peaches are relatively low

(Samara *et al.*, 2017), because differences in production or harmful effects were not observed when comparing healthy and PPV-D infected trees in Canada, except for symptoms in fresh fruits that rendered them unmarketable (Figure 1c). Nevertheless, most of the fruit could be used for canned product, even though they presented symptoms. The crop is scarcely affected by the predominant PPV-D isolates endemic in some regions (mainly in early-season producing areas of nectarines along the Mediterranean coast). PPV-M was detected in 2016, however, in medium and late-season peach-producing areas, where the main estimated losses have associated with preventive eradication campaigns.

For plum trees, early cultivars of Japanese plum (*P. salicina*) are the most cultivated, whereas European plums (*P. domestica*) are of little importance. Together, these plum species represent 5.8% (about 16,000 ha) of the Spanish stone fruit growing area, with average annual production of 222,020 t during 1995 to 2023. Rejection rates are estimated at 1.0% of annual harvests, resulting in annual estimated losses of €1,110,100 (based on €0.5 kg^{-1} in 100 kg pallets). Over the evaluated period, this accounts for more than €31 million in losses. However, this is probably an under-estimate because the selling price in 2021-2022 was €0.90 kg^{-1}.

Apricot tree cultivation was for 4.4% (approx. 20,000 ha) of the Spanish stone fruit growing area during 1995 to 2023, with average annual production estimated at 154,000 t. The crop was severely impacted by the prevalent PPV-D strain from 1984 to 1995, particularly in early cultivars grown along the Mediterranean coast (Martínez-Gómez *et al.* 2000). This lead to an estimated 5% of unmarketable fruits. However, inoculum reduction was achieved through a voluntary eradication programme which removed 2.3 million trees, mainly apricot, as well as use of certified virus-free planting material and adoption of PPV-tolerant cultivars. This led to decreased proportions of unmarketable fruit to approx. 1–2% of the annual harvests from 1995 to 2023. These improvements helped Spain maintain its position as the leading international exporter of high-quality fresh apricots. With an average price at origin of €0.59 kg^{-1} (2010-2020), the losses are estimated at approx. €1.81 million year^{-1}, totalling more than €50.6 million for 1995 to 2023.

Currently, no fruit losses are associated with sharka for cherries and almonds in Spain, where PPV-D is the prevalent strain, and PPV-M outbreaks are under eradication from eastern Spain. Consequently, the total estimated direct harvest losses due to sharka amount to approx. €81.76 million for 1995 to 2023. The value of direct compensation for tree eradication (i.e., subsidies and compensations) relating to outbreaks of PPV-D and

PPV-M was €17.75 million, bringing the total value of direct losses to more than €99.51 million.

The total indirect costs associated with surveys, sampling, and laboratory analyses are calculated at €6.37 million during 1995 to 2023. Approx. 35,000 samples were analyzed annually, primarily using ELISA tests based on universal and strain-specific monoclonal antibodies, at a cost of €5 per test, including field sample collection. This leads to an estimated cost of more than €5 million, which includes costs for several identification procedures based on molecular amplification and sequencing techniques. The extent of surveys conducted in Prunus nurseries and in the field, especially for PPV-M prevention, is estimated at 39,500 ha year^{-1}, with an estimated cost of €35 ha^{-1}, totalling €1.38 million during 1995 to 2023.

In summary, the total direct costs (€99.51 million) and the primary indirect costs (€6.38 million) associated with sharka management in Spain, excluding indirect trade losses, amount to approx. €105.89 million for the period 1995 to 2023. This represents an average of €3.782 million per year, which is about 0.32 % of the average annual value of the production of apricots, peaches, and plums in Spain (estimated at approx. €1,174 million). This estimate was made for the current epidemiological situation: PPV-D is prevalent in some areas, whereas PPV-M remains in isolated pockets under eradication programmes in the Northeast Iberian Peninsula.

Case study for Türkiye, at the Europe Asia boundary

Türkiye is a major world stone fruit-producing country (FAO, 2024). For apricots, Türkiye is a leading producer, and exports substantial amounts of apricots as fresh or, particularly, dried product, playing an important role in the country's agricultural sector and in international trade. Although the first report of sharka was in 1968, the disease was confined to germplasm collection orchards and home gardens. Sharka did not spread to commercial orchards until the early 2000s (Çağlayan and Gazel, 1998; Çağlayan and Yurdakul, 2017). When severe PPV symptoms were observed in commercial stone fruit orchards in 2004, the Ministry of Agriculture and Forestry organized extensive surveys in 56 of the 81 provinces of Türkiye. A total of 5,762 samples were collected from almond, apricot, mahaleb, cherry, nectarine, plum, peach, sweet and sour cherry orchards, and were tested for PPV by biological indexing, ELISA, and RT-PCR. Among these samples, 222 plants were found to be infected with PPV (Akbaş et al., 2011).

Greater incidence and impact of sharka has occurred since 2013. Therefore, assessment of damage and costs associated with the disease have been evaluated over the past 10 years, by crops according to TURKSTAT (2023) and for some local sources. Peach cultivation in Türkiye ranks fourth in production area after apricots, cherries, and almonds, and ranks third in world production (1,008,185 t) (FAOSTAT, 2023). For 2023 production, the average proportion of peach fruit that could not be marketed due to PPV is estimated at 0.05%, resulting in a loss of approx. €873,000 year^{-1}. This totals more than €8.7 million for the 10 years evaluated, based on 2023 sales prices (1.73€ kg^{-1}). Peach production is important for Türkiye, and strict eradication projects are being carried out to attempt to prevent these losses.

Plum production is modest compared to other stone fruit varieties in terms of area, with cultivation occurring on an average of 21,342 ha. Green plum (*Prunus cerasifera*) has gained importance in the Aegean and Mediterranean Regions, on the sea coastlines. In the interior and transition regions, European (*P. domestica*) and Japanese (*P. salicina*) plums, along with cultivars suitable for storage and drying, are more common. All plum varieties had national production of 355,132 t in 2023. The impact of PPV on yields is estimated to be 0.1 %, resulting in a loss of €490,082 year^{-1}. This is valued at approx. €5 million in the 10-year period where presence of sharka was declared. Calculations were based on an average selling price of 1.38 € kg^{-1}.

For apricot, Türkiye produced approx. 22 to 25% of world apricot production, and ranks first in production. A significant portion of this production comes from the Malatya and Elazığ provinces, which contribute, respectively, 63.5% and 7.6% of the national apricot production. These two provinces have been designated as PPV-free regions, which results in a low impact of sharka for commercial apricot production in this country.

For almonds and cherry, there have been isolated sharka detections in almonds, but these plants do not exhibit symptoms (Akbaş *et al.* 2011). For cherry, PPV-T has been so far detected in a single plant, and no infections were found within a 10 km radius of this tree. Since 2019 approx. €30 support has been paid to the producer for each tree eradicated due to PPV (Coşkan et al 2022). The total number of eradicated trees from 2019 to 2023 has been approx. 2,000, so the amount paid to producers is approx. €60,000. The total estimated direct harvest losses due to PPV are approx. €13.7 million. The indirect costs associated with PPV and sharka management within the scope of the PPV-free area programme, is calculated to be €340,000, with the greatest proportion of total indirect costs related to tree eradication, analysis, and project expenses being ELISA tests at €209,000. Identification procedures are estimated to cost approx.

€38,000. Surveys carried out cost at least €54,583 (Birişik *et al.* 2021; Morca *et al.*, 2022).

In summary, the estimated indirect costs of sharka were almost €0.5 million, excluding commercial fruit losses. The direct and indirect losses are estimated to be approx. €13.5 million for 2014 to 2023, which is equivalent to an average of €1.35 million year^{-1}. This represents about 0.06% of the average annual value of production of apricots, peaches, and plums produced (estimated at approx. €2.325 thousand million).

Since the detected PPV strains are PPV-D, -M, -Rec, and -T, special attention and monitoring must be maintained to prevent potential sharka damage, which has not yet occurred to the robust Turkish stone fruit industry.

Case study for Chile

Chile is an important stone fruit producing country in the Southern hemisphere. In 2023, the value of the exported stone fruit from Chile was of €670,500,000. PPV was detected in 1993 (Acuña, 1993; Herrera, 2013), with PPV-D the only strain found since its initial discovery (Rosales *et al.*, 1998; Fiore *et al.*, 2010). Direct losses associated with sharka have been as follows:

For peaches and nectarines, the cultivated area of peach trees has been decreasing since 2003, while the area of nectarine trees has remained stable. The main reason for this situation is the shift towards cherry trees, which is currently the main stone fruit produced in Chile. However, Chile continues to be the main producer of nectarine peaches in Latin America and ninth in the world, with an estimated production of 312,907 t (FAOSTAT, 2023). The peach production is mainly dedicated to the canning industry, where sharka disease does not represent a major problem. Nectarines are produced for export as fresh fruit and therefore, the symptoms caused by sharka do represent a serious problem. However, there is no record of fruit losses or rejections associated with sharka in packaging warehouses in the interior of the country, probably because in general, farms dedicated to exports have strict control measures in place to minimize sharka symptoms. Currently, there are no official evaluations for losses in fresh market nectarines. However, it is here estimated that a loss of 0.05% is prudent, which is similar to that in other exporting countries. This is equivalent to a loss of 42.5 t per year, from annual production of 85,000 t and value of €1,288 per t. The estimated cost associated with sharka during the last 28 years is approx. €1.532 million.

Plum is the second most important stone fruit produced in Chile, with the European plum being the main cultivated type (14,316 ha), followed by Japanese plum (3,465 ha). In 2023, the industry exported 225,198.5 t of plums, with a value of €561,705,000 (FOB). Chilean plum production is estimated at 424,887 t (FAOSTAT, 2023), ranking fifth in the world and first in South America. The cultivated area for plum trees has shown sustained growth from 1997 (12,398 ha) to 2023 (17,781 ha), although the plum tree proportion relative to the total area of stone fruit trees has decreased, due to rapid expansion of sweet cherry production. There is no official estimation of plum losses, but these are here estimated to be approx. 0.05% of fruits, representing 212.4 t year^{-1} and value of approx. €9.247 million during 28 years (at a price of €1,555 t^{-1}).

Apricot cultivation showed has decreased in Chile, with the latest registry (2021) indicating 539 ha planted. Symptoms caused by PPV in apricots are severe, and investing in apricot trees is considered high-risk. Losses due to rejection of fresh fruit are here estimated at approx. 0.05%. Therefore, on national apricot production of 4,562 t with an average value of €1,834 t^{-1}, these losses represent 2.3 t year^{-1}, or €4,218 year^{-1}. Consequently, these estimated losses amount to approx. €118,104 in the period 1995 to 2023.

For almond and cherry, no fruit losses are currently associated with sharka.

Indirect costs associated with PPV are primarily related to the surveillance and sharka containment, which has been managed through official control measures directed by the Agricultural and Livestock Service (SAG). Official sharka control involves annual costs for the Chilean government and private companies producing stone fruit. Annually, nurserymen must declare the mother plants from which propagation material will be obtained, and these plants must be analyzed by laboratories recognized by the SAG. The costs of these analyses are borne by the nursery companies. Between 1995 and 2023, 423,150 official analyses were conducted using RT-PCR tests, except for in the early years of this period when the ELISA technique was used in combination with RT-PCR. The total cost of these analyses is estimated to be €2.556 million. Of the total analyzed plants, 0.29% tested positive for PPV, resulting in eradication of 1,232 plants at a cost carried by the private industry sector. The official PPV control regulation in Chile does not provide for compensation.

These costs, along with those associated with human resources for sample collection, and laboratory analyses, have estimated value of approx. €5 million. Additionally, the government of Chile, through SAG, invests human resources dedicated to orchard surveillance and ensuring compliance with disease control regulations. For the period between 1995 and 2023, this investment is estimated to

be €10.384 million including laboratory analyses (ELISA and RT-PCR) by SAG laboratories for samples collected during orchard surveillance and surveys. In addition, the Government of Chile invested €940,000 primarily for epidemiological studies and for PPV strain identification. Only PPV-D has been detected, which has left cherries unaffected. Cherry is the main stone fruit exported from Chile, accounting for 56.9% of the total volume of exported stone fruit during 2023. The approx. annual total value of plums and peaches/nectarines produced in Chile is €670.447 million (Chilean customs, 2020).

In summary, the total estimated direct costs of sharka in Chile exceed €12.298 million, with main indirect costs totalling approx. €13.890 million associated with sharka management in that country (excluding indirect trade losses, and costs for administrative procedures). Together, these losses amount to approx. €26.188 million for the period 1995-2023. This equates to almost €1 million per year, representing approx. 0.14% of the average annual value of peach/nectarine and plum production in Chile in 2023.

Case study for Greece, where sharka is endemic

Stone fruit trees are the most important fresh fruit trees in Greece, occupying 67,000 ha and producing 1,124,000 t, with peaches and nectarines accounting for 80% of these totals (FAOSTAT, 2023). PPV was first reported in Greece in 1967, and within 10 years, PPV became widespread in areas of intensive Prunus cultivation, with apricot being the most affected. The Grecian share of World production of processed apricots diminished from 35% to 13% in 1995 (USDA/FAS). Widespread PPV occurrence led to the implementation of an eradication programme in the late 1980s, resulting in the disappearance of traditional apricot early-sensitive cultivars (e.g., 'Early of Tyrinth', and 'Diamantopoulou') of excellent quality and flavour, and considerable reductions of the cultivated area and production, particularly of apricots. Natural infections of almonds have been recorded (Kaponi *et al.*, 2012), but without consequences for production. The virus has not been detected from sweet or sour cherries, cultivation of which has doubled in the last 25 years. The majority of Greek PPV isolates have been classified as PPV-M and particularly belonging to the Ma clade of Mediterranean isolates, although there have been a few cases (three of 28) where PPV-D isolates were identified (Dimitriadou, 2015). Research projects to generate new tolerant varieties, evaluate the susceptibility of foreign varieties under local conditions, the modes of virus spread in the field, and PPV incidence in germplasm collections and nurseries, have been implemented for several years (Drogoudi and Pantelidis,

2017; Varveri, 2017). Considerable effort is being made regarding the production of PPV-free plant propagation material, and the immediate eradication of diseased trees in orchards, a practice often adopted by growers. Nevertheless, the economic damage of PPV on Prunus cultivation remains high and annual rejections of apricot and peach fruit during packaging are estimated to be at least 30% of the total production.

For apricot, as a result of the PPV eradication programme which started in 1988, the area cultivated in 1995 was 4,670 ha with production of 42,800 t, the lowest ever recorded in the country. Since then, production has increased 2.6-fold (112,000 t, FAOSTAT, 2023) due to cultivation of foreign tolerant varieties, and Greek varieties (e.g. 'Tyrbe' and 'Nostos') issued from national breeding projects of the Institute of Plant Breeding and Genetic Resources, at Naoussa. The currently preferred cultivars are 'Mogador', 'Mirlo Blanco', 'Pricia', 'Lilly cot', and 'Wondercot'. The PPV-sensitive variety 'Early of Tyrinth' currently occupies 580 ha, only 6% of the total apricot area [Greek Payment Authority of Common Agricultural Policy (C.A.P.) Aid Schemes-OPEKEPE, 2023]. Old local varieties of intermediate susceptibility, such as 'Bebecou', are still cultivated (2,160 ha, OPEKEPE, 2023) for their preferred characteristics, particularly as processed product (pulp or canned fruit), although the lifetime of cans is reduced to 3 years due to PPV. Rejections during fruit packaging are estimated at about 35% of the production, totalling approx. 39.2 tons per year. At €0.59 per kilogram, this implies direct losses of more than €23 million per year.

For peach and nectarine, quality of peaches is also affected by PPV, the main problem being softening of the fruit. Peach production has diminished principally for commercial reasons, particularly in the last 10 years. In 1995, the area cultivated with peach and nectarine trees was 53,504 ha with production of 1,034,400 t, but currently these crop areas have diminished to 38,220 ha and production of 894,510 t, a production reduction of 13.5% (FAOSTAT, 2023). Early peach cultivars (e.g., 'François', 'Lolita') are the most susceptible to PPV, exhibiting symptoms on 50-65% of their fruit, which are rejected during fruit packaging, and these cultivars are being replaced by late ripening ones. The overall rejections of late varieties during packaging are estimated at approx. 30% of peach production each year (direct losses of about €26,8 million year^{-1} at value €0.10 kg^{-1}). Studies conducted at the Institute of Plant Breeding and Genetic Resources evaluated the PPV resistance of different peach and nectarine cultivars, identifying tolerant varieties such as 'Tasty Free', 'Jerseyland', 'Gialla Precoce Morettini', 'Desert Gold' and 'Springtime'.

Plum production is less important in Greece than other stone fruit, but has been steadily increasing. In 1995, the area cultivated with plum trees was 719 ha with a production of 3,737 t, but at present these have increased to 2,140 ha and 24,380 t, a production increase >550% (FAOSTAT, 2023). The 'Angelino' Japanese plum cultivar, which is moderately sensitive to PPV, is the most common, covering more than 25% of the total plum tree cultivated area. Annual fruit rejections during packaging are estimated at around 11% of the production (direct losses of about €1.4 million/year at a price of €0.54/kg).

The losses in Greece due to sharka outlined above show that this disease has significant economic impacts on the stone fruit industry in that country. These total approx. €51 million per year.

Costs due to sharka in world Prunus industry

The presence of PPV and management of sharka in the 54 countries that have officially declared presence of the virus, including efforts toward eradication, indicate that this disease has considerable international economic impacts. An accurate international evaluation of the associated costs to Prunus industries is difficult, due to uncertainties in estimating actual direct crop losses due to the disease. This is especially relevant due to the weight and influence on the final estimation of the associated losses in China, where Prunus production and marketing have become major industries. Estimation of real direct losses is also difficult due to the different approaches to PPV management in different countries. For example, central European countries where PPV is endemic, unlike recently or locally infested countries, do not perform PPV eradication programmes but rely on cultivation of tolerant Prunus genotypes. Also, there are no available and accurate data on the actual sharka impacts from some territories, so erroneous estimations for these areas could lead to unreliable conclusions. Therefore, conservative estimates have been made in the following sections of this review, addressed by crops, and also considering the PPV strains present in each country, the actions or programmes available in the literature, and information supplied by expert colleagues and personnel from national Plant Health or Plant Protection Services. These general data are summarized in Table 1.

*Common apricot (*Prunus armeniaca*) and Japanese apricot (*P. mume*)*

Apricot, alongside the European plum, is the most fruit type affected by sharka (Martínez-Gómez *et al.*, 2000). According to FAOSTAT (2023), the great-

est apricot-producing countries where PPV has been detected (based on historical data), are: Türkiye (one of the largest producers of apricots), Iran, China (a world leading apricot producer), Uzbekistan (the major apricot-producing country in Central Asia), Italy: (a prominent apricot producer in Europe), and Spain and France (high-quality producers of apricots). The main Prunus producers with declared PPV presence are (in alphabetical order): Argentina, China, Cyprus, Canada, Croatia, Egypt, France, Germany, India, Iran, Israel, Italy, Japan, Jordan, Kazakhstan, Mexico, Pakistan, Portugal, Russia, Spain, Syria, Türkiye, Tunisia, Uzbekistan, and Ukraine, with an estimated total average global production of 2,320,000 t. Due to uncertainties about actual production in these countries, the present study uses a conservative average of 2% of fruit rejected, which represent approx. 46,400 t. With an average price of €0.30 kg^{-1} for fresh or dried fruit in pallets of 100 kg, this represents €13,920,000 year^{-1}, indicating, over the last 28 years, accumulated losses of approx. €389,760,000. This amount must be added to the losses incurred in countries where PPV-M is prevalent and other PPV strains causing more damage are also present, estimated at an average of 5% of the total apricot production. These countries include Albania, Bulgaria, Bosnia and Herzegovina, Greece, Moldova, North Macedonia, Poland, Romania, Serbia, Slovakia, and Slovenia, with a combined estimated production of apricots of approx. 418,200 t. With estimated losses of 20.91 million kg at an average price of €0.30 kg^{-1}, this represents annual losses of €6,273,000, amounting to approx. €175,644,000 over the period 1996 to 2023. Consequently, the total direct costs for apricot losses associated with sharka during this period amount to approx. €565,404,000 (Table 1).

*Japanese, Chinese plums (*Prunus salicina*) and European plums (*P. domestica*)*

Japanese and Chinese plums dominate world fresh fruit markets whereas European plums are also common in some regions, mainly in Europe, America, and Asia (FAOSTAT, 2023). Since China, especially Sichuan province, is the largest producer these plum species (Liu, 2018), accounting for almost 58% of the world plum production, that country should have the greatest weight in estimation of losses due to sharka. However, uncertainty is high related to Chinese production and the prevalence of PPV.

PPV-D symptoms on Japanese plums are rare, although the virus reduces numbers of marketable fruit. Conversely, incidence of sharka on *P. domestica* is important in Europe where PPV-M is the prevalent

strain. For plums, evaluation of losses has been carried out based production and the local presence of specific PPV strains in production regions.

The European Union (EU), particularly central and eastern Europe, is where major losses have been associated with sharka in European plum, and the diseases is also important in Southern European and Mediterranean countries, where Japanese plums predominate. Direct losses of 5% are estimated in the demanding plum markets of the European Union. In an average world production of 1,300,000 t, losses due to sharka would represent 65,000 t of fruit rejects per year, with a value (at €0.5 kg^{-1}) of €32,500,000 year^{-1} in the EU (€910 million from 1996 to 2023) (Table 1).

The second area with direct fruit losses associated with sharka is China, where estimated 0.1% of rejects due to the disease is here made, with uncertainty due to lack of reported data. This would represent 6,700 t loss from production of 6.7 million t, which at a local price of €0.2 kg^{-1}, would cause losses valuing approx. €1,340,000 year^{-1} (€37,520,000 assuming PPV has been present since 1995).

Ranking third is a group of countries which include (in order of plum production): Serbia, Iran, Türkiye, Chile, India, Ukraine, Russia, and Uzbekistan. This group have combined annual plum production estimated at 2,600 t. Sharka could cause losses, estimated on a country-by-country basis, of 79.56 t annually, valued at €39,78 year^{-1}, which totals €1,113,840 for 1996 to 2023.

The countries with least plum production are Mexico, Moldova, Bosnia and Herzegovina, Kazakhstan, Argentina, Turkmenistan, Syria, Israel, Armenia, and North Macedonia (ranked by decreasing amounts produced). Their combined production is approx. 464 t. It is here estimated, with uncertainty, that these countries could experience direct fruit losses of approx. 8.66 t annually, with an estimated value of €4,330/year, totaling €121,240 from 1996 to 2013.

Total world direct losses caused by sharka in plum production are estimated at €33,884,110 year^{-1}, equivalent to €948,755,000 for 1996 to 2023 (Table 1).

Peaches

Peaches (*Prunus persica*) suffers minor losses from infections of the predominant PPV-D strain (Samara *et al.*, 2017). However, the amount of fruit rejected could be significant in areas where other strains of PPV are present. In areas where peach production is primarily focused on canning industries, sharka does not pose major problems. The top ten countries where peach production is most concentrated, and where PPV is present, have substantial average production volumes.

These countries, in order of annual peach and nectarine production during 1996 to 2023 are: China (13 million t); followed by Spain and Italy (totalling 2 million t); the USA (0.8 million t); Greece (0.8 million t), Türkiye (0.7 million t), Iran (0.4 million t), Egypt (0.36 million t), Chile (0.33 million t), and Argentina (0.24 million t). Their total annual peach production, excluding the USA (where PPV was eradicated), is 17.83 million t. In addition, PPV is present in other important peach producing countries, such as: India (0.24 million t) and France (0.2 million t), totalling peach production 0.44 million t per year. Consequently, production of peaches is at least 18,270,000 t each year in countries where sharka occurs. Estimated losses due to the disease of 0.025% (because peaches showing superficial symptoms can be used peeled for canning, and only nectarines are rejected), could cause 45,675 t of discarded fruit, amounting to economic losses of approx. €18.32 million year^{-1} at an average estimated cost of €0.4 kg^{-1}. From 1996 to 2023, these losses could total approx. €511.56 million (Table 1), which does not include costs of the mandatory sharka eradication programmes adopted in Canada and USA.

Cherries

The top ten producers of sour cherry (*P. cerasus*) and sweet cherry (*P. avium*) are Türkiye, Chile, Uzbekistan, USA, Spain, Italy, Iran, Greece, Poland, and Syria. These countries produced, in 2022, approx. 75% of world cherries. Including other producers, the average annual production during 2008-2022 was approx. 2.35 million t (FAOSTAT, 2023; Palmieri, 2024). Among the PPV strains that severely affect both cherry species, PPV-C has been found in Russia, Moldova, Germany, Italy, Hungary, Croatia, and Belarus. PPV-CR and PPV-CV have been detected only in Russia (estimated annual cherry production of 294,000 t) (FAOSTAT, 2024). PPV-C can reduce the productivity of some *P. cerasus* cultivars and hybrids by 38 to 45% (Sheveleva *et al.*, 2021). These losses were obtained from 152 fruit-bearing sour cherry trees in the Tatarstan region of Russia, so they are an uncertain basis for determining generalized sharka losses for sour cherry production. Nevertheless, neither premature fruit drop nor sharka fruit symptoms are observed on sour cherry in Russia, although the disease probably causes losses, but these have not been precisely evaluated.

Almonds

No losses due to sharka have been reported from any country where almond (*P. dulcis*) trees are grown and the disease sharka is present, even in endemic situations.

CONCLUSIONS

The estimated total world costs of €2,394,119,080 (approx. €2.4 thousand million; '€2.4 billion') (Table 1) associated with the prevention and management of PPV and sharka from 1995 to 2023, despite the high value, indicates a significant reduction compared to the €10 thousand million incurred in previously evaluated period from the 1970s to 2006 (Cambra *et al.*, 2006a). Cumulative world losses from the sharka pandemic since the decade of 1910 to 1920 should surpass €13 thousand million in nominal terms (without inflation adjustments). The first evaluated period was 30 years up to 2006, characterized as the most severe period of sharka in Europe and onset of the disease in America and Asia. During that period, social and political impacts of the disease were severe (Capote *et al.*, 2006; Damsteegt, 2008; Barba *et al.*, 2011; Sochor *et al.*, 2012), with significant loss of biodiversity in traditional fruit cultivars across Europe. At that time, current detection and diagnostic methods and kits were not available or commonly used on large scales (Cambra *et al.*, 2011), and the trade and traffic of plant material was frequent, especially between neighboring countries, but also over long distances, in an expanding fruit production industry.

The reduction in costs related to PPV indicates improvements in sharka management practices (along with other possible factors) have contributed to reducing the economic effects of PPV and sharka. Based primarily on the reports of Gottwald *et al.* (2013), Welliver *et al.* (2014), Rimbaud *et al.* (2015), García *et al.* (2014; 2024), the major factors that have collectively contributed to the reductions in these economic impacts from 1995 to 2023, compared to 1970 to 2006, were:

Advances in disease management:
• Improved prevention, eradication, and integrated control methods;
• Use of more PPV-tolerant cultivars and PPV-free nursery plants;
• Enhanced monitoring and quarantine measures;
• Effective eradication or reduction of PPV inoculum in key areas.

Technological improvements:
• Development of more accurate and rapid diagnostic tools;
• Enhanced sampling methodologies for large-scale pathogen testing;
• Early detection facilitating timely intervention and containment.

Education and awareness:
• Increased awareness and education in PPV prevention and management among farmers, nurserymen and stakeholders.
• Improved knowledge and legislative framework leading to better disease management and reducing illegal plant material traffic.

Support and co-operation:
• National and international support for research, surveillance, and control programmes;
• International co-operation facilitating dissemination of best practices, and co-ordinated efforts through common research projects, networks, and international diagnostic standards.

Industry adaptation:
• Diversification of production, such as increasing cherry cultivation in areas without cherry-adapted PPV isolates, facilitated by more favourable market conditions for expanding cherry production.
• Investment in disease-resistant/tolerant cultivars developed through different conventional and new technologies;
• Implementation of rigorous phytosanitary measures and improved nursery practices.

Nevertheless, the evaluated total cost of €2.4 thousand million from 1996 to 2023 is significant. This represents approx. 0.17% of the value of the stone fruit industry (average annual estimated value of production for 1995 to 2023 approx. €51 thousand million), according to FAO. These costs are likely affected by increased globalization and the interconnectedness of economies, which have facilitated the spread of sharka to new regions, often through uncontrolled movement of PPV-infected plant material. Additionally, lack of effective control measures and efficient biosecurity practices in many areas have allowed sharka to persist and spread, thereby exacerbating the economic impacts of the disease. Overall, the factors that have contributed to these substantial costs, can be summarized as follows:
• **Continued spread of PPV:** Despite control measures, PPV has persisted in many regions, requiring ongoing application of disease management.
• **Aphid vector transmission:** PPV has continued to spread locally through aphid species vectors, necessitating constant insect monitoring and control, especially in plant nurseries.
• **High direct losses:** Significant losses from unmarketable infected stone fruit, especially European plums, has severely impacted the industry.

- **Indirect costs:** Ongoing expenses for sample collection, ELISA and PCR-based testing, surveys, research, and control strategies.
- **Expensive eradication and containment programmes:** The difficulties and costs of PPV eradication and the lack of success in many areas, require integrated and costly containment measures that frequently result in maintenance of pathogen inoculum.
- **International trade restrictions:** The rejection of sharka symptomatic fruit in international markets, and precautions and careful selection to avoid export of symptomatic fruit.
- **Research and development:** Continued investment in research and scientific networks to develop disease management strategies and resistant or more agronomically tolerant cultivars, along with the costs of field trials.
- **Exclusion of certain costs:** This study did not account for trade costs, genetic erosion of traditional cultivars, loss of biodiversity, research and development for PPV resistant/tolerant cultivars, or measures to prevent and avoid PPV entry in certain areas, including the implementation of phytosanitary controls at entry points and legal frameworks, indicating additional hidden impacts.

Investments made in each country for sharka management, usually but not always, align with national significance as producers and exporters of stone fruit, aiming to maintain competitiveness in increasingly demanding markets, and to ensure the future for the respective fruit production industries. For instance, primarily in Southern European Union countries, such as Italy, France, and Spain, significant economic efforts have been made to contain sharka, which in Spain's case represents about 0.32% of the average annual value of apricot, peach, and plum production. Furthermore, with PPV being downgraded to RNQP for the European Union (EU regulation 2016/2031), the future may be more uncertain, as private control is usually less or non-effective for successfully managing sharka (Martinez *et al.*, 2024). In other countries, despite investments in containment, and considering PPV as a quarantine pest, the efforts have not been sufficient in relation to the total values of stone fruit production and the quantities of exported fruit. Robust programmes to manage sharka are needed in high-value stone fruit industries. Countries with less significant stone fruit industries probably invest less in disease management, posing risks for other areas by maintaining PPV reservoirs, from which infected material could be illegally transported (for cultural or traditional reasons) to other

regions or countries where PPV and sharka is effectively contained, or has been eradicated.

Distribution of total losses due to PPV across regions for 1995 to 2023 reflects the extent of the regions. Asia experienced the largest total economic losses and associated costs (direct and indirect). Europe and the Americas together had similar losses despite the large differences in land use and agricultural practices in these regions. The African continent, despite risks of PPV introduction, probably applies the lowest costs for prevention. As the region with least land area, Oceania accounts for the lowest indirect total associated economic losses, which are mainly devoted to efficient prevention of PPV entry and establishment.

An uncertainty for estimating costs is the value applied to losses associated with sharka. Fluctuations in stone fruit prices can be caused by several factors, including supply and demand. Increases in agricultural input and labour costs can also impact fruit market prices, as well as competition, especially in case of oversupply. Government interventions, including tariffs, agricultural subsidies, and trade regulations, can also impact stone fruit prices. combinations of these factors, and others, cause variable markets prone to abrupt fluctuations. However, once fruit losses were estimated in this study, with uncertainties in some cases due to lack of transparency in officially acknowledging the losses where these have not been published, they were assigned value likely to be appropriate. Sharka affects trees differently in each stone fruit production area, depending on PPV strain(s) and the predominant or majority strain(s). Yield losses in infected cherry trees have been reported, but it is difficult to establish exact loss amounts. Accurately determination of these losses has yet to be achieved, as the pathogen strains must be prevented given the substantial growth in cherry cultivation.

Resilience through the use of ´agronomically tolerant cultivars´ (e.g., domestic plum cultivars produced at the Fruit Research Institute at Čačak in Serbia) is being pursued in Central and Eastern Europe, in areas where sharka is endemic. The PPV-resistant, genetically engineered HoneySweet cultivar was deregulated in 2007 in the USA, after numerous international field trials and analytical assays, and was released to breeders and growers concerned about the threats of PPV (Scorza *et al.*, 2007). This or a similar engineered cultivar has not yet been approved for release in the European Union.

The combined use of certified virus-free plants, even those sensitive to PPV, produced in approved nurseries, along with multiplication of PPV-resistant or tolerant cultivars, is allowing the maintenance of stone fruit production in countries where sharka has not been eradicated.

Research efforts on PPV must remain active and innovative in several topic areas, such as in advanced diagnostic and detection techniques, sampling methodologies for eradication, or accurate testing to determine the PPV-free status of plant material, as well as plant-virus interaction studies aimed at interfering with virus spread. Establishment of certification programmes for *Prunus* spp. should be globally promoted. Consistent and durable financial support for advanced technical and scientific assistance to the Prunus industries is advisable, proportional to the value of the industry in each country. Active dissemination through educational programmes should emphasize the imprudence of moving plant material without comprehensive sanitary guarantees. Urgent development and application of conventional, transgenic, or genome-editing techniques to obtain tolerant or, preferably, resistant stone fruit cultivars (Cirili *et al.*, 2016; De Mori *et al.*, 2020; García *et al.* 2024) are also important for sharka disease management, and should be strongly promoted.

LITERATURE CITED

Acuña R., 1993. Outbreaks of Plum pox virus in Chile. *European and Mediterranean Plant Protection Organization (EPPO) Conference Plum pox virus*, Bordeaux, France. 5–8 August. EPPO, Paris, France.

Akbaş B., Değirmenci K., Çiftçi O., Kaya A., Yurtmen M.,…Türkölmez Ş., 2011. Update on plum pox virus distribution in Turkey. *Phytopathologia Mediterranea* 50 (1): 75–83. https://doi.org/10.14601/Phytopathol_Mediterr-8646.

Atanasoff, D., (1932. Plum pox. A new virus disease. *Annals of the University of Sofia, Faculty of Agriculture and Silviculture* 11: 49–69.

Barba M., Hadidi A., Candresse T., Cambra M., 2011. Plum pox virus. In: *Virus and Virus-like Diseases of Pome and Stone Fruits* (A. Hadidi, M. Barba, T. Candresse, W. Jelkmann, ed.), APS, St. Paul, MN, USA, 185–197 https://doi.org/10.1094/9780890545010.036.

Batlle I., Cantin C. M., Badenes M. L., Rios G., Ruiz D., … García-Brunton J., 2018. Frutales de hueso y pepita. In: *Influencia del cambio climático en la mejora genética de plantas* (J. García Brunton, O. Pérez Tornero, J.E. Cos Terrer, L. Ruiz García, E,. Sánchez López, ed.), Comunidad Autónoma de la Región de Murcia, Sociedad Española de Ciencias Hortícolas, Sociedad Española de Genética, Murcia, Spain, 97–130. https://www.imida.es/documents/13436/877249/INFLUENCIA+DEL+CAMBIO+CLIMATICO+EN+LA+MEJORA+GENÉTICA+DE+PLANTAS-IMIDA-WEB.pdf/3fce9e5f-17da-4bd7-b227-830289d48409

Birişik N., Morca A. F., Erilmez S., Çiftçi O., Yurtmen M., … Öntepeli M L., 2021. Assessment of a six-year national survey and eradication program for Plum pox virus in Turkey. *Plant Protection Bulletin* 61(2): 19–32. https://doi.org/10.16955/bitkorb.793804

Bolat I., Ak B.E., Acar I., Ikinci A., 2017. Plum culture in Turkey. *Acta Horticulturae* 1175: 15–18 https://doi.org/10.17660/ActaHortic.2017.1175.4.

Çağlayan K., Gazel M.H., 1998. Virus and virus-like diseases of stone fruits in the Eastern Mediterranean

area of Turkey. *Acta Horticulturae* 42: 527–529. https://doi.org/10.17660/ActaHortic.1998.472.66

Çağlayan K., Yurdakul S., 2017. Sharka disease (Plum pox virus) in Turkey: the past, present and future. *Acta Horticulturae* 1163: 69–74. https://doi.org/10.17660/ActaHortic.2017.1163.11

Cambra M., Vidal E., 2017. Sharka, a vector-borne disease caused by Plum pox virus: vector species, transmission mechanism, epidemiology and mitigation strategies to reduce its natural spread. *Acta Horticulturae* 1163: 57–68. https://doi.org/10.17660/actahortic.2017.1163.10

Cambra M., Capote N., Myrta A., Llácer, G., 2006a. Plum pox virus and the estimated costs associated with sharka disease. *EPPO Bulletin* 36: 202–204. https://doi.org/10.1111/j.1365-2338.2006.01027.x

Cambra M.A., Serra J., Cano A., Cambra, M., 2006b. Plum pox virus (PPV) in Spain. 215 pp. In: A review of Plum pox virus. Current status of Plum pox virus and sharka disease worldwide. (N. Capote, M. Cambra, G. Llácer, F. Petter, LG Platts, A.S. Roy, I.M. Smith, ed). *EPPO Bulletin* 36: 205–218.

Cambra M., Boscia D., Gil M., Bertolini E., Olmos, A., 2011. Immunology and immunological assays applied to the detection, diagnosis and control of fruit tree viruses. In: *Virus and Virus-like Disease of Pome and Stone Fruits* (A. Hadidi, M. Barba,T. Candresse, W. Jelkmann, ed.), APS. Press, St. Paul, MN, USA, 303–313. https://doi.org/10.1094/9780890545010.055

Candresse T., Saenz P., García, J.A., Boscia, D., Navratil, M.,… Cambra, M. 2011. Analysis of the epitope structure of Plum pox virus coat protein. *Phytopathology* 101: 611–619. https://doi.org/10.1094/PHYTO-10-10-0274

Capote N., Cambra M., Llácer G., Petter F., Platts L.G, …Smith, I. M., (eds)., 2006. A review of Plum pox virus. *EPPO Bulletin* 36(2): 201–349. https://gd.eppo.int/reporting/article-1121

Capote N., Bertolini E., Olmos A., Vidal E., Martinez M.C., Cambra M., 2009. Direct sample preparation methods for the detection of Plum pox virus by real-time RT-PCR. *International Microbiology* 12: 1–6. https://doi.org/10.2436/20.1501.01.75

Capote N., Cambra M. A., Botella P., Gorris M. T., Martínez M. C.,…Cambra M., 2010. Detection, characterization, epidemiology and eradication of Plum pox virus Marcus type in Spain. *Journal of Plant Pathology* 92: 619–628. https://www.jstor.org/stable/41998850

Chilean customs, Aduanas de Chile., 2020. Dynamic Export database. Customs. Accessed, 19 november, 2020, from https://www.aduana.cl/base-de-datos-dinamicas-de-exportaciones/aduana/2020-11-19/151830.html

Chirkov S., Sheveleva A., Gasanova T., Kwon D., … Osipov G., 2022. New cherry-adapted plum pox virus phylogroups discovered in Russia. *Plant Disease* 106: 2591–2600. https://doi.org/10.1094/PDIS-01-22-0006-RE

Cirili M., Geuna F., Babini A.R., Bozhkova V., Catalano L., … Bassi D., 2016. Fighting Sharka in Peach: Current Limitations and Future Perspectives. *Frontiers in Plant Science* 7: 1290. https://doi.org/10.3389/fpls.2016.01290

Coşkan S., Morca A.F., Akbaş B., Çelik A., Santosa A. I. 2022. Comprehensive surveillance and population study on plum pox virus in Ankara Province of Turkey. *Journal of Plant Diseases and Protection* 129: 981–991. https://doi.org/10.1007/s41348-022-00597-5

CREDA, 2023. Estimated production cost of stone fruit (peaches) for the farmer. Centro de Investigación en Economía y Desarrollo Agroalimentario, Spain. Accessed June 2024, from https://www.creda.es/es/coste-produccion-fruta-hueso-agricultores/

Culliney, T.W., 2014. Crop losses to arthropods. In: *Integrated Pest Management. Pesticide problems* (D. Pimentel, R.Pestrin, ed.), Springer Nature, 201–225.

Damsteegt V. D., 2008. *Plum pox virus (sharka). CABI Compendium.* https://doi.org/10.1079/cabicompendium.42203

De Mori G., Savazzini F., Geuna F., 2020. Molecular tools to investigate sharka disease in *Prunus* species. In: *Applied Plant Biotechnology for Improving Resistance to Biotic Stress* (P. Poltronieri, Y. Hong, ed.), Academic Press, Elsevier Inc., Oxford, 203–223.

Dimitriadou A., 2015. *Serological and molecular characterisation of Plum pox virus (PPV) populations in Greece.* MSc Thesis, Aristotle University of Thessaloniki. https://doi.org/10.26262/heal.auth.ir.286908

Drogoudi P., Pantelides G., 2017. Results of evaluation of agronomic and qualitative characteristics of new and older varieties of apricot cultivated in Greece. In: *Sharka virus and apricot tree: new data. Proceedings of the Conference organized by the Association of Agronomists of Argolida* (D. Dimou, ed.)., Argos, Greece, 35–48 (in Greek).

EC, 2022. European Comission DG Agri E2-F&V-2022. EU fruit and vegetables market observatory. Stone fruit subgroupe. Vol. 032-Trade fresh. The peaches and nectarines market in the EU 27: Trade on fresh products.

EPPO, 2020. Plum pox virus. EPPO datasheets on pests recommended for regulation. Accessed April 25, 2024, from https://gd.eppo.int

EPPO, 2023. PM 7/32 (2) Plum pox virus. *EPPO Bulletin* 53: 518–539. https://doi.org/10.1111/epp.12948

EPPO, 2024. Plum pox virus. EPPO datasheets on pests recommended for regulation. Accessed April 25,

2024, from https://gd.eppo.int. EPPO code PPV000. Last updated: 2023-09-11.

EPPO PRA, 2012. Pest Risk Analysis for Plum pox virus. https://pra.eppo.int› getfile.

EU 2023. DG AGRI DASI-BOARD. Peaches and nectarines EU weekly prices for peaches (ex-packaging station, €/100 kg). Accessed April 25, 2024, from https://agriculture.ec.europa.eu/document/download/7edd5ce4-8bed-4209-aa48-3f58118b4d47_en?filename=dashboard-peaches_en_0.pdf

EU regulation 2016/2031. Regulation of the European Parliament of the Council of 26 October 2016 on protective measures against pests of plants, amending Regulations (EU) No 228/2013, (EU) No 652/2014 and (EU) No 1143/2014 of the European Parliament and of the Council and repealing Council Directives 69/464/EEC, 74/647/EEC, 93/85/EEC, 98/57/EC, 2000/29/EC, 2006/91/EC and 2007/33/EC. http://data.europa.eu/eli/reg/2016/2031/oj

FAOSTAT, 2023. Faostat. Data retrieved for years between 1995 and 2023. Accessed April 25, 2024, from https://www.fao.org/faostat/es/#data

FAOSTAT, 2024. Faostat. Data retrieved for 2024. Accessed April 25, 2024, from https://www.fao.org/faostat/es/#data

Fiore N., Araya C., Zamorano A., González F., Mora R., … Rosales I.M., 2010. Tracking Plum pox virus in Chile throughout the year by three different methods and molecular characterization of Chilean isolates. *Julius-Kühn-Archiv* 427: 156–161.

García J. A., Glasa M., Cambra M., Candresse T., 2014. Plum pox virus and sharka: a model potyvirus and a major disease. *Molecular Plant Pathology* 15: 226–41. https://doi.org/10.1111/mpp.12083

García J. A., Rodamilans B., Martínez-Turiño S., Valli A. A., Simón-Mateo C., Cambra M., 2024. Plum pox virus: An overview of the potyvirus behind sharka, a harmful stone fruit disease. *Annals of Applied Biology* (*in press*).

Ghahremani. A., Ebrahim Ganji E., Marjani A., 2023. Growth, yield, and biochemical behaviors of important stone fruits affected by plant genotype and environmental conditions. *Scientia Horticulturae* 321: 112–211. https://doi.org/10.1016/j.scienta.2023.112211

Gildow F., Damsteegt V., Stone A., Scheider W., Luster D., Levy L., 2004. Plum pox in North America: identification of aphid vectors and a potential role for fruit in virus spread. *Phytopathology* 94(8): 868–874. https://doi.org/10.1094/PHYTO.2004.94.8.868

Glasa M., Prikhodko Y., Predajna L., Nagyova A., Shneyder Y., … Candresse T., 2013. Characterization of sour cherry isolates of Plum pox virus from the Volga basin in Russia reveals a new cherry strain of the virus. *Phytopathology* 103: 972–979. https://doi.org/10.1094/PHYTO-11-12-0285-R

Gottwald T. R., Wierenga E., Luo W. Q., Parnell S., 2013. Epidemiology of Plum pox "D" strain in Canada and the USA. *Canadian Journal of Plant Pathology* 35: 442–457. https://doi.org/10.1080/07060661.2013.844733

Guillesky S., 2018. China-Peoples Republic of; Stone fruits annual, 2018. Global Agriculture Information Network Report, GAIN report CH 18037. USDA Foreign Agricultural Service. https://apps.fas.usda.gov/newgainapi/api/report/downloadreportbyfilename?filename=Stone%20Fruit%20Annual_Beijing_China%20-%20Peoples%20Republic%20of_6-29-2018.pdf

Guo M., Qi D., Dong J., Dong S., Yang X., Qian Y., Zhou X., Wu J., 2023. Development of Dot-ELISA and Colloidal Gold Immunochromatographic Strip for Rapid and Super-Sensitive Detection of Plum Pox Virus in Apricot Trees. *Viruses* 15(1): 169. https://doi.org/10.3390/v15010169

Gutiérrez-Jara J.P., Vogt-Geisse K., Correa M.C.G., Vilches-Ponce K., Pérez L.M., Chowell G., 2023. Modeling the impact of agricultural mitigation measures on the spread of sharka disease in sweet cherry orchards. *Plants* 12(19): 3442. https://doi.org/10.3390/plants12193442

Hadidi A., Barba M., 2011. Economic impact of pome and stone fruit viruses and viroids. In: *Virus and Virus-like Diseases of Pome and Stone Fruits* (A. Hadidi, M. Barba, T. Candresse, W. Jelkmann, ed), APS, St. Paul, MN, USA, 1–7. https://doi.org/10.1094/9780890545010

Herrera G., 2013. Investigations of the Plum pox virus in Chile in the past 20 years. *Chilean Journal of Agricultural Research* 73(1): 60–65. https://doi.org/10.4067/S0718-58392013000100009

Huang H., Che g Z., Zhang Z., Wang Y., 2008. History of cultivation and trends in China. In: *The Peach. Botany, Production and Uses* (D.R. Layne, D. Bassi, ed.), CABI, Wallingford, AMA Dataset Ltd, UK, 37–60. https://doi.org/10.1079/9781845933869.0037

IPPC-FAO, 2018. International standards for phytosanitary measures: diagnostic protocols: Plum pox virus. *ISPM 27, Annex 2* (DP2). https://assets.ippc.int/static/media/files/publication/en/2019/07/DP_02_2018_En_PlumPox_Rev_2018-09-21.pdf

ISTAT, 2023. Prunus fruit production in Italian regions. Accessed May 15, 2024, from http://dati.istat.it/Index.aspx?QueryId=33705

Jelkmann W., Sanderson D., Berwarth C., James D., 2018. First detection and complete genome characterization of a Cherry (C) strain isolate of plum pox virus from

sour cherry (*Prunus cerasus*) in Germany. *Journal of Plant Diseases and Protection* 125(3): 267–272. https://doi.org/10.1007/s41348-018-0155-7

Jones R. A. C., Naidu R. A., 2019. Virus Diseases: Current Status and Future Perspectives. *Annual Review of Virology* 6: 387–409. https://doi.org/10.1146/annurev-virology-092818-015606

Kaponi M., Axarli E.A., Koutretsis P., Nikoloudakis N., Drogoudi P., Berbati M.G., 2012. First report of plum pox virus in almond trees in Greece in the context of Phytosanitary control. In: *Abstracts of the 16th Panhellenic Phytopathlogical Congress*, Thessaloniki, Greece, October 2012, 143 (in Greek).

Kegler H., Hartmann W., 1998. Present status of controlling conventional strains of Plum pox virus. In: *Plant Virus Disease Control* (A. Hadidi, R.K. Khetarpal, H. Koganezawa, ed.), APS Press St. Paul, MN, USA, 616–628.

Kimura K., Usugi T., Hoshi H., Kato A., Ono T., … Tsuda S., 2016. Surveys of Viruliferous Alate Aphid of Plum pox virus in *Prunus mume* Orchards in Japan. *Plant Disease* 100(1): 40–48. https://doi.org/10.1094/PDIS-05-15-0540-RE

Labonne G., Quiot J.B., 2001. Aphids can acquire plum pox virus from infected fruits. *Acta Horticulturae* 550: 79–83. https://doi.org/10.17660/ActaHortic.2001.550.8

Labonne G., Yvon M. Quiot J.B., Avinent L. Llacer G., 1995. Aphids as potential vectors of plum pox virus: comparison of methods of testing and epidemiological consequences. *Acta Horticulturae* 386: 207–218. https://doi.org/10.17660/ActaHortic.1995.386.27

Lebas B. S. M., Ochoa-Corona F. M., Elliott D. R., Double B., Smales T., Wilson J. A., 2006. Control and monitoring: quarantine situation of Plum pox virus in New Zealand. *EPPO Bulletin* 36: 296–301. https://doi.org/10.1111/j.1365-2338.2006.00999.x

Levy L., Damsteegt V., Welliver R., 2000. First report of Plum pox virus (sharka disease) in Prunus persica in the United States. Plant Disease 84(2): 202. https://doi.org/10.1094/PDIS.2000.84.2.202B

Liu J., 2018. Plum and apricot industry: present status and future perspectives in Sichuan, China. *Acta Horticulturae* 1214: 19–22. https://doi.org/10.17660/ActaHortic.2018.1214.4

Loera-Muro A., Gutiérrez-Campos R., Delgado M., Hernández-Camacho S., Holguín-Peña R. J., 2017. Identification of Plum pox virus causing sharka disease on peach (Prunus persica L.) in Mexico. *Canadian Journal of Plant Pathology* 39(1): 83–86. http://doi.org/10.1080/07060661.2017.1292549

Madariaga M., Ramírez I., Vega R., Meza P., Nova N., Devia J., Sepúlveda K., Defilippi B., 2024. Effect of storage temperature on viral RNA accumulation in Plum pox virus-infected Red Lyon plum fruit from the Central Valley of Chile. *Discov Appl Sc* 6: 417. https://doi.org/10.1007/s42452-024-06078-8

MAPA 2021. Ministerio de Agricultura, Pesca y Alimentación. Ministry of Agriculture, Fisheries and Food. Anuario de Estadística 2021. Boletín de precios fruta de hueso campañas 2021, semana 22, de 2021(31 mayo-6 junio), en palés de 100 kg. Accessed May 15, 2024. https://www.mapa.gob.es/es/agricultura/temas/producciones-agricolas/boletinsemanalpreciosfrutadehueso202131_maya6_jun_tcm30-563516.pdf and https://www.mapa.gob.es/es/agricultura/temas/producciones-agricolas/frutas-y- hortalizas/boletin_fruta_de_hueso.aspx, and www.mapa.gob.es

Martinez C., Courtois P., Thébaud G., Tidball M., 2024. The private management of plant disease epidemics: Infection levels and social inefficiencies. *European Review of Agricultural Economics* 51(2): 248–274. https://doi.org/10.1093/erae/jbae009

Martínez-Gómez P., Dicenta F., Audergon J. M., 2000. Behaviour of apricot (*Prunus armeniaca* L.) cultivars in the presence of sharka (plum pox potyvirus): a review. *Agronomie* 20: 407–422. https://hal.science/hal-00886049

Matthews R. E. F., Hull R., 2002. *Plant Virology*. Academic Press, San Diego.

Morca A.F., Coşkan S., Akbaş B., 2022. Detection, Characterization, and Monitoring of Plum pox virus in Zonguldak Province. *KSU Journal of Agriculture and Nature* 25(6): 1369–1377 (in Turkish). https://doi.org/10.18016/ksutarimdoga.vi.1015786

Mulderij R., 2018. Overview global stonefruit market. Fresh Plaza. Accessed July 30, 2024, from https://www.freshplaza.com/north-america/article/9021519/overview-global-stonefruit-market/

NAPPO 2009. RSPM 35. *Guidelines for the Movement of Stone and Pome Fruit Trees and Grapevines into a NAPPO Member Country*. NAPPO, Ottawa. Canada. https://www.nappo.org/application/files/4715/9452/9276/RSPM_35-e.pdf

Nemchinov L., Crescenzi A., Hadidi A., Piazzolla P., Verderevskaya T., 1998. Present status of the new cherry subgroup of plum pox virus (PPV-C). In: *Plant Virus Disease Control* (A. Hadidi, R.K. Khetarpal, H. Koganezawa, ed.), APS Press, St Paul, Minnesota, USA, 629-638.

Németh M., 1994. History and importance of plum pox virus in stone-fruit production. *EPPO Bulletin* 24: 525–536. https://doi.org/10.1111/j.1365-2338.1994.tb01065.x

Oerke E. C., Dehne, H.W. Schönberck, F., Weber, A., 1994. *Crop Production and Crop Protection: Estimated*

Losses in Major Food and Cash Crops. Elsevier Science B.V., Amsterdam.

Oishi M., Inoue Y., Kagatsume R., Shukuya T., Kasukabe R., …Y. Maeda 2018. First Report of Plum pox virus Strain M in Japan. *Plant Disease* 102 (4): 829. https://doi.org/10.1094/PDIS-08-17-1327-PDN

OPEKEPE 2023. Ο.Π.Ε.Κ.Ε.Π.Ε.-Ενιαία Αίτηση Ενίσχυσης 2023. Organization of Agricultural Payments and Markets in Greece. Accessed April 15, 2024, from https://www.opekepe.gr/opekepe-organisation-gr/opekepe-e-services-gr/efarmoges-ypostiriksis-synallagon-me-ton-politi/eniaia-aitisi-enisxysis-2023

Palmieri A., 2024. The evolution of cherry production over the last 15 years. Cherry times. Accessed June 15, 2024, from https://cherrytimes.it/en/news/The-evolution-of-cherry-production-over-the-last-5-years.

Paulus A.O., Ullstrup S.E., 1978. *Economic Impact of Plant Disease*. Academic Press.

Pedrelli A., Panattoni A., Clotrozzi L., 2024. The sharka disease on stone fruits in Italy: a review, with a focus on Tuscany. *European Journal of Plant Pathology* 169: 287–300. https://doi.org/10.1007/s10658-024-02827-y

Rao G.P., Reddy G.M., 2020. Overview of yield losses due to plant viruses. In: *Applied Plant Virology. Advances, detection and antiviral strategies* (L.P. Awasthi, ed.), Academic Press, 531–550. https://doi.org/10.1016/B978-0-12-818654-1.00038-4

Ravelonandro M., Scorza R., Polak J., Callahan A., Krška B., Kundu J., Briard P., 2013. HoneySweet Plum. A Valuable Genetically Engineered Fruit-Tree Cultivar. *Food and Nutrition Sciences* 4: 45–49. http://dx.doi.org/10.4236/fns.2013.46A005

Retamales J. B., 2011. World temperate fruit production: Characteristics and challenges. *Revista Brasileira de Fruticultura* 33: 121–130. https://doi.org/10.1590/S0100-29452011000500015

Rezende J. A. M., Camelo V. M., Kitajima E. W., 2016. First Report on detection of Plum pox virus in imported peach fruits in Brazil. *Plant Disease* 100(4): 869. *Disease note*. https://doi.org/10.1094/PDIS-09-15-1015-PDN

Rimbaud L., Dallot S., Gottwald T., Decroocq V., Jacquot E., Soubeyrand S., Thébaud G., 2015. Sharka epidemiology and worldwide management strategies: learning lessons to optimize disease control in perennial plants. *Annual Review of Phytopathology* 53: 357–378. http://dx.doi.org/10.1146/annurev-phyto-080614-120140

Rodoni B., Merriman P., Moran J., Whattam M., 2006. Control and monitoring: phytosanitary situation of Plum pox virus in Australia. *EPPO Bulletin* 36: 293–295.

Rodoni B., Sarec R., Mann R., Moran J., Merriman P., Ochoa-Corona F., Lovelock D., 2020. *National Diagnostic Protocol of Australia*. Plum pox virus (PPV). NDP2 V4. Subcommitte on Plant Health Diagnostics. https://www.plantbiosecuritydiagnostics.net.au/app/uploads/2020/12/NDP-2-Plum-pox-virus-V4.pdf

Rosales M., Hinrichsen P., Herrera G., 1998. Molecular characterization of Plum pox virus isolated from apricots, plums and peaches in Chile. *Acta Horticulturae* 472: 401–407. https://dx.doi.org/10.17660/ActaHortic.1998.472.47

Samara R., Hunter D. H., Stobbs L. W., Greig N., Lowery D. T., Delury N. C., 2017. Impact of Plum pox virus (PPV-D) infection on peach tree growth, productivity and bud cold hardiness. *Canadian Journal of Plant Pathology* 39(2): 218–228. https://doi.org/10.1080/07060661.2017.1336489

Savary S., Willocquet L., Pethybridge S. J., Esmjker P., McRoberts N., Nelson A., 2019. The global burden of pathogens and pests on major food crops. *Nature Ecology and Evolution* 3: 430–439. https://doi.org/10.1038/s41559-018-0793-y

Scholthof K-B. G., Adkins S., Czosnek H., Palukaitis P., Jacquot E., … Foster G. D., 2011. Top 10 plant viruses in molecular plant pathology. *Molecular Plant Pathology* 12(9): 938–954. https://doi.org/10.1111/j.1364-3703.2011.00752.x

Scorza R., Hily J.M., Callahan A., Malinwski T., Cambra M., … Ravelonandro M., 2007. Deregulation of Plum Pox Resistant Transgenic Plum 'HoneySweet'. *Acta Horticulturae* 738: 669–673. https://doi.org/10.17660/ActaHortic.2007.738.88

Scorza R., Ravelonandro M., Callahan A., Zagrai I., Polak J., … Dardick C., 2016. HoneySweet' (C5), the First Genetically Engineered Plum pox virus-resistant Plum (*Prunus domestica* L.) Cultivar. *HortScience* 51(5): 601–603. https://doi.org/10.21273/HORTSCI.51.5.601

Sheveleva A., Osipov G., Gasanova T., Ivanov P., Chirkov S., 2021. Plum pox virus strain C isolates can reduce sour cherry productivity. *Plants* 10(11): 2327. https://doi.org/10.3390/plants10112327

Simões D., de Andrade E., Sabino R., 2023. Fungi in One Health Perspective. *Encyclopedia* 3(3), 900–918. https://doi.org/10.3390/encyclopedia3030064

Snover-Clift K. L., Clement P. A., Jablonski R., Mungari R. J., Mavrodieva V. A., Negvi S., Levy L., 2007. First Report of Plum pox virus on Plum in New York State. *Plant Disease* 91(11): 1512. https://doi.org/10.1094/PDIS-91-11-1512C

Sochor J., Babula P., Adam V., Krska B., Kizek R., 2012. Sharka: The Past, The Present and The Future. *Viruses* 4(11): 2853–2901. https://doi.org/10.3390/v4112853

Strange R. N., Scott P. R., 2005. Plant disease: A threat to global food security. *Annual Review of Phytopathology* 43: 3.1–3.34. https://doi.org/10.1146/annurev.phyto.43.113004.133839

Thomson D., 2006. Plum pox virus (PPV) in Canada. In: *A Review of Plum Pox Virus. Current Status of Plum Pox Virus and Sharka Disease Worldwide* (N. Capote, M. Cambra, G. Llácer, F. Petter, L.G. Platts, A.S. Roy, I.M. Smith, ed.) *EPPO Bulletin* 36: 205–218.

Thompson D., McCann M., MacLeod M., Lye D., Green M., James D., 2001. First Report of Plum Pox Potyvirus in Ontario, Canada. *Plant Disease* 85(1): 97. https://doi.org/10.1094/PDIS.2001.85.1.97C

Thresh J. M., Fargette D., Otim-Nape G. W., 1994. Effects of African cassava mosaic virus on the yield of cassava. *Tropical Science* 26: 34–37.

TURKSTAT 2023. Türkiye Statistical Institute. Ministry of Agriculture and Forest (MoAF) and published by TurkStat within the scope of the Official Statistics Program. Accessed May 20, 2024, https://biruni.tuik.gov.tr/medas/?kn=92&locale=tr

USDA 2019. USDA declares United States free from Plum pox virus. Accessed February 28, 2024, from https://www.aphis.usda.gov/aphis/newsroom/news/sa_by_date/sa-2019/plum-pox-declaration

Varveri C., 2017. Plum pox virus and its integrated management. In: *Sharka Virus and Apricot Tree: New Data*. In: *Proceedings of the Conference organized by the Association of Agronomists of Argolida* (Dimou D., ed.). Argos, Greece, June 2017, 25–34 (in Greek).

Vidal E., Moreno A., Bertolini E., Pérez-Panadés J., Carbonell E.A., Cambra M., 2010. Susceptibility of *Prunus* rootstocks to natural infection of Plum pox virus and effect of mineral oil treatments. *Annals of Applied Biology* 157: 447–457. https://doi.org/10.1111/j.1744-7348.2010.00436.x

Vidal E., Zagrai L.A., Malinowski T., Soika G., Warabieda W., Cambra M., 2020. Statistical model for Plum pox virus prediction in *Prunus* nursery blocks using vector and virus incidence data in four different European ecological areas. *Annals of Applied Biology* 177(3): 308–324. https://doi.org/10.1111/aab.12617

Waterworth H. E., Hadidi A., 1998. Economic losses due to plant viruses. In: *Plant Virus Disease Control* (A. Hadidi, R. K. Khetarpal, H. Koganezawa, ed.) APS Press, St. Paul, MN, USA, 1–13.

Welliver R., Valley K., Richwine N., Clement G., Albright D., 2014. Expelling a Plant Pest Invader: The Pennsylvania Plum Pox Eradication Program, A Case Study in Regulatory Cooperation. Posted September 2014. PennState, Pennsylvania Department of Agriculture and APHIS. Accessed January 20, 2024, from https://www.agriculture.pa.gov/Plants_Land_Water/PlantIndustry/plant-protection/PlumPox/Documents/PA%20PPV%20Eradication%209-2014.pdf

Xing F., Wang H.Q., Li S. 2017. Risk assessment of Plum pox virus in China. *Acta Horticulturae* 1163: 141–146. https://doi.org/10.17660/ActaHortic.2017.1163.21

Zhou J., Xing F., Wang H., Shifang L., 2021. Occurrence, distribution and genomic characteristics of plum pox virus isolates from common apricot (*Prunus armeniaca*) and Japanese apricot (*P. mume*) in China. *Plant Disease* 105(11): 3474-3480. https://doi.org/10.1094/PDIS-09-20-1936-RE

Research Papers

Identification of powdery mildew on *Prunus rufoides* in China, caused by *Podosphaera prunigena*

ORCID:
ZW: 0000-0001-8734-1729
WL: 0000-0002-0983-7910
YH: 0009-0002-8988-9012
KF: 0009-0000-4501-7883
LL: 0000-0001-8044-1006
TF: 0009-0007-4913-6370
QY: 0009-0001-5237-0586
GW: 0009-0004-1767-0817

Zhilong WANG[1,*], Wen LI[1], Yueqiu HE[1], Feng LIU[1], Kai FENG[1], Liang LIU[1], Tao FU[1], Qi YE[1], Guoliang WANG[2]

[1] *Ningbo City College of Vocational Technology, Ningbo Zhejiang, 315000, China*
[2] *College of Biological and Environmental Sciences, Zhejiang Wanli University, Ningbo Zhejiang, 315000, China*
*Corresponding author. E-mail: wangzhl01@163.com

Summary. *Prunus rufoides* is a deciduous wild tree, native to China, which is also used as an ornamental. From late March to December in the years 2018 to 2023, *P. rufoides* plants growing in Siming Mountain (29°71'08"N, 121°15'12"E), Ningbo, Zhejiang Province, were severely affected by powdery mildew. The disease initially emerged in late March each year, and was characterized as white, irregular mycelial patches on the adaxial surfaces of young leaves. Between July and August, the powdery mildew colonies on affected parts of leaves disappeared, leaving only irregular yellow-brown spots. The disease recurred in September and persisted until late December. Chasmothecia containing asci and ascospores were observed on the leaves in December. Morphological analyses of the chasmothecia indicated a *Podosphaera* sp. as the causative agent. Molecular identification, based on the internal transcribed spacer (ITS) region (primers ITS4/ITS5) confirmed the identity of the pathogen as *Podosphaera prunigena*. Koch's postulates were fulfilled by inoculation tests in which the same pathogen was identified from the inoculated leaf tissue. This study represents the first report confirming the powdery mildew disease on *P. rufoides* in China to be caused by *P. prunigena*.

Keywords. *Erysiphaceae*, morphology, molecular analysis, taxonomy.

INTRODUCTION

Cerasus is classified as a subgenus of *Prunus* L. (*Rosaceae*), and is primarily distributed in tropical and subtropical regions (Willis, 1985; Mabberley, 1997). Most species within this subgenus are important for their ornamental and economic values, and these plants include *P. avium* (L.)L. (sweet cherry), *P. pseudocerasus* Lindl. (Chinese cherry), *P. serrulata* Lindl. (Japanese cherry), and *P. cerasoides* Buch.-Ham. ex D.Don (Lee and Wen, 2001). *Prunus rufoides* C.K.Schneid., originally described from China, is widely distributed and is an important flowering tree species in early spring (Wang, 2014; Zhu *et al.,* 2018).

Powdery mildews are widespread, common, and detrimental diseases on plant species, including *Prunus* spp., which can lead to substantial economic losses (Frye and Innes, 1998). Some species of *Podosphaera* are known to cause diseases on *Rosaceae* hosts. Notably, *Po. clandestina*, *Po. leucotricha*, and *Po. pannosa*, are important and frequently occurring species that cause powdery mildews on cultivated plants (Braun and Cook, 2012; Hubert *et al.*, 2012; Farr and Rossman, 2019). Among *Prunus* spp. hosts, *Po. tridactyla* (*s. lat.*) has been identified as the most common species causing powdery mildew (Braun and Cook, 2012; Meeboon *et al.,* 2015). In a recent morpho-phylogenetic analysis of *Po. tridactyla s. lat.*, Meeboon *et al.* (2020) proposed dividing this organism into ten species, comprising seven new species and three previously recognized species. These authors identified *Po. prunigena* as one of the seven new species. *Podosphaera prunigena*, an Asian species on hosts of *Prunus* sub gen. *Cerasus*, is distinct from *Po. tridactyla s. str.* in morphology and phylogenetic characteristics. This pathogen has been reported on three *Prunus* host species including *P. apetala*, *P. leveilleana*, and *P. serulata* (Meeboon *et al.,* 2020). Shirouzu *et al.* (2020) reported *Po. prunigena* on *Cerasus kumanoensis* in Japan, and amended the circumscription of this powdery mildew species, including detailed description of the anamorph.

From 2018 to 2023, symptoms of powdery mildews were observed on *P. rufoides* trees in Siming Mountain, Ningbo, China. The disease predominantly affected 1-year-old plants in a nursery, with more than 80% of cherry plants infected by this fungus. To identify the pathogen, cherry leaf samples were collected and examined in a laboratory. Morphological, molecular, and pathogenicity tests were carried out, to provide information for development of effective disease management strategies.

MATERIALS AND METHODS

Plant material and pathogen Isolation

The infected leaf samples were deposited in the Herbarium of Ningbo City College of Vocational Technology, under the accession number NBCC2018016. Morphological analysis of the pathogen was carried out using the procedure outlined by Meeboon and Takamatsu, 2020. Mycelium and chasmothecia were taken from infected leaf surfaces using a clean needle and mounted on microscope slides. All samples were examined in water. Fifty conidia, chasmothecia, ascospores, and asci were measured, and photographs were taken using a light microscope (Leica DM3000), and dimensions of the fungal structures were measured.

Pathogenicity tests

Twenty 1-year-old healthy *P. rufoides* plants were each inoculated with a 1×10^8 mL^{-1} suspension of conidia. Ten healthy plants were treated with sterile distilled water served as negative experimental controls. The *P. rufoides* plants were grown in a greenhouse chamber for 1 year using the shoot cutting method. Prior to fungal inoculations, plant leaves were washed in sterilized water to remove adhering soil and were then air-dried. Inoculated plants were maintained in a greenhouse chamber at 25°C with a 12 h light 12 h dark daily cycle. Different treatment groups were separated to prevent cross-contamination. Symptoms were observed 9 to 10 d post-inoculation. Disease symptom observations, and morphological and molecular analyses of the fungus, were carried out as described above. All plant disease characteristics on inoculated leaves were compared with those of the initially affected greenhouse plants.

Pathogen DNA extraction, amplification, and sequencing

The genomic DNA was extracted separately from mycelium and chasmothecia, using the cetyl trimethyl ammonium bromide (CTAB) method (Doyle, 1991). DNA concentrations were measured using a NanoDrop 2000 OneC Microvolume UV-Vis Spectrophotometer (Thermo Scientific). Polymerase chain reaction (PCR) and DNA sequencing were carried out as follows: DNA was diluted to a concentration of 100 ng µL^{-1} in water. Each 50 µL PCR reaction contained 2.5 µL of template DNA, 2.5 µL of each forward and reverse primer, 25 µL of Taq buffer, 5 µL of DNA polymerase, and 12.5 µL of dd H$_2$O (Li *et al.,* 2021). The primer pairs used were ITS4 and ITS5 (White *et al.,* 1990; Kusaba and Tsuge, 1995). The PCR amplification process included an initial denaturation at 95°C for 5 min, followed by 34 cycles each of 95°C for 30 sec, 55°C for 30 sec, and 72°C for 1 min, a final extension at 72°C for 10 min, and a 4°C hold. The PCR products were visualized through gel electrophoresis on a 1.5% agarose gel with a TAE running buffer containing 4S Green Plus Nucleic Acid Stain (Sangon Biotech Co., Ltd.). The results were captured using a gel documentation system equipped with a digital camera (UVP GelDoc-It2 Image System). The expected bands were excised and purified using the SanPrep Column DNA Gel Extraction Kit (B518131-0050, Sangon Biotech Co., Ltd.,), following the manufacturer's instructions. The samples were subsequently sent for sequencing to Tsingke Biotechnology Co., Ltd. The obtained sequences were initially analyzed using NCBI-BLAST-Nucleotide BLAST, available at https://blast.ncbi.nlm.

Table 1. Specimen and accession numbers of sequences used for phylogenetic analyses.

| *Podosphaera* spp. and vouchers	GenBank accession number of ITS
Podosphaera longiseta	AB000945.1
Podosphaera pruni-avium voucher 47899	MK530456.1
Podosphaera pruni-cerasoidis voucher 6861	MK530447.1
Podosphaera prunigena isolate WZL09	MT820800
Podosphaera prunigena TNS: F-89227	LC529409.1
Podosphaera prunigena	AB026147.1
Podosphaera prunigena voucher 5266	MK530446.1
Podosphaera pruni-japonicae	AB000943.1
Podosphaera pruni-lusitanicae voucher VPRI 22158	AY833655.1
Podosphaera prunina KUSF26292	JQ517296.1
Podosphaera prunina voucher 5209	MK530442.1
Podosphaera salatai	AB525929.1
Podosphaera sibirica MUMH303	AB026144.1
Podosphaera tridactyla	AF011318.1
Podosphaera tridactyla voucher 65909	MK530463.1
Podosphaera xanthii voucher MUMH68	D84387.1

nih.gov/Blast.cgi. The sequences generated from the ITS region were aligned with other *Podosphaera* sequences using ClustalW (Larkin *et al.,* 2007). The sequence data were deposited in GenBank, and the accession numbers were obtained from https://www.ncbi.nlm.nih.gov/gen-bank/. Phylogenetic analyses were conducted on the data using the Maximum likelihood method. The sequences were first aligned using the Clustal W method, and then the phylogenetic analysis was carried out in MEGA7, with a bootstrap value of 1000 (Kumar *et al.,* 2016).

RESULTS

Disease symptoms and morphological characterization

From 2018 to 2023, the *P. rufoides* plants growing in Siming Mountain exhibited severe powdery mildew symptoms. The disease began in late March to early April each year, mainly affecting the young cherry blossom plants, including leaves, petioles, and young shoots, especially the tender leaves which were most susceptible to the disease (Figure 1, A, B and C).The affected areas initially had chlorotic spots with indistinct margins, which gradually expanded, and white powdery mildew colonies developed on these spots (Figure 1 D). In severe cases, these patches merged, and caused defoliation. Between July and August, the white powdery mildew colonies on the affected parts disappeared, leaving irregular yellow-brown leaf spots (Figure 1 E). In September, white powdery mildew colonies re-appeared on the diseased leaves, and persisted until December. By the end of December, small brown dots were visible on the leaf spots, and were identified as the teleomorph of the pathogen (chasmothecia). These were accompanied
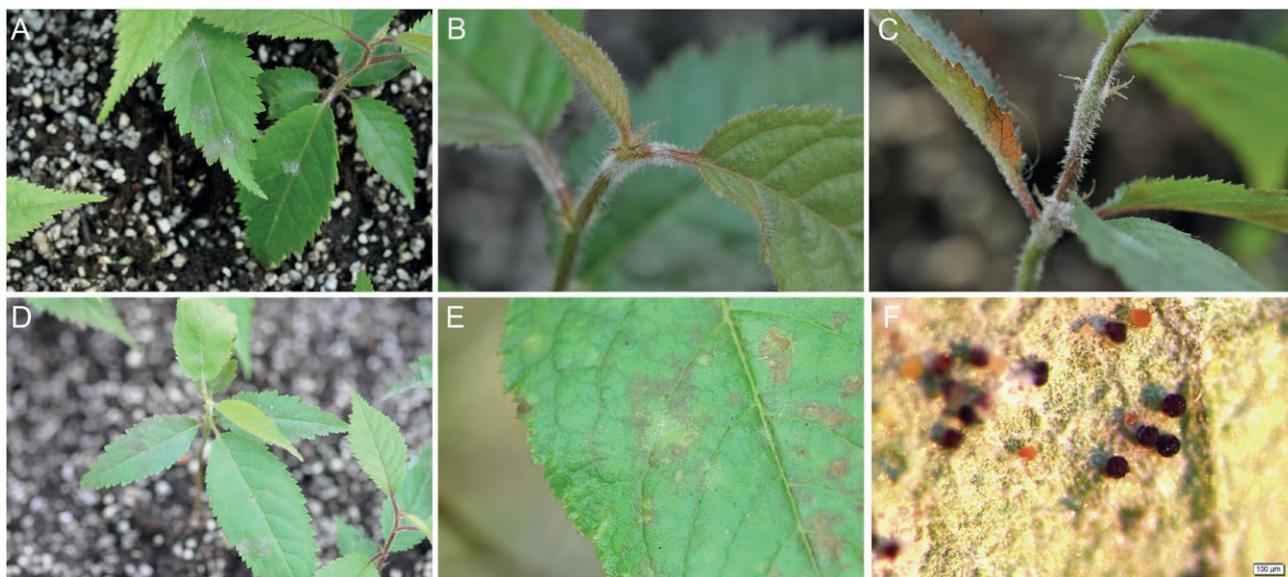
Figure 1. A, B and C. Disease symptoms on *Prunus rufoides* leaves, petioles and young shoots infected by *Podosphaera prunigena*. D. The affected areas show chlorotic spots with indistinct margins at edges the initial infection stage. E. Irregular yellow-brown spots on a leaf between July and August. F. Chasmothecia on the fallen cherry blossom leaf.

Figure 2. Morphology of *Podosphaera prunigena*, isolate WZL09. A, conidia. B, conidiophore with foot-cell. C, chasmothecium. D, chasmothecium appendage. E, ascus. F, ascospore with germ tube. Scale bars: A, B, E, and F = 10 μm; C and D = 20 μm.

by re-emergence of white mycelium until December, when the chasmothecia on fallen host leaves became mature, forming asci and ascospores (Figure 1 F). Leaves from diseased plants tended to detach earlier than those from healthy plants. The disease predominantly affected 1-year-old plants in a nursery, with more than 80% of the cherry plants infected by the fungus.

A voucher specimen affected by the pathogen was deposited at the in School Landscape Ecology of City College of Vocational Technology·Utilization of Ningbo (Accession WZL09).

To identify the causal agent of this disease, morphological examination was conducted on 20 infected leaves. The hyphae and conidia were hyaline. The foot cells of the conidiophores were straight, cylindrical, and measured 28–62 × 7–10 μm (n = 50) (Figure 2 B). The conidia were ellipsoid to ovate, measuring 20–32 × 14–21 μm (n = 50) (Figure 2 A). The conidia were produced in chains and contained well-developed fibrosin bodies. Conidium germ tubes were simple and lateral (Figure 2 F). Chasmothecia were each globose or depressed globose, with a diameters of 60–110 μm (average 81.9 μm; n = 100) (Figure 2 C), and had the chasmothecia had 2 to 5 appendages in the upper halves, and these were gregarious, straight or somewhat curved, were of dimensions 90–180 × 8–10 μm (n = 50), and each appendage had a 1–4 septate thick-walled stalk, with septae throughout or only in the lower half. The stalks were brown in the lower parts, and apices that were 3 to 5 times regularly and dichotomously branched. Tips of the ultimate branchlets were knob-like, and not recurved (Figure 2 D). Each ascus was

subglobose to broad ellipsoid-ovoid, measuring 58–94 × 50–83 μm (n = 40), with a thick wall (4–5 μm), and contained eight ascospores (Figure 2 E). The ascospores were ellipsoid-ovoid to subglobose, 16–25 × 12–18 μm (n = 50), and colourless.

The morphological characteristics of the pathogen suggested it was a species of *Podosphaera* sect. *Podosphaera* subsect. *Tridactyla* [*Podosphaera tridactyla* complex] (Braun and Cook, 2012), and molecular identification was performed to determine the species of the pathogen.

Pathogenicity testing

All inoculated leaves developed powdery mildew within 9 to 10 d post-inoculation, while the control plants remained asymptomatic (Figures. 3, A and B). Specimens from the inoculated plants showed that the fungus on the infected leaves was identical to that originally observed on the naturally infected plants. Molecular analyses confirmed the identity of the fungus with that of the inoculated fungus. These results fulfilled Koch's postulates for the inoculated pathogen.

Phylogenetic analysis

To confirm the morphological identification of the pathogen, genomic DNA from mycelium and chasmothecia was extracted independently, and the internal transcribed spacer (ITS) region along with a portion
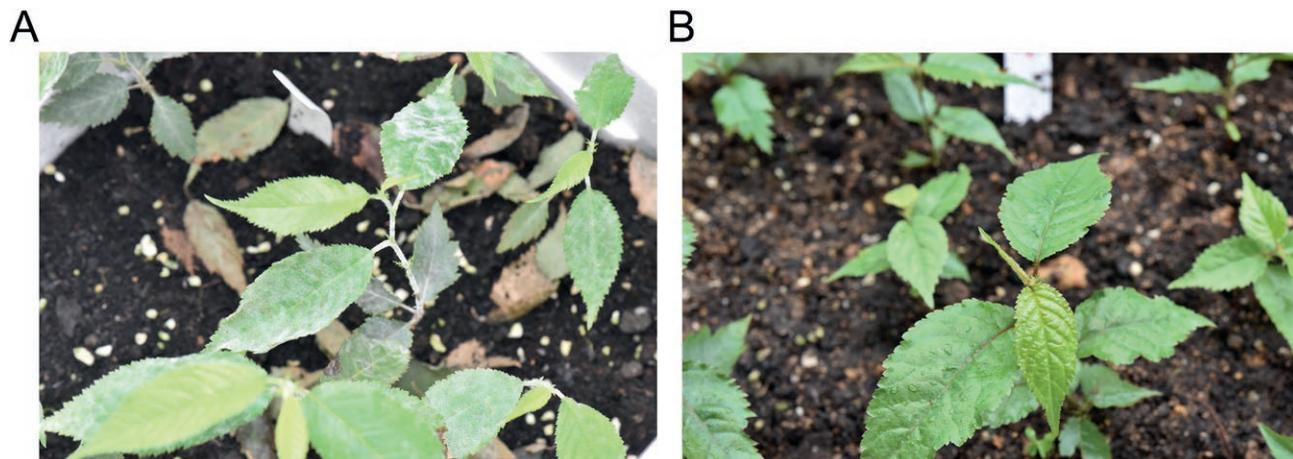
Figure 3. Pathogenicity test. Koch's postulates were fulfilled after inoculating 20 *Prunus rufoides* plants with powdery mildew (A) or with sterilized water (B). These photographs were taken at 10 d post inoculation.

of the 28S gene were amplified using polymerase chain reaction (PCR) and sequenced. The results indicated that the ITS sequences from mycelium and chasmothecia were identical, confirming that the anamorph and teleomorph were one species. The ITS sequence was deposited in GenBank (accession number MT820800). BLAST analysis showed that the ITS sequence had 99% similarity with *Po. prunigena* voucher 5266 (1166/1168, 99%, MK530446). To further confirm this phylogeny, ITS sequences from 15 other *Podosphaera* strains were retrieved from the NCBI database. A phylogenetic tree

was constructed using bootstrap analysis with 1,000 replicates in MEGA 7. The other *Podosphaera* strains used in the phylogenetic analysis are listed in Table 1.

The fungus formed a strongly supported clade with *Po. prunigena* (GenBank: AB026147, LC529409 and MK530446) (Figure 4). Two additional strains, *Po. xanthii* and *Po. sibirica* MUMH303, were used as outgroups. In conjunction with the morphological analyses described above, it was concluded that the powdery mildew found in China on *Prunus rufoides* was caused by *Po. prunigena*.
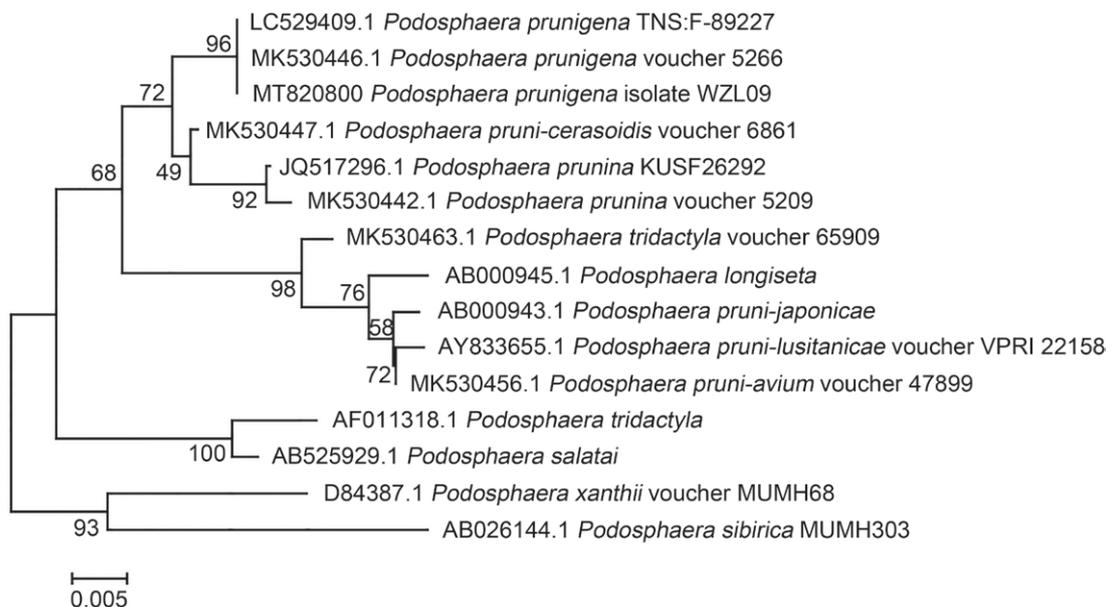
Figure 4. This phylogenetic tree was constructed in MEGA 7. These results inferred from the ITS sequences positioned the sequence obtained from powdery mildew on *Prunus rufoides* in China within the *Podosphaera prunigena* clade.

Table 2. Characteristics of five *Podosphaera* strains.

Name	Conidia	Foot-cells	Chasmothecia	Appendages	Ascus	Ascospores	Host	References
Podosphaera prunigena WZL09	20 to 32 × 14 to 21 µm	28 to 62 × 7 to 10 µm	60 to 110 µm	2 to 5, 90–180 × 8–10 µm	58–94 × 50–83 µm	16–25 × 12–18 µm	*Prunus rufoides*	The present study
Podosphaera prunigena Meeboon, S. Takam. & U. Braun, sp. nov.	-	-	100 to 130 µm	3 to 5, 85–205× 8–11.5 µm	87.5–100 × 73–78 µm	30–35 × 17–25 µm	*Prunus apetala*	Meeboon *et al.* (2020)
Podosphaera prunigena	-	-	75 to 95 µm	–	65–81 × 50–69 µm	18.5–27 × 10.5–12 µm	*Cerasus kumanoensis*	Shirouzu *et al.* (2020)
Podosphaera tridactyla voucher 65909 (= *Po. prunina*)	20 to 32 × 14 to 21 µm	28 to 62 × 7 to 10 µm	65 to 112 µm	2 to 4, –	66–86 × 47–76 µm	15–27 × 12–18 µm	*Prunus hypoleuca*	Bai *et al.* (2015); Meeboon *et al.* (2020)
Podosphaera wuyishanensis Z.X. Chen et Yao	-	-	80 to 110 µm	1 to 2, × 7.5–9 µm	75–97.5 × 67.5–90 µm	20–24 × 32.5–12.5 µm	*Prunus fukienensis* Yu et Ku	Chen and Yao, (1989)

DISCUSSION

Powdery mildews can cause widespread and severe diseases of wild and cultivated plants, and can reduce host growth and cause economic losses. Several studies have shown the pathogenicity of powdery mildews on *Prunus* spp. (Chen and Yao, 1989; Schulze-Lefert and Vogel, 2000; Bai *et al.,* 2015). In the present study, the powdery mildew WZL09 was examined, which caused severe disease on *P. rufoides* plants, primarily affecting 1-year-old cherry plants in a nursery in China. Based on morphology of the pathogen and results of sequence analyses, the causative agent of this powdery was identified as *Podosphaera prunigena*. This is the first unequivocal record of this species from China, with *P. rufoides* as a new host. The retrieved sequence clustered within the *Po. prunigena* clade. Morphology of chasmothecia found on *P. rufoides* agree with the original description of this species by Meeboon *et al.* (2020), except that the pathogen examined here had much smaller chasmothecia, which were described by Meeboon *et al.* (2020) to be 100 to 130 µm in diameter. However, Shirouzu *et al.* (2020) published an emended description for *Po. prunigena*, with chasmothecia of diameter 75 to 95 µm, which is similar to dimensions for the Chinese specimens. The amended description of *Po. prunigena* by Shirouzu *et al.* (2020) was based on a re-examination of type material of this species, and measurements of Japanese material found on *Cerasus kumanoensis*. This showed the size of the chasmothecia was incorrect in the Meeboon *et al.* (2020) description.

Podosphaera tridactyla and *Po. wuyishanensis* are in the *Po. tridactyla* complex that has also been reported on *Prunus* spp. in China. As shown in Table 1, a sequence obtained from a Chinese specimen of *Po. tridactyla s. lat.* on *Prunus hypoleuca* reported by Bai *et al.* (2015) was included the phylogenetic taxonomic revision of the *Po. tridactyla* complex, and was shown to belong to *Po. prunina*. Other older records of *Po. tridactyla s. lat.* cannot be compared with *Po. prunigena* since they refer to the heterogenous *Po. tridactyla* complex which has been divided into numerous species. Sequences for *Po. wuyishanensis* are not yet available in GenBank, but this species is unique and morphologically clearly distinguished from all other species of the *Po. tridactyla* complex by having only 1-2(-3) terminal cleithothecial appendages.

Flowering cherries, including *P. rufoides*, are popular ornamental plants, that have aesthetically beautiful flowers in early spring. The powdery mildew caused by *Po. prunigena* can infect cherry leaves from early spring to late autumn. This disease leads to early host defoliation and affects the growth and ornamental value of cherry plants, resulting in substantial losses for farmers and the industries involved. The present study has identified the pathogen causing powdery mildew on *P. rufoides*, which is information to support evaluation of appropriate methods to control this disease.

LITERATURE CITED

Bai L.C., Cao Z.M., Li P.Q., Liang C., 2015. First report of powdery mildew *Podosphaera tridactyla* on *Prunus hypoleuca* in China. *Plant Disease* 99(2): 289. https://doi.org/10.1094/PDIS-09-14-0914-PDN

Braun U., Cook R.T.A., 2012. *The Taxonomic Manual of the* Erysiphales *(Powdery Mildews)*. CBS Biodiversity Series No. 11. CBS-KNAW Fungal Biodiversity Centre, Utrecht, 707.

Chen Z.X., Yao Y.J., 1989. *Podosphaera wuyishanensis* Z. X. Acta. *Mycologica Sinica* 8(4): 256–258. https://doi.org/10.13346/j.mycosystema

Doyle J., 1991. DNA protocols for plants. In: Molecular Techniques in Taxonomy. Berlin Heidelberg: Springer; 283–293.

Farr D.F., Rossman A.Y. U.S., National Fungus Collections, ARS, USDA. Fungal Databases. Available at: https://nt.ars-grin.gov/fungaldatabases/

Frye C.A., Innes R.W., 1998. An *Arabidopsis* mutant with enhanced resistance to powdery mildew. *Plant Cell* 10(6): 947–956. https://doi.org/10.1105/tpc.10.6.947

Hubert J., Fourrier C., Payen C., Fournie J.L., Loos R., 2012. First report of powdery mildew caused by *Podosphaera pannosa* on *Prunus cerasus* in France. *Plant Disease* 96(9): 1375–1375. https://doi.org/10.1094/PDIS-02-12-0218-PDN

Kumar S., Stecher G., Tamura K., 2016. MEGA7: Molecular Evolutionary Genetics Analysis version 7.0 for bigger datasets. *Molecular Biology and Evolution* 33: 1870–1874. https://doi.org/10.1093/molbev/msw054

Kusaba M., Tsuge T., 1995. Phylogeny of *Alternaria* fungi known to produce host-specific toxins on the basis of variation in internal transcribed spacers of ribosomal DNA. *Current Genetics* 28(5): 491–498. https://doi.org/10.1007/BF00310821

Larkin M.A., Blackshields G., Brown N.P., Chenna R., McGettigan P.A., Higgins D.G., 2007. ClustalW and ClustalX version 2. *Bioinformatics* 23: 2947–2948. https://doi.org/10.1093/bioinformatics/btm404

Lee S., Wen J., 2001. A phylogenetic analysis of *Prunus* and the *Amygdaloideae* (*Rosaceae*) using ITS sequences of nuclear ribosomal DNA. *American Journal of Botany* 88(1): 150–160. https://doi.org/10.2307/2657135

Li W., He Y.Q., Wang J.Y., Wang G.L., Wang Z.L., 2021. Isolation and identification of pathogen causing anthracnose on *Zinnia elegans* Jacq. and fungicides screening. *Chinese Journal of Pesticide Science* 23(2): 341–347. https://doi.org/10.16801/j.issn.1008-7303.2021.0017

Mabberley D.J., 1997. *The Plant-book, a Portable Dictionary of the Vascular Plants*. 2nd ed. Cambridge University Press, Cambridge, UK.

Meeboon J., Takamatsu S., 2015. *Erysiphe takamatsui*, a powdery mildew of lotus: rediscovery of teleomorph after 40 years, morphology and phylogeny. *Mycosphere* 56: 159–167. https://doi.org/10.1016/j.myc.2014.05.002

Meeboon J., Takamatsu S., Braun U., 2020. Morphophylogenetic analyses revealed that *Podosphaera tridactyla* constitutes a species complex. *Mycologia* 112(2): 244–266. https://doi.org/10.1080/00275514.2019.1698924

Schulze-Lefert P., Vogel J., 2000. Closing the ranks to attack by powdery mildew. *Trends in Plant Science* 5(8): 343–348. https://doi.org/10.1016/S1360-1385(00)01683-6

Shirouzu T., Fujita A., Nakamura M., Takamatsu S., 2020. *Podosphaera prunigena* occurred on leaves of *Cerasus kumanoensis* and its emended description. *Japanese Journal of Mycology* 61: 33–39. https://doi.org/10.18962/jjom.jjom.R01-12

Wang X.R., 2014. *An Illustrated Monograph of Cherry Cultivars in China*. Beijing, China, Science Press.

White T.J., Bruns T., Lee S., 1990. *PCR Protocols: A Guide to Methods and Applications*. Academic Press, San Diego, CA, USA, 315.

Willis J.C., 1985. A dictionary of the flowering plants and ferns. 8th ed. Cambridge, UK: Cambridge University Press.

Zhu H., Zhu S.X., Li Y.F., Wang X.R., 2018. Leaf phenotypic variation in natural populations of *Cerasus dielsiana*. *Chinese Journal of Plant Ecology* 42(12): 1168–1178. https://doi.org/10.17521/cjpe.2018.0196

ORCID:
IM: 0000-0001-8045-240X
VB: 0000-0003-4757-8339
GP: 0000-0001-8630-2760
VG: 0000-0003-3188-7743
EL: 0000-0001-6981-6364

New or Unusual Disease Reports

Colletotrichum fioriniae, causal agent of postharvest avocado fruit rot in Southern Italy

Ilaria MARTINO[1], Roberto SORRENTINO[2], Giulio PICCIRILLO[2], Valerio BATTAGLIA[2], Giancarlo POLIZZI[3], Vladimiro GUARNACCIA[1,4,*], Ernesto LAHOZ[2]

[1] *Department of Agricultural, Forest and Food Sciences (DISAFA), University of Torino, Largo Braccini 2, 10095 Grugliasco (TO), Italy*
[2] *Research Center for Cereal and Industrial Crops - Council for Agricultural Research and Economics (CREA-CI), Via Torrino 3, 81100 Caserta (CE), Italy*
[3] *Department of Agriculture, Food and Environment (Di3A), University of Catania, Catania 95123 (CT), Italy*
[4] *Interdepartmental Centre for Innovation in the Agro-Environmental Sector, AGROINNOVA, University of Torino, 10095 Grugliasco (TO), Italy*
*Corresponding author. E-mail: vladimiro.guarnaccia@unito.it

Summary. *Colletotrichum* includes pathogens affecting different plant hosts in tropical, subtropical, and temperate regions. Anthracnose caused by these pathogens is a prevalent and severe postharvest disease of tropical fruits, including avocado. In 2021, avocado fruit with typical anthracnose symptoms was found during storage, and on very ripe fruit, in Caserta, Campania region, Italy. Avocado cultivation and production is increasing in this region, so the etiology of this disease was examined. Molecular and phylogenetic analyses on four genomic loci (ITS, *gapdh*, *act* and *tub2*) combined with morphology identified selected representative isolates as *Colletotrichum fioriniae*, in the *C. acutatum* species complex. Pathogenicity of isolates was confirmed by inoculating them on healthy avocado fruit (cv. Pinkerton). This is the first report of *C. fioriniae* causing post-harvest fruit rot on avocado in Italy. This pathogen merits further epidemiological and ecological investigations, to provide basic knowledge supporting development of management of its spread and mitigating possible impacts on avocado production.

Keywords. Anthracnose, *Colletotrichum acutatum* species complex, *Persea americana*.

INTRODUCTION

Avocado (*Persea americana* Mill.) is native to Mexico, and is cultivated in tropical and subtropical regions, with Spain, Portugal and Greece as the three major European countries for commercial production (FAOSTAT, 2024). In Italy, avocado plants were initially introduced for ornamental purposes; then, they began to be cultivated along the coasts, where climatic conditions were favourable for their growth (Guarnaccia *et al.*, 2016). During recent years, the increasing demand of avocado fruit, mainly due to their health benefits, has resulted in increased avocado cultivation, with Sic-

ily, Calabria, Campania, Puglia and Sardinia currently being main productive regions of the Italian peninsula (Migliore *et al.*, 2017).

Colletotrichum pathogens are ranked eighth in terms of economic damage and importance, causing anthracnose, leaf spots, shoot dieback and postharvest rot and decay on many tropical and temperate fruit types (Dean *et al.*, 2012; Aiello *et al.,* 2015; Guarnaccia *et al.*, 2021a; 2021b). Twenty *Colletotrichum* spp., belonging to the gloeosporioides, acutatum, boninense, gigasporum, dematium and magnum Species Complexes (SC), have been reported affecting avocado in the main productive countries, including Australia, Chile, China, Colombia, Israel, Italy, Mexico, Turkey and New Zealand (Guarnaccia *et al.*, 2016; Sharma *et al.*, 2017; Giblin *et al.*, 2018; Fuentes-Aragón *et al.*, 2020; Hofer *et al.*, 2021; Bustamante *et al.*, 2022; USDA, Fungal Database, 2024). Symptoms on avocado leaves are usually yellow spots and necrotic lesions at the tips or between veins. Fruit symptoms develop around lenticels as small brown to black lesions that become larger and sunken after harvest (Talhinhas and Baroncelli, 2023).

In March 2021, avocado fruit originating from trees cultivated in an experimental orchard at the Centre for Olive, Fruit and Citrus Crops located in Caserta (Campania, Italy) showed typical symptoms of anthracnose and *Colletotrichum* spp. infections after 10 d storage at 18 ± 2°C. Because of the diversity of *Colletotrichum* spp. reported on avocado, the present study aimed to identify and characterize the causal agent of this post-harvest disease, through molecular and phylogenetic analyses, assessment of morphological features, and pathogenicity tests.

MATERIALS AND METHODS

Isolation and morphological observations

Forty symptomatic mature avocado fruits were obtained from the experimental orchard at the Centre for Olive, Fruit and Citrus Crops, located in Caserta (41°04'24.5"N, 14°19'04.7"E). Small sections (3×3 mm diam.) were excised with a scalpel from the margins of circular spots. The fragments were surface disinfected three times in a 2% sodium hypochlorite solution for 1 min, then rinsed in sterile distilled water (SDW) for 1 min, dried in laminar flow cabinet, and transferred onto potato dextrose agar (PDA, Oxoid) amended with 100 mg L^{-1} streptomycin sulphate (Merck) in Petri plates. Conidia were also harvested from the conidial masses developing on 80% of the field-collected symptomatic fruits and placed on PDA-S. All the plates were incubated in the dark at 24 ± 2°C for 2 to 3 d. Developing

colonies morphologically resembling *Colletotrichum* spp. were placed on new PDA-S plates. After 7 d, single conidium cultures were established. A total of ten isolates was obtained, and two representative isolates were used for analyses.

Morphological features of the isolates were observed on the growing colonies using a light microscope (Olympus BH-2). Culture colours were determined according to Rayner (1970). Conidia were examined by mounting fungal structures in sterile water and the length and width of 30 conidia were measured for each isolate using a light microscope at ×40 magnification. The average dimensions and standard deviations were calculated.

Molecular characterization and phylogenetic analyses

DNA was extracted from two representative isolates (GP1 and GP2) using the DNeasy Plant Mini Kit (Qiagen). The PCR reactions were each carried out with 10 ng of DNA template, with the primer pair ITS1/ITS4 (White *et al.,* 1990) to amplify the internal transcribed spacer region (ITS) of the nuclear ribosomal RNA operon, including the 3' end of the 18S rRNA, the first internal transcribed spacer region, the 5.8S rRNA gene, the second internal transcribed spacer region and the 5' end of the 28S rRNA gene. The primer pair Btub2Fd/Btub4Rd was used for amplification of part of the β-tubulin II region (Stielow *et al.,* 2015). The primer pair GDF1/GDR1 (Guerber *et al.,* 2003) was used to amplify the glyceraldehyde-3-phosphate dehydrogenase locus, and ACT512F/ACT783R (Carbone and Kohn, 1999) was used to amplify actin locus. The reactions were each prepared in a total volume of 50 μL containing 1× of reaction buffer, 200 μM of dNTPs set, 500 mM of each primer, and 1 unit of Q5 Hi-Fi DNA polymerase (New England Biolabs). Reaction tubes were incubated in the thermocycler, at 94°C for 1 min, followed by 35 cycles of 20 s at 94°C, 30 s at 58–62°C and 30 s at 72°C, and a final extension at 72°C for 5 min. Amplicons were purified using the Nucleospin Extract- Kit (Macherey-Nagel), and were sequenced by BMR Genomics (Padova, Italy). The nucleotide sequences were analysed by BLASTn (http://blast.ncbi.nlm.nih.gov/Blast.cgi) with the default parameters described by Altschul *et al.* (1990). Reference sequences were retrieved among the closest relative species, and *Colletotrichum* spp. reported as pathogens of *P. americana* were also retrieved to obtain a taxonomic framework of the analysed isolates.

The sequences obtained were initially aligned with reference sequences using MAFFT v. 7 online server (https://mafft.cbrc.jp/alignment/server/index.html)

(Katoh and Standley, 2013) for each considered locus. A manual adjustment in MEGA v. 7 (Kumar *et al.*, 2016) was then made to determine multi-locus phylogenies based on Maximum Parsimony (MP) and Bayesian Inference (BI) criteria. Phylogenetic Analysis Using Parsimony (PAUP) v.4.0b10 (Swofford, 2003) was used for MP phylogeny. Heuristic searches with 100 random additional sequences estimated the phylogenetic relationships. Tree bisection-reconnection was used. The branch swapping option was set on "best trees" and all characters were weighted equally. Alignment gaps were considered as "fifth base". The analysis calculated the following parameters: tree length (TL), consistency index (CI), retention index (RI) and rescaled consistence index (RC). A total of 1000 replications were set for the bootstrap analyses (Hillis and Bull, 1993). For the BI analysis, MrModeltest v.2.3 (Nylander, 2004) was run to determine the best evolutionary model for each considered locus. The determined model was incorporated in the analyses performed with MrBayes v. 3.2.5 (Ronquist *et al.*, 2012) to generate phylogenetic trees, following optimal criteria for each locus. The Markov Chain Monte Carlo (MCMC) analysis started from a random tree topology, and four chains were used. The heating parameter was set at 0.3 and the sampling frequency at 1000 generations. Analyses stopped when the average standard deviation of split frequencies was below 0.01. Sequences generated in the present study were deposited in GenBank (Table 1).

Pathogenicity tests

Pathogenicity tests were carried out using the isolates GP1 and GP2, to assess fulfilment of Koch's postulates. The isolates were inoculated on wounded (1 mm diam.) fruit of *P. americana* cv. Pinkerton. The trial was conducted using ten fruit for each tested isolate. A total of 20 fruit for each isolate were washed, dipped in 1.5% sodium hypochlorite for 30 sec, rinsed twice in sterile distilled water (SDW) for 1 min and then dried on absorbent paper. Each fruit was wounded at three points with a sterile needle, and for each wound 5 μL of conidium suspension (10^4 conidia mL^{-1}) was applied. Conidium suspensions of each isolate were prepared by adding SDW to 10 day old cultures grown on PDA-S, scraping the mycelia and conidium masses and filtering the mixture through muslin cloth. Inoculation control fruits were each treated with 5 μL of SDW. After inoculation, the fruits were placed in plastic containers covered with plastic film, and were incubated in growth chamber at 25°C 100% RH for 3 d. The assay was carried out two times.

The collected fruit showed depressed circular spots, and developed orange-pink mucilaginous lumps after storage (Figure 1). The fungal colonies obtained from isolations and directly from conidium masses were identified as *Colletotrichum* spp., based on their morphologies. The cultures of the two representative isolates (GP1 and GP2) had light grey to pink mycelium with abundant salmon pink masses of conidia on the upper surfaces, and pinkish mycelium with black spots on the reverse surfaces. The conidia were hyaline, narrowly elliptical, with guttulae, and measured (mean ± SD length and width) $13 \pm 4.5 \times 3.3 \pm 1.6$ μm.

The multi-locus phylogeny, which allowed precise identification of the two representative isolates, consisted of 57 sequences, including the outgroup (*Monilochaetes infuscans*, CBS 896.96), and included a total of 1709 characters (ITS: 1–581; *gapdh*: 588–895; *act*: 902–1183; *tub2*: 1190–1709). A total of 565 characters was parsimony-informative, 349 characters were variable and parsimony-uninformative, and 767 were constant. A maximum number of 1000 equally most parsimonious trees was saved (Tree length = 2255, CI = 0.659, RI = 0.900 and RC = 0.593). Bootstrap values obtained with the MP analysis are indicated on the BI phylogenetic tree in Figure 2. For the BI analysis, the following models, recommended by MrModeltest, were used: GTR + I + G for ITS, HKY + G for *gapdh*, and GTR + G for *act* and *tub2*. In the BI analysis, the ITS locus had 159 unique site patterns, the *gapdh* locus had 255, the *act* locus had 162, and the *tub2* locus had 267 unique site patterns. The analysis ran for 1,550,000 generations, resulting in 3102 trees, of which 2327 were used to calculate the posterior probabilities. In the multi-locus analyses, the isolates GP1 and GP2 obtained from the present study clustered with three reference strains of *C. fioriniae*.

For the pathogenicity assessments, all the inoculated fruits showed symptoms similar to those observed on the sample collected in the orchard (Figure 1), while non-inoculated control fruit did not show symptoms. After 10 d post inoculation, all the fruits inoculated with the two isolates were completely rotten. The inoculated fungi were successfully re-isolated from lesions of the inoculated fruits, fulfilling Koch's postulates.

The genus *Colletotrichum* includes 340 recognised species, which are grouped into 20 species complexes, and several species belonging to this genus are pathogens of cultivated plants in tropical, subtropical and temperate regions (Dean *et al.,* 2012). In particular, anthracnose caused by *Colletotrichum* spp. is the most widespread and serious postharvest disease of many

Table 1. Details of *Colletotrichum* isolates used in phylogenetic analyses, and their corresponding GenBank accession numbers. Isolates from the present study are indicated in bold font.

Species	Code*	Country	Host species	GenBank Accession Number			
				ITS	tub2	act	gapdh
Colletotrichum acutatum	CBS 112996 t	Australia	*Carica papaya*	JQ005776	JQ005860	JQ005839	JQ948677
Colletotrichum aenigma	ICMP 18608 t	Israel	*Persea americana*	JX010244	JX010389	JX009443	JX010044
Colletotrichum aeschynomenes	ICMP 17673 t	USA	*Aeschynomene virginica*	JX010176	-	JX009483	JX009930
Colletotrichum alatae	ICMP 17919	India	*Dioscorea alata*	JX010190	-	JX009471	JX009990
Colletotrichum alienum	ICMP 12071 t	New Zealand	*Malus domestica*	JX010251	-	JX009572	JX010028
Colletotrichum asianum	ICMP 18580, CBS 130418	Thailand	*Coffea arabica*	JX010196	-	JX009584	JX010053
Colletotrichum brisbanense	CBS 292.67 t	Australia	*Capsicum annuum*	JQ948291	JQ949942	JQ949612	JQ948621
Colletotrichum chrysanthemi	CBS 126518	The Netherlands	*Carthamus* sp.	JQ948271	JQ949922	JQ949592	JQ948601
Colletotrichum chrysophilum	CMM4268 t	Brazil	*Musa* sp.	KX094252	KX094285	KX093982	KX094183
Colletotrichum cigarro	ICMP 18539 t	Australia	*Olea europaea*	JX010230	JX010434	JX009523	JX009966
Colletotrichum clidemiae	ICMP 18658	USA (Hawaii)	*Clidemia hirta*	JX010265	-	JX009537	JX009989
Colletotrichum cordylinicola	ICMP 18579 t	Thailand	*Cordyline fructicosa*	JX010226	JX010440	JX009586	JX009975
Colletotrichum cosmi	CBS 853.73 t	The Netherlands	*Cosmos* sp.	JQ948274	JQ949925	JQ949595	JQ948604
Colletotrichum costaricense	CBS 330.75 t	Costa Rica	*Coffea arabica*	JQ948180	JQ949831	JQ949501	JQ948510
Colletotrichum cuscutae	IMI 304802 t	Dominica	*Cuscuta* sp.	JQ948195	JQ949846	JQ949516	JQ948525
Colletotrichum fioriniae	ATCC 28992	USA	*Malus domestica*	JQ948297	JQ949948	JQ949618	JQ948627
Colletotrichum fioriniae	CBS 129916	USA	*Vaccinium* sp.	JQ948317	JQ949968	JQ949638	JQ948647
Colletotrichum fioriniae	CBS 293.67	Australia	*Persea americana*	JQ948310	JQ949961	JQ949631	JQ948640
Colletotrichum fioriniae	**GP1**	**Italy**	**Persea americana**	**MZ613321**	**PQ295819**	**OR767286**	**OR767287**
Colletotrichum fioriniae	**GP2**	**Italy**	**Persea americana**	**PQ283879**	**PQ295820**	**PQ295821**	**PQ295822**
Colletotrichum gloeosporioides	ICMP 17821, CBS 112999	Italy	*Citrus sinensis*	JX010152	JX010445	JX009531	JX010056
Colletotrichum godetiae	CBS 133.44 t	Denmark	*Clarkia hybrida*	MH856119	JQ950053	JQ949723	JQ948733
Colletotrichum guajavae	IMI 350839 t	India	*Psidium guajava*	JQ948270	JQ949921	JQ949591	JQ948600
Colletotrichum horii	C1180.1	Japan	*Diospyros kaki*	GQ329690	JX010450	JX009533	GQ329685
Colletotrichum indonesiense	CBS 127551 t	Indonesia	*Eucalyptus* sp.	JQ948288	JQ949939	JQ949609	JQ948618
Colletotrichum jiangxiense	GCMCC 3.17363 t	China	*Camellia sinensis*	NR_152279	OK236389	-	-
Colletotrichum karsti	CBS 106.91	Brazil	*Carica papaya*	JQ005220	JQ005654	JQ005568	JQ005307
Colletotrichum kinghornii	CBS 198.35 t	UK	*Phormium* sp.	JQ948454	JQ950105	JQ949775	JQ948785
Colletotrichum laticiphilum	CBS 112989 t	India	*Hevea brasiliensis*	JQ948289	JQ949940	JQ949610	JQ948619
Colletotrichum limetticola	CBS 114.14 t	USA	*Citrus aurantifolia*	JQ948193	JQ949844	JQ949514	JQ948523
Colletotrichum lupini	CBS 109225 t	Ukraine	*Lupinus albus*	JQ948155	JQ949806	JQ949476	JQ948485
Colletotrichum melonis	CBS 159.84 t	Brazil	*Cucumis melo*	JQ948194	JQ949845	JQ949515	JQ948524
Colletotrichum nupharicola	CBS 470.96	USA	*Nuphar polysepala*	JX010187	JX010398	-	-
Colletotrichum nymphaeae	CBS 100065	The Netherlands	*Anemone* sp.	JQ948225	JQ949876	JQ949546	JQ948555
Colletotrichum nymphaeae	CBS 129928	USA	*Fragaria × ananassa*	JQ948228	JQ949879	JQ949549	JQ948558

(Continued)

Table 1. (Continued).

| Species	Code*	Country	Host species	Genbank Accession Number			
				ITS	tub2	act	gapdh
Colletotrichum nymphaeae	CBS 231.49	Portugal	Olea europaea	JN121201	JN121288	JQ949523	JQ948532
Colletotrichum nymphaeae	IMI 370491	Brazil	Malus pumila	JQ948204	JQ949855	JQ949525	JQ948534
Colletotrichum orchidophilum	CBS 632.80 t	USA	Dendrobium sp.	JQ948151	JQ949802	JQ949472	JQ948481
Colletotrichum paxtonii	IMI 165753 t	Saint Lucia	Musa sp.	JQ948285	JQ949936	JQ949607	JQ948615
Colletotrichum perseae	CBS 141365	Israel	Persea americana	KX620308	KX620341	KX620145	KX620242
Colletotrichum phormii	CBS 118194 t	Germany	Phormium sp.	JQ948446	JQ950097	JQ949768	JQ948777
Colletotrichum pseudoacutatum	CBS 436.77 t	Chile	Pinus radiata	JQ948480	JQ950131	JQ949801	JQ948811
Colletotrichum psidii	CBS 145.29 t	Italy	Psidium sp.	JX010219	JX010443	JX009515	JX009967
Colletotrichum pyricola	CBS 128531 t	New Zealand	Pyrus communis	JQ948445	JQ950096	JQ949766	JQ948776
Colletotrichum queenslandicum	ICMP 1778	Australia	Carica papaya	JX010276	JX010414	JX009447	JX009934
Colletotrichum rhombiforme	CBS 129953 t	Portugal	Olea europaea	JQ948457	JQ950108	JQ949778	JQ948788
Colletotrichum roseum	INIA<CHL>:RGM 2685	Chile	Lapageria rosea	MK903611	MK903607	MK903604	MK903603
Colletotrichum salicis	CBS 607.94 t	The Netherlands	Salix sp.	JQ948460	JQ950111	JQ949781	JQ948791
Colletotrichum salsolae	ICMP 19051	Hungary	Salsola tragus	JX010242	JX010403	JX009562	JX009916
Colletotrichum scovillei	CBS 126529 t	Indonesia	Capsicum sp.	JQ948267	JQ949918	JQ949588	JQ948597
Colletotrichum siamense	ICMP 18578	Thailand	Coffea arabica	JX010171	-	JX009518	JX009924
Colletotrichum simmondsii	CBS 122122 t	Australia	Carica papaya	JQ948276	JQ949927	JQ949597	JQ948606
Colletotrichum theobromicola	CBS 124945	Panama	Theobroma cacao	JX010294	JX010447	JX009444	JX010006
Colletotrichum tropicale	ICMP 18653	Panama	Theobroma cacao	JX010264	JX010407	JX009489	JX010007
Colletotrichum walleri	CBS 125472 t	Vietnam	Coffea sp.	JQ948275	JQ949926	JQ949596	JQ948605
Colletotrichum xanthorrhoeae	BRIP 45094 t	Australia	Xanthorrhoea preissii	JX010261	JX010448	JX009478	JX009927
Monilochaetes infuscans	CBS 869.96	South Africa	Ipomoea batatas	JQ005780	JQ005864	JQ005843	JX546612

* t = type culture.
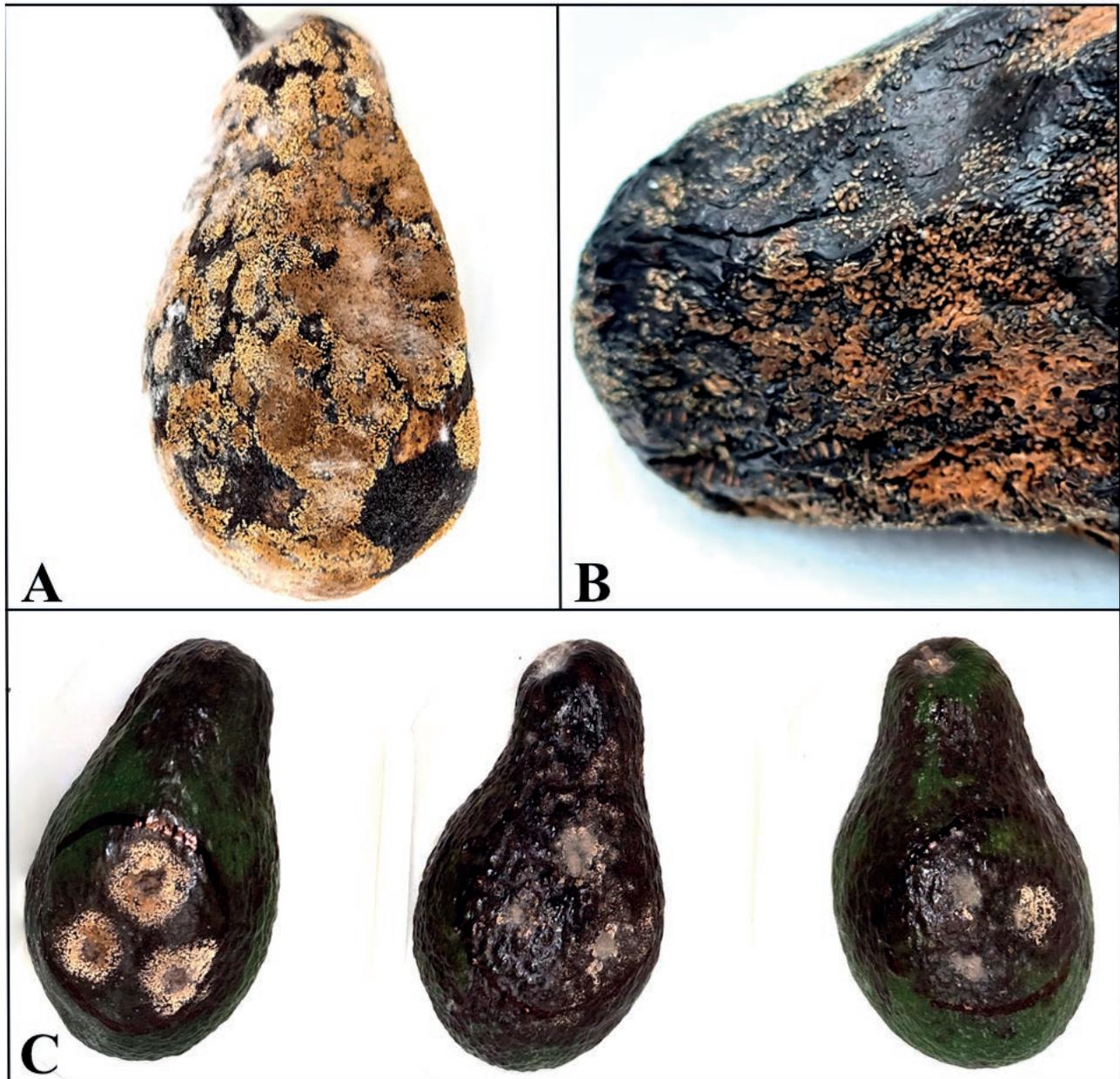
Figure 1. A and **B**, Symptomatic avocado fruit (cv. Pinkerton), showing sunken necrotic lesions and conidium masses on fruit epidermis; **C**, Avocado fruits (cv. Pinkerton) showing symptoms 7 d after inoculation with isolate GP1 of *Colletotrichum fioriniae*.

tropical fruits including avocado, lychee, mango and papaya (Zakaria, 2021; Talhinhas and Baroncelli, 2023).

Investigating the etiology of anthracnose has presented several challenges. The most reliable methods for identifying species within *Colletotrichum* involve the use of multi-locus phylogenies combined with morphological feature assessments (Bhunjun *et al.*, 2021). In the present study, the molecular and phylogenetic analyses, and morphological assessments identified the isolates found

in association with avocado fruit rot as belonging to *C. fioriniae*. In addition, pathogenicity of this species on avocado fruit was demonstrated. This is the first report of *C. fioriniae* infecting avocado in Italy.

Colletotrichum fioriniae has been previously identified from avocado in Mexico and Australia (Fuentes-Aragón *et al.*, 2020; USDA Fungal Database, 2024). In general, in recent years, *C. fioriniae* has been reported as the causal agent of fruit rot and leaf spots on sev-
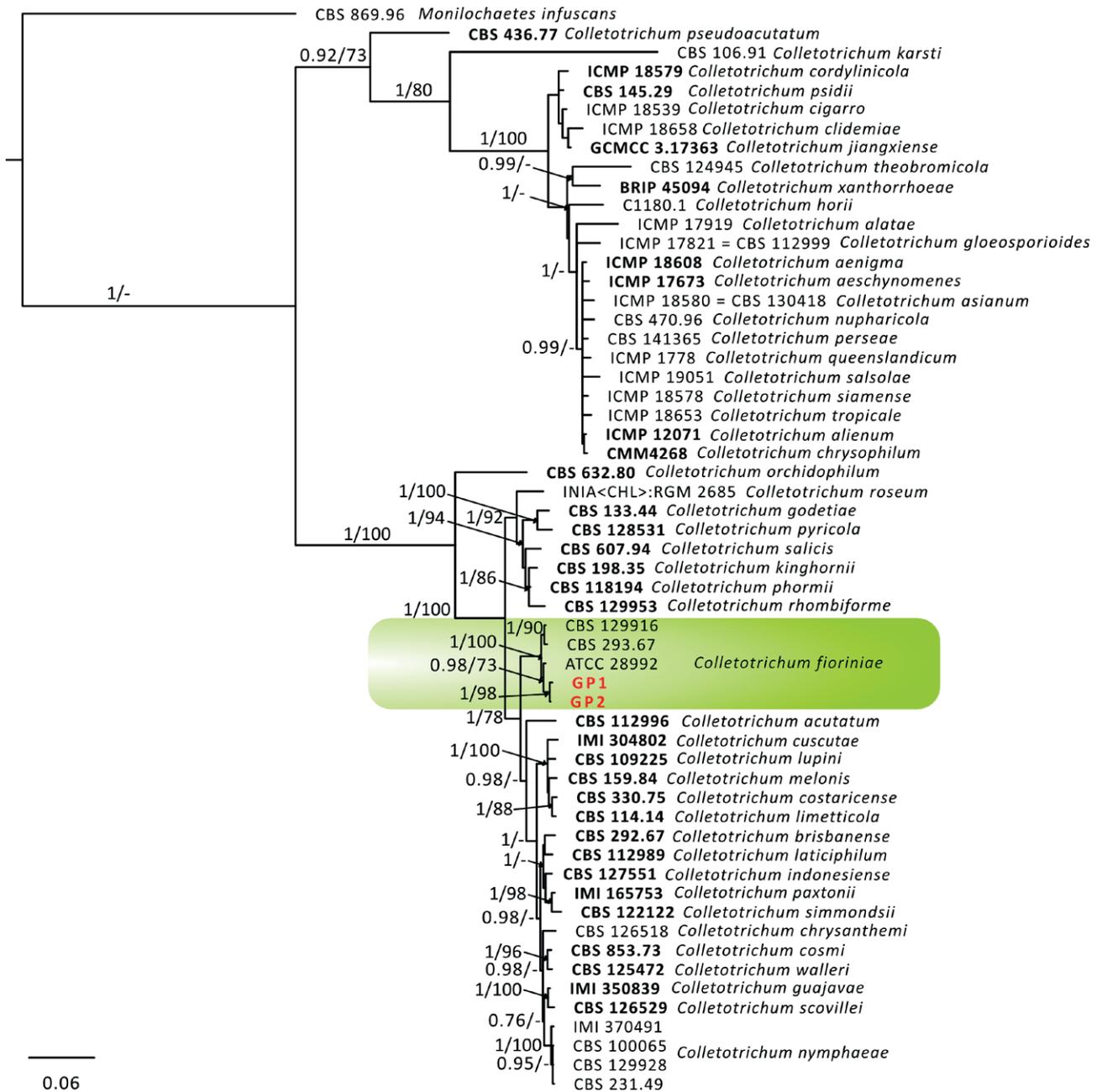
Figure 2. Consensus phylogram resulting from a Bayesian analysis of the combined ITS, *gapdh*, *act* and *tub2* sequences of *Colletotrichum* spp. Bayesian posterior probability values (BI) and Bootstrap support values (MP) are indicated at the nodes. The isolates collected and species found in the present study are indicated in red font. Ex-type strains are indicated in bold. The tree was rooted to *Monilochaetes infuscans* (CBS 869.96).

eral plant hosts, including apple, pear, peach, walnut, hazelnut and tomato (Kou *et al.,* 2014; Munda, 2014; Sezer *et al.,* 2017; Chechi *et al.,* 2019; USDA, Fungal Database, 2024). In Italy, this fungus has been reported as the causal agent of apple bitter rot (ABR), leaf spots on sage (*Salvia leucantha)* and mahonia (*Mahonia aquifolium*), and anthracnose on walnut (Guar-

naccia *et al.,* 2019; 2021a; Carneiro and Baric, 2021; Luongo *et al.,* 2022). Several of the above mentioned horticultural crops are important crops cultivated in Campania region. Thus, *C. fioriniae* infecting avocado poses a serious threat to cultivation of this host, and to other relevant host crops with possible significant economic impacts on their supply chains. Latent infec-

tions not detectable at harvest may also occur, increasing difficulty to minimize losses caused by *Colletotrichum* pathogens (De Silva *et al.*, 2017). Further investigations should be carried out to determine possible cross-infection patterns considering other possible hosts, and to understand effects of the mild climate of Southern Italy on plant-pathogen interactions and disease development to investigate the epidemiology and eventual spread of *C. fioriniae*.

ACKNOWLEDGEMENT

LITERATURE CITED

Aiello D., Carrieri R., Guarnaccia V., Vitale A., Lahoz E., Polizzi G., 2015. Characterization and pathogenicity of *Colletotrichum gloeosporioides* and *C. karstii* causing preharvest disease on *Citrus sinensis* in Italy. *Journal of Phytopathology* 163: 168–177. https://doi.org/10.1111/jph.12299.

Altschul S.F., Gish W., Miller W., Myers E.W., Lipman D.J., 1990. Basic local alignment search tool. *Journal of Molecular Biology* 215: 403–410. https://doi.org/10.1016/S0022-2836(05)80360-2.

Bhunjun C.S., Phukhamsakda C., Jayawardena R.S., Jeewon R., Promputtha I., Hyde, K.D., 2021. Investigating species boundaries in *Colletotrichum*. *Fungal Diversity* 107: 107–127. https://doi.org/10.1007/s13225-021-00471-z

Bustamante M.I., Osorio-Navarro C., Fernández Y., Bourret T.B., Zamorano A., Henríquez-Sáez J.L., 2022. First record of *Colletotrichum anthrisci* causing anthracnose on avocado fruits in Chile. *Pathogens* 11: 1204. https://doi.org/10.3390/pathogens11101204

Carbone I., Kohn L.M., 1999. A method for designing primer sets for speciation studies in filamentous ascomycetes. *Mycologia* 91: 553–556. https://doi.org/10.1080/00275514.1999.12061051

Carneiro G.A., Baric S., 2021. *Colletotrichum fioriniae* and *Colletotrichum godetiae* causing postharvest bitter rot of apple in South Tyrol (Northern Italy). *Plant Disease* 105: 3118–3126. https://doi.org/10.1094/PDIS-11-20-2482-RE.

Chechi A., Stahlecker J., Zhang M., Luo C.X., Schnabel G., 2019. First report of *Colletotrichum fioriniae* and *C. nymphaeae* causing anthracnose on cherry tomatoes in South Carolina. *Plant Disease* 103: 1042–1042. https://doi.org/10.1094/PDIS-09-18-1696-PDN.

Dean R., Van Kan J.A.L., Pretorius Z.A., Hammond-Kosack K.E., Di Pietro A., …, Foster G.D., 2012. The top 10 fungal pathogens in molecular plant pathology. *Molecular Plant Pathology* 13: 414–430. https://doi.org/10.1111/j.1364-3703.2011.00783.x.

De Silva D.D., Crous P.W., Ades P.K., Hyde K.D., Taylor P.W., 2017. Life styles of *Colletotrichum* species and implications for plant biosecurity. *Fungal Biology Reviews* 31 155–168. https://doi.org/10.1016/j.fbr.2017.05.001

FAOSTAT, 2024. *FAOSTAT*. https://www.fao.org/faostat/en/#data/QCL. Accessed on July 2024.

Fuentes-Aragón D., Silva-Rojas H.V., Guarnaccia V., Mora-Aguilera J.A., Aranda-Ocampo S., …, Téliz-Ortíz D., 2020. *Colletotrichum* species causing anthracnose on avocado fruit in Mexico: Current status. *Plant Pathology* 69: 1513–1528. https://doi.org/10.1111/ppa.13234

Giblin F.R., Tan Y.P., Mitchell R., Coates L.M., Irwin J.A.G., Shivas R.G., 2018. *Colletotrichum* species associated with pre-and post-harvest diseases of avocado and mango in eastern Australia. *Australasian Plant Pathology* 47: 269–276. https://doi.org/10.1007/s13313-018-0553-0

Guarnaccia V., Vitale A., Cirvilleri G., Aiello D., Susca A., …, Polizzi G., 2016. Characterisation and pathogenicity of fungal species associated with branch cankers and stem-end rot of avocado in Italy. *European Journal of Plant Pathology* 146: 963–976. https://doi.org/10.1007/s10658-016-0973-z

Guarnaccia V., Gilardi G., Martino I., Garibaldi A., Gullino M.L., 2019. Species diversity in *Colletotrichum* causing anthracnose of aromatic and ornamental Lamiaceae in Italy. *Agronomy* 9: 613. https://doi.org/10.3390/agronomy9100613

Guarnaccia V., Martino I., Gilardi G., Garibaldi A., Gullino M.L., 2021a. *Colletotrichum* spp. causing anthracnose on ornamental plants in northern Italy. *Journal of Plant Pathology* 103: 127–137. https://doi.org/10.1007/s42161-020-00684-2

Guarnaccia V., Martino I., Brondino L., Garibaldi A., Gullino M.L., 2021b. Leaf anthracnose and defoliation of blueberry caused by *Colletotrichum helleniense* in Northern Italy. *Phytopathologia Mediterranea* 60: 479–491. https://doi.org/10.36253/phyto-12377

Guerber J.C., Liu B., Correll J.C., Johnston P.R., 2003. Characterization of diversity in *Colletotrichum acutatum* sensu lato by sequence analysis of two gene

introns, mtDNA and intron RFLPs, and mating compatibility. *Mycologia* 95: 872–895. https://doi.org/10.1080/15572536.2004.11833047

Hillis D.M., Bull J.J., 1993. An empirical test of bootstrapping as a method for assessing confidence in phylogenetic analysis. *Systematic Biology* 42: 182–192

Hofer K.M., Braithwaite M., Braithwaite L.J., Sorensen S., Siebert B., …, Toome-Heller M. 2021. First report of *Colletotrichum fructicola*, *C. perseae*, and *C. siamense* causing anthracnose disease of avocado (*Persea americana*) in New Zealand. *Plant Disease* 105: 1564. https://doi.org/10.1094/pdis-06-20-1313-pdn

Katoh K., Standley D.M., 2013. MAFFT Multiple sequence alignment software version 7: improvements in performance and usability. *Molecular Biology and Evolution* 30: 772–780.

Kumar S., Stecher G., Tamura K., 2016. MEGA7: Molecular Evolutionary Genetics Analysis version 7.0 for bigger datasets. *Molecular Biology and Evolution* 33: 1870–1874.

Kou L.P., Gaskins V., Luo Y.G., Jurick W.M., 2014. First report of *Colletotrichum fioriniae* causing postharvest decay on 'Nittany' apple fruit in the United States. *Plant Disease* 98: 993. https://doi.org/10.1094/PDIS-08-13-0816-PDN.

Luongo L., Galli M., Garaguso I., Petrucci M., Vitale S., 2022. First report of *Colletotrichum fioriniae* and *C. nymphaeae* as causal agents of anthracnose on walnut in Italy. *Plant Disease* 106: 327. https://doi.org/10.1094/PDIS-05-21-1062-PDN.

Migliore G., Farina V., Tinervia S., Matranga G., Schifani G., 2017. consumer interest towards tropical fruit: factors affecting avocado fruit consumption in Italy. *Agricultural and Food Economics* 5: 24. https://doi.org/10.1186/s40100-017-0095-8.

Munda A., 2014. First report of *Colletotrichum fioriniae* and *C. godetiae* causing apple bitter rot in Slovenia. *Plant Disease* 98: 1282. https://doi.org/10.1094/PDIS-04-14-0419-PDN.

Nylander J.A.A., 2004. MrModeltest v. 2. Program distributed by the author. Uppsala Evolutionary Biology Centre Uppsala University

Rayner R.W., 1970. *A Mycological Colour Chart*. Kew, Commonwealth Mycological Institute & British Mycological Society, pp. 34

Ronquist F., Teslenko M., Van der Mark P., Ayres D.L., Darling A., …, Huelsenbeck J.P., 2012. MrBayes 3.2: efficient Bayesian phylogenetic inference and model choice across a large model space. *Systematic Biology* 61: 539–542.

Sezer A., Dolar F.S., Ünal F., 2017. First report of *Colletotrichum fioriniae* infection of hazelnut. *Mycotaxon* 132: 495–502.

Sharma G., Maymon M., Freeman S., 2017. Epidemiology, pathology and identification of *Colletotrichum* including a novel species associated with avocado (*Persea americana*) anthracnose in Israel. *Scientific Reports* 7: 15839. https://doi.org/10.1038/s41598-017-15946-w

Stielow J.B., Lévesque C.A., Seifert K.A., Meyer W., … Robert V., 2015. One Fungus, Which Genes? Development and Assessment of Universal Primers for Potential Secondary Fungal DNA Barcodes. *Persoonia* 35: 242–263. https://doi.org/10.3767/003158515X689135.

Swofford D.L., 2003. Phylogenetic analysis using parsimony (and Other Methods), v. 4.0b10. Sinauer Associates, Sunderland

Talhinhas P., Baroncelli R., 2023. Hosts of *Colletotrichum*. *Mycosphere* 14: 158–261. https://doi.org/10.5943/mycosphere/14/si2/4

USDA Fungal Databases, 2024. https://fungi.ars.usda.gov/. Accessed on July 2024.

White T.J., Bruns T., Lee S., Taylor J.W., 1990. Amplification and direct sequencing of fungal ribosomal RNA genes for phylogenetics. In: *PCR Protocols: A Guide to Methods and Applications* 18: 315–322.

Zakaria L., 2021. Diversity of *Colletotrichum* species associated with anthracnose disease in tropical fruit crops – A review. *Agriculture* 11: 297. https://doi.org/10.3390/agriculture11040297.

Research Papers

Molecular and morphological characterisation of a new record of *Bursaphelenchus arthuri* (Nematoda: Aphelenchoididae) from a new host, *Pinus pinea,* in Europe

Hugo SILVA[1], Joana M.S. CARDOSO[1], Ricardo M.F. DA COSTA[2], Isabel ABRANTES[1], Luís FONSECA[1,3,*]

[1] *University of Coimbra, Centre for Functional Ecology-CFE, Associate Laboratory for Sustainable Land Use and Ecosystem Services-TERRA, Department of Life Sciences, Coimbra, Portugal*
[2] *University of Coimbra, Molecular Physical-Chemistry R&D Unit, Department of Chemistry, LAQV Requimte, Coimbra, Portugal*
[3] *FITOLAB – Laboratory for Phytopathology, Instituto Pedro Nunes (IPN), Coimbra, Portugal*
*Corresponding author. E-mail: luis.fonseca@uc.pt

ORCID:
HS: 0000-0002-0046-4716
JMSC: 0000-0002-8720-8845
RMFC: 0000-0002-5426-412X
IA: 0000-0002-8761-2151
LF: 0000-0001-7405-8916

Summary. Nematodes with morphological characters of *Bursaphelenchus arthuri*, a species of the Fungivorus group, first described in 2005 in China from imported coniferous packaging wood, were extracted from a centennial *Pinus pinea* tree with wilting symptoms in Coimbra, Portugal. Nematodes were transferred to *Botrytis cinerea* cultures to establish a nematode isolate which was characterised using morphological, morphometrical and molecular methods. Restriction fragment length polymorphism (RFLP) analysis carried out with five endonucleases of amplified internal transcribed spacer (ITS) of the rDNA region, revealed the characteristic restriction pattern described for *Bursaphelenchus arthuri*. Sequencing of the D2-D3 expansion region of the large subunit (LSU) of rDNA confirmed this identification. Phylogenetic analysis based on multiple sequence alignment of selected D2-D3 sequences showed that the Portuguese *B. arthuri* isolate formed a separate group, along with the other *B. arthuri* isolate from Taiwan available in GenBank, from those of other isolates of closely related nematodes species belonging to the Fungivorus group. This study is the first report of *B. arthuri* in Europe and from *P. pinea*.

Keywords. Centennial tree, D2-D3 expansion region sequencing, morphobiometrics, nematode, PCR-ITS-RFLP.

INTRODUCTION

Bursaphelenchus can be divided into several groups based on morphological and molecular analyses. The Xylophilus group includes the phytoparasitic species *Bursaphelenchus xylophilus* Steiner and Buhrer, 1934 (Nickle, 1970), the causal agent of pine wilt disease (EPPO, 2024). *Bursaphelenchus arthuri*

Burgermeister, Gu and Braasch, 2005, a mycetophagous nematode species first described in China from coniferous packaging wood imported from Taiwan and South Korea (Burgermeister *et al.,* 2005), belongs to the Fungivorus group, which comprises other species such as: 1) *B. hunti* (Steiner, 1935) Giblin-Davis and Kaya, 1983; 2) *B. sychnus* Rühm, 1956; 3) *B. steineri* Rühm, 1956; 4) *B. fungivorus* Franklin and Hooper, 1962; 5); *B. gonzalezi* Loof, 1964; 6) *B. seani* Giblin-Davis and Kaya, 1983; 7) *B. thailandae* Braasch and Braasch-Bidasak, 2002; 8) *B. willibaldi* Schönfeld, Braasch and Burgermeister, 2006; 9) *B. braaschae* Gu and Wang, 2010; 10) *B. kiyoharai* Kanzaki, Maehara, Aikawa, Masuya and Giblin-Davis, 2011; 11) *B. arthuroides* Gu, Wang and Zeng, 2012; 12) *B. parathailandae* Gu, Wang and Chen, 2012; 13) *B. tadamiensis* Kanzaki, Taki, Masuya and Okabe, 2012; 14) *B. penai* Kanzaki, Giblin-Davis, Carrillo, Duncan and Gonzalez, 2014; 15) *B. sycophilus,* Kanzaki, Tanaka, Giblin-Davisa and Davies 2014*;* 16) *B. kesiyae* Kanzaki, Aikawa, Maehara and Thu, 2016; 17) *B. rockyi* Wang, Fang, Maria, Gu and Ge, 2019; and 18) *B. suri* Kanzaki, Kruger, Greeff and Giblin-Davis, 2022 (Gu *et al.,* 2012; Wang *et al.,* 2019; Kanzaki *et al.,* 2014; 2016; 2022). Since the first detection of *B. arthuri* in China from coniferous packaging wood imported from Taiwan and South Korea, this nematode was later identified in imported wood from Republic of Korea, the United States of America, China, and Japan (Gu *et al.,* 2006; 2008).

In the present study, wood samples from an isolated *P. pinea* Linnaeus, 1753 tree displaying severe wilting symptoms were collected, and were assessed for presence of the EPPO A2 quarantine organism, *B. xylophilus* (the pinewood nematode), and for other *Bursaphelenchus* species. Nematodes resembling *B. arthuri* were separated from these samples and propagated in fungus cultures. Subsequent characterisation and identification were accomplished based on the morphological and morphometric characteristics of females and males and based on molecular characteristics of the ITS rDNA region using PCR ITS-RFLP and D2-D3 LSU rDNA sequencing. A phylogenetic analysis was also built with the multiple sequence alignment between D2-D3 LSU rDNA sequences available on databases.

MATERIALS AND METHODS

Nematodes extraction and culture establishment

Wood samples (trunk and branches) were collected from a centennial *P. pinea* tree showing wilting symptoms in Coimbra, Portugal. The samples were then cut into small pieces (< 1 cm wide). Nematodes were extract-

ed from these pieces using the tray method (Whitehead and Hemming, 1965; EPPO, 2013) and were handpicked and transferred to *Botrytis cinerea* grown at 25°C on malt extract agar to obtain a nematode isolate, as described by Fonseca *et al.* (2008). The nematode isolate obtained was identified (see below) as *Bursaphelenchus arthuri* and designated as BaPt1.

Morphobiometrical characterisation

Fifteen females and 15 males were killed by heat in a drop of water on a cavity glass slide, and were mounted in water, photographed, and their morphological and morphometric characters were analysed. Photographs were taken with a Leica DM 2500 bright field light microscope (Leica) using a LeicaDFC 450 digital camera (Leica). Measurements (Tables 1 and 2) were carried out using Microsystem LAS Interactive Measurement Software Version 4.0.0. (Leica) (Silva *et al.,* 2023).

DNA extraction and amplification of ITS-rDNA and D2-D3 rDNA regions

DNA from nematodes collected from a culture plate (mixed developmental stages) was extracted with the DNeasy Blood and Tissue Mini Kit (Qiagen), following manufacturer's instructions, and were quantified using Nanodrop 2000C (ThermoScientific). The ITS rDNA region containing partial 18S and 28S and complete ITS1, 5.8S and ITS2 sequences was amplified using 50 ng of extracted DNA, 1× of NZYTaq II Master Mix (Nzytech), and 0.4 μM of the primers 18SF 5'-CGTAACAAGGTAGCTGTAG-3' (Ferris *et al.,* 1993; EPPO 2023) and 28SR 5'-TTTCACTCGCCGTTACTAAGG-3' (Vrain, 1993; EPPO, 2023). Reactions were carried out in a Thermal Cycler (Bio-Rad), with an initial denaturation step of 95°C for 2.5 min, followed by 40 reaction cycles of 95°C for 30 s, annealing at 55°C for 30 s, extension at 72°C for 1 min, and a final extension at 72°C for 5 min. The resulting amplification product was used for RFLP analysis.

The D2-D3 expansion region of LSU rDNA was amplified in a 50 μL reaction using 50 ng of DNA, 1× NZYTaq II Master Mix (Nzytech), and 0.4 μM of primers D2A (5' ACAAGTACCGTGAGGGAAAGTTG-3') and D3B (5'-TCGGAAGGAACCAGCTACTA-3') (Ley *et al.,* 1999). All reactions were conducted in a Bio-Rad Thermal Cycler, with an initial denaturation step of 95°C for 2.5 min, followed by 40 reaction cycles of 95°C for 30 s, annealing at 56°C for 30 s, extension at 72°C for 1 min, and a final extension at 72°C for 5 min. The resulting amplification product was purified with the

NZYGelpure Kit (Nzytech), according to manufacturer instructions, and used for sequencing.

Restriction fragment length polymorphism analysis

RFLP analysis was carried out on the amplified ITS rDNA PCR product following Burgermeister *et al.* (2009) and EPPO (2023) protocols, using the five restriction endonucleases *Hinf*I, *Alu*I, *Hae*III, *Msp*I, and *Rsa*I (Amersham Biosciences), according to the manufacturer's instructions. The restriction products were separated by electrophoresis on 1.5% agarose gel.

Sequencing and phylogenetic analysis

The amplified D2-D3 LSU rDNA product was sequenced in both strands using an Automatic Sequencer 3730xl with BigDyeTM terminator cycling conditions, at Macrogen Company (Seoul, Korea), employing the same primers used in the PCR (above). Sequences obtained were analyzed with BioEdit (Hall, 1999). BLAST (Altschul *et al.*, 1997) was used to search for homologous sequences in the databases, and selected sequences were aligned using BioEdit. Phylogenetic analysis was carried out in MEGA 11 (Tamura *et al.*, 2021), using the Neighbor-Joining method (Saitou and Nei, 1987) with 1000 bootstrap replications, and employing the Jukes-Cantor substitution model. Ambiguous positions were removed from each sequence pair (pairwise deletion option) using the D2-D3 LSU sequences alignment.

<div align="center">RESULTS</div>

Morphobiometrical characterisation

Female and male nematodes (Figure 1, A to F) had key diagnostic morphological characters consistent with the original description of *B. arthuri* (Burgermeister *et al.*, 2005): heat relaxed form almost straight, only slightly ventrally arcuate when heat-killed; lip region offset by a constriction; head with six lips; stylet slender with only very slight basal swellings; median bulb rounded to elongated oval with conspicuous valve plates centrally placed (Figure 1 E); nerve ring located closely posterior to the median bulb; excretory pore position approx. half to one body diameter behind the median bulb at level with intestine. Female (Figure 1 A): vulva a transverse slit without flap; ovary outstretched; conspicuous post uterine branch extending over two-thirds of vulva

to anus distance (Figure 1 B); anus slightly protruding; tail slightly ventrally bent and with finely rounded terminus (Figure 1 C). Male (Figure 1 D): tail region sharply curled ventrally when killed by heat; posterior anus lip slightly protruding; spicules paired and straight with a high rounded condylus and rostrum in the middle position; distal ends of spicules rounded without a cucullus; tail with a distinct, oval-shaped terminal bursa with a pointed terminus, which can be seen in dorso-ventral position; small tubercle observed close to the anus indicates presence of a single pre-anal papilla (Figure 1 F).

Morphometrics of the female and male nematodes were compared with other morphometric data for *B. arthuri* (Burgermeister *et al.*, 2005). Most of the morphometric data for the females and males were within the range of the nematodes measured in the original species description (Burgermeister *et al.*, 2005), apart of the total body length, and *a* and *c* ratios, which were smaller than those in the original description (Tables 1 and 2).
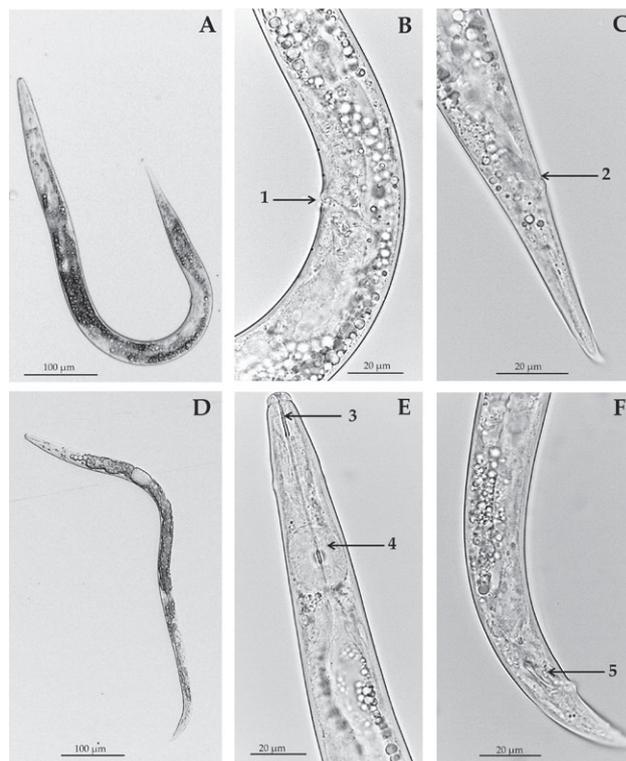
Figure 1. Light micrographs of the Portuguese *Bursaphelenchus arthuri* isolate (BaPt1). A; female (entire body): B; part of a female reproductive system; C; female tail: D; male (entire body): E; anterior region: F; male tail. 1; vulva: 2; anus: 3; stylet: 4; median bulb: 5; spicule.

Table 1. Morphometric data of *Bursaphelenchus arthuri* females from Portugal (BaPt1) and Taiwan. Values are means ± SD, and those in parentheses are minima and maxima.

Character	Females	
	Portugal (n = 15) (BaPt1, this study)	Taiwan (n = 15) (Burgermeister *et al.*, 2005)
Linear (μm)		
Body length (L)	709.3 ± 55.9 (601.5–828.8)	961.9 ± 62.4 (827–1069)
Greatest body width (GBW)	24.4 ± 2.3 (21.3–29.5)	-----
Stylet length	15.0 ± 0.7 (14.1–16.8)	16.4 ± 1.0 (14.0–17.7)
Median bulb length	22.6 ± 1.5 (19.9–25.7)	-----
Median bulb diameter	17.2 ± 1.6 (15.2–21.7)	-----
Anterior end to end of median bulb (AEMB)	70.9 ± 5.9 (56.3–78.6)	-----
Tail length (TL)	60.1 ± 4.7 (47.4–65.2)	-----
Body width at anus (BWA)	12.0 ± 0.9 (10.7–13.8)	-----
Anterior end to vulva	499.0 ± 40.4 (432.2–583.9)	
Vulva to anus	153.9 ± 17.2 (131.2–191.1)	-----
Ratio		
a = L/GBW	29.2 ± 1.7 (25.0–31.7)	33.9 ± 1.5 (31.2–35.7)
b_1=L/AEMB	10.1 ± 1.2 (8.4–12.4)	-----
c=L/TL	11.9 ± 0.8 (10.6–13.6)	15.0 ± 1.7 (13.6–19.1)
c'=TL/BWA	5.0 ± 0.5 (3.9–5.6)	4.8 ± 0.4 (4.2–5.4)
Percentage		
V = Distance anterior end to vulva x 100/L	70.4 ± 1.3 (68.5–73.0)	72.3 ± 1.0 (70.8–73.7)

Table 2. Morphometric data of *Bursaphelenchus arthuri* males from Portugal (BaPt1) and Taiwan. Values are means ± SD, and those in parentheses are minima and maxima.

Character	Males	
	Portugal (n = 15) (BaPt1, this study)	Taiwan (n = 15) (Burgermeister *et al.*, 2005)
Linear (μm)		
Body length (L)	671.4 ± 63.3 (564.2–784.7)	922.8 ± 35.3 (882–980)
Greatest body width (GBW)	24.0 ± 2.6 (20.0–29.8)	-----
Stylet length	14.2 ± 0.8 (12.7–15.7)	15.7 ± 0.8 (15.1–17.4)
Median bulb length	20.4 ± 1.9 (17.9–24.7)	-----
Median bulb diameter	16.0 ± 1.9 (13.5–19.8)	-----
Anterior end to end of median bulb (AEMB)	69.0 ± 5.8 (56.3–79.6)	-----
Tail length (TL)	34.4 ± 3.2 (29.9–40.4)	-----
Body width at anus (BWA)	14.0 ± 1.4 (12.4–17.7)	-----
Spicule length	14.4 ± 1.0** (12.9–15.8)	19.4± 1.4* (16.0–20.9)
Ratio		
a=L/GBW	28.1 ± 1.8 (24.7–30.8)	31.9 ± 3.0 (27.0–36.0)
b_1=L/DAEMB	9.8 ± 1.1 (8.5–11.3)	-----
c=L/TL	19.6 ± 1.6 (17.7–23.1)	27.3 ± 1.2 (25.9–29.8)
c'=TL/BWA	2.5 ± 0.3 (1.8–2.9)	2.2 ± 0.1 (2.1–2.3)

* Measured as bow.
** Measured by curved median line.

Molecular identification

Restriction fragment length polymorphism analysis

The BaPt1 ITS rDNA regions PCR amplification resulted in a product with length approx. 950 bp. The restriction patterns obtained through digestion with the five endonucleases (Figure 2), corresponded with those previously described for *B. arthuri* (Burgermeister *et al.*, 2009; EPPO, 2023).

Sequencing and phylogenetic analysis

The sequence of BaPt1 D2-D3 LSU rDNA was deposited in the GenBank database under the accession number PQ304253. Phylogenetic analysis revealed that the corresponding BaPt1 D2-D3 LSU rDNA clusters together with other *B. arthuri* isolate submitted in the GenBank and formed a clear separate group (Figure 3). This analysis confirms the identity of isolate BaPt1 as *B. arthuri*.
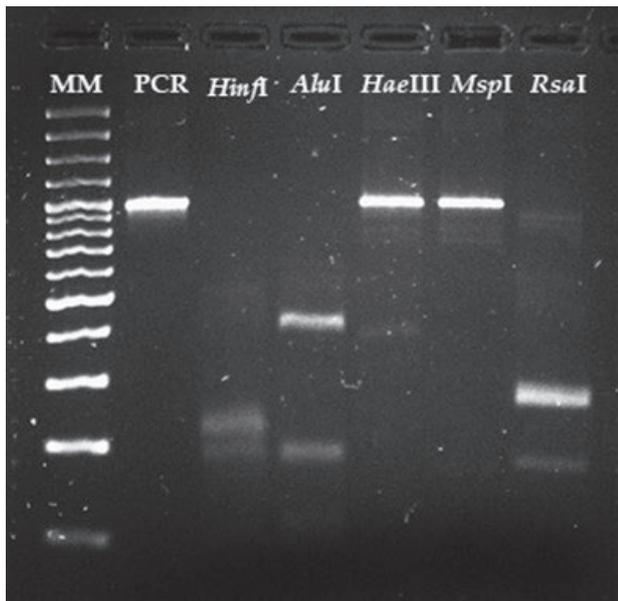
Figure 2. ITS-RFLP patterns of the Portuguese *Bursaphelenchus arthuri* (BaPt1) with the restriction endonucleases *Hinf*I, *Alu*I, *Hae*III, *Msp*I and *Rsa*I. MM—DNA Molecular Marker (Gene Ruller™ 100 bp Plus DNA Ladder).

DISCUSSION

To date, *B. arthuri* has only been detected in Ningbo Port, China, from coniferous packaging wood imported from Taiwan, South Korea, USA, China and Japan (Burgermeister *et al.,* 2005; Gu *et al.,* 2006; 2008). In the present study, *B. arthuri* was detected, for the first time, associated with a *P. pinea* tree. In addition, from this tree, other *Aphelenchoididae* nematodes were found co-existing, including *Potensaphelenchus stammeri* (Silva *et al.*, 2023), demonstrating that wilting coniferous trees can be reservoirs of different nematode species.

The morphology of the Portuguese *B. arthuri* BaPt1 isolate, is consistent with the diagnostic morphological characters outlined in the original description of this nematode (Burgermeister *et al.,* 2005), and most of the morphometric data of females and males are in accordance with the original description (Burgermeister *et al.,* 2005). The morphometric differences found in total body length and *a* and *c* ratios could be because nematodes measured in the present study were previously maintained in fungus cultures for a few weeks. Previous nematode morphometric studies have demonstrated correlations between some morphometric characters and environmental variables (Amin, 2007; Grzelak *et al.,* 2020; Nguyen *et al.,* 2023).

Bursaphelenchus arthuri morphological and morphometric differentiation is difficult within the Fungi-
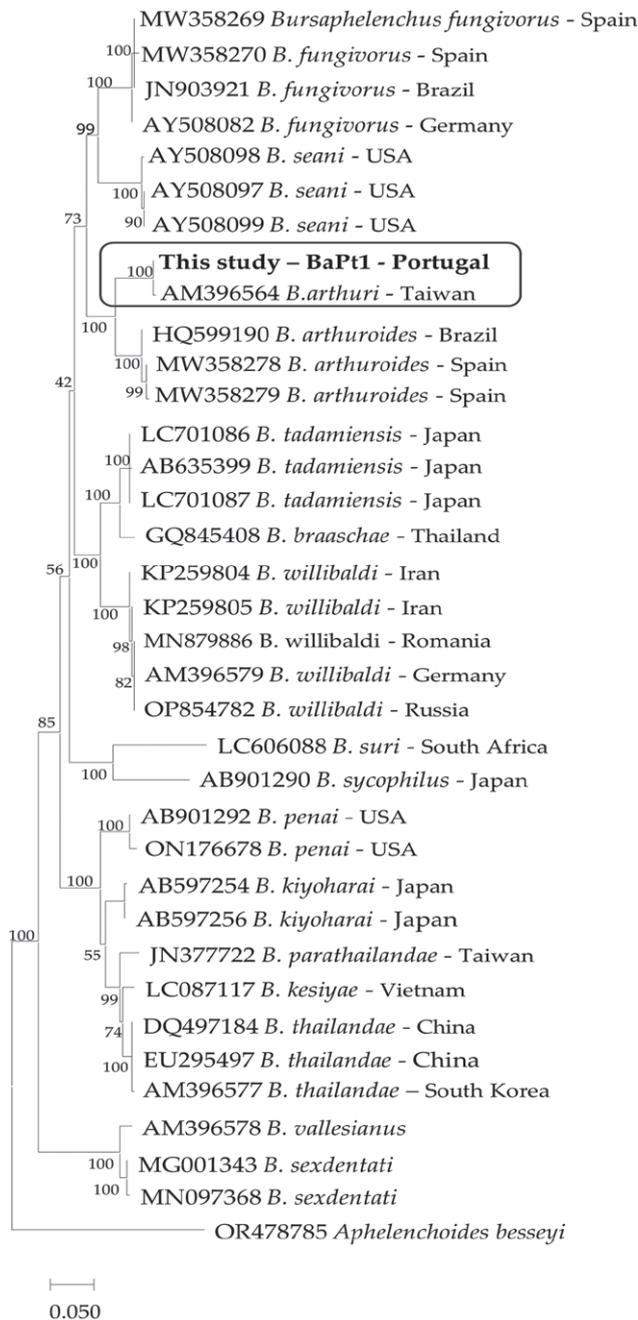
Figure 3. Phylogenetic tree generated by the Neighbor-Joining method using the multiple sequence alignment between D2-D3 LSU rDNA sequences. A *Aphelenchoides besseyi* sequence was used as the outgroup. Bootstrap values are shown at branch points, and the scale bar indicates 0.050 substitutions per site.

vorus group (Burgermeister *et al.*, 2005), making molecular methods (ITS-RFLP analysis and rDNA region sequencing) useful for the species diagnosis. ITS-RFLP analysis, through digestion with *Hinf*I, *Alu*I, *Hae*III, *Msp*I, and *Rsa*I endonucleases, matched with the previ-

ously described pattern for *B. arthuri* species (Burgermeister *et al.,* 2009; EPPO, 2023), confirmed the species identification. Furthermore, the phylogenetic analysis, using the BaPt1 D2-D3 rDNA sequence, showed that the Portuguese isolate clustered together with other *B. arthuri* isolate with D2-D3 sequences available in the databases, making a separate phylogenetic group from those formed by other isolates closely related to nematodes of the Fungivorus group. This clearly identified the BxPta1 isolate as belonging to *B. arthuri*.

Kanzaki *et al.* (2016) divided the Fungivorus group into four subgroups based on morphological characteristics, and placed *B. arthuri* in the same subgroup as *B. hunti*, *B. gonzalezi*, *B. fungivorus*, *B. seani*, and *B. arthuroides*. In the present study, phylogenetic analysis placed together, in the same phylogenetic branch, the species *B. fungivorus*, *B. seani*, *B. arthuroides*, and *B. arthuri* available in GenBank, supporting the previously made subgroup division (Gu *et al.,* 2006). Among these species, phylogenetic analysis showed that *B. arthuroides* is most closely related to *B. arthuri*. Morphologically, these two species are also very similar, with small differences in the shapes of the female tail and in the spicule (Gu *et al.,* 2012).

The present study is the first report of the presence of *B. arthuri* in Portugal and in Europe. Species identification was based on species-specific morphological diagnostic characters and was confirmed by PCR-ITS-RFLP analysis and D2-D3 LSU rDNA sequencing. In addition, this study identifies *P. pinea* as a new host for *B. arthuri* adding new information to the occurrence of *Bursaphelenchus* species in Europe.

ACKNOWLEDGEMENTS

LITERATURE CITED

Amin B., 2007. Host and temperature preference, male occurrence and morphometrics of fungivorous nematode, *Aphelenchus avenae* isolates from Japan. *Jurnal Agripet* 7: 39–47. https://jurnal.usk.ac.id/agripet/article/view/3312

Altschul S.F., Madden T.L., Schaffer A.A., Zhang J.H., Zhang Z., Miller W., Lipman, D.J., 1997. Gapped BLAST and PSI-BLAST: a new generation of protein database search programs. *Nucleic Acids Research* 25: 3389–3402. https://www.ncbi.nlm.nih.gov/pmc/articles/PMC146917/

Burgermeister W., Gu J, Braasch H., 2005. *Bursaphelenchus arthuri* sp. n. (Nematoda: Parasitaphelenchidae) in packaging wood from Taiwan and South Korea-a new species belonging to the fungivorus group. *Journal of Nematode Morphology and Systematics* 8: 7–17. https://revistaselectronicas.ujaen.es/index.php/jnms/article/view/85

Burgermeister W., Braasch H., Metge K., Gu J, Schröder T., Woldt E., 2009. ITS-RFLP analysis, an efficient tool for differentiation of *Bursaphelenchus species*. *Nematology* 11: 649–668. https://brill.com/view/journals/nemy/11/5/article-p649_2.xml

EPPO, 2013. PM 7/119 (1) Nematode extraction. *EPPO Bulletin* 43: 471–495. https://doi.org/10.1111/epp.12077

EPPO, 2023. PM 7/4 (4) *Bursaphelenchus xylophilus EPPO Bulletin* 53: 156–183**.** https://doi.org/10.1111/epp.12915

EPPO, 2024. *Bursaphelenchus xylophilus*. EPPO datasheets on pests recommended for regulation. https://gd.eppo.int (accessed 2024-09-02).

Fonseca L., Santos M.C.V., Santos M.S., Curtis R.H.C., Abrantes I.M.O., 2008. Morpho-biometrical characterisation of Portuguese *Bursaphelenchus xylophilus* isolates with mucronate, digitate or round tailed females. *Phytopathologia Mediterranea* 47: 223–233. https://oajournals.fupress.net/index.php/pm/article/view/5252

Ferris V.R., Ferris J.M., Faghihi J., 1993. Variation in spacer ribosomal DNA in some cyst-forming species of plant parasitic nematodes. *Fundamental Applied Nematology* 16: 177–184. https://horizon.documentation.ird.fr/exl-doc/pleins_textes/fan/40289.pdf

Grzelak K., Gluchowska M., Kędra M., Błażewicz M., 2020. Nematode responses to an Arctic sea-ice regime: morphometric characteristics and biomass size spectra. *Marine Environmental Research* 162: 105181. https://www.sciencedirect.com/science/article/pii/S0141113620305456

Gu J., Braasch H., Burgermeister W., Zhang J., 2006. Records of *Bursaphelenchus* spp. intercepted in imported packaging wood at Ningbo, China. *Forest Pathology* 36: 323–333. https://onlinelibrary.wiley.com/doi/abs/10.1111/j.1439-0329.2006.00462.x

Gu J., Zhang J., Chen X., Braasch H., Burgermeister W., 2008. *Bursaphelenchus* spp. in wood packaging intercepted in China. In: *Pine Wilt Disease: A Worldwide Threat to Forest Ecosystems* (M. Mota, P. Vieira, ed), Springer. pp. 83–88. https://link.springer.com/book/10.1007/978-1-4020-8455-3

Gu J., Wang J., Zheng J., 2012. Description of *Bursaphelenchus arthuroides* sp. n. (Nematoda: Aphelenchoididae), a second parthenogenetic species of *Bursaphelenchus* Fuchs, 1937. *Nematology* 14: 51–63. https://brill.com/view/journals/nemy/14/1/article-p51_5.xml

Hall T.A., 1999. BioEdit: a user-friendly biological sequence alignment editor and analysis program for Windows 95/98/NT. *Nucleic Acids Symposium Series* 41: 95–98. https://www.academia.edu/2034992/

Kanzaki N., Tanaka R., Giblin-Davis R.M., Davies K.A., 2014. New plant-parasitic nematode from the mostly mycophagous genus *Bursaphelenchus* discovered inside figs in Japan. *PLoS One* 9: e99241. https://pubmed.ncbi.nlm.nih.gov/35385500/

Kanzaki N., Aikawa T., Maehara N., Thu P.Q., 2016. *Bursaphelenchus kesiyae* n. sp. (Nematoda: Aphelenchoididae), isolated from dead wood of *Pinus kesiya* Royle ex Gordon (Pinaceae) from Vietnam, with proposal of new subgroups in the *B. fungivorus* group. *Nematology* 18: 133–146. https://brill.com/view/journals/nemy/18/2/article-p133_2.xml

Kanzaki N., Kruger M.S., Greeff J.M., Giblin-Davis M., 2022. *Bursaphelenchus suri* n. sp.: A second *Bursaphelenchus* syconial parasite of figs supports adaptive radiation among section Sycomorus figs. *PLoS One* 17: e0265339. https://journals.plos.org/plosone/article?id=10.1371/journal.pone.0099241

Ley P.D., Felix M., Frisse L., Nadler S., Sternberg P., Thomas, W.K., 1999. Molecular and morphological characterisation of two reproductively isolated species with mirror-image anatomy (Nematoda: Cephalobidae). *Nematology* 1: 591–612. https://brill.com/view/journals/nemy/1/6/article-p591_2.xml

Nguyen M.Y., Vanreusel A., Lins L., Thanh T.T., Bezerra T.N., Nghia S.H., Xuan Q.N., 2023. Nematode's morphometric shifts related to changing environmental conditions in the Mekong estuaries Ba Lai and Ham Luong, Vietnam. *Environmental Science and Pollution Research* 30: 70974–70984. https://pubmed.ncbi.nlm.nih.gov/37160517/

Saitou N., Nei M., 1987. The Neighbor-Joining method – a new method for reconstructing phylogenetic trees. *Molecular Biology and Evolution* 4: 406–425. https://academic.oup.com/mbe/article/4/4/406/1029664

Silva H., Cardoso J.M.S., da Costa R.M.F., Abrantes I., Fonseca L., 2023. *Potensaphelenchus stammeri* (Körner, 1954) Gu, Liu, Abolafia & Pedram, 2021 (Nematoda: Aphelenchoididae) from *Pinus pinea* Linnaeus, 1753 in Portugal. *Forests* 14: 962. https://www.mdpi.com/1999-4907/14/5/962

Tamura K., Stecher G., Kumar S., .2021. MEGA 11: Molecular Evolutionary Genetics Analysis Version 11. *Molecular Biology and Evolution* 38: 3022–3027. https://academic.oup.com/mbe/article/38/7/3022/6248099

Vrain T.C., 1993. Restriction Fragment Length Polymorphism separates species of the *Xiphinema americanum* group. *Journal of Nematology* 25: 361–364. https://www.ncbi.nlm.nih.gov/pmc/articles/PMC2619403/pdf/361.pdf

Wang X., Fang Y., Maria M., Gu J., Ge J., 2019. Description of *Bursaphelenchus rockyi* n. sp. (Nematoda: Aphelenchoididae) in peat moss from Russia. *Nematology* 21: 253–265. https://brill.com/view/journals/nemy/21/3/article-p253_3.xml

Whitehead A.G., Hemming J.R., 1965. A comparison of some quantitative methods of extracting small vermiform nematodes from soil. *Annals of Applied Biology* 55: 25–38. https://onlinelibrary.wiley.com/doi/abs/10.1111/j.1744-7348.1965.tb07864.x

ORCID:
MMA: 0000-0002-2415-4384
GEA: 0000-0003-2333-1104
SP: 0009-0004-6489-715X
AMC: 0009-0000-7775-7472
SM: 0000-0003-4985-8641
MGLDN: 0000-0001-5201-0057
LS: 0000-0002-9737-2593

Short Notes

Alternaria alternata causing necrosis on leaves, fruits, and pedicels of olive plants in Italy

Meriem Miyassa ACI[†], Giovanni E. AGOSTEO[†], Sonia PANGALLO, Anna Maria CICHELLO, Saveria MOSCA, Maria Giulia LI DESTRI NICOSIA, Leonardo SCHENA*

Department of Agriculture, Università degli Studi Mediterranea di Reggio Calabria, Reggio Calabria, Italy
† Authors contributed equally to this research
*Corresponding author. E-mail: lschena@unirc.it

Summary. This paper is the first report of symptoms caused by *Alternaria alternata* on aboveground organs of olive plants in Italy. On leaves, symptoms included spots and necroses frequently associated with damage caused by the olive thrips (*Liothrips oleae*). On fruits, symptoms included browning and necroses of pedicels, necroses of fruitlets soon after fruit set, and rot and mummification of mature fruit. Several isolates of *A. alternata* with identical morphological features and DNA sequences were associated with all the different symptoms. The impacts of *A. alternata* on olive production can be severe, and infections to fruit pedicels are particularly relevant as they cause severe fruit fall soon after fruit set.

Keywords. *Olea europaea*, leaf spot, fruit rot.

INTRODUCTION

The presence of *Alternaria spp.* on olive plants (*Olea europaea* L.) was first associated with infections of drupes and high yield losses in 2001 in the Languedoc-Roussillon region of France (Alaux, 2002). In 2008, *Alternaria alternata* (Fries) Keissler was isolated in Spain and was associated with soft rot of mature olive drupes showing grey-white skins and mummification (Moral *et al.*, 2008). A survey conducted in in Morocco showed presence of *A. alternata* in all the sampled olive orchards (Chliyeh *et al.*, 2014). More recently, *A. alternata* has been identified as a causal agent of olive leaf spots in Turkey (Basım *et al.*, 2017), leaf and fruit spots in Pakistan (Alam and Munis, 2019), bud and blossom blight in Greece and Bosnia and Herzegovina (Lagogianni *et al.*, 2017; Crnogorac *et al.*, 2023), and necroses on olive tree cuttings in Greece (Tziros *et al.*, 2021). In the last 8-10 years, in Calabria (Southern Italy), similar symptoms have been observed in olives, which did not match any disease previously reported in Italy. These Symptoms had different frequencies and severities, depending on microclimatic
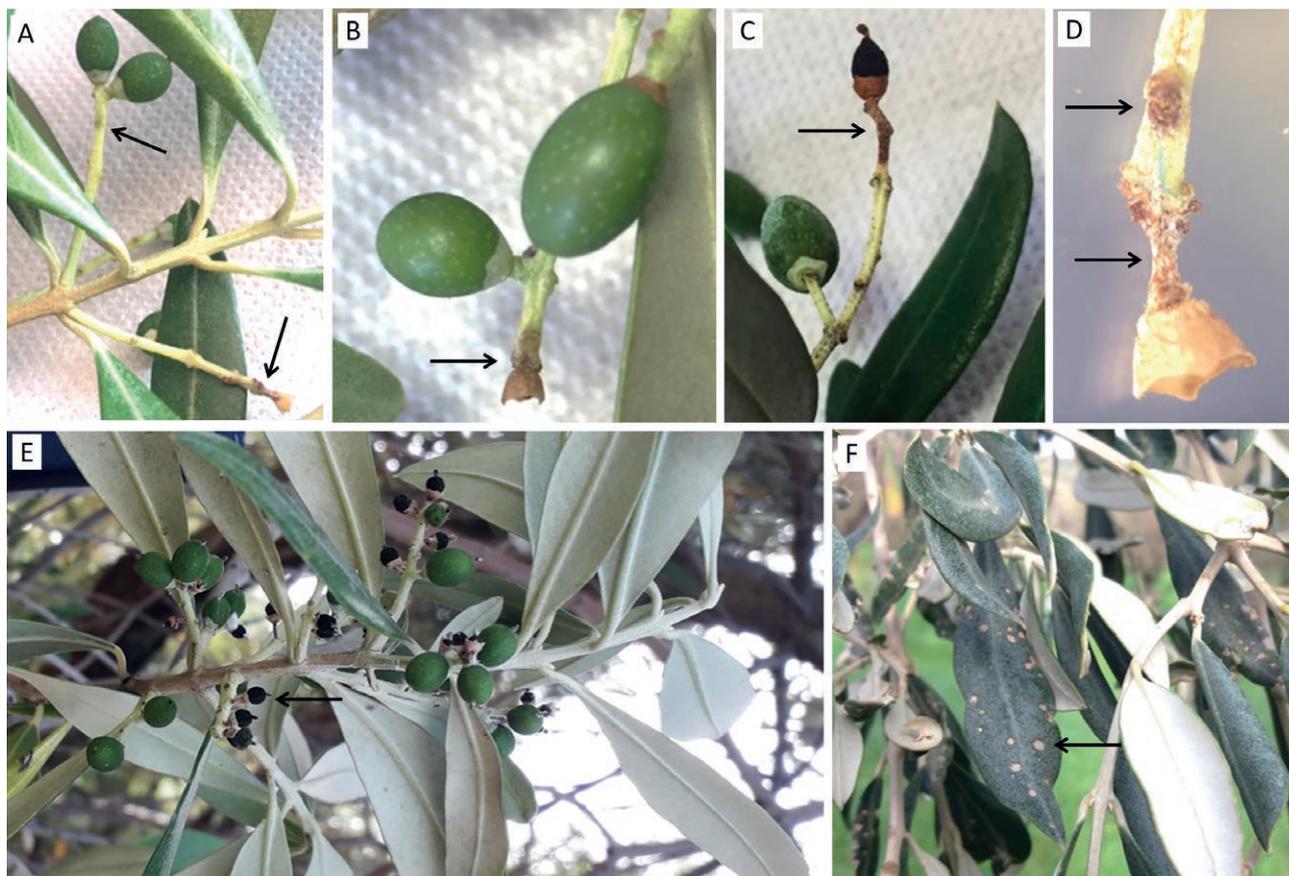
Figure 1. Symptoms caused by infections of *Alternaria alternata* on pedicels and leaves of *Olea europaea*. (A) Localized browning (top arrow) and extended necrosis (bottom arrow) of the pedicel. (B) Necrosis of the apical part of a pedicel and detachment of the fruitlet. (C) Extended necrosis of a pedicel and consequent death of the fruitlet, which remained attached to the plant. (D) Close-up of a necrotic pedicel. (E) Olive branch with dead fruitlets due to infections of *A. alternata* on the pedicels. (F) Leaf spots caused by *A. alternata*, probably in association with *Liothrips oleae*.

areas (orchards), olive cultivars and years. Overall, however, symptoms were observed in a large area extending for more than 150 km in the east coastal area of Catanzaro and Reggio Calabria. Often, whole production areas were lost. Symptoms included (i) browning and necroses of fruit pedicels (Figure 1 A, B, C, D, E); (ii) leaf spots and necroses frequently associated with damage caused by the olive thrips, *Liothrips oleae* (Figure 1 F); (iii) necroses on fruitlets soon after setting (Figure 2A, B); immature fruits (Figure 2C); and (iv) rots of mature fruits with grey-white skins and subsequent mummification (Figure 2 D).

The present study aimed to determine if *A. alternata* was responsible for all the symptoms described above, carrying our *in vitro* isolations and re-inoculations to confirm the role of this fungus as a pathogen of olive plants.

MATERIALS AND METHODS

Pathogen isolation

Samples of symptomatic olive tree organs (leaves, pedicels, fruitlets, and mature fruits) were collected in 2017 and 2022 from a representative orchard of cv. Carolea located in Sellia Marina, Catanzaro, southern Italy (GPS 38.894225, 16.716885), and *in vitro* isolation of the causal agent was attempted. Olive tree samples were surface sterilized by dipping them for 15 s in a 2% sodium hypochlorite solution, rinsed twice in sterile distilled water, and then dried on sterile absorbent paper. Small pieces of tissues were dissected and placed on Potato Dextrose Agar (PDA) plates, containing ampicillin and streptomycin (200 μg mL^{-1}) to prevent bacterial growth. The plates were then incubated at 25±1°C under a 12 h

Figure 2. Symptoms caused by *Alternaria alternata* infections on olive fruits in different growing phases. (A and B) Necrotic areas around the floral calyx and in the equatorial zone of young fruits soon after setting. (C) Necrotic areas on an immature fruit. (D) Rotten mature fruit.

light 12 h dark regime. Dark mycelium developed from most of the dissected tissues, and mycelium from the margins of these colonies was transferred to fresh PDA plates to establish pure cultures. Stock cultures of these isolates are maintained at 4°C and at -20°C at the University of Reggio Calabria.

Morphological, molecular and phylogenetic analyses of isolated fungi

The morphology of colonies, hyphae and conidia of sixteen representative isolates (four from each of the sampled olive organs) was observed after growing pure cultures on PDA at 23°C for 10–15 d. Four isolates (one from each sampled olive organ) were identified by Sanger-sequencing six gene regions (ITS, GAPDH, RPB2, TEF1, ALTA1, and ENDOPG) commonly used as barcode genes for *Alternaria* sect. *Alternaria* (Woudenberg *et al.*, 2015). DNA extraction, amplification, and sequencing were carried out as described by Schena *et al.* (2014), and sequences of each gene were manually curated using the software ChromasPro v.2.1.10.1.

A phylogenetic tree was built with concatenated sequences of the six genes, using representative reference sequences of *Alternaria* sect. *Alternaria* (Woudenberg *et al.*, 2015). In addition, sequences were aligned and compared with available sequences of *A. alternata* previously associated with olive diseases (Alam and Munis, 2019; Tziros *et al.*, 2021; Crnogorac *et al.*, 2023). Sequences were aligned with MUSCLE, and were used to build a phylogenetic tree using the Maximum Likelihood method and the Tamura–Nei

model with 1,000 bootstraps, as implemented in MEGA 11 (Tamura *et al.*, 2021).

Pathogenicity tests

Pathogenicity tests were carried out on detached fruits and leaves of three olive varieties (Coratina, Leccino, and Nocellara etnea). Fruits and leaves ($n = 40$ per organ and cultivar) were surface sterilized by immersion in a 1% sodium hypochlorite solution for 1 min, washed twice with tap water, air-dried, and then wounded in the equatorial zones with a needle (fruits) or a scalpel (leaves). Half of the fruits and leaves ($n = 20$ for each cultivar) were each inoculated with 20 μL of a conidium suspension ($\approx 10^5$ conidia mL^{-1}) of the pathogen, while the other half ($n = 20$ for each cultivar) were inoculated with sterile water. These detached leaves and fruits were then placed in plastic boxes to maintain high relative humidity. A similar set of tests were carried out for leaves of 2-year-old potted plants ($n = 3$) of the olive cultivar Carolea. Due to practical difficulties for surface sterilizing potted plants, leaves ($n = $ ten per plant) were each wounded with a scalpel without preliminary sterilization, and were then inoculated as above and covered with a transparent plastic bag. A set of ten leaves for each plant were inoculated with sterile water as inoculation controls. Lesion diameters on detached fruits and leaves was recorded 7 d after inoculation, and differences between plant varieties were assessed tested using ANOVA of these data. Data analyses were carried out with R v4.4.0 (R Core Team, 2020), using *Base R* and *stats* packages for statistical tests and the *ggplot2* package (Wikman, 2009) for data visualization.

RESULTS AND DISCUSSION

Five days after isolation, white mycelium developed from most dissected tissues, and this turned dark later due to abundant sporulation (Figure 3 A). Developing conidiophores were dark green to brown and were short, septate, and branched. Conidia were ellipsoidal each with a short beak and many transverse septa. Sixteen representative isolates (four from each of the sampled olive organs) had identical morphological features of colonies, hyphae, and conidia, were tentatively identified as *Alternaria* spp. (Simmons 2007).

The molecular analyses of the four sequenced isolates gave identical results for the ITS, GAPDH, RPB2, TEF1, ALTA1, and ENDOPG genes (GenBank Accession number, respectively, PP762481, PP783612, PP783614, PP783613, PP783615, and PP783616). BLAST analyses of the sequences showed 100% identity with several corresponding sequences of reference strains of *Alternaria alternata* (GenBank Accession numbers KP124341, KP124195, KP125117, KP124809, KP123889, and KP124042). The phylogenetic analysis confirmed the identity of the isolates from olive (Figure 3 B). After trimming sequences to an even length, ITS, TEF,

and ENDOPG sequences of the isolates were identical across all isolates previously reported on olive (Alam and Munis, 2019; Tziros *et al.*, 2021; Crnogorac *et al.*, 2023). Furthermore, ALT1 sequences were identical to three of five previously reported sequences in Bosnia and Herzegovina (OP972865, OP972866) (Crnogorac *et al.*, 2023) and Greece (MN512439) (Lagogianni *et al.*, 2017), differing for a single base (C instead of T) compared to the other two Greek sequences (MN512440, MN512441). Greater diversity was found within the RPB2 gene, as seven bases differentiated the present study isolates from two other isolates from Bosnia and Herzegovina (OP038921 and OP038922) (Crnogorac *et al.*, 2023).

For the pathogenicity tests, after 6 d at 20 ± 2°C, all detached leaves (Figure 4 A) and fruits (Figure 5) inoculated with *A. alternata* developed dark lesions resembling those of natural infections, while non-inoculation control fruits and leaves remained asymptomatic. *Alternaria alternata* was re-isolated from symptomatic samples, fulfilling Koch's postulates. Similarly, for the second set of tests on potted plants, all the inoculated leaves developed necroses (Figure 4 B), while all the non-inoculated control leaves were asymptomatic. ANOVA revealed statistically significant differences of sensitivity to inocu-
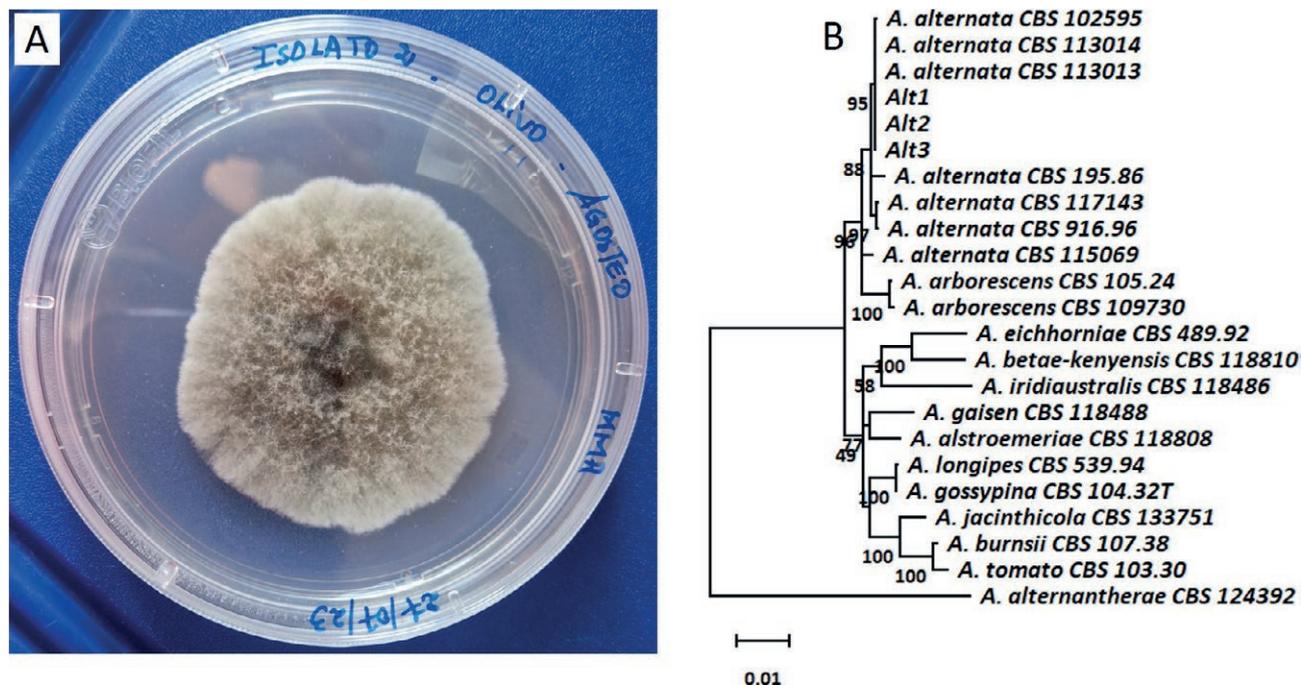
Figure 3. (A) Representative colony of *Alternaria alternata* isolated from a young fruit of *Olea europaea* on potato dextrose agar after 4 d incubation. (B) Phylogenetic tree constructed using concatenated sequences of ITS, GAPDH, RPB2, TEF1, ALTA1, and ENDOPG gene regions (Woudenberg *et al.*, 2015). Representative sequences obtained in the present study (Alt1, Alt2, and Alt3) were analyzed with reference sequences of *Alternaria* sect. *Alternaria* (Woudenberg *et al.*, 2015). Sequences were aligned with MUSCLE and used to build a phylogenetic tree using the Maximum Likelihood method and the Tamura–Nei model with 1,000 bootstraps, as implemented in MEGA 11 (Tamura *et al.*, 2021).
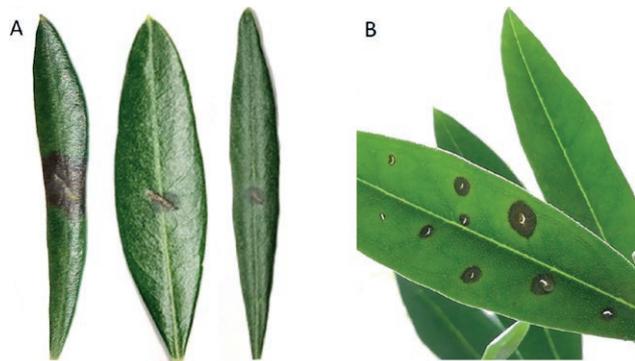
Figure 4. (A) Symptoms on detached leaves of cultivars Coratina (left), Leccino (middle), and Nocellara etnea (right), 6 d after inoculation with *Alternaria alternata*. (B) Symptoms on leaves of a potted olive plant cultivar Carolea 6 d after inoculation *Alternaria alternata*.

lation among the cultivars, on leaves ($F_{2, 57} = 68.65$, $P < 0.001$) and fruits ($F_{2, 57} = 62.78$, $P < 0.001$). Tukey's post-hoc contrasts showed that on fruits, mean lesion diameters (Figure 6, mean ± sd) were greatest for the cultivar Leccino (11.50 ± 0.32 mm), followed by Coratina (7.42 ± 0.72 mm) and Nocellara etnea (4.08 ± 0.16 mm). Leaves

of Coratina were more sensitive (mean lesion diameter = 11.09 ± 0.97 mm) than those of Leccino (3.97 ± 0.12 mm) and Nocellara etnea (1.19 ± 0.42 mm).

As indicated above, previous studies have reported *A. alternata* as the cause of diseases in olive plants. However, this is the first report of infections on olive fruit pedicels. This is also the first report of the occurrence of *A. alternata* on olive plants in Italy. The same pathogen has been shown to cause all the previously reported symptoms on olive (Moral *et al.*, 2008; Basım *et al.*, 2017; Lagogianni *et al.*, 2017; Alam and Munis, 2019; Crnogorac *et al.*, 2023).

The present study results also showed differences in susceptibility to *A. alternata* for different olive varieties. The close similarity between sequences of the present study isolates with those previously reported indicated that observed differences in symptom incidence and severity are likely to be related to environmental conditions and host genotype rather than *A. alternata* strain. This emphasises the importance of the cultivar choice for to prevent the spread of this disease. Although further investigations are required, the impacts of disease caused by this pathogen were severe in the region surveyed in the present study. Infections of fruit pedicels

Figure 5. Symptoms on fruits of Coratina (top), Leccino (middle), and Nocellara etnea (bottom) 6 d after inoculation with *Alternaria alternata*.
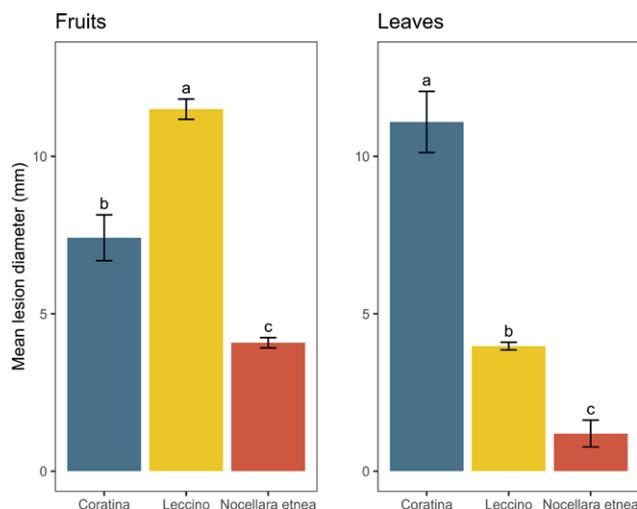
Figure 6. Mean lesion diameters on olive fruits (left) and leaves (right) of cultivars Coratina, Leccino, and Nocellara etnea 6 d after inoculation with *Alternaria alternata*. Barplots are means ± sd for each group. Pairwise comparisons are indicated as letters on top of each barplot (Tukey's multiple comparison procedure).

were the most relevant, as these caused many fruits to fall from trees during the first developmental phases.

LITERATURE CITED

Alam T., Munis M.F.H., 2019. *Alternaria alternata* Causing Leaf and Fruit Spot of Olive in Pakistan. *Plant Disease* 103: 762–762. https://doi.org/10.1094/PDIS-08-18-1448-PDN

Alaux C., 2002. La présenc d'alternaria, une source d'inquiétude pour les oliveraies du Languedoc. *Phytoma* 552: 24–25 (in French).

Basım E., Basım H., Abdulai M., Baki D., Öztürk N., 2017. Identification and characterization of Alternaria alternata causing leaf spot of olive tree (*Olea europaea*) in Turkey. *Crop Protection* 92: 79–88. https://doi.org/10.1016/j.cropro.2016.10.013

Chliyeh M., Rhimini Y., Selmaoui K., Touhami A.O., Filali-Maltouf A., … Douira A., 2014. Survey of the fungal species associated to olive-tree (*Olea europaea* L.) in Morocco. *International Journal of Recent Biotechnology* 2 (2): 15–32.

Crnogorac A., Mandić A., Godena S., Petrović E., Matić S., 2023. First report of *Alternaria alternata* causing bud and blossom blight on olive in Bosnia and Herzegovina. *New Disease Reports* 48. https://doi.org/10.1002/ndr2.12214

Lagogianni C.S., Tjamos E.C., Antoniou P.P., Tsitsigiannis D.I., 2017. First report of *Alternaria alternata* as the causal agent of alternaria bud and blossom blight of olives. *Plant Disease* 2151. https://doi.org/10.1094/PDIS-04-17-0527-PDN

Moral J., De la Rosa R., León L., Barranco D., Michailides T.J., Trapero A., 2008. High Susceptibility of Olive Cultivar FS-17 to *Alternaria alternata* in Southern Spain. *Plant Disease* 92: 1252–1252. https://doi.org/10.1094/PDIS-92-8-1252A

R Core Team, 2020. R: A language and environment for statistical computing. R Foundation for Statistical Computing, Vienna, Austria. https://www.r-project.org/

Schena L., Mosca S., Cacciola S.O., Faedda R., Sanzani S.M., … Magnano di San Lio G., 2014. Species of the *Colletotrichum gloeosporioides* and *C. boninense* complexes associated with olive anthracnose. *Plant Pathology* 63: 437–446. https://doi.org/10.1111/ppa.12110

Simmons E.G., 2007. *Alternaria*: an Identification Manual. APS Press, St. Paul, MN

Tamura K., Stecher G., Kumar S., 2021. MEGA11: Molecular evolutionary genetics analysis version 11. *Molecular Biology and Evolution* (F.U. Battistuzzi, ed.), Oxford University Press 38: 3022–3027. https://doi.org/10.1093/molbev/msab120

Tziros G.T., Karpouzis A., Lagopodi A.L., 2021. *Alternaria alternata* as the cause of decline and necrosis on olive tree cuttings in Greece. *Australasian Plant Disease Notes* 16: 7. https://doi.org/10.1007/s13314-021-00422-2

Wickham H., 2009. ggplot2: Elegant graphics for data analysis. Springer-Verlag New York. https://ggplot2.tidyverse.org.

Woudenberg J.H.C., Seidl M.F., Groenewald J.Z., de Vries M., Stielow J.B., … Crous P.W., 2015. *Alternaria* section *Alternaria* : Species, *formae speciales* or pathotypes? *Studies in Mycology* 82: 1–21. https://doi.org/10.1016/j.simyco.2015.07.001

New or Unusual Disease Reports

Cryptostroma corticale in Italy: new reports of sooty bark of *Acer pseudoplatanus* and first outbreak on *Acer campestre*

Rebekka SCHLÖSSER¹, Alberto SANTINI¹, Alessia Lucia PEPORI¹, Tiziana BASCHIERI², Carlo CAMPANI³, Dario FERRARI², Giorgio MARESI⁴, Domenico RIZZO³, Leonel STAZIONE⁵, Giovanni BISCIONI⁵, Luisa GHELARDINI⁵,⁶,*

¹ National Research Council, Institute for Sustainable Plant Protection (CNR-IPSP), Sesto Fiorentino, Firenze, Italy
² Regione Emilia-Romagna, Settore Fitosanitario e Difesa delle Produzioni, Bologna, Italy
³ Regione Toscana, Direzione Agricoltura e Sviluppo Rurale, Settore Servizio Fitosanitario Regionale e di Vigilanza e Controllo Agroforestale, Firenze, Italy
⁴ Fondazione Edmund Mach, Centro Trasferimento Tecnologico, San Michele all'Adige, Trento, Italy
⁵ University of Florence, Department of Agriculture, Food, Environment and Forestry (DAGRI), Firenze, Italy
⁶ National Biodiversity Future Center (NBFC), Palermo, Italy
*Corresponding author. E-mail: luisa.ghelardini@unifi.it

Summary. Monitoring of emerging plant diseases in the Apennine mountains (central Italy) identified *Cryptostroma corticale* as the cause of the disease sooty bark of maple trees. The identified sites were located in rural or forested areas, next to buildings, in villages or suburbs, and one site was in a forest. Samples of symptomatic tissues were taken from *Acer pseudoplatanus* and/or *A. campestre*, as well as asymptomatic samples from *A. campestre* and *Aesculus hippocastanum*. All samples tested positive to a species-specific qPCR assay for the presence of *C. corticale*, indicating wide incidence of the disease in the northern Apennines of Italy, after attempted eradication of the first small group of infected plants were found in 2012.

Keywords. Maple, alien invasive species, emerging plant diseases, opportunistic pathogens, human health.

INTRODUCTION

Maple species (*Acer* spp.) are minority but important components of forest biodiversity (Spiecker *et al.*, 2009), and are commonly used in urban settings (Pauleit *et al.*, 2002; Sjöman *et al.*, 2012) in Europe and in North America due to their environmental adaptability (Pasta *et al.*, 2016). Maples are commonly planted in urban areas of Southern Europe, and the use of European maple species has been encouraged due to their low pol-

len allergenicity compared to *Acer negundo*, which is frequently found in cities (Acar *et al.*, 2007; Lacan and McBride, 2009; Chaparro and Terradas, 2010; Calatayud and Cariñanos, 2024). In Italy, maples trees are widely favoured as urban greenery, and are common in all major cities of the Alpine, Po Valley and Apennine regions, as well as in other Mediterranean areas (Bartoli *et al.*, 2021). For example, in Rome, use of maple trees has been encouraged because of their high rooting and carbon sequestration capacities and low ozone-forming potential. *Acer platanoides* is also valued for resistance to wind damage and air pollution, and *A. pseudoplatanus* has phytostabilising activity against soil contaminants (Mirabile *et al.*, 2015).

The health of maple trees is being increasingly challenged by *Cryptostroma corticale* (Ellis & Everh.) P.H. Greg. & S. Waller (Ellis and Everhart, 1889; Gregory and Waller, 1951), a pathogenic ascomycete considered non-native in Europe, and the causal agent of the disease sooty bark.

Cryptostroma corticale as first described by Ellis and Everhart (1889) as *Coniosporium corticale*. The first report of its presence in Europe was in 1945, in Wanstead Park in London, United Kingdom (Gregory and Waller, 1951). The fungus is known as a pathogen and saprophyte (Dickenson, 1980; Enderle *et al.*, 2020), and the endophytic stage was long assumed but only recently proven (Schlößer *et al.*, 2023). *Cryptostroma corticale* is opportunistic and causes symptoms when host trees suffer stress caused by abiotic factors such as high temperatures and drought (Dickenson, 1980; Enderle *et al.*, 2020). Reports of sooty bark periodically appeared after especially warm and dry summer periods as occurred in the 1960s and 1980s (Gregory and Waller, 1951; Moreau and Moreau, 1951; Townrow, 1953; Plate and Schneider, 1965; Young, 1978; Dickenson, 1980; Abbey and Stretton, 1985). Reports of *C. corticale* in Europe have increased since the drought years of 2003 and 2005 (Cech, 2004 ; Metzler, 2006 ; Robeck *et al.*, 2008; Langer *et al.*, 2013; Koukol *et al.*, 2014).

In Italy, the only published report of *C. corticale* was in 2012, when a small plantation of heavily damaged trees, clustered together, were identified at the forest edge on a mountain top in Bologna (Oliveira Longa *et al.*, 2016). No symptoms were observed on other *Acer* plants growing in the surroundings, and the outbreak was promptly eradicated.

Sooty bark symptoms include wilting, shoot dieback, greenish yellow wood discolouration, and development of blisters under host tree bark with subsequent heavy sporulation after the blisters burst (Gregory and Waller, 1951). Young's (1978) experimental evidence (reported in Dickenson, 1980) suggested that it takes a year or more for severe disease development, although small young trees may die within 10 months. The released spores of *C. corticale* can also cause hypersensitive pneumonitis in mammals (Towey *et al.*, 1932; Braun *et al.*, 2021). Humans with heavy exposure to the spores, such as forest or paper mill workers, as well as people with pre-existing lung diseases, are particularly at risk (Braun *et al.*, 2021).

This paper reports new outbreaks of the sooty bark identified in the northern Apennines in Central Italy.

MATERIALS AND METHODS

Study sites and sampling procedure

Diseased plants were observed between 2022 and 2024 at seven locations in or at the base of the Apennines (Figure 1). Details of these observations are listed below.

– About 15 symptomatic *A. pseudopatanus* trees (c. 15-years-old), in a mixed species plantation with *Fraxinus excelsior*, were found at Le Sassane (Gaggio Montano. 44.233890 N, 10.975204 E, 700 m a.s.l.) in the province of Bologna. The trees had been planted on a slight slope with a potentially wet depressed area at the slope base. The trees resembled those at the first outbreak in Montovolo. Most of the trees were severely damaged with typical sooty bark symptoms, and some were dead. Samples of bark, fungal stroma and wood were taken from five of the symptomatic trees.

– Two dead *A. pseudopatanus* trees with sooty bark symptoms were found on a road alongside a cultivated field near Riola (Vergato, 44.237902 N, 11.052955 E, c 420 m a.s.l.) in the province of Bologna. Wood and fungal stroma were sampled from both trees.

– Symptomatic *A. pseudoplatanus* trees were found in Castellonchio, in the province of Parma (44.546420 N, 10.004982 E, c. 910 m a.s.l.), which was followed by a report issued by the Regione Emilia Romagna (Ferrari and Bariselli, 2023). Here, in a small mountain village surrounded by forests, a group of young planted sycamores (circa hundred trees approx. 20-years-old) were heavily affected by the disease. The trees had severe crown dieback, bark cracking with abundant black stroma and fresh sporulation, and many were dead at the time of discovery.

– A mature *A. pseudoplatanus* plant (approx. 100 years old) with sooty bark symptoms (death of most of the crown and conspicuous stroma with active fungal
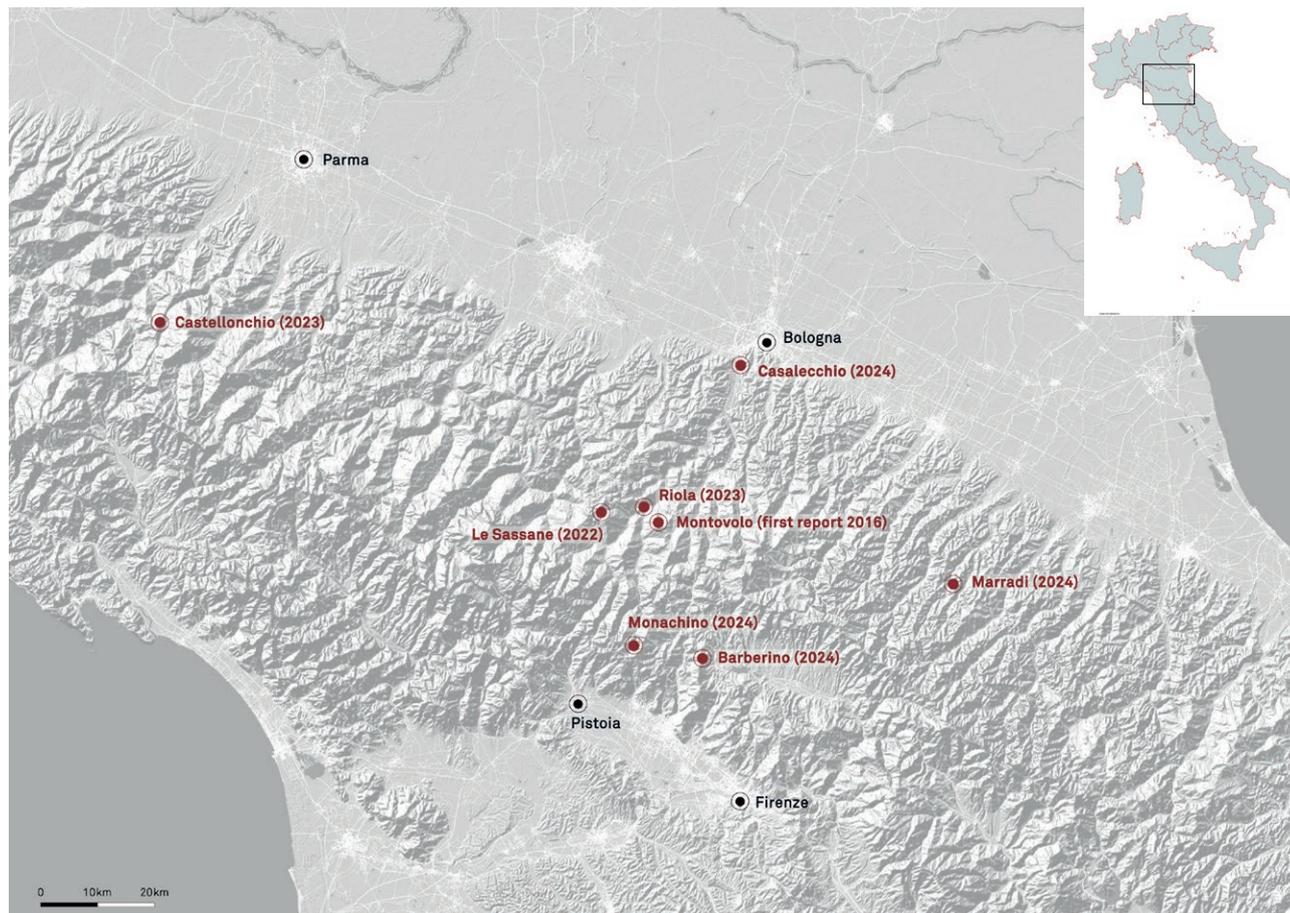
Figure 1. Infection sites (red dots, with year of discovery in parentheses) along the Appenines in Emilia Romagna (Bologna and Parma) and Tuscany (Pistoia and Firenze). The geographical image is a shaded relief from Esri, DigitalGlobe, GeoEye, i-cubed, USDA FSA, USGS, AEX, Getmapping, Aerogrid, IGN, IGP, swisstopo, and the GIS User Community (modified). The insert map of Italy was created at https://www.mapchart.net/italy.html.

sporulation on the stems and branches) was identified in Monachino, a group of houses in a mountain forest area in the province of Pistoia (44.02122 N, 11.03270 E, c. 710 m a.s.l.). The record was reported by the Phytosanitary service of Tuscany (Regione Toscana, 2024). Bark and fungal stroma were sampled from the main stem of the plant. Next to the diseased *A. pseudoplatanus,* an asymptomatic *Aesculus hippocastanum* L. tree was growing. Since *A. hippocastanum* is a known host of *C. corticale* (Young, 1978), and a recent report from Germany showed that *C. corticale* also caused symptoms on *Ae. hippocastanum* (Brenken *et al.*, 2024), twig samples from this tree were taken and analysed.

– In the vicinity of Marradi, province of Firenze (44.103722 N, 11.73475 E, c. 515 m a.s.l.), five symptomatic *A. pseudoplatanus* trees of unknown origin in the private garden of an isolated country house

were affected. Samples of the bark with stroma were taken from all the symptomatic trees as well as twigs of one asymptomatic *A. campestre* tree growing among the diseased trees.

– In Barberino di Mugello, province of Firenze (43.997781 N, 11.181664 E, c. 695 m a.s.l.), approx. 15 symptomatic *A. pseudoplatanus* trees with 3- to 4-year-old sooty bark symptoms were observed in a forested area close to the ancient monastic settlement of Montecuccoli. Symptomatic bark tissue was sampled from three of these trees.

– In Casalecchio di Reno (44.473327 N, 11.283565 E, c. 70 m a.s.l.), 42 *A. campestre* trees of putative natural origin were found to be dead or symptomatic (extensive crown dieback and visible fungal stroma from bark cracks on the main stems and branches) in a forested area, part of a large historic garden which is transformed into a peri-urban park. Three addi-

tional symptomatic *A. pseudoplatanus* trees were also surrounding private buildings in the immediate vicinity. Bark and stroma were sampled from five of the *A. campestre* trees.

Except in Riola and Barberino del Mugello, where it was not known how long the maple trees had been showing sooty bark symptoms, in the other cases decline and death of the plants was rapid, as reported by the locals or as observed by the authors of the present paper, i.e. over one or two growing seasons.

Samples from all sites, consisting of a part of fungal stroma, symptomatic shoots and wood samples, were brought to the University of Florence for morphological characterisation, and CNR laboratory facilities for molecular characterisation. Samples were taken from trees with stromatal spots on the trunks. Trunk tissues were scraped to obtain spores, or pieces of bark with stroma were excised with an axe and collected in sterile plastic bags. A branch (approx. 2 cm at the base), with multiple twigs, was cut from the asymptomatic *Ae. hippocastanum* (in Monachino), and from the asymptomatic *A. campestre* (in Marradi), to determine endophytic presence of *C. corticale*.

Morphological and molecular identifications of samples

Spore samples were microscopically examined. Parts of these samples were also inoculated onto malt extract agar (3% MEA, Biotec) and then incubated at room temperature with ambient light in order to isolate the fungus. Isolation of *C. corticale* was attempted for all samples including spores.

DNA extraction

When isolations were achieved, isolates were grown until they reached the margins of 90 mm diam. Petri dishes containing 3% MEA covered by cellophane discs (Celsa) of the same diameter. The mycelium was then scraped from the cellophane and placed in 2 mL capacity Eppendorf tubes each containing two tungsten beads (3 mm, Qiagen) and placed at -80°C for 20 min. DNA was likewise extracted from wood, bark and spore samples. These samples were then ground using a Retsch Mill (MM 400, Retsch), set to 25 oscillations sec^{-1} for 2 min. DNA was extracted from ground mycelium using the EZNA Plant DNA Kit (Omega Bio-tek), according to the manufacturer's protocol. Total DNA concentrations were estimated using the Tecan Infinite M Plex (Nano-Quant Plate™). Eluted DNA samples were kept at -20°C until analysis.

DNA amplification

PCR was conducted only on the mycelium DNA, using the ITS1 and ITS4 primer set (White *et al.*, 1990) to amplify internal transcribed spacers 1, 2 and the 5.8S gene. The PCR products were purified using the mi-PCR Purification kit (Metabion International,), and were sent for sequencing to Macrogen (Milan, Italy). The acquired sequences (PQ339922, PQ339923, PQ339924) were analysed using the BLASTn function on www.ncbi.nlm.nih.gov.

DNA was also extracted from all samples, including wood, spores and mycelium, and analysed by qPCR, using the species-specific primers for *C. corticale* described by Kelnarová *et al.* (2017) and Muller *et al.* (2023). Asymptomatic samples taken from *A. campestre* collected from Marradi and *Ae. hippocastanum* at the Monachino site, were also analysed using qPCR.

RESULTS AND DISCUSSION

The spores observed with a microscope were morphologically identified as *C. corticale*. The spores were dark brown and ovoid, with average size of 5.7 × 3.9 µm (5.1-6.7 µm × 3.4-4.4 µm; n = 20; Figure 2), which is consistent with the descriptions of *C. corticale* by Gregory and Waller (1951) and Ellis and Everhart (1889). The outgrowing mycelium from spores placed on MEA was initially white and later turned brownish, as is characteristic for this fungus. *Cryptostroma corticale* cultures were successfully obtained from symptomatic trees of *Acer pseudoplatanus* in Monachino and Marradi, and of *A. campestre* in Casalecchio di Reno. For all the other field sites, it was not possible to obtain cultures because the stroma were dried. The BLASTn results for amplified DNA extracts showed a 100% identity and query cover matches for *C. corticale* strain CBS 216.52 (MH857008), and for several other *C. corticale* strains.

The qPCR yielded positive results for *C. corticale* for all the tested samples, including plant material from asymptomatic maples and from *Ae. hippocastanum*. This confirms presence of the fungus in the sampled asymptomatic woody tissues. Although no symptoms were observed on *Ae. hippocastanum*, the present results confirm previous observations that *C. corticale* can colonize alternative hosts. Young (1978) reported saprophytic infections by *C. corticale* on *Ae. hippocastanum*, and Dickenson (1980) reported that *C. corticale* can sporulate on sterile autoclaved wood of several plant species, including *Ae. hippocastanum*. In 2022 a diseased *Ae. hippocastanum* tree, exhibiting black spore fissures, loss
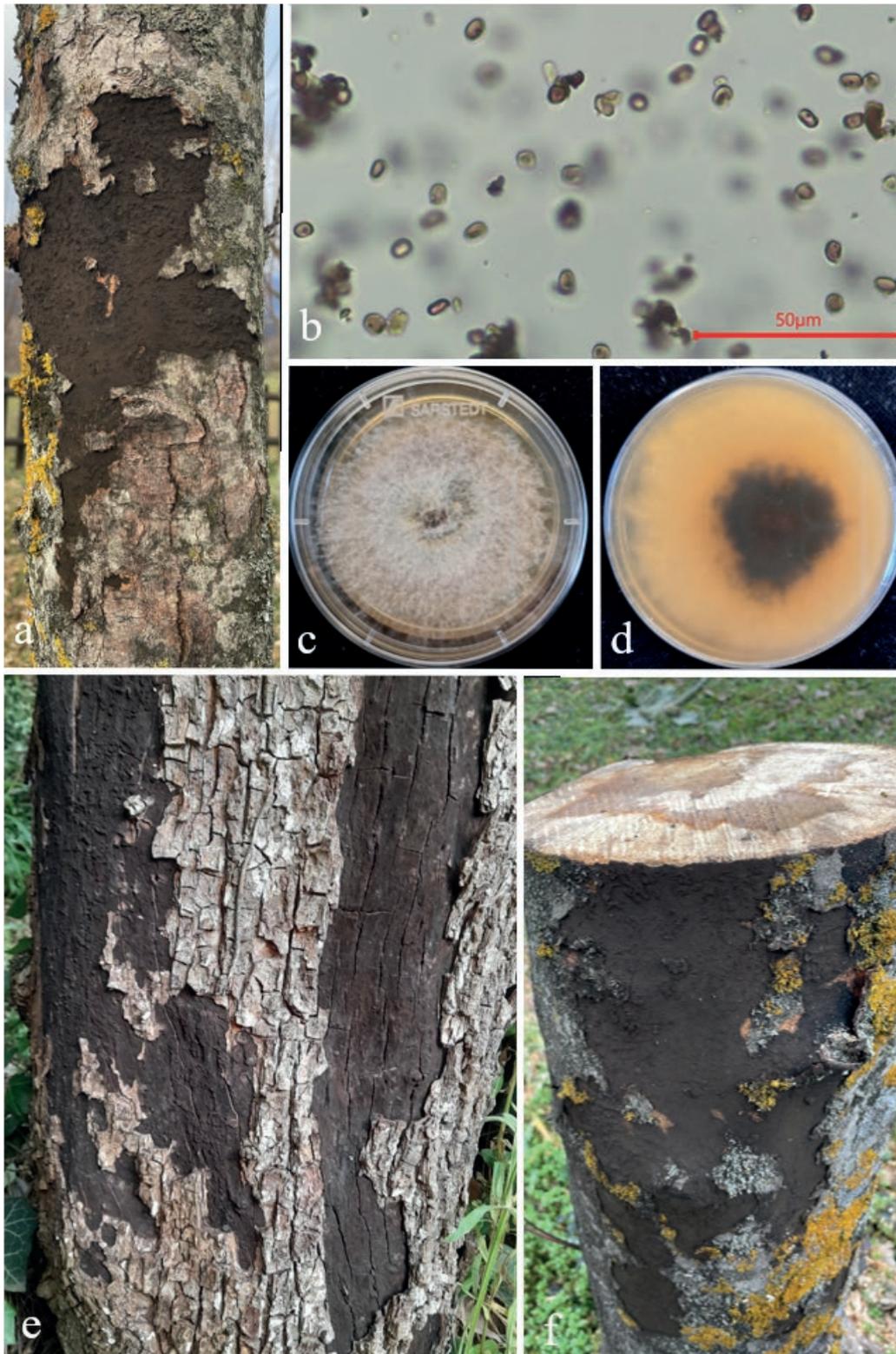
Figure 2. a) Sporulation on an *Acer pseudoplatanus* tree (photo credit: Stefano Romei). b) Spores of *Cryptostroma corticale* obtained during sampling. c) Culture of *C. corticale* isolated from material from Marradi (Accession number: PQ339924). d) View of the underside of the same culture. e) Symptoms of *C. corticale* infection on *Acer campestre*. f) *Acer pseudoplatanus* trunk with sporulation of *C. corticale* and cut surface with typical staining and white rot (photo credits: Stefano Romei).

of bark and death of crown parts, was identified in Trier, Germany (Brenken *et al.*, 2024). This report showed that in central Europe *C. corticale* is also causing isolated damage on *Ae. hippocastanum*, posing a threat to urban areas in central Italy. During the monitoring of the present study, symptomatic (Casalecchio di Reno, Figure 2) and asymptomatic (Marradi) *A. campestre* trees were found to be infected by *C. corticale*. From the present study, *Acer campestre* hence appears to be a similarly common host for *C. corticale*. Dickenson (1980) showed that *A. campestre* was similarly susceptible to *C. corticale* infections as *A. pseudoplatanus*, but this host has rarely been observed to show natural symptoms in Europe (Moreau and Moreau, 1951; Anon, 1952 cited in Dickenson, 1980). This is most likely due to the sporadic occurrence of *A. campestre* in central Europe.

Cryptostroma corticale usually causes disease when trees are stressed by drought and above average temperatures (Gregory and Waller, 1951; Dickenson, 1980; Enderle *et al.*, 2020). Over the course of the monitoring carried out in the present study, recent disease outbreaks with viable spores were found in Sassane, Castellonchio, Monachino and Casalecchio di Reno. The trees in Casalecchio di Reno had died over the course of the previous year. The symptoms observed in Riola and Barberino di Mugello were not fresh, and very few spores could be found. The symptoms from these two regions were estimated to be approx. 2–4 years old. The disease in Barberino di Mugello could have been due to a change in the forest structure, due to establishment of a fire protection strip, where few solitary trees were left standing. The sudden change from a closed forest to open field conditions is likely to have triggered the sooty bark outbreak in this area. The report in Barberino del Mugello is the only report of this disease in a forested area and not close to buildings. Outbreaks in urban areas would generally be unsurprising due to increased temperatures, harsh insolation, pollution and soil compression conditions, and trees standing at large distances from each other. This combination of conditions is known to cause severe water deficit in crowns of maple trees (Close *et al.*, 1996).

Sooty bark outbreaks are currently found along a portion of the northern Apennines in central Italy. Further spread of this disease is likely along the Apennines and to urban areas. Spores of *C. corticale* are estimated to disperse within a radius of at least 300 km (Muller *et al.*, 2023). Burgdorf *et al.*, (2022) reported a *C. corticale* spore count of 277 spores cm^{-2} d^{-1} during July and August 2019 in northern Bavaria, Germany, a year with many reported infections. Fifty-four percent of sycamore trees in the surveyed stand had visible sporulating trunk fissures. Numbers of counted spores varied over the year and were greatest during summer and early autumn (Burgdorf *et al.*, 2022). These results indicate potentially high infection pressure during summer period in northern Bavaria, where trees are stressed due to high temperatures and drought.

Identifying the pathway for introduction and the local sources of inoculum will be challenging, since *C. corticale* can survive endophytically for long periods before becoming pathogenic (Kelnarová *et al.*, 2017), and infection pressure can be high when bark fissures are present (Burgdorf *et al.*, 2022). The potentially infested area is assumed to be large, especially regarding the reports of *C. corticale* spread by Muller *et al.*, (2023). Often outbreaks are not detected or identified due to lack of knowledge and awareness, or effective controls, and are not eradicated prior to spore production, furthering spread of the fungus.

Emergence of sooty bark poses a threat for trees in the Mediterranean region. A large part of Italy has climatic characteristics favourable to the establishment of *C. corticale*. Furthermore, summer drought is forecast to occur during the next few decades in the Mediterranean region and parts of temperate Europe (Kottek *et al.*, 2006). This and the popularity of maples as urban greenery (Pauleit *et al.*, 2005; Augustinus *et al.*, 2024) increases the importance of selecting suitable provenances and genotypes of *A. pseudoplatanus* and *A. campestre,* which can adapt to the increasingly challenging environmental conditions that are likely to occur.

This emphasizes the need for awareness and caution regarding the disease sooty bark of maple trees. Especially for urban areas, this disease poses threats for conservation of established and valuable trees, but potentially also for human health.

ACKNOWLEDGMENTS

LITERATURE CITED

Abbey S.D., Stretton R.J., 1985. Some environmental factors affecting *Cryptostroma corticale*. *Microbios* 44: 157–167.

Acar C., Acar H., Eroğlu E., 2007. Evaluation of ornamental plant resources to urban biodiversity and cultural changing: A case study of residential landscapes in Trabzon city (Turkey). *Building and Environment* 42: 218–229. https://doi.org/10.1016/j.buildenv.2005.08.030.

Anon, 1952. Sooty Bark Disease in Sycamore. In: *Forestry Commission Leaflet*, H.M.S.O.

Augustinus B.A., Abegg M., Queloz V., Brockerhoff E.G., 2024. Higher tree species richness and diversity in urban areas than in forests: Implications for host availability for invasive tree pests and pathogens. *Landscape and Urban Planning* 250: 105144. https://doi.org/10.1016/j.landurbplan.2024.105144.

Bartoli F., Savo V., Caneva G., 2021. Biodiversity of urban street trees in Italian cities: a comparative analysis. *Plant Biosystems - An International Journal Dealing with all Aspects of Plant Biology* 156: 649–662. https://doi.org/10.1080/11263504.2021.1906347.

Braun M., Klingelhöfer D., Groneberg D.A., 2021. Sooty bark disease of maples: the risk for hypersensitivity pneumonitis by fungal spores not only for woodman. *Journal of Occupational Medicine and Toxicology* 16: 2. https://doi.org/10.1186/s12995-021-00292-5.

Brenken A.-C., Kehr R., Riebesehl J., Esch J., Enderle R., 2024. First report of *Cryptostroma corticale* on *Aesculus hippocastanum* causing sooty bark disease in Germany. *Journal of Plant Diseases and Protection* 131: 1087–1092. https://doi.org/10.1007/s41348-024-00891-4.

Burgdorf N., Härtl L., Hahn W.A., 2022. Sooty Bark Disease in Sycamore: Seasonal and Vertical Variation in Spore Release of *Cryptostroma corticale*. *Forests* 13: 1956. https://doi.org/10.3390/f13111956.

Calatayud V., Cariñanos P., 2024. Mapping pollen allergenicity from urban trees in Valencia: A tool for green infrastructure planning. *Environmental Research* 252: 118823. https://doi.org/10.1016/j.envres.2024.118823.

Cech T.L., 2004. Bermerkenswerte Pilzkrankheiten in 2004. *Forstschutz Aktuell* 32: 31–34.

Chaparro L., Terradas J., 2010. Ecosystem services of urban forest. CREAF, Ajuntament de Barcelona.

Close R., Nguyen P., Kielbaso J.J., 1996. Urban vs. Natural Sugar Maple Growth: I. Stress Symptoms and Phenology in Relation to Site Characteristics. *Arboriculture & Urban Forestry* 22: 144–150. https://doi.org/10.48044/jauf.1996.021.

Dickenson S.J., 1980. *Biology of* Cryptostroma corticale *and the Sooty Bark Disease of Sycamore*. Dissertation, University of Bath, Ascot, 126 pp.

Ellis J.B., Everhart, B.M., 1889. New species of hyphomycetes fungi. *Journal of Mycology* 5: 68–72.

Enderle R., Riebesehl J., Becker P., Kehr R., 2020. Rußrindenkrankheit an Ahorn - Biologie, Pathologie und Entsorgung von Schadholz. In: *Jahrbuch der Baumpflege 2020* (D. Dujesiefken, ed.), Braunschweig, Haymarket Media, 85–100.

Ferrari D., Bariselli M., 2023. Corteccia fuligginosa dell'acero - *Cryptostroma corticale*. *Regione Emilia Romana - Agricoltura, caccia e pesca*. Available at: https://agricoltura.regione.emilia-romagna.it/fitosanitario/avversita/schede/avversita-per-nome/acero-corteccia-fuligginosa. Accessed June 18, 2024.

Gregory P.H., Waller S., 1951. *Cryptostroma corticale* and sooty bark disease of sycamore (*Acer pseudoplatanus*). *Transactions of the British Mycological Society* 34: 579–597. https://doi.org/10.1016/S0007-1536(51)80043-3.

Kelnarová I., Černý K., Zahradník D., Koukol O., 2017. Widespread latent infection of *Cryptostroma corticale* in asymptomatic *Acer pseudoplatanus* as a risk for urban plantations. *Forest Pathology* 47: e12344. https://doi.org/10.1111/efp.12344.

Kottek M., Grieser J., Beck C., Rudolf B., Rubel F., 2006. World Map of the Köppen-Geiger climate classification updated. *Meteorologische Zeitschrift* 15: 259–263. https://doi.org/10.1127/0941-2948/2006/0130.

Koukol O., Kelnarová I., Černý K., 2014. Recent observations of sooty bark disease of sycamore maple in Prague (Czech Republic) and the phylogenetic placement of *Cryptostroma corticale*. *Forest Pathology* 45: 21–27. https://doi.org/10.1111/efp.12129.

Lacan I., McBride J.R., 2009. War and trees: The destruction and replanting of the urban and peri-urban forest of Sarajevo, Bosnia and Herzegovina. *Urban Forestry & Urban Greening* 8: 133–148. https://doi.org/10.1016/j.ufug.2009.04.001.

Langer G.J., Bressem U., Habermann M., 2013. Vermehrt Pilzkrankheiten an Bergahorn in Nordwestdeutschland. *AFZ-Der Wald* 6: 22–26.

Metzler B., 2006. *Cryptostroma corticale* an Bergahorn nach dem Trockenjahr 2003. *Mitteilungen aus der Biologischen Bundesanstalt für Land- und Forstwirtschaft* 400: 161–162.

Mirabile M., Bianco P.M., Silli V., Brini S., Chiesura A., … Gaudioso D., 2015. *Guidelines of Sustainable Urban Forestry for the Municipality of Rome*. (ISPRA, ed.), ISPRA Roma Capitale.

Moreau C., Moreau M., 1951. La 'Suie' des Sycamores a Paris. *Bulletin de la Société Mycologique de France* 67: 404–418.

Muller E., Dvořák M., Marçais B., Caeiro E., Clot B., … Gomez-Gallego M., 2023. Conditions of emergence of the Sooty Bark Disease and aerobiology of *Cryptostroma corticale* in Europe. *NeoBiota* 84: 319–347. https://doi.org/10.3897/neobiota.84.90549.

Oliveira Longa C.M., Vai N., Maresi G., 2016. *Cryptostroma corticale* in the northern Apennines (Italy). *Phytopathologia Mediterranea* 55: 136–138. https://doi.org/10.14601/Phytopathol_Mediterr-17164.

Pasta S., de Rigo D., Caudullo G., 2016. *Acer pseudoplatanus* in Europe: distribution, habitat, usage and threats. In: *The European Atlas of Forest Tree Species: Modelling, Data and Information on Forest Tree Species* (J. San-Miguel-Avanz, D. de Rigo, G. Caudullo, T. Houston Durant and A. Mauri, ed.), Luxembourg, Publ. Off. EU, e01665a+.

Pauleit S., Jones N., Garcia-Martin G., Garcia-Valdecantos J.L., Rivière L.M., … Randrup T.B., 2002. Tree establishment practice in towns and cities – Results from a European survey. *Urban Forestry & Urban Greening* 1: 83–96. https://doi.org/10.1078/1618-8667-00009.

Pauleit S., Jones N., Nyhuus S., Pirnat J., Salbitano F., 2005. Urban Forest Resources in European Cities. In: *Urban Forests and Trees* (C. Konijnendijk, K. Nilsson, T. Randrup and J. Schipperijn, ed.), Berlin/Heidelberg, Springer-Verlag, 49–80.

Plate H.P., Schneider R., 1965. Ein Fall von asthmaartiger Allergie, verursacht durch den Pilz *Cryptostroma corticale*. *Nachrichtenblatt des deutschen Pflanzenschutzdienstes* 17: 100–101.

Regione Toscana, 2024. Prima segnalazione in Toscana della "Corteccia fuligginosa dell'acero." *Regione Toscana - Agricoltura e Alimentazione - Servizion Fitosanitario Regionale*. Available at: https://www.regione.toscana.it/-/prima-segnalazione-in-toscana-della-corteccia-fuligginosa-dell-acero-un-fungo-che-pu%C3%B2-provocare-irritazioni-polmonari. Accessed June 18, 2024.

Robeck P., Heinrich R., Schumacher J., Feindt R., Kehr R., 2008. Status der Rußrindenkrankheit des Ahorns in Deutschland. In: *Jahrbuch der Baumpflege, Braunschweig 2008*: 238–244.

Schlößer R., Bien S., Langer G.J., Langer E.J., 2023. Fungi associated with woody tissues of *Acer pseudoplatanus* in forest stands with different health status concerning sooty bark disease (*Cryptostroma corticale*). *Mycological Progress* 22: 13. https://doi.org/10.1007/s11557-022-01861-6.

Sjöman H., Östberg J., Bühler O., 2012. Diversity and distribution of the urban tree population in ten major Nordic cities. *Urban Forestry & Urban Greening* 11: 31–39. https://doi.org/10.1016/j.ufug.2011.09.004.

Spiecker H., Hein S., Makonnen-Spiecker K., Thies M., 2009. Distribution of valuable broadleaved forests in Europe, Appendix B. In: *Valuable Broadleaved Forests in Europe*, Joensuu, Finland, European Forest Institute, 256.

Towey J.W., Sweany H.C., Huron W.H., 1932. Severe bronchial Astma apprently due to fungus spores found in marple bark. *Journal of the American Medical Association* 99: 453–459. https://doi.org/10.1001/jama.1932.02740580021005.

Townrow J.A., 1953. The Biology of *Cryptostroma corticale* and the Sooty Bark Disease of Sycamore. In: *Report on Forest Research*, H.M.S.O., London, 118–120.

White T.J., Bruns T., Lee S.J.W.T., Taylor J., 1990. Amplification and direct sequencing of fungal ribosomal RNA genes for phylogenetics. *PCR protocols: a Guide to Methods and Applications* 18: 315–322.

Young C.W.T., 1978. *Sooty Bark Disease of Sycamore*. London u.a, Stationery Office Books, Department of Environment, 1–8 pp.

ORCID:
BFA: 0000-0002-6605-8462
AHZ: 0000-0002-7507-5969
SAE-B: 0009-0005-2150-662X
HME-G: 0009-0002-9134-517X
YMR: 0000-0002-7702-8023
KMAE-H: 0009-0009-4069-2025
SAE-S: 0000-0002-2230-8087

Research Papers

Metallic oxide nanoparticles enhance chickpea resistance to root rot and wilt

Bandar F. ALMIMAN[1], Ahmed H. ZIAN[2,*], Salama A.S. EL-BLASY[2], Hala M. EL-GENDY[2], Younes M. RASHAD[3], Kamar M. ABD EL-HAI[2], Sahar A. EL-SAYED[1,2]

[1] *Biology Department, Faculty of Science, Al-Baha University, Al-Baha, 65779, Saudi Arabia*
[2] *Leguminous and Forage Crop Diseases Department, Plant Pathology Research Institute, Agricultural Research Center, Giza, 12619, Egypt*
[3] *Plant Protection and Biomolecular Diagnosis Department, Arid Lands Cultivation Research Institute (ALCRI), City of Scientific Research and Technological Applications (SRTA-City), New Borg El-Arab, 21934, Egypt*
*Corresponding author. E-mail: ahmed_hanafy1001@yahoo.com

Summary. Antifungal properties of nanoparticles (NPs) of copper oxide (CuO), titanium dioxide (TiO$_2$), and silica dioxide (SiO$_2$) were compared to the fungicide thiophanate-methyl for controlling root rot and wilt of chickpea, caused by, respectively, *Rhizoctonia solani* and *Fusarium oxysporum* f. sp. *ciceris*. Different concentrations (10, 20, or 40 ppm) of the NPs were assessed for their ability to inhibit fungal growth *in vitro*. All the nanoparticles had antifungal activity, with greatest effects at 40 ppm. CuO NPs at 40 ppm gave 61% reduction for Rhizoctonia rot and 65% reduction for Fusarium wilt. Alterations in the ultrastructure of the fungal mycelia were observed in response to treating with CuO NPs. No differences in *in vivo* tests were observed between CuO NPs and thiophanate-methyl for reducing root rot or wilt. Applications of CuO NPs also enhanced growth and yield of chickpea plants. CuO NPs had antifungal properties, increased activities of peroxidase and polyphenol oxidase in chickpea plants, and increased plant phenol contents. These results indicate that CuO NPs have potential as effective, eco-friendly alternatives to conventional fungicides for controlling of root rot and wilt of chickpea.

Keywords. *Rhizoctonia solani*, *Fusarium oxysporum* f. sp. *ciceris*.

INTRODUCTION

Chickpea (*Cicer arietinum* L.) is a highly nutritious legume, which is grown in more than fifty countries and is as a major source of proteins and carbohydrates for human and animal consumption. Through biological nitrogen fixation, chickpea plants also improve soil fertility (Jukanti *et al.*, 2012).

Chickpea plants are susceptible to wilt, caused by *Fusarium oxysporum* Schlecht emend. Snyd. & Hans. f. sp. *ciceris* (Padwick) Snyd. & Hans., and root rot caused by *Rhizoctonia solani* J.G. Kühn (Choudhary *et al.*, 2013; Zian

et al., 2023). These diseases may adversely affect chickpea growth metrics and crop productivity.

Using fungicides for control of fungal diseases offers several benefits, including availability, effectiveness, and fast action. However, the compounds have disadvantages, including potential harmful impacts on human and animal health, and development of fungicide resistant pathogen races (Yadav *et al.*, 2020). Environmental hazards resulting from fungicide use have also been demonstrated, and recent studies have been conducted to find alternative treatments (Al-Askar *et al.*, 2014; Rashad *et al.*, 2018; Rashad *et al.*, 2020a; Rashad *et al.*, 2022; Zian *et al.*, 2024). Novel approaches have therefore been assessed to managed fungal diseases, and safeguard and fortify worldwide food security while mitigating financial setbacks, by seeking methods to limit the use of fungicide compounds.

Nanotechnology can enhance crop production by boosting input efficiency and reducing losses. The most important benefit of using active nanomaterials is the large specific surface area they provide to fertilizers and pesticides. Furthermore, nanomaterials are can be carriers of agrochemicals, providing precise and targeted delivery of nutrients, leading to enhanced plant protection. Gogos *et al.* (2012) indicated that nanotechnology can alleviate issues related to food production as well as climate change by benefiting the environment and aiding in disease management (Worrall *et al.*, 2018). Nanoparticle materials have unique physicochemical features, including surface and quantum effects, that distinguish them from bulk materials. These effects enhance their ability to interact with fungi and perform therapeutic functions (Boxi *et al.*, 2016). Nanoparticles have minute diameters (1 to 100 nm). They adhere to fungal surfaces and penetrate and deposit into fungal cells, and have been shown to exhibit antifungal properties. These features include capacity to mechanically and physically harm cell walls and membranes, and to alter cellular signals by dephosphorylating potential integral peptide substrates that are essential for cell survival and division. Permeability of membranes is also increased, water channels are obstructed, and microbial enzymes are deactivated, reactive oxygen species effectively produced, respiration is halted, and other metabolic pathways are modified. All of these actions contribute to inhibition of fungal growth (Allahverdiyev *et al.*, 2011; Wang *et al.*, 2014). Nanoparticles can stimulate cell division, host callus development, enhance root structure, increase shoot length, leaf numbers, and overall biomass in many plant species under stress and also in normal conditions (Gohari *et al.*, 2020).

Silicon (Si) NPs can prevent pathogen infections by enhancing host plant disease resistance. Because plants transpire less, those with nanosilicon coatings have protection from high temperatures (Rastogi *et al.,* 2019; Rashad *et al.*, 2021). Plant growth and yield can be also be enhanced by Si NPs (Siddiqui and Al-Whaibi 2014; Suriyaprabha *et al.*, 2014). White rot was shown to be less common in garlic and onion plants when exogenous Si and silicate salts enhanced the action of host systemic defense enzymes (Elshahawy *et al.,* 2021). Silica treatment triggered potato resistance against late blight by improving the ethylene and jasmonic acid metabolism in separated foliage and in whole plants (Xue *et al.*, 2021).

Due to their photocatalytic and antibacterial characteristics, nanoparticles of titanium dioxide (TiO$_2$ NPs) and of other metal oxides have promise as agricultural additives. TiO$_2$ NPs increased photosynthetic activity of cucumber and reduced infections caused by *Pseudomonas syringae* pv. *lachrymans* and *Pseudoperonospora cubensis* in field research conducted by Cui *et al.* (2009). Servin *et al.* (2015) demonstrated how systemic acquired resistance or direct suppression of disease-causing organisms by nanoparticles of TiO$_2$, CuO, and ZnO could enhance in disease control programs.

Studies have demonstrated antifungal action of copper oxide nanoparticles (CuO NPs) on *F. oxysporum* that causes tomato wilt (Kanhed *et al.*, 2014), and *R. solani* (El-Shewy *et al.*, 2019; Ismail, 2021). Abou-Salem *et al.* (2022) also tested CuO NPs against *F. oxysporum, Macrophomina phaseolina,* and *Pectobacterium carotovorum*, which cause root rot in sugar beet. That study showed that CuO NPs at 150 µg mL^{-1} was an effective treatment, reducing disease incidence while enhancing vegetative growth, improving physiological traits, and boosting antioxidant enzyme activity. Elmer and White (2016) found when eggplant and tomato plants were cultivated in soil inoculated with *F. oxysporum* f. sp. *lycopersici* and *Verticillium dahliae*, CuO was more effective than other tested nanomaterials, including MnO, ZnO, NiO, TiO, FeO, and AlO.

Systemic resistance induced by abiotic agents has been extensively studied, since it enhances plant defense against a wide range of phytopathogens. Triggered systemic resistance involves several processes, including generation of salicylic acid and antibiotics, and expression of the antioxidant enzymes peroxidase (POD), polyphenol oxidase (PPO), and other phenolic compounds. Copper has many functions in plant physiological and biochemical processes as an enzyme activator, and is integral to numerous enzymes. Copper is also essential for plant growth and nutrition (Bowler *et al.,* 1992; Kasana and AliNiazee, 1997). Previous studies Nair and

Chung (2014) showed that treatments with copper oxide nanoparticles (CuO NPs) enhanced activities of ascorbate peroxidase (APX) and peroxidase (POD). Sarkar *et al.* (2020) demonstrated that lentil plants treated with CuO NPs had high activity of APX and superoxide dismutase (SOD). Potato plants treated with CuO NPs had enhanced PPO and POD activities (Ismail, 2021).

The present study aimed to investigate the efficacy of nanoparticles of CuO, TiO$_2$, and SiO$_2$ nanoparticles in comparison with the fungicide thiophanate-methyl, for suppressing *R. solani* and *F. oxysporum* f. sp. *ciceris*, enhancing chickpea defense responses, affecting plant growth parameters. Effects of CuO NPs on chickpea ultrastructure were also assessed.

MATERIALS AND METHODS

Chickpea seeds

Chickpea seeds (cv. Giza-2) were obtained from the Legume Research Department, Field Crops Research Institute, ARC, Giza, Egypt.

Nanoparticles and fungicide

The three tested nanomaterials were purchased from Nanotechnology & Advanced Nano-Materials Laboratory (NANML), Plant Pathology Research Institute (PPRI), Giza, Egypt. These were: CuO NP (25 ± 5 nm particle size (Supplementary data), and previously characterized by Ismail (2021); Ti$_2$O NP (45 ± 5 nm particle size (Supplementary data); and SiO$_2$ NP (50 ± 23 nm particle size) (Supplementary data). Sterilized distilled water was used to produce all stock solutions. A Transonic 420 sonicator (Elma) was used to sonicate nanoparticle suspensions for 30 min before they were applied as seed soakings or included in sterilized plant growth medium. The chemical fungicide (thiophanate-methyl (Topsin-M70° 70% WP, Cairo Chemical Company, Egypt) was used for comparisons with the three nanomaterials.

Chickpea root rot and wilt pathogens

Two virulent isolates (Zian *et al.*, 2023), one of *R. solani* (accession No. OR074128) and the other of *F. oxysporum* f. sp. *ciceris* (accession No. OR074126), were used in this study. These isolates were previously obtained from chickpea fields in the Ismailia governorate, Egypt, where they had caused symptoms of wilt and root rot.

Screening the tested nanoparticles for antifungal activity

CuO NP, TiO$_2$ NP, and SiO$_2$ NP were each assessed at 10, 20, and 40 ppm against *R. solani* and *F. oxysporum* f. sp. *ciceris* and compared to thiophanate-methyl. Initial stock solutions of nanoparticles were prepared at concentrations of 1000 ppm, and were diluted with sterile deionized water to obtain these concentrations. Before being utilized in experiments, the solutions were maintained at 4°C. The agar dilution procedure reported by Fraternale *et al.* (2003) was used for *in vitro* assays. The prepared concentrations of nanoparticles and thiophanate-methyl at 200 ppm were added to sterilized potato dextrose agar (PDA) before solidification, and the amended agar was poured into Petri dishes (9 cm diam.). Agar discs (5 mm diam.) were taken from the margins of 7-d-old cultures of the test fungi and placed individually in the center of each plate. PDA plates without nanoparticle or fungicide amended media and inoculated with the assessed fungi served as experimental controls. The plates were then incubated at 25 ± 2°C for 7 d, and radial growth of the fungi was measured after 4 and 7 d of incubation. Each treatment was applied in four replicates, and the assay was repeated twice. Inhibition of mycelium growth of the two tested fungi was calculated using the procedure of Kaur *et al.* (2012).

The equation used for calculating inhibition percentage of the fungi was:

$$\text{Inhibition \%} = \frac{C - T}{C} \times 100$$

where C = radial growth in control plates, and T = radial growth in the treatment.

Transmission electron microscopy studies

Effects of CuO NP on the ultrastructure of the *R. solani* and *F. oxysporum* f. sp. *ciceris* were assessed by taking samples from cultures used in the nanoparticle antifungal assessments (above), after 3 d incubation. Morphological modifications in the hyphal cell structures of the two fungi were assessed using transmission electron microscopy (TEM). Specimens (1 mm^2 each) were taken from each treated colony. The samples were added to phosphate buffer and then washed in a 3% glutaraldehyde solution, and then fixed in potassium permanganate solution for 5 min. The specimens were then dehydrated for 30 min using absolute ethanol, with immersion in nine ethanol concentrations (10 to 90%), for 15 min in each concentration. The samples were then treated in a graded epoxy resin and acetone series, fol-

lowed by immersion in pure wax, then loaded onto copper grids, followed by staining in uranyl acetate and lead citrate. A JEOL JEM 1010 transmission electron microscope running at 70 kV was used to observe the stained sections (Amin, 2016; Amin *et al.*, 2020; Amin *et al.*, 2022).

Cytotoxicity bioassay

Cytotoxicity bioassays were carried out using the cell line WI-38, ATCC® CCL-75 (normal human fetal lung fibroblasts). For preparation of the cell monolayer, the cells were grown on fetal bovine serum (FBS) medium and adjusted at 5×10^5 cell mL^{-1}. In a 96 well plate, 200 μL of cell culture was added to each well, except the peripheral wells which were used as blanks. The plate was then incubated at 37°C for 24 h. To investigate CuO NP cytotoxicity, the nanoparticles were serially diluted in culture medium. The test was carried out in three replicates, with three plates (media only) as experimental controls. After 24 h, the plate was assessed using MTT assay on a microplate ELISA reader (M965 Mate 2.0). Inhibition percentages were calculated for each nanoparticle each concentration (Rashad *et al.*, 2021). The half-maximum inhibitory concentrations (IC$_{50}$s) were determined using the Graph Pad Prism program.

Hemolytic activity assay

This assay was carried out using 2 mL capacity tubes, and the procedure of Farias *et al.* (2013), with minor adjustments. CuO NP was serially diluted in 0.9% NaCl solution. 100 μL of 1% rabbit red blood cell solution was combined with 900 μL of the each nanoparticle dilution in each microtube, and the microtubes were incubated at 37°C for 1 h and then centrifuged for 5 min at 3000 rpm. Supernatant was then poured into a 96-well plate (200 μL per well), and the absorbance of the supernatant was determined (at 540 nm) using a spectrophotometer. Experimental controls each used 900 μL of 0.9% NaCl combined with 100 μL of the red blood cell suspension. The CuO NP concentration required to achieve a 50% inhibition of red blood cell hemolysis was used to obtain the IC$_{50}$ value for the tested nanoparticles.

Pot experiments

For inoculum preparation, Inoculum of the two fungal pathogens (*F. oxysporum* and *R. solani*) was prepared after the fungi were cultured on sorghum/sand (2:1 v/v)

medium. This sterilized at 121°C and 1.5 air pressure for 20 min. Agar discs (5 mm diam.) from 4-d-old *R. solani* culture (mycelium) or 7-d-old *F. oxysporum* culture (mycelium and spores) were used to inoculate the sterilized media. The bottles containing the inoculated media for soil inoculation in pot tests were then incubated at 25 ± 2°C for 15 d.

Pot experiments were carried out under natural conditions to compare effects of CuO, TiO$_2$, or SiO$_2$ NPs with thiophanate-methyl for effects on root rot and wilt of chickpea. The two pathogens were separately cultured in glass bottles on sorghum/sand (3:1 w/w) medium for 15 d at 25 ± 2°C. Each plastic pot (approx. 30 cm diam.) was filled with 6 kg of soil (clay plus sand, 1:1 v/v) which had been disinfected with formalin. Fungal inoculum (mycelium and sclerotia of *R. solani*, mycelium and conidia of *F. oxysporum*) was added at 2% of the soil weight, as by Papavizas and Devey (1962). Inoculated soil was watered and then allowed to rest for 1 week to allow proliferation of the fungi. The Nanoparticles of CuO, TiO$_2$ or SiO$_2$ were prepared at 40 ppm, along with 0.2% Tween 80, and were each used as chickpea seed soaks for 2 h before planting. The fungicide thiophanate-methyl was applied at 3 g kg^{-1} seeds. The treated seeds were then planted in the pots (five seeds per pot), and the pots were regularly watered and fertilized. Each experimental treatment was applied to four replicate pots, and additional pots, seeded in sterile soil, were used as non-inoculated controls for comparisons with the treated pots containing the pathogens. The pots were arranged in completely randomize experimental design, and the experiment was repeated twice.

Assessments of damping-off and root rot of the chickpea plants were carried out at 30 and 90 d after planting. Numbers of plants affected were assessed as percentages, respectively, of early and late wilt, in a similar manner, at 30 an 90 days using the following equations:

$$\text{Damping-off \%} = \frac{\text{No. of un-germinated seeds after 15 days + no.of dead seedlings after 30 days}}{\text{Total No. of sown seeds}} \times 100$$

$$\text{Root rotted plants \%} = \frac{\text{No. of rotted seedlings after 90 days}}{\text{Total No. of sown seeds}} \times 100$$

$$\text{Early wilt \%} = \frac{\text{No. of wilted plants after 30 days}}{\text{Total No. of sown seed}} \times 100$$

$$\text{Late wilt \%} = \frac{\text{No. of wilted plants after 90 days}}{\text{Total No. of sown seed}} \times 100$$

$$\text{Survived plants \%} = \frac{\text{No. of survival plants after 90 days}}{\text{Total No. of sown seeds}} \times 100$$

The percentage that was reduced or increased above the infested control was also determined using the subsequent calculation:

$$\text{Reduction or Increasing \%} = \frac{\text{DI of Control} - \text{DI of treatment}}{\text{DI of Control}} \times 100$$

Effects of nanoparticles on the antioxidant enzymes and total phenol contents

Fresh leaves were picked from chickpea plants 15 d after seed sowing, and extracts were made from the leaves. The peroxidase (POD) and total phenol contents (PPO) in these extracts were assessed (four replicates each). POD activity in the chickpea leaf extracts was assayed using the procedure of Chakraborty and Chatterjee (2007). PPO was extracted and assayed based on the protocol of Sadasivam and Manickam (1996), and total phenol content in the plants was determined as described by Zilesin and Ben-Zaken (1993).

Field experiments

Field experiments were carried out at the Sers El-Layian and Etai El-Baroud farms of the Agricultural Research Station during 2021/2022, assess the efficacy of CuO, TiO$_2$ and SiO$_2$ nanoparticles for managing chickpea root rot and wilt. Three replicates of each treatment were used a randomized block design field trial. Each replicate comprised four rows (each 3 m long and 50 cm wide, covering 6 m^2 (2 × 3 m). Before planting, chickpea seeds were soaked for 2 h in the same nanoparticle treatments used in the pot experiment (described above). In each plot, one seed per hill was planted on either side of the row ridge, 25 cm between each seed. The experimental control treatment comprised soaking seeds in distilled water for 2 h.. At both sites, all normal agricultural practices were followed during the trials. Proportions of damping-off, rotten seedlings, wilted plants, and surviving plants were recorded. At harvest, measurements of plant height, number of branches, number of capsules, seed weight, weights of 100 seeds and total seed yield were determined.

Statistical analyses

The statistical program COSTAT version 6.4 was used for statistical analyses of data. Mean values from different treatments were compared using Duncan's multiple-range test, and significance standards for comparisons of means were indicated as $P \le 0.01$ and $P \le 0.05$.

RESULTS

Effects of nanoparticles on the fungal growth

As indicated in Table 1, all the assessed nanoparticles (CuO, TiO$_2$ and SiO$_2$) at all tested concentrations decreased mycelium growth of the two fungi. CuO NPs

Table 1. Mean colony diameters of *Rhizoctonia solani* and *Fusarium oxysporum* f. sp *ciceris* in agar amended with different concentrations of three nanoparticles, or the fungicide thiophanate-methyl.

Treatment	Concentration (ppm)	*R. solani*		*F. oxysporum* f. sp. *ciceris*	
		Mean fungal growth (mm)	% reduction	Mean fungal growth (mm)	% reduction
Control	-	90.0 ± 0 [a]	0.0	90.0 ± 0 [a]	0.0
CuO-NPs	10	71.0 ± 1.0 [d]	21.2	70.2 ± 0.2 [d]	22.0
	20	56.1 ± 1.2 [f]	37.6	54.4 ± 0.7 [f]	39.6
	40	35.4 ± 0.5 [h]	60.7	31.1 ± 0.9 [i]	65.3
TiO$_2$-NPs	10	81.8 ± 1.2 [b]	09.0	75.8 ± 0.8 [b]	15.7
	20	61.4 ± 0.6 [e]	31.7	59.1 ± 0.9 [e]	34.4
	40	40.8 ± 0.7 [g]	54.6	38.3 ± 0.7 [g]	57.3
SiO$_2$-NPs	10	74.8 ± 0.7 [c]	16.8	72.7 ± 0.6 [c]	19.1
	20	57.8 ± 0.7 [f]	35.7	55.1 ± 0.8 [f]	38.8
	40	39.5 ± 1.3 [g]	56.2	36.4 ± 0.5 [h]	59.4
Thiophanate-methyl	200	00.0 ± 0 [i]	100.0	00.0 ± 0 [j]	100.0

Means in each column accompanied by different letters are different ($P \le 0.01$), as indicated by Duncan's multiple-range test. Standard deviations of the means are also indicated.

at 40 ppm gave the greatest antifungal effects, by 61.7% for *R. solani* and 65.3% for *F. oxysporum* f. sp. *ciceris*. SiO$_2$ and TiO$_2$ NPs at 40 ppm also reduced growth of these fungi. TiO$_2$-NP at 10 ppm gave the least suppression of mycelium growth for both fungi. Inhibition of fungal growth decreased with reductions in nanoparticle concentrations, and *F. oxysporum* was less sensitive to nanoparticles than *R. solani*. The fungicide thiophanate-methyl completely suppressed growth of both fungi.

TEM observations

Figure 1 contains transmission electron micrographs of transverse sections of *R. solani* hyphae. A normal and organized cell (Figure 1a) is enclosed by a thin electron-dense cell wall and a thin electron-lucent plasma membrane. The cytoplasm contains a normal nucleus, vacuoles, and electron-lucent glycogen granules. In contrast, *R. solani* hyphae treated with CuO NPs (Figure 1b) had abnormal disorganized cells with cytoplasmic granulation, numerous mitochondria and electron-dense bodies that were enclosed by electron-dense cell walls.

Figure 2 a shows a normal untreated cell of *F. oxysporum* f. sp. *ciceris*. The cell has a thin cell wall, a thin plasma membrane, a normal nucleus, and mitochondria in the cytoplasm. Numerous electron-lucent glycogen bodies were also present. Mycelium of *F.*

oxysporum, treated with CuO NPs had many ultrastructural alterations (Figure 2b). The treated cell was irregular with thickening of the cell wall and plasma membrane. Cytoplasmic granulation, an irregular large vacuole and many electron-dense particles were also present.

Cytotoxicity of CuO-NPs

The CuO NPs had toxic effects on human lung fibroblast cells (WI-38), particularly at high concentrations. Cytotoxicity of CuO NPs increased with increasing concentration, reaching complete mortality at 255 ppm (Figure 3a). At 40 ppm, the CuO NPs gave 80% cytotoxicity, while its IC$_{50}$ was 25.2 ppm. In contrast, the hemolytic activity assay showed that CuO NPs did not have substantial adverse effects on red blood cells (no toxicity at 100 ppm; Figure 3b). At 40 ppm, the CuO NPs gave 8% hemolytic activity of red blood cells, and the IC$_{50}$ for the CuO NPs was 440.1 ppm.

Pot experiments

All the treatments (nanoparticles or thiophanate-methyl) reduced damping-off, root rot and wilt diseases (Table 2). Thiophanate-methyl exhibited the greatest efficacy. Least occurrences of root rot and wilt were recorded after treatments with CuO NPs. Plants treated with
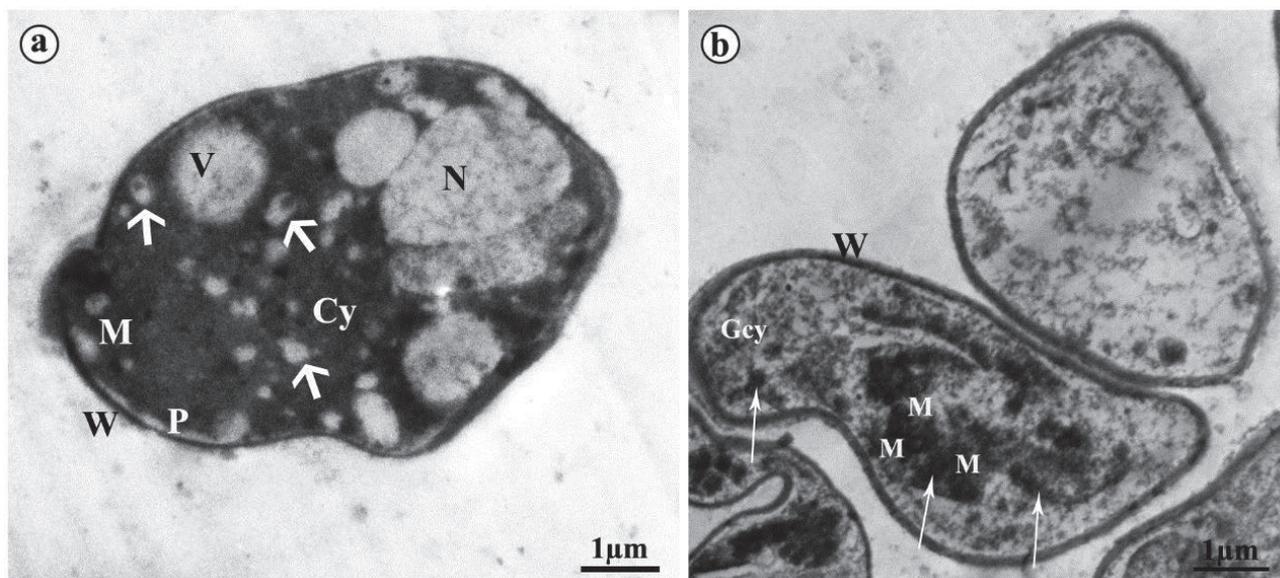
Figure 1. Transmission electron micrographs transverse section of hyphae of *Rhizoctonia solani*. a) An untreated hypha has a thin electron-dense cell wall (W) and a thin electron-lucent plasma membrane (P). The cytoplasm (Cy) has a normal nucleus (N), vacuoles (V), and electron-lucent glycogen granules (arrowheads). b) A hypha of *R. solani* which was treated with CuO NPs has granulated cytoplasm (Gcy), many mitochondria (M), and electron-dense bodies (arrows) that are enclosed by an electron-dense cell wall (W).
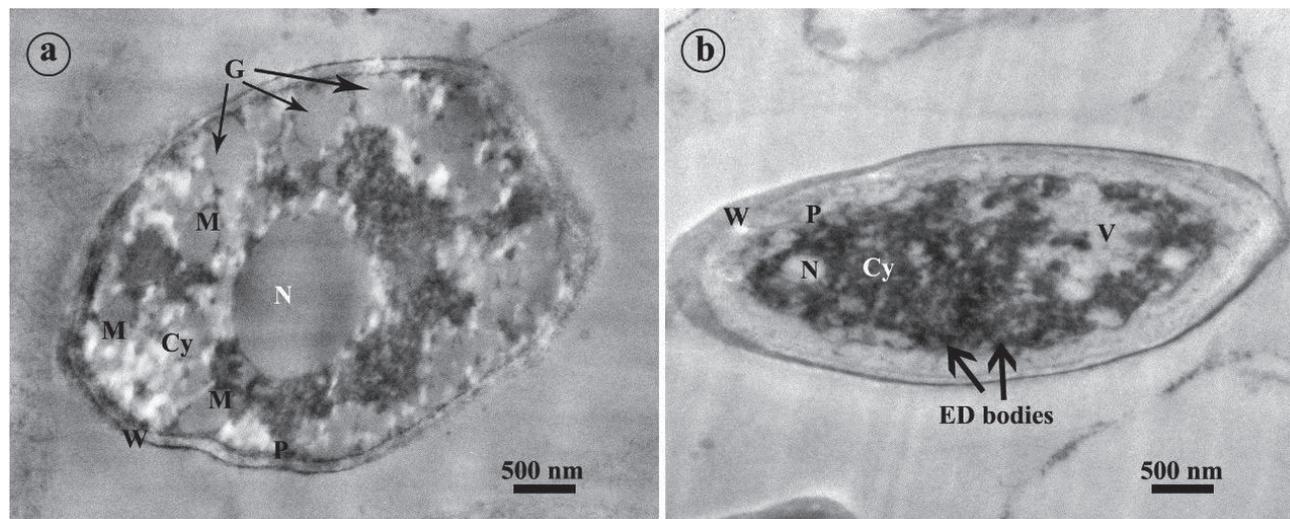
Figure 2. Transmission electron micrographs of transverse sections of hyphae of *Fusarium oxysporum* f. sp. *ciceris*. a) An untreated hypha with a thin cell wall (W), a thin plasma membrane (P), a normal nucleus (N), and mitochondria (M) in the cytoplasm (Cy). Numerous electron-lucent glycogen bodies (G) were also observed. b) A hypha of *F. oxysporum* which was treated with CuO-NPs had a thickened cell wall (W) and plasma membrane (P). Cytoplasmic granulation (Cy), an irregular large vacuole (V) and many electron-dense particles were also observed.
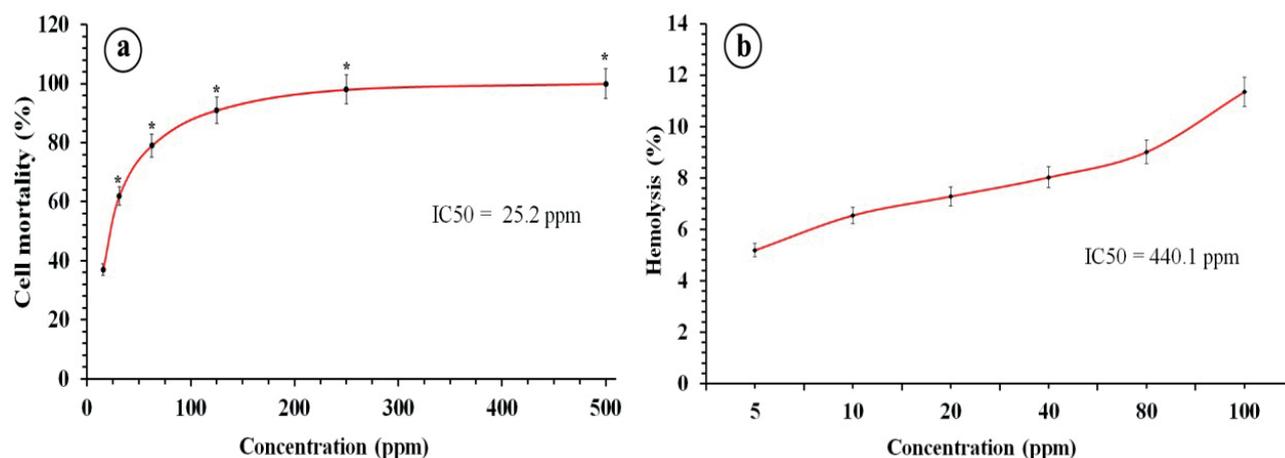
Figure 3. Cytotoxicity bioassay of CuO-NPs. Bioassay carried out at exposure time of 24 h on (a) human fetal lung fibroblasts (Vero), plus (b) lung epithelial cells (BEAS-2B). Each value is the mean of three replicates (± standard error). IC_{50} = the half-maximal inhibitory dose. * = significant at $P \leq 0.05$, compared with experimental controls.

SiO_2 or TiO_2 NPs also had reductions in these diseases, but to lesser extents than from CuO NPs. When the plants were inoculated with either *R. solani* or *F. oxysporum* f. sp. *ciceris,* greatest plant survival occurred after treatments with CuO NPs.

Effects of nanoparticles on the antioxidant enzymes and total phenol contents

Applications of the different nanoparticles increased oxidative enzyme activity and total phenol contents in chickpea plants (Table 3). For inoculations with *R. solani*, CuO NPs gave the greatest POD activity, followed by TiO_2 NPs and thiophanate-methyl. PPO activity also increased in response to CuO NP treatment, thiophanate-methyl, or SiO_2 NP treatments. In the plants inoculated with *F. oxysporum* f. sp. *ciceris*, the CuO NP treatments resulted in the greatest activity levels of both POD and PPO.

The chickpea plants treated with nanoparticles had high total phenolic contents. The greatest total phenolic content was recorded for plants treated with CuO NPs. Total phenol contents increased after treatments with

Table 2. Mean disease parameters in pot trials, where chickpea plants were exposed to *Rhizoctonia solani* (A) or *Fusarium oxysporum* (B) after treatments with different nanoparticles, or the fungicide thiophanate-methyl.

(A) *Rhizoctonia solani*:

Treatment	Damping-off %		Rotted seedlings %		Surviving plants %	% increase
	Incidence %	% reduction	Incidence %	% reduction		
CuO NPs	5.0 ± 10 [cd]	80.0	10.0 ±11.5 [b]	50.0	85.0 ± 10 [bc]	54.5
TiO$_2$NPs	15.0 ± 10 [b]	40.0	10.0 ± 11.5 [b]	50.0	75.0 ± 10 [d]	36.3
SiO$_2$ NPs	10.0 ± 11.5 [bc]	60.0	10.0 ± 11.5 [b]	50.0	80.0 ± 0 [cd]	45.4
Thiophanate-methyl	5.0 ± 10 [cd]	80.0	5.0 ± 10 [bc]	75.0	90.0 ± 11.5 [b]	63.6
Inoculated control	25.0 ± 10 [a]	-	20.0 ± 0 [a]	-	55.0 ± 10 [e]	-
Non-inoculated control	0.0 ± 0 [d]	-	0.0 ± 0 [c]	-	100.0 ± 0 [a]	-

(B) *Fusarium oxysporum* f. sp. *ciceris*:

Treatment	Wilted plants %				Surviving plants %	% increase
	Early wilt		Late wilt			
	Incidence %	% reduction	Incidence %	% reduction		
CuO-NPs	5.0 ± 10 [bc]	66.7	5.0 ± 10 [b]	80.0	90.0 ± 11.5 [bc]	50.0
TiO$_2$-NPs	5.0 ± 10 [bc]	66.7	10.0 ± 11.5 [b]	60.0	85.0 ± 10 [cd]	41.7
SiO$_2$ -NPs	10.0 ± 11.5 [ab]	33.4	10.0 ± 11.5 [b]	60.0	80.0 ± 0 [d]	33.4
Thiophanate-methyl	0.0 ± 0 [c]	100.0	5.0 ± 10 [b]	80.0	95.0 ± 10 [ab]	58.4
Inoculated control	15.0 ± 10 [a]	-	25.0 ± 10 [a]	-	60.0 ± 0 [e]	-
Non-inoculated control	0.0 ± 0 [c]	-	0.0 ± 0 [b]	-	100.0 ± 0 [a]	-

Means in each column accompanied by different letters are different ($P \leq 0.05$), as indicated by Duncan's multiple-range test. Standard deviations of the means are also indicated.

CuO NPs, TiO$_2$ NPs, and thiophanate methyl, although this effect was least for the fungicide. However, in comparison to the control, the use of SiO$_2$ NP treatments had the least effects on overall phenol contents.

Field experiments

All the experimental treatments decreased root rot and wilt of field-grown chickpea plants. Thiophanate-methyl gave the greatest disease reductions at Etai El-Baroud (Table 4), followed by treatments with CuO or TiO$_2$ NPs, which also reduced disease incidence. The SiO$_2$ NP treatment gave the least reduction in incidence of the two diseases. At Sers El-Layian, thiophanate-methyl was again the most effective treatment, giving the greatest reduction in disease incidence. CuO and SiO$_2$ NP treatments also had disease reduction efficacy, but to a lesser extent than thiophanate-methyl. However, The TiO$_2$ NP treatment was the least effective of the tested treatments

Effects of nanoparticles on the chickpea growth parameters in field conditions

After the nanoparticle treatments, chickpea growth and yields were increased at both field trial sites (Table 5). Applications of thiophanate-methyl or CuO NP treatments increased plant heights. All the treatments increased chickpea branch numbers compared to the experimental control. Thiophanate-methyl was most effective treatment at Etai El-Baroud experiment, followed by CuO NP and TiO$_2$ NP treatments. At the Sers El-Layian Agricultural Research Station, thiophanate-methyl was again the most effective treatment, followed by treatments with CuO NPs or SiO$_2$ NPs.

In contrast to the control treatment, all yield parameters were increased by the different experimental treatments, including 100 seed weights, numbers of capsules per plant, and plant seed weights. The treatments with thiophanate-methyl or CuO NPs at both trial sites produced the greatest yield parameters. Thiophanate-methyl gave

Table 3. Mean peroxidase and polyphenoloxidase activities, and total phenols, in chickpea plants receiving different nanoparticle and fungicide treatments, and inoculations with either *Rhizoctonia solani* (A) or *Fusarium oxysporum* f. sp. *ciceris* (B).

Treatment	Peroxidase (unit/mg protein/min)		Polyphenoloxidase (unit /mg protein/min)		Total phenols (mg/g fresh leave weight)	
	Activity	% increase	Activity	% increase	Activity	% increase
(A) *Rhizoctonia solani*						
CuO-NPs	1.46 ± 0.03 [a]	217.3	1.48 ± 0.02 [a]	139.4	4.24 ± 0.03 [a]	100.7
TiO$_2$-NPs	1.12 ± 0.04 [b]	142.6	1.13 ± 0.03 [c]	82.4	3.54 ± 0.02 [b]	67.7
SiO$_2$-NPs	0.83 ± 0.1 [c]	79.8	1.28 ± 0.02 [b]	107.4	2.64 ± 0.01 [c]	24.9
Thiophanate-methyl	1.33 ± 0.02 [a]	188.5	1.42 ± 0.02 [a]	128.9	2.68 ± 0.02 [c]	27.1
Inoculated control	0.46 ± 0.01 [d]	-	0.62 ± 0.01 [d]	-	2.11 ± 0.01 [d]	-
Non-inoculated control	0.36 ± 0.01 [d]	-	0.51 ± 0.01 [e]	-	1.93 ± 0.02 [e]	-
(B) *Fusarium oxysporum* f. sp. *ciceris*						
CuO-NPs	1.49 ± 0.03 [a]	208.8	1.57 ± 0.02 [a]	114.8	4.25 ± 0.02 [a]	97.5
TiO$_2$-NPs	1.21 ± 0.01 [c]	150.1	1.16 ± 0.01 [c]	58.9	3.78 ± 0.02 [b]	75.8
SiO$_2$-NPs	0.93 ± 0.02 [d]	92.3	1.32 ± 0.02 [b]	79.9	2.88 ± 0.02 [d]	34.0
Thiophanate-methyl	1.37 ± 0.01 [b]	182.6	1.52 ± 0.02 [a]	107.5	2.96 ± 0.01 [c]	37.6
Inoculated control	0.48 ± 0.01 [e]	-	0.73 ± 0.02 [d]	-	2.15 ± 0.02 [e]	-
Non-inoculated control	0.36 ± 0.01 [f]	-	0.51 ± 0.01 [e]	-	1.93 ± 0.02 [f]	-

Means in each column accompanied by different letters are different ($P \leq 0.01$), as indicated by Duncan's multiple-range test. Standard deviations of the means are also indicated.

Table 4. Mean incidences of damped-off, rotted chickpea seedlings, or and wilted plants in two field trials (A and B) carried out during the 2021/2022 growing seasons.

Treatment	Damping- off		Rotted seedlings		Wilted plant		Surviving plants %	% increase
	Incidence %	% reduction	Incidence %	% reduction	Incidence %	% reduction		
(A) Etai El-baroud Agricultural Research Station								
CuO-NPs	3.7 ± 1.5 [b]	66.3	4.0 ± 1.0 [b]	58.7	4.0 ± 0 [b]	69.2	88.3 ± 2.5 [ab]	33.2
TiO$_2$-NPs	4.0 ± 2.0 [b]	63.6	3.7 ± 1.5 [b]	61.8	6.0 ± 1.0 [b]	53.8	86.3 ± 1.5 [bc]	30.1
SiO$_2$-NPs	5.0 ± 1.0 [b]	54.5	5.4 ± 1.1 [b]	44.3	6.0 ± 1.0 [b]	53.8	83.6 ± 1.5 [c]	26.0
Thiophanate-methyl	2.7 ± 0.5 [b]	75.4	3.0 ± 0 [b]	69.0	4.0 ± 1.0 [b]	69.2	90.3 ± 0.5 [a]	36.2
Control	11.0 ± 1.0 [a]	-	9.7 ± 1.5 [a]	-	13.0 ± 2.6 [a]	-	66.3 ± 2.5 [d]	-
(B) Sers El-layian Agricultural Research Station								
CuO-NPs	2.7 ± 0.5 [c]	66.2	3.0 ± 0 [cd]	55.2	4.3 ± 1.1 [bc]	70.5	90.0 ± 1.7 [a]	27.3
TiO$_2$-NPs	5.0 ± 1.0 [b]	37.5	4.7 ± 0.5 [b]	29.8	6.7 ± 0.5 [b]	54.1	83.6 ± 0.5 [b]	18.2
SiO$_2$-NPs	4.7 ± 1.1 [b]	41.2	4.0 ± 1.0 [bc]	40.3	6.0 ± 1.7 [b]	58.9	85.3 ± 3.7 [b]	20.6
Thiophanate-methyl	2.4 ± 1.1 [c]	70.0	2.0 ± 1.0 [d]	70.1	2.6 ± 1.1 [c]	82.2	93.0 ±1.0 [a]	31.5
Control	8.0 ± 1.0 [a]	-	6.7 ± 0.5 [a]	-	14.6 ± 1.1 [a]	-	70.7 ± 0.5 [c]	-

Means in each column accompanied by different letters are different ($P \leq 0.05$), as indicated by Duncan's multiple-range test. Standard deviations of the means are also indicated.

the greatest yield increases at Etai El-Baroud, followed by treatments with CuO NPs and TiO$_2$ NPs. The greatest seed production obtained at Sers El-Layian was from treatments with thiophanate-methyl, CuO NPs or SiO$_2$ NPs.

DISCUSSION

Plant disease control can be difficult in crop production, and increases in fungicide resistance in phytopath-

Table 5. Mean chickpea plant parameters at two field sites after applications of different treatments in two field trials (A and B) in the 2021/2022 growing season.

Treatment	Plant height (cm)	Number of branches/plant	Number of capsules/plant	Weight (g) of seeds/plant	Weight (g) of 100 seeds	Seed yield (kg/feddan)
(A) Etai El-baroud Agricultural Research Station						
CuO NPs	81.4 ± 5.5 [a]	4.8 ± 1.3 [a]	26.6 ± 1.0 [a]	11.7 ± 0.8 [b]	29.0 ± 1.1[b]	1110.3 ± 1.5 [b]
TiO$_2$ NPs	81.0 ± 2.5 [a]	4.3 ± 0.3 [ab]	25.4 ± 1.2 [ab]	11.3 ± 0.8 [bc]	27.9 ± 0.5 [b]	1098.0 ± 23.4 [b]
SiO$_2$ NPs	77.4 ± 3.0 [a]	3.6 ± 1.0 [b]	23.8 ± 1.3 [b]	10.5 ± 0.1 [c]	27.4 ± 0.5 [b]	1065.0 ± 7.2 [c]
Thiophanate-methyl	82.3 ± 5.9 [a]	4.9 ± 0.6 [a]	27.1 ± 1.6 [a]	12.7 ± 0.2 [a]	32.0 ± 2.0 [a]	1204.3 ± 13.6 [a]
Control	67.0 ± 1.7 [b]	1.8 ± 0.2 [c]	19.4 ± 0.8 [c]	7.0 ± 0.2 [d]	18.5 ± 0.7 [c]	720.0 ± 12.4 [d]
(B) Sers El-layian Agricultural Research Station						
CuO-NPs	104.3 ± 4.1[a]	5.4 ± 0.5 [a]	27.1 ± 1.4 [ab]	13.4 ± 0.1 [b]	31.4 ± 3.2 [ab]	1167.4 ± 26.6 [b]
TiO$_2$ NPs	89.6 ± 4.0 [bc]	4.0 ± 1.7 [ab]	25.5 ± 1.0 [c]	11.7 ± 0.2 [c]	27.7 ± 0.6 [b]	1092.0 ± 10.1 [c]
SiO$_2$ NPs	94.0 ± 3.4 [b]	4.5 ±1. [a]	26.4 ± 1.1 [bc]	12.3 ± 0.1 [c]	28.3 ± 0.7 [b]	1110.7 ± 1.5 [c]
Thiophanate-methyl	106.3 ± 3.0 [a]	5.5 ± 1.3 [a]	28.3 ± 0.8 [a]	14.5 ± 0.9 [a]	34.7 ± 4.5 [a]	1213.4 ± 18.9 [a]
Control	81.6 ± 5.7 [c]	2.3 ± 0.05 [b]	20.1 ± 0.5 [d]	8.6 ± 0.4 [d]	20.4 ± 0.5 [c]	780.4 ± 5.5 [d]

Means in each column accompanied by different letters are different ($P \leq 0.05$), as indicated by Duncan's multiple-range test. Standard deviations of the means are also indicated

ogenic fungi have become important. Fungicides are frequently used to manage fungal infections and protect crops, and frequent and inappropriate use of these compounds has induced resistance in many economically important fungi (Goffeau, 2008).

Significant effort has been applied to create non-hazardous disease management practices. Nanoparticles have been proposed as possible pesticide substitutes for managing diseases caused by pathogenic bacteria. Nanoparticles can also have antifungal capabilities, are environmentally benign, and are also cost-effective (Gupta and Gupta, 2005; Nel, *et al.*, 2006).

The present study has demonstrated that nanoparticles of CuO, TiO$_2$, and SiO$_2$, at different concentrations, reduced the fungal growth of *F. oxysporum* f. sp. *ciceris* and *R. solani*, which are important pathogens of chickpea. CuO NPs at 40 ppm had the greatest inhibitory effects on these fungi, with growth reduction of 35% for *R. solani* and 31% for *F. oxysporum* f. sp. *ciceris*. These results are similar to those from previous studies. Hermida-Montero *et al.* (2019) showed that CuO NPs contributed to development of reactive oxygen species (ROS) and caused membrane damage in *F. oxysporum*. They also reported decreases in fungal radial growth and alterations in hyphal morphology of this fungus. El-Shewy *et al.* (2019), using CuO NPs at 200 μL L^{-1}, decreased growth of *R. solani* by 55%. Oussou-Azo *et al.* (2020) noted that Cu NPs at 200 mg mL^{-1} suppressed growth of *Colletotrichum gloeosporoides* by 77%. Kanhed *et al.* (2014) recorded strong activity of CuO NPs against

F. oxysporum, Alternaria alternata, Phoma distructiva and *Curvularia lunata*.

Nanoparticles can physically and mechanically damage fungal cell walls and membranes, give these materials their antifungal properties. They can penetrate and accumulate within fungal cells, and can influence cellular signaling at the molecular level by dephosphorylating peptide substrates that are essential for cell viability and division. They can also enhance membrane permeability, block water channels, inhibit enzymes, and increase production of reactive oxygen species produced. These activities can disrupt essential metabolic pathways leading to the death or inhibition of fungi (Allahverdiyev *et al.*, 2011; Wang *et al.*, 2014). Perez-de-Luque and Rubiales (2009) also reported that extracellular enzymes and metabolites may be released as a result of using nanoparticles.

Transmission electron micrographs of hyphae of *F. oxysporum* f. sp. *ciceris* and *R. solani* verified the damage caused by CuO NP treatments. Treating *R. solani* mycelium with CuO NPs gave abnormal and disorganized cells with cytoplasm granulation, numerous mitochondria, and electron-dense bodies enclosed by electron-dense cell walls. Treated cells of *F. oxysporum* were irregular with thickened cell walls and plasma membranes. Cytoplasmic granulation, irregular large vacuoles and many electron-dense particles were also observed. El-Shewy *et al.* (2019) and Ismail (2021) observed similar effects to those observed in the present study.

Results from the cytotoxicity assay showed that CuO NPs were toxic to the test cells (IC$_{50}$ = 25.2 ppm). At 40

ppm, CuO NPs were toxic to WI-38 human lung fibroblast cells, giving 80% cell mortality. This corroborated the conclusions of Katsumiti *et al.* (2018), who reported high toxicity for CuO NPs towards human lung epithelial cells (TT1 cells), with LC_{50} of 9.05 ppm. Cytotoxicity can be caused by generation of reactive oxygen species which cause oxidative stress to human cells and increases in ROS production as the mechanisms of cytotoxicity of CuO NPs. However, these cytotoxic effects depend on numerous factors, including surface functionalization, type of the tested cells, and concentration, size, shape, exposure time, and dose of CuO NPs (Naz *et al.* 2020). In contrast, no hemolytic effects were recorded from CuO NPs on red blood cells (IC_{50} = 440.1 ppm).

The pot and field experiments of the present study supported the findings from the *in vitro* experiments, demonstrating that the nanoparticles reduced development of root rot and wilt in chickpea plants. Among the nanoparticles assessed, CuO NPs had the greatest disease reduction efficacy. CuO NPs had effects comparable with the commercial fungicide thiophanate -methyl, with CuO NPs and the fungicide giving the least root rot and wilt incidences, compared to experimental controls. This result is similar to those of El-Shewy *et al.* (2019) who reported complete elimination of black scurf of potato in field trials using CuO-NPs. Copper-based nanoparticles have also been shown to be efficacious against fungal diseases, including tomato late blight caused by *Phytophthora infestans* (Giannousi *et al.*, 2013), and Fusarium wilt and Verticillium wilt of tomato (Elmer and White, 2016). The study by Servin *et al.* (2015) showed that nanoparticles of zinc oxide, titanium dioxide, and copper oxide provided effective disease management by direct inhibition of pathogens or stimulation of systemic acquired host resistance.

Previous research has demonstrated the mechanisms of action of nanomaterials towards phytopathogens. The biocidal effects of CuO NPs can be attributed to their direct impacts, or through release of copper ions. Because of the extensive surface area of CuO NPs, they can strongly attach to microbial cells, releasing essential cellular components and disrupting cell permeability (Raffi *et al.,* 2010). Oussou-Azo *et al.* (2020) showed that copper interacts with microbes through permeabilization of cell membranes, lipid peroxidation, alteration of proteins, and nucleic acid denaturation, leading to cell death.

The present study has shown that the assessed nanoparticles, particularly CuO NPs, have the ability to activate host plant defense systems against infections caused by *R. solani* and *F. oxysporum* f. sp. *ciceris*. Activity levels of POD and PPO enzymes, and total phenols were enhanced by all experimental nanoparticle treatments compared to the untreated experimental controls. CuO NPs exhibited greatest stimulation of these defense mechanisms among the experimental treatments applied. Previous investigations have given similar results, where copper-based nanoparticles augmented antioxidant mechanisms in plants, including the actions of SOD as well as PPO enzymes, and total antioxidant levels (Regier *et al.*, 2015; Singh *et al.*, 2017). El-Shewy *et al.* (2019) reported that potato plants treated with CuO NPs had increased POD and PPO activity. Nair and Chung (2014) reported that soybean plants treated with CuO NPs had increased PPO and lignin levels. They also showed high nanoparticle concentrations increased enzyme activity. Sarkar *et al.* (2020) presented results showing that presence of CuO NPs mediated catalase activation, ascorbate peroxidase, PPO, and SOD enzymes in tobacco plants.

Phenolic compounds have important roles in the plant resistance against fungi and plant diseases through mechanisms including causing hypersensitive cell death and the lignification of cell walls (Rashad *et al.*, 2020b). The present study demonstrated that CuO NPs gave the greatest phenol contents, which is similar to the results of Sarkar *et al.* (2020). They reported increased production of phenols and flavonoids after application of an optimum concentration of CuO NPs. Biswas *et al.* (2012) also discussed the role of phenols in the disease resistance. Additionally, nanoparticles of ZnO, TiO_2 and CuO have been shown to have uses in pathogen control programs by direct inhibition of disease-causing organisms or induction of systemic acquired resistance in host plants (Servin *et al.* 2015).

The present study field trials showed that the tested nanoparticles reduced root rot and wilt of chickpea, with CuO NPs) having the greatest disease reduction activity, comparable to that achieved with the fungicide thiophanate-methyl . The disease reductions from nanoparticle treatments was probably due to the large nanoparticle surface areas, facilitating robust adsorption to pathogen organisms, compromising cell permeability, and releasing vital components (Raffi *et al.,* 2010). These results are similar to those from other studies demonstrating elimination of black scurf of potato by CuO NPs (El-Shewy *et al.,* 2019) and efficacy of copper-based nanoparticles against several fungal pathogens (Giannousi *et al.*, 2013; Elmer and White, 2016). Previous research has also shown the effectiveness of nanoparticles of zinc oxide titanium dioxide, and CuO for disease control by either directly inhibiting pathogens or enhancing systemic acquired resistance (Servin *et al.,* 2015).

Applying nanoparticles of CuO, SiO_2, or TiO_2 through seed soaking increased chickpea growth and

yield parameters. These enhancements were associated with reductions in disease incidence, indicating possible induction of disease resistance in chickpea. Treatment with CuO NPs had the greatest positive impact on chickpea growth and yield parameters. These results align with previous studies demonstrating the beneficial role of copper for promoting plant growth and productivity. Ngo *et al.* (2014) reported beneficial effects of copper on plant growth. Elmer and White (2016) found that CuO NPs outperformed other metallic oxide nanoparticles for enhancing growth parameters of tomato and eggplant cultivated in soil inoculated with specific pathogens. Immersing wheat plants in Cu NPs accelerated their growth (Yasmeen *et al.*, 2015). Hafeez *et al.* (2015) demonstrated that wheat growth was increased in soils amended with Cu NPs at concentrations between 10 and 30 ppm. Baskar *et al.* (2018) showed that treating eggplants with CuO NP at 100 mg L^{-1} increased seedling root and shoot lengths. Badawy *et al.* (2021) found that CuO NPs (50 ppm) enhanced growth parameters of wheat plants. The present study gave similar results, showing that CuO NPs increased chickpea plant growth and yield parameters in the field trials. These increased seed yields indicate that use of CuO NPs is likely to be advantageous for augmenting profitability of chickpea farming.

This study assessed nanoparticles of CuO, SiO_2 and TiO_2 for antifungal effects against *R. solani* and *F. oxysporum* f. sp. *ciceris*. *In vitro* experiments demonstrated that increasing the concentrations of these nanoparticles increased inhibition rates of fungal growth and reduced the fungal populations. In the pot experiments, the tested nanoparticles, particularly at high concentrations, enhanced the resistance of chickpea plants against root rot and wilt. This was associated with increased levels of host defense compounds. TEM observations showed harmful alterations in cellular ultrastructures of *R. solani* and *F. oxysporum* f. sp. *ciceris* due to exposure to CuO NPs. These results indicate the potential for incorporating CuO NPs into management of Rhizoctonia rot and Fusarium wilt of chickpea plants. The field experiments further supported the effectiveness of these nanoparticles for reducing disease incidence and promoting chickpea growth and yield. CuO NP treatments are therefore recommended as potential alternative to potentially hazardous fungicides for managing chickpea root rot and wilt.

LITERATURE CITED

Abou-Salem E., Ahmed A.R., Elbagory M., Omara A.E.D., 2022. Efficacy of biological copper oxide nanoparticles on controlling damping-off disease and growth dynamics of sugar beet (*Beta vulgaris* L.) plants. *Sustainability* 14(19): 12871. https://doi.org/10.3390/su141912871

Al-Askar A.A., Abdulkhair W.M., Rashad Y.M., Hafez E.E., Ghoneem K.M., Baka Z.A., 2014. *Streptomyces griseorubens* E44G: A Potent Antagonist Isolated from Soil in Saudi Arabia. *Journal of Pure and Applied Microbiology* 8: 221–230.

Allahverdiyev A.M., Emrah S.A., Malahat B., Miriam R., 2011. Antimicrobial effects of TiO_2 and Ag_2O nanoparticles against drug-resistant bacteria and leishmania parasites. *Future Microbiology* 6: 933-940. https://doi.org/10.2217/fmb.11.78

Amin B.H., 2016. Isolation and characterization of antiprotozoal and antimicrobial metabolite from *Penicillium roqueforti*. *African Journal of Mycology and Biotechnology* 21(3): 13–26.

Amin B.H., Abou-Dobara M.I., Diab M.A., Gomaa E.A., El-Mogazy M.A., Salama H.M., 2020. Synthesis, characterization, and biological investigation of new mixed-ligand complexes. *Applied Organometallic Chemistry* 34(8): 1–18. https://doi.org/10.1002/aoc.5689

Amin B.H., Amer A., Azzam M., Abd El-Sattar N.E.A., Mahmoud D., Hozzein W.N., 2022. Antimicrobial and anticancer activities of *Periplaneta americana* tissue lysate: An *in vitro* study. *Journal of King Saud University*–Science 34: 102095. https://doi.org/10.1016/j.jksus.2022.102095

Badawy A.A., Nilly A.H.A., Salem S.S., Mohamed F.A., Amr F., 2021. Efficacy assessment of biosynthesized copper oxide nanoparticles (CuO-NPs) on stored grain insects and their impacts on morphological and physiological traits of wheat (*Triticum aestivum* L.) plant. *Biology* 10: 233. https://doi.org/10.3390/biology10030233

Baskar V., Nayeem S., Kuppuraj S.P., Muthu T., Ramalingam S., 2018. Assessment of the effects of metal oxide nanoparticles on the growth, physiology and metabolic responses *in vitro* grown eggplant (*Solanum melongena*). *3 Biotech* 8: 362. https://doi.org/10.1007/s13205-018-1386-9

Biswas S.K., Pandey N.K., Rajik M., 2012. Inductions of defense response in tomato against Fusarium wilt

through inorganic chemicals as inducers. *Journal of Plant Pathology & Microbiology* 3: 1–7. https://doi.org/10.4172/2157-7471.1000128

Bowler C., Montagu M.V., Inze D., 1992. Superoxide dismutase and stress tolerance. *Annual Review of Plant Biology* 43: 83–116.

Boxi S.S., Mukherjee K., Paria S., 2016. Ag doped hollow TiO_2 nanoparticles as an effective green fungicide against *Fusarum solani* and *Venturia inaequalis* phytopathogens. *Nanotechnology* 27: 085103. https://doi.org/10.1088/0957-4484/27/8/085103

Chakraborty M.R., Chatterjee N.C., 2007. Interaction of *Trichoderma harzianum* with *Fusarium solani* during its pathogenesis and the associated resistance of the host. *Asian Journal of Experimental Sciences* 21: 351–355.

Choudhary A.K., Kumar S., Patil B.S., Sharma M., Kemal S.,…Vijayakumar A.G., 2013. Narrowing yield gaps through genetic improvement for Fusarium wilt resistance in three pulse crops of the semi-arid tropics. SABRAO *Journal of Breeding and Genetics* 45: 341–370. http://oar.icrisat.org/id/eprint/1079

Cui H., Zhang P., Gu W., Jiang J., 2009. Application of anatasa TiO_2 sol derived from peroxotitannic acid in crop diseases control and growth regulation. *NSTI-Nanotech* 2: 286–289.

Elmer W.H., White J.C., 2016. The use of metallic oxide nanoparticles to enhance growth of tomatoes and eggplants in disease infested soil or soilless medium. *Environmental Science. Nano* 3: 1072–1079. https://doi.org/10.1039/C6EN00146G

Elshahawy I.E., Osman S.A., Abd-El-Kareem F., 2021. Protective effects of silicon and silicate salts against white rot disease of onion and garlic, caused by *Stromatinia cepivora*. *Journal of Plant Pathology* 103: 27–43. https://doi.org/10.1007/s42161-020-00685-1

El-Shewy E.S.A., Mohemed F.G., Abd-latif F.M., Hafez E.M., Mansour S.A., 2019. The efficacy of copper oxide, tri-calcium phosphate and silicon dioxide nanoparticles in controlling black scurf disease of potato. *Annals of Agricultural Science Moshtohor* 57: 129–138. https://doi.org/10.21608/assjm.2019.42223

Farias D.F., Souza T.M., Viana M.P., Soares B.M., Cunha A.P., … Carvalho A.F.U., 2013. Antibacterial, antioxidant, and anticholinesterase activities of plant seed extracts from Brazilian semiarid region. *BioMed Research International* 1: 510736. https://doi.org/10.1155/2013/510736

Fraternale D., Giamperi L., Ricci D., 2003. Chemical composition and antifungal activity of essential oil obtained from *in vitro* plants of *Thymus mastichina* L. *Journal of Essential Oil Research* 15: 278–281.

Giannousi K., Avramidis I., Dendrinou S.C., 2013. Synthesis, characterization and evaluation of copper-based nanoparticles as agrochemicals against *Phytophthora infestans*. *RSC Advances* 3: 21743–21752. https://doi.org/10.1039/C3RA42118J

Goffeau A., 2008. Drug resistance: The fight against fungi. *Nature* 452: 541-542. https://doi.org/10.1038/452541a

Gogos A., Knauer K., Bucheli T.D., 2012. Nanomaterials in plant protection and fertilization: current state, foreseen applications, and research priorities. *Journal of Agricultural and Food Chemistry* 60(39): 9781–9792 . https://doi.org/10.1021/jf302154y

Gohari G., Mohammadi A., Akbari A., Panahirad S., Dadpour M.R., Kimura S., 2020. Titanium dioxide nanoparticles (TiO_2 NPs) promote growth and ameliorate salinity stress effects on essential oil profile and biochemical attributes of Draco-cephalum moldavica. *Scientific Reports* 10(1): 1–14. https://doi.org/10.1038/s41598-020-57794-1

Gupta A.K., Gupta M., 2005. Synthesis and surface engineering of iron oxide nanoparticles for biomedical applications. *Biomaterials* 26: 3995–4021. https://doi.org/10.1016/j.biomaterials.2004.10.012

Hafeez A., Razzaq A., Mahmood T., Jhanzab H.M. 2015. Potential of copper nanoparticles to increase growth and yield of wheat. *Journal of Nanoscience with Advanced Technology* 1: 6–11. https://doi.org/10.24218/jnat.2015.02.

Hermida-Montero L.A., Nicolaza P.A.I, Mtz-Enriquez G.C., Paraguay-Delgado F., Greta R.S., 2019. Aqueous-phase synthesis of nanoparticles of copper/copper oxides and their antifungal effect against *Fusarium oxysporum*. *Journal of Hazardous Materials* 380: 120850. https://doi.org/10.1016/j.jhazmat.2019.120850

Ismail A.M., 2021. Efficacy of copper oxide and magnesium oxide nanoparticles on controlling black scurf disease on potato. *Egyptian Journal of Phytopathology* 49(2): 116-130 . http://dx.doi.org/10.21608/ejp.2021.109535.1050

Jukanti A.K., Gaur P.M., Gowda C.L.L., Chibbar R.N., 2012. Nutritional quality and health benefits of chickpea (*Cicer arietinum* L.): a review. *British Journal of Nutrition* 108: (S1) S11–S26. https://doi.org/10.1017/S0007114512000797

Kanhed P., Birla S., Gaikwad S., Gade A., Seabra A.B., Rai M., 2014. *In vitro* antifungal efficacy of copper nanoparticles against selected crop pathogenic fungi. *Materials Letters* 115: 13–17. https://doi.org/10.1016/j.matlet.2013.10.011

Kasana A., AliNiazee M.T., 1997. A thermal unit summation model for the phenology of *Rhagoietis completa* (Diptera: Tephritidae). *Journal of the Entomological Society of British Columbia* 94: 13–18.

Katsumiti A., Thorley A.J., Arostegui I., Reip P., Valsami-Jones E., Cajaraville M.P., 2018. Cytotoxicity and cellular mechanisms of toxicity of CuO NPs in mussel cells *in vitro* and comparative sensitivity with human cells. *Toxicology In Vitro* 48: 146–158. https://doi.org/10.1016/j.tiv.2018.01.013

Kaur P., Thakur R., Choudhary A., 2012. An *in vitro* study of the antifungal activity of silver/chitosan nanoformulations against important seed borne pathogens. *International Journal of Science and Technology Research* 1: 83–86.

Nair P.M.G., Chung I.M., 2014. Impact of copper oxide nanoparticles exposure on Arabidopsis thaliana growth, root system development, root lignification, and molecular level changes. *Environmental Science and Pollution Research* 21: 12709–12722. https://doi.org/10.1007/s11356-014-3210-3

Naz S., Gul A., Zia M., 2020. Toxicity of copper oxide nanoparticles: a review study. *IET Nanobiotechnology* 14(1): 1-13. https://doi.org/10.1049/iet-nbt.2019.0176

Nel A.E., Xia T., Madler L., Li N., 2006. Toxic potential of materials at the nanolevel. *Science* 311: 622–627. https://doi.org/10.1126/science.1114397

Ngo B.Q., Dao T.T., Nguyen C.H., Tran X.T., Nguyen T.V., Huynh T.H., 2014. Effects of nanocrystalline powders (Fe, Co and Cu) on the germination, growth, crop yield and product quality of soybean (Vietnamese species DT-51). *Advances in Natural Sciences: Nanoscience and Nanotechnology* 5: 015016. https://doi.org/10.1088/2043-6262/5/1/015016

Oussou-Azo A.F., Nakama T., Nakamura M., Futagami T., Vestergaard M.C.M., 2020. Antifungal potential of nanostructured crystalline copper and its oxide forms. *Nanomaterials* 10: 1–13. https://doi.org/10.3390/nano10051003

Papavizas G.C., Davey C.B., 1962. Isolation and pathogenicity of Rhizoctonia saprophytically existing in soil. *Journal of Phytopathology* 52: 834–840.

Perez-de-Luque A., Rubiales, D., 2009. Nanotechnology for parasitic plant control. *Pest Management Science* 65: 540–545. https://doi.org/10.1002/ps.1732

Raffi M., Mehrwan S., Bhatti T.M., Akhter J.I., Yawar A.W., Masood ul Hasan, M., 2010. Investigations into the antibacterial behavior of copper nanoparticles against *Escherichia coli*. *Annals of Microbiology* 60(1): 75–80. https://doi.org/10.1007/s13213-010-0015-6

Rashad Y.M., Aseel D.G., Hafez E.E., 2018. Antifungal potential and defense gene induction in maize against Rhizoctonia root rot by seed extract of *Ammi visnaga* (L.) Lam. *Phytopathologia Mediterranea* 57(1): 73–88. https://doi.org/10.14601/Phytopathol_Mediterr-21366

Rashad Y.M., Abbas M.A., Soliman H.M., Abdel-Fattah G.G., Abdel-Fattah G.A., 2020a. Synergy between endophytic *Bacillus amyloliquefaciens* GGA and arbuscular mycorrhizal fungi induces plant defense responses against white rot of garlic and improves host plant growth. *Phytopathologia Mediterranea* 59(1): 169–186. https://doi.org/10.36253/phyto-11019

Rashad Y.M., Aseel D.G., Hammad S.M., 2020b. Phenolic Compounds Against Fungal and Viral Plant Diseases. In: *Plant Phenolics in Sustainable Agriculture* (Lone R., Shuab R., Kamili A., ed.). Springer Nature Singapore Pte Ltd. pp. 201–219, from https://doi.org/10.1007/978-981-15-4890-1_9

Rashad Y.M., El-Sharkawy H.H., Belal B.E., Abdel Razik E.S., Galilah D.A., 2021. Silica nanoparticles as a probable anti-oomycete compound against downy mildew, and yield and quality enhancer in grapevine: field evaluation, molecular, physiological, ultrastructural, and toxicity investigations. *Frontiers in Plant Science* 12: 763365. https://doi.org/10.3389/fpls.2021.763365

Rashad Y.M., El-Sharkawy H.H., Elazab, N.T., 2022. *Ascophyllum nodosum* extract and mycorrhizal colonization synergistically trigger immune responses in pea plants against rhizoctonia root rot, and enhance plant growth and productivity. *Journal of Fungi* 8(3): 268. https://doi.org/10.3390/jof8030268

Rastogi A., Tripathi D.K., Yadav S., Chauhan D.K., Živčák M., Brestic M., 2019. Application of silicon nanoparticles in agriculture. *3 Biotech* 9(3): 90. https://doi.org/10.1007/s13205-019-1626-7

Regier N., Cosio C., Von Moos N., Slaveykova V.I., 2015. Effects of copper-oxide nanoparticles, dissolved copper and ultraviolet radiation on copper bioaccumulation, photosynthesis and oxidative stress in the aquatic macrophyte Elodea nuttallii. *Chemosphere* 128: 56–61. https://doi.org/10.1016/j.chemosphere.2014.12.078

Sadasivam S., Manickam A., 1996. *Biochemical Methods*. Second Ed. New Age Int. Pvt. Ltd. Pub. and T.N. Agril. Univ. Coimbatore, Tamil Nadu, India, pp. 108–110.

Sarkar J., Chakraborty N., Chatterjee A., Bhattacharjee A., Dasgupta D., Acharya K., 2020. Green synthesized copper oxide nanoparticles ameliorate defense and antioxidant enzymes in *Lens culinaris. Nanomaterials* 10(2): 312. https://doi.org/10.3390/nano10020312

Servin A., Elmer W., Mukherjee A., Torre-Roche R., Hamdi H., … Dimkpa C., 2015. A review of the use of engineered nanomaterials to suppress plant disease and enhance crop yield. *Journal of Nanoparticle Research* 17: 92. https://doi.org/10.1007/s11051-015-2907-7

Siddiqui M.H., Al-Whaibi M.H., 2014. Role of nano-SiO$_2$ in germination of tomato (*Lycopersicum esculentum* seeds Mill.) *Saudi Journal of Biological Sciences* 21(1): 13–17. https://doi.org/10.1016/j.sjbs.2013.04.005

Singh A., Singh N.B., Hussain I., Singh H., 2017. Effect of biologically synthesized copper oxide nanoparticles on metabolism and antioxidant activity to the crop plants *Solanum lycopersicum* and *Brassica oleracea* var. *botrytis*. *Journal of Biotechnology* 262: 11–27. https://doi.org/10.1016/j.jbiotec.2017.09.016

Suriyaprabha R., Karunakaran G., Yuvakkumar R., Rajendran V., Kannan N., 2014. Foliar application of silica nanoparticles on the phytochemical responses of maize (*Zea mays* L.) and its toxicological behavior. *Synthesis and Reactivity in Inorganic, Metal-Organic, and Nano-Metal Chemistry* 44(8): 1128–1131. https://doi.org/10.1080/15533174.2013.799197

Wang X.P., Liu X.Q., Chen J.N., Han H.Y., Yuan Z.D., 2014. Evaluation and mechanism of antifungal effects of carbon nanomaterials in controlling plant fungal pathogen. *Carbon* 68: 798–806. https://doi.org/10.1016/j.carbon.2013.11.072

Worrall E.A., Hamid A., Mody K.T., Mitter N., Pappu H.R., 2018. Nanotechnology for plant disease management. *Agronomy* 8(12): 285. https://doi.org/10.3390/agronomy8120285

Xue X.J., Geng T.T., Liu H.F., Yang W., Zhong W.R., Zhang Z.L., 2021. Foliar application of silicon enhances resistance against *Phytophthora infestans* through the ET/JA- and NPR1-dependent signaling pathways in potato. *Frontiers in Plant Science* 12: 609870. https://doi.org/10.3389/fpls.2021.609870

Yadav R.K., Singh N.B., Singh A., Yadav B., Bano C., Niharika, 2020. Expanding the horizons of nanotechnology in agriculture: recent advances, challenges and future perspectives. *Vegetos* 33: 203–221. https://doi.org/10.1007/s42535-019-00090-9

Yasmeen F., Razzaq A., Iqbal M.N., Jhanzab H.M., 2015. Effect of silver, copper and iron nanoparticles on wheat germination. *International Journal of Biosciences* 6: 112–117. https://doi.org/10.12692/ijb/6.4.112-117

Zian A.H., El-Blasy S.A., El-Gendy H.M., El-Sayed S.A., 2023. Plant defense activation and down-regulation root rot and wilt in chickpea diseases by some abiotic substances. *E3S Web of Conferences* 462: 02014. https://doi.org/10.1051/e3sconf/202346202014

Zian A.H., El-Blasy S.A.S., Khalil M.S.M., El-Gammal Y.H., 2024. Improving the Efficiency of Bioagents Using Certain Chemical Inducers against Root Rot and Wilt Diseases of Soybean. *Journal of Plant Protection and Pathology* 15(10): 335–346. https://doi.org/10.21608/jppp.2024.320903.1266

Zilesin N., Ben-Zaken R., 1993. Peroxidase activity and presence of phenolic substances in peduncles of rose flowers. *Plant Physiology and Biochemistry* 31: 333–339.

ORCID:
VM: 0000-0001-8565-4166
OP: 0009-0003-7182-3143
FN: 0000-0002-8273-0052
SP: 0000-0001-8806-1905
GL: 0000-0002-5154-7829
FF: 0000-0003-1063-0607

Short Notes

Isolation and molecular characterization of a *Xylella fastidiosa* subsp. *multiplex* strain from almond (*Prunus dulcis*) in Apulia, Southern Italy

Vito MONTILON[1], Oriana POTERE[1], Leonardo SUSCA[1], Francesco MANNERUCCI[1], Franco NIGRO[1], Stefania POLLASTRO[1,*], Giuliana LOCONSOLE[2], Francesco PALMISANO[3], Claudio ZAZA[3], Marco CANTATORE[3], Francesco FARETRA[1]

[1] *University of Bari Aldo Moro, Department of Soil, Plant and Food Sciences (DiSSPA), Via Amendola 165/A, 70126 Bari, Italy*
[2] *National Research Council, Institute for Sustainable Plant Protection, Via Amendola, 122/D, 70126 Bari, Italy*
[3] *Regional Plant Protection Service-Apulia Region, Lungomare Nazario Sauro, 51, 70100 Bari, Italy*
*Corresponding author. E-mail: stefania.pollastro@uniba.it

Summary. *Xylella fastidiosa* is a xylem-limited phytopathogenic bacterium under regulation in the European Union as a priority pest. Given the potential risk posed by this pathogen to cultivated and ornamental plants, mandatory annual surveys and laboratory testing are required in Member States to early detect outbreaks. In the course of surveys carried out during early spring 2024 in the Apulia region (Southern Italy), *X. fastidiosa* subsp. *multiplex* was identified using quantitative real-time Polymerase Chain Reaction (qPCR), in a non-symptomatic sample from an almond tree (*Prunus dulcis*) in an orchard located in Santeramo in Colle, in Bari province. Multilocus sequence typing (MLST) was used to identify the subspecies and sequence type (ST) of the bacterium using the genomic DNAs extracted from the infected sample. Comparative sequence analysis of the seven MLST allele genes indicated that the obtained nucleotide sequences completely matched allele sequences of *X. fastidiosa* in PubMLST database corresponding to the allelic profile (Sequence Type) ST26 related to subsp. *multiplex*. Bacterial colonies consistent in morphology with *X. fastidiosa* were isolated from asymptomatic host samples and identity was confirmed by real-time PCR analysis. This is the first report of detection of *X. fastidiosa* subsp. *multiplex* ST26 in the EU.

Keywords. *Xanthomonadaceae*, MLST, priority pest, sequence type, xylem-limited bacterium.

INTRODUCTION

Xylella fastidiosa (*Xanthomonadaceae*) (Wells *et al.*, 1987) is a gram-negative plant pathogenic bacterium comprising several subspecies, which are pathogenic to a broad spectrum of host plants including agricultural crops

of economic importance, ornamentals and natural vegetation (EFSA, 2023). The pathogen is limited to host plant xylem tissues (Purcell and Hopkins, 1996), leading to symptoms generally related to xylem vessel occlusion, which include scorching of leaves and dieback that vary in severity depending on the host susceptibility. The pathogen is naturally transmitted by xylem sap-feeding leafhoppers (*Cicadellidae*) and spittlebugs (*Cercopidae*) (Hopkins, 1989), and is spread over long distances through movement of infected plant material or infectious insect vectors (Purcell and Hopkins, 1996; Loureiro *et al.*, 2024).

Following the first confirmed report of *X. fastidiosa* in the European Union (EU) in 2013, in Salento, Apulia Region, Southern Italy (Saponari *et al.*, 2013), where a strain of *X. fastidiosa* subsp. *pauca* Sequence Type (ST) 53 (Giampetruzzi *et al.*, 2015; Giampetruzzi *et al.*, 2017) was found to cause the Olive Quick Decline Syndrome (OQDS) (Martelli, 2016; Saponari *et al.*, 2017), EU emergency measures against plant pests were updated with the new plant health Regulation (EU) 2016/2031 (European Commission, 2016). Under this regulation, *X. fastidiosa* became a priority pest (European Commission, 2019), and has been since subjected to mandatory annual surveys by Member States to prevent its entrance and spread within the EU (European Commission, 2020; European Commission, 2024). As a result of extensive survey activities, *X. fastidiosa* has also been detected in France, Spain, and Portugal (Denancé *et al.*, 2017; Olmo *et al.*, 2017; Marco-Noales *et al.*, 2021; Carvalho-Luis *et al.*, 2022; EFSA, 2023), in which several sequence types (STs) of the bacterium belonging to different subspecies were identified on various plant species. More recently, *X. fastidiosa* subsp. *multiplex* ST87 has been found in the Tuscany region of Italy (Saponari *et al.*, 2019), and a new outbreak of the subspecies *fastidiosa* ST1 emerged in a location in the province of Bari in Apulia (Cornara *et al.*, 2024).

Official inspections performed for the detection and identification of the bacterium and its subspecies are regulated by Commission Implementing Regulation (EU) 2020/1201, amended and corrected by Commission Implementing Regulation (EU) 2024/2507, that specify which molecular tests must be used for the identification of *X. fastidiosa* and its subspecies.

Inspections are based on visual surveys, and collection of representative plant samples for pathogen diagnosis to species level by real-time Harper PCR (Harper *et al.*, 2010, erratum 2013). Following the diagnostic confirmation of the positive detection of *X. fastidiosa* in previously free areas or in new plant host species, multilocus sequence typing (MLST) analysis (Yuan *et al.*, 2010) is the most common test used for the assignment of

positive samples to subspecies and Sequence Type (ST). Real-time PCR methods based on Dupas *et al.* (2019) and Hodgetts *et al.* (2021) can also be used for subspecies assignment (CI Regulation (EU) 2024/2507).

This paper reports identification of *X. fastidiosa* subsp. *multiplex* ST26 in a non-symptomatic sample from an almond tree (*Prunus dulcis*) in an orchard in Apulia, in the province of Bari (Southern Italy) (Europhyt outbreak notification n. 2549). This discovery occurred in the context of the regional surveillance program for *X. fastidiosa* associated with OQDS, enforced by the Plant Health Service of the Apulia Region, and carried out by the Regional Agency for Irrigation and Forestry Activities (ARIF).

MATERIALS, METHODS, AND RESULTS

Samples were randomly collected in March 2024, from a site that included orchards in the municipal territory of Santeramo in Colle, a few tens of kilometres from the west of the *X. fastidiosa* subsp. *pauca* ST53 demarcated area (DA). The plant material delivered to the laboratory of the Department of Soil, Plant and Food Sciences, University of Bari (Italy) consisted of mature lignified branches from non-symptomatic almond trees, which were refrigerated until testing.

Samples were prepared by debarking the hardwood cuttings and scraping the exposed surfaces of the wooden tissues with a sterile razor blade. From each sample, 0.5 g of wood shavings were placed in extraction bags (BIOREBA®) and then ground in 5 mL (1:10 weight:volume) of CTAB extraction buffer using a semi-automated homogenizer (Homex 7, BIOREBA®). Total nucleic acids were extracted using a cetyltrimethylammonium bromide (CTAB) based method (Loconsole *et al.*, 2014; EPPO, 2023). Samples from an OQDS-infected and a non-infected plant were included in the DNA extraction as positive (PIC) and negative (NIC) isolation controls (EPPO, 2023).

DNA extracts were analysed by quantitative polymerase chain reaction (qPCR) assays carried out according to Appendix 5 of the EPPO Diagnostic Standard for *X. fastidiosa* PM 7/24 (5) based on the protocol of Harper *et al.* (2010, erratum 2013). Total nucleic acids of PIC and NIC were run alongside the samples, and a negative amplification control (NAC) was included. A positive amplification control (PAC) consisting of a suspension at a known concentration of *X. fastidiosa* subsp. *pauca* ST53 cells was also included in the same plate of the qPCR assay. According to the guidelines issued by the Plant Health Service of the Apulia Region (DDS no. 31 of 13 May 2022) for the

monitoring and eradication of the pathogenic bacterium at regional level, samples that produced by qPCR (Harper *et al.*, 2010) a quantification cycle (Cq) ≤32 were considered positive, while samples that did not exhibit exponential amplification were considered negative. If the Cq was greater than 32 the result was considered undetermined, and the sample was re-tested.

The qPCR assays for individual trees revealed presence of *X. fastidiosa* in one almond tree identified with the code ID 19107. The Cq value produced for this sample by qPCR was 28,54. Both the negative (NIC and NAC) and positive (PIC and PAC) controls produced the respective expected results.

Consequently, an aliquot of DNA of this sample was used for multilocus sequence typing (MLST) analysis (Yuan *et al.*, 2010), according to the Appendix 16 of the EPPO Diagnostic Standard PM 7/24 (5) (EPPO, 2023), to further characterize the *X. fastidiosa* genotype detected outside the *X. fastidiosa* DA. Amplicons with the expected size were sequenced by Macrogen Inc., Seoul, South Korea. Allele sequences were then assembled by BioEdit Sequence Alignment Editor version 7.2.5 software and analyzed using the PubMLST database (http://pubmlst.org/xfastidiosa/) to identify allele types. Allele

sequences amplified from the infected almond tree had 100% nucleotide identity with those of alleles *leuA*_5, *petC*_3, *malF*_3, *cysG*_3, *holC*_6, *nuoL*_3, and *gltT*_5 corresponding to the ST26 genotype belonging to *X. fastidiosa* subsp. *multiplex* (EPPO, 2023). The sequences obtained for the MLST alleles were deposited in GenBank under accession numbers: *leuA* allele 5, PQ535574; *petC* allele 3, PQ535575; *malF* allele 3, PQ535576; *cysG* allele 3, PQ535577; *holC* allele 6, PQ515132; *nuoL* allele 3, PQ535578; and *gltT* allele 5, PQ535579. A phylogenetic network, inferred through the concatenation of the MLST sequences of all *X. fastidiosa* (STs) retrieved from the PubMLST database (Jolley *et al.*, 2018), and conducted using the Neighbor-Net method implemented in Splits Tree4 (version 4.12.2) (Huson and Bryant, 2006), indicated that the genotype ST26 shared close similarity to a complex of strains of subsp. *multiplex* (Figure 1).

An aliquot of the DNA sample extracted from the infected almond tree was also analyzed by real-time tetraplex PCR assay (Dupas *et al.*, 2019) to further confirm the isolated bacterium subspecies. This test was carried out using the reaction volumes and amplification conditions validated in the test performance study for the *X. fastidiosa* subspecies identification previously con-
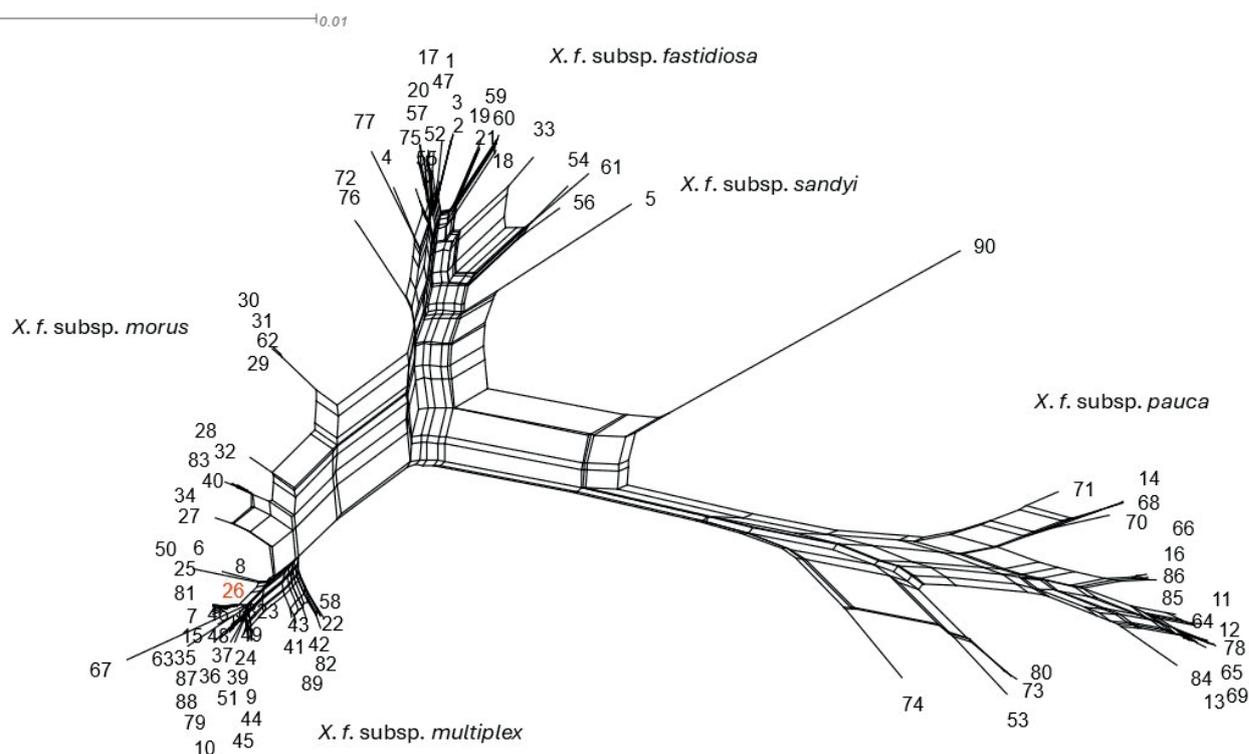
Figure 1. Neighbor net network analysis based on concatenated sequence alignments of the seven MLST genes representing distribution and phylogenetic relationships of the 90 sequence types (STs) of *X. fastidiosa* belonging to the subspp. *multiplex*, *morus*, *fastidiosa*, *sandyi* or *pauca* identified to date. The nextwork tree includes the ST26 (red font) identified in the present study.
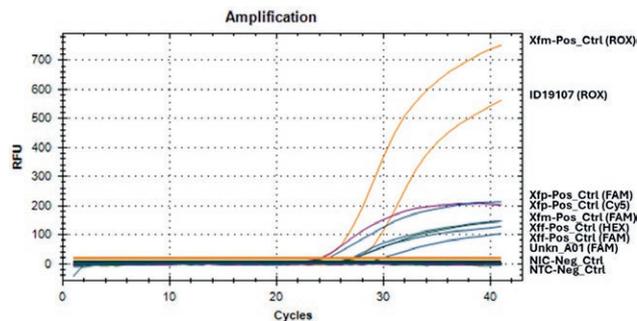
Figure 2. Results from multiplex real-time PCR based on primer sets reported in Dupas *et al.* (2019). The blue exponential curves were generated by the primer-probe set, labelled with fluorophore FAM, which detected bacteria at species levels in the positive controls, and in the sample ID 19107. The green exponential curve was generated by the primer-probe set, labelled with HEX, which specifically detected subsp. *fastidiosa* in the positive control (Xff-Pos_Ctrl). The orange exponential curves were generated by the primer-probe set, labelled ROX, which detected the subsp. *multiplex* in the positive control Xfm-Pos, and in the sample ID 19107. The violet exponential curve was generated by t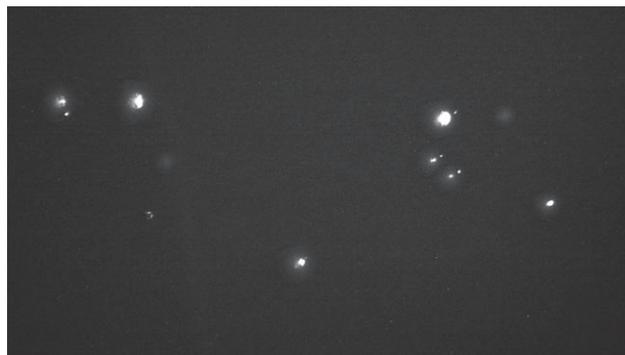he primer-probe set, labelled Cy5, which detected subsp. *pauca* in the positive control Xfp-Pos. Negative amplification controls (NIC-Neg_Ctrl and NTC-Neg_Ctrl) are also indicated. Quantification cycles are indicated on the x axis, and relative fluorescence units (RFUs) are indicated on the y axis.

Figure 3. Bacterial colonies of *X. fastidiosa* subsp. *multiplex* ST26 isolated from almond tree branches on buffered cysteine yeast extract (BCYE) agar 30 d after isolation.

ducted by the Official Laboratories of the Italian National Plant Protection Organization (NPPO), with coordination of the National Reference Laboratory, constituted by the Council for Agricultural Research and Economics, Research Centre for Plant Protection and Certification (CREA-DC) (Pucci *et al.*, 2023). For the assay, PACs were provided by CREA-DC and consisted of DNA extracted from plant samples infected by isolates of *X. fastidiosa* subsp. *fastidiosa*, subsp. *multiplex* or subsp. *pauca*. The tetraplex real-time PCR assay detected and identified subsp. *multiplex* in the sample ID 19107, producing a Cq value of 27.47 (Figure 2). All DNAs extracted from the PAC tested positive for the corresponding target subspecies of *X. fastidiosa* when using the appropriate subspecies-specific primers and probes, while no amplification reaction occurred for the other subspecies. No signal amplification was observed for the NAC.

Attempts were made to isolate the bacterium. Lignified portions (length 4 to 8 cm) recovered from cuttings of non-symptomatic host plant branches that had tested positive by qPCR were surface sterilized in a laminar flow hood by soaking for 2 min in 2% (v/v) sodium hypochlorite solution and 2 min in 70% ethanol, and then rinsed three times each for 2 min in sterile distilled water. The tissue portions were then each cut in half, squeezed with sterile pliers by pressing the external ends, and the freshly cut faces were blotted onto buffered cysteine-yeast extract

(BCYE) medium (Wells *et al.*, 1981). The inoculated plates were then incubated at 28°C in the dark for at least 30 d and were periodically observed using a light microscope for appearance of colonies with morphological characteristics typical of *X. fastidiosa* (Wells *et al.*, 1981; 1987) (Figure 3). Typical colonies were re-isolated and their identity as *X. fastidiosa* was confirmed using the qPCR assay of Harper *et al.* (2010, erratum 2013).

DISCUSSION

The subsp. *multiplex* of *X. fastidiosa* is native to North America (Nunney *et al.*, 2019), and is known to have a wide plant species host range. This includes peach (*P. persica*), plum (*P. domestica*), almond (*P. dulcis*), and several forest and shade trees (Schaad *et al.*, 2004; Nunney *et al.*, 2013; Nunney *et al.*, 2019). Strains of *X. fastidiosa* subsp. *multiplex* have also been reported in associations with olive (Krugner *et al.*, 2014), and with grapevine (Almeida and Purcell, 2003). To date, in the European Union, strains belonging to the ST6, ST7, ST81 and ST87 of *X. fastidiosa* subsp. *multiplex* have been reported on almond and other hosts, including cultivated and ornamental species in Corsica, mainland France, the Balearic Islands, in Spain, and in Italy in Tuscany and Lazio (EFSA, 2022; Trkulja *et al.*, 2022). The strain ST26 identified in Apulia is distinct from those found in other Italian and European regions, indicating that ST26 has been introduced from a different and unknown location.

Xylella fastidiosa subsp. *multiplex* ST26 has been previously detected only on *P. domestica* in Brazil, where it was thought to have been introduced from the North America (Coletta-Filho *et al.*, 2017). ST26 is reported to mainly affect stone fruit trees (*Prunus* spp.), particularly plum (Coletta-Filho *et al.*, 2017; Nunney *et al.*, 2019).

After the notification of detection of *X. fastidiosa* multiplex ST26 to the competent Plant Health Service of the Apulia Region, a DA was established, and emergency control measures have been carried out to limit the spread of the bacterium to surrounding areas, in accordance with the legislative provisions under Regulation (EU) 2020/1201 (European Commission, 2020) amended by Regulation (EU) 2024/2507 (European Commission, 2024). A monitoring campaign is currently underway (in 2024) to determine the extent of the epidemic outbreak. Further research is required to consider the host range of ST26, seasonal development of the leaf scorch symptoms this strain causes, and the presence of infective vectors.

LITERATURE CITED

Almeida R.P.P., Purcell A.H., 2003. Biological Traits of *Xylella fastidiosa* Strains from Grapes and Almonds. *Applied and Environmental Microbiology* 69(12): 7447–7452. https://doi.org/10.1128/AEM.69.12.7447-7452.2003

Carvalho-Luis C., Rodrigues J.M., Martins L.M., 2022. Dispersion of the Bacterium *Xylella Fastidiosa* in Portugal. *Journal of Agricultural Science and Technology A* 12(1). https://doi.org/10.17265/2161-6256/2022.01.005

Coletta-Filho H.D., Francisco C.S., Lopes J.R., Muller C., Almeida R.P., 2017. Homologous Recombination and *Xylella Fastidiosa* Host–Pathogen Associations in South America. *Phytopathology* 107(3): 305–312. https://doi.org/10.1094/PHYTO-09-16-0321-R

Cornara D., Boscia D., D'Attoma G., Digiaro M., Ligorio A., … Saponari M., 2024. An Integrated Strategy for Pathogen Surveillance Unveiled *Xylella Fastidiosa* ST1 Outbreak in Hidden Agricultural Compartments in the Apulia Region (Southern Italy). *European Journal of Plant Pathology*. https://doi.org/10.1007/s10658-024-02945-7

Denancé N., Legendre B., Briand M., Olivier V., de Boisseson C., … Jacques M.A., 2017. Several Subspecies and Sequence Types Are Associated with the Emergence of *Xylella Fastidiosa* in Natural Settings in France. *Plant Pathology* 66(7): 1054–1064. https://doi.org/10.1111/ppa.12695

Dupas E., Briand M., Jacques M.A., Cesbron S., 2019. Novel Tetraplex Quantitative PCR Assays for Simultaneous Detection and Identification of *Xylella Fastidiosa* Subspecies in Plant Tissues. *Frontiers in Plant Science* 10: 1732. https://doi.org/10.3389/fpls.2019.01732

European Commission, 2016. Regulation (EU) 2016/2031 of the European Parliament of the Council of 26 October 2016 on protective measures against pests of plants, amending Regulations (EU) No 228/2013, (EU) No 652/2014 and (EU) No 1143/2014 of the European Parliament and of the Council and repealing Council Directives 69/464/EEC, 74/647/EEC, 93/85/EEC, 98/57/EC, 2000/29/EC, 2006/91/EC and 2007/33/EC. *Official Journal of the European Union L* 317: 4–104. http://data.europa.eu/eli/reg/2016/2031/oj/eng

European Commission, 2019. Commission Delegated Regulation (EU) 2019/1702 of 1 August 2019 supplementing Regulation (EU) 2016/2031 of the European Parliament and of the Council by establishing the list of priority pests. *Official Journal of the European Union L* 260: 8–10. http://data.europa.eu/eli/reg_del/2019/1702/oj/eng

European Commission, 2020. Commission Implementing Regulation (EU) 2020/1201 of 14 August 2020 as regards measures to prevent the introduction into and the spread within the Union of *Xylella fastidiosa* (Wells *et al.*). *Official Journal of the European Union L* 269: 2–39. http://data.europa.eu/eli/reg_impl/2020/1201/oj/eng

European Commission, 2024. Commission Implementing Regulation (EU) 2024/2507 of 26 September 2024 amending and correcting Implementing Regulation (EU) 2020/1201 as regards measures to prevent the

introduction into and spread within the Union of *Xylella fastidiosa* (Wells *et al.*) and amending Implementing Regulation (EU) 2020/1770 as regards the list of plant species not exempted from the traceability code requirement for plant passports. *Official Journal of the European Union L.* http://data.europa.eu/eli/reg_impl/2024/2507/oj/eng

EFSA (European Food Safety Authority), Delbianco A., Gibin D., Pasinato L., Morelli M., 2022. Update of the *Xylella* spp. host plant database: systematic literature search up to 30 June 2021. *EFSA Journal* 20(1): 7039. https://doi.org/10.2903/j.efsa.2022.7039

EFSA (European Food Safety Authority), Gibin D., Pasinato L., Delbianco A., 2023. Update of the *Xylella* Spp. Host Plant Database – Systematic Literature Search up to 31 December 2022. *EFSA Journal* 21(6): 8061. https://doi.org/10.2903/j.efsa.2023.8061

EPPO (European Plant Protection Organization), 2023. PM 7/24 (5) *Xylella Fastidiosa*. *EPPO/OEPP Bulletin* 53(2): 205-276. https://doi.org/10.1111/epp.12923

Giampetruzzi A., Chiumenti M., Saponari M., Donvito G., Italiano A., … Saldarelli P., 2015. Draft Genome Sequence of the *Xylella fastidiosa* CoDiRO Strain. *Genome Announcements* 3(1): e01538-14. https://doi.org/10.1128/genomeA.01538-14

Giampetruzzi A., Saponari M., Almeida R.P.P., Essakhi S., Boscia D., ... Saldarelli P., 2017. Complete Genome Sequence of the Olive-Infecting Strain *Xylella fastidiosa* subsp. *pauca* De Donno. *Genome Announcements* 5(27): 10.1128/genomea.00569-17. https://doi.org/10.1128/genomea.00569-17

Harper S.J., Ward L.I., Clover G.R.G., 2010. Development of LAMP and Real-Time PCR Methods for the Rapid Detection of *Xylella fastidiosa* for Quarantine and Field Applications. *Phytopathology*® 100(12): 1282–1288. (erratum 2013). https://doi.org/10.1094/PHYTO-06-10-0168

Hodgetts J., Glover R., Cole J., Hall J., Boonham N., 2021. Genomics informed design of a suite of real-time PCR assays for the specific detection of each *Xylella fastidiosa* subspecies. *Journal of Applied Microbiology* 131(2): 855–872. https://doi.org/10.1111/jam.14903

Hopkins D.L., 1989. *Xylella Fastidiosa*: Xylem-Limited Bacterial Pathogen of Plants. *Annual Review of Phytopathology* 27(1): 271–290. https://doi.org/10.1146/annurev.py.27.090189.001415

Huson D.H., Bryant D., 2006. Application of Phylogenetic Networks in Evolutionary Studies. *Molecular Biology and Evolution* 23(2): 254–267. https://doi.org/10.1093/molbev/msj030

Jolley K.A., Bray J.E., Maiden M.C.J., 2018. Open-Access Bacterial Population Genomics: BIGSdb Software, the PubMLST.Org Website and Their Applications. *Wellcome Open Research* 3: 124. https://doi.org/10.12688/wellcomeopenres.14826.1

Krugner R., Sisterson M.S., Chen J., Stenger D.C., Johnson M.W., 2014. Evaluation of Olive as a Host of *Xylella fastidiosa* and Associated Sharpshooter Vectors. *Plant Disease* 98(9): 1186–1193. https://doi.org/10.1094/PDIS-01-14-0014-RE

Loconsole G., Potere O., Boscia D., Altamura G., Djelouah K., … Saponari M., 2014. Detection of *Xylella fastidiosa* in olive trees by molecular and serological methods. *Journal of Plant Pathology* 96(1): 7–14. https://doi.org/10.4454/JPP.V96I1.041

Loureiro T., Serra L., Martins A., Cortez I., Poeta P., 2024. *Xylella Fastidiosa* Dispersion on Vegetal Hosts in Demarcated Zones in the North Region of Portugal. *Microbiology Research* 15(3): 1050–1072. https://doi.org/10.3390/microbiolres15030069

Marco-Noales E., Barbé S., Monterde A., Navarro-Herrero I., Ferrer A., … Roselló M., 2021. Evidence that *Xylella fastidiosa* is the Causal Agent of Almond Leaf Scorch Disease in Alicante, Mainland Spain (Iberian Peninsula). *Plant Disease* 105(11): 3349–3352. https://doi.org/10.1094/PDIS-03-21-0625-SC

Martelli G.P., Boscia D., Porcelli F., Saponari M., 2016. The Olive Quick Decline Syndrome in South-East Italy: A Threatening Phytosanitary Emergency. *European Journal of Plant Pathology* 144(2): 235–243. https://doi.org/10.1007/s10658-015-0784-7

Nunney L., Vickerman D.B., Bromley R.E., Russell S.A., Hartman J.R., … Stouthamer R., 2013. Recent Evolutionary Radiation and Host Plant Specialization in the *Xylella Fastidiosa* Subspecies Native to the United States. *Applied and Environmental Microbiology* 79(7): 2189–2200. https://doi.org/10.1128/AEM.03208-12

Nunney L., Azad H., Stouthamer R., 2019. An Experimental Test of the Host-Plant Range of Nonrecombinant Strains of North American *Xylella Fastidiosa* subsp. *multiplex*. *Phytopathology*® 109(2): 294–300. https://doi.org/10.1094/PHYTO-07-18-0252-FI

Olmo D., Nieto A., Adrover F., Urbano A., Beidas O., ... Landa B.B., 2017. First Detection of *Xylella fastidiosa* Infecting Cherry (*Prunus avium*) and *Polygala myrtifolia* Plants, in Mallorca Island, Spain. *Plant Disease* 101(10): 1820–1820. https://doi.org/10.1094/PDIS-04-17-0590-PDN

Pucci N., Scala V., Cesari E., Crosara V., Fiorani R., … Loreti S., 2023. An Inter-Laboratory Comparative Study on the Influence of Reagents to Perform the Identification of the *Xylella Fastidiosa* Subspecies Using Tetraplex Real Time PCR. *Horticulturae* 9(9): 1053. https://doi.org/10.3390/horticulturae9091053

Purcell A.H., Hopkins D.L., 1996. Fastidious xylem-limited bacterial plant pathogens. *Annual Review of Phytopathology* 34: 131–151. https://doi.org/10.1146/annurev.phyto.34.1.131

Saponari M., Boscia D., Nigro F., Martelli G.P., 2013. Identification of Dna Sequences Related to *Xylella fastidiosa* in Oleander, Almond and Olive Trees Exhibiting Leaf Scorch Symptoms in Apulia (southern Italy). *Journal of Plant Pathology* 95(3): 668. https://doi.org/10.4454/JPP.V95I3.035

Saponari M., Boscia D., Altamura G., Loconsole G., Zicca S., ... Martelli G.P., 2017. Isolation and Pathogenicity of *Xylella Fastidiosa* Associated to the Olive Quick Decline Syndrome in Southern Italy. *Scientific Reports* 7(1): 17723. https://doi.org/10.1038/s41598-017-17957-z

Saponari M., D'Attoma G., Kubaa R.A., Loconsole G., Altamura G., … Boscia D., 2019. A new variant of *Xylella fastidiosa* subspecies *multiplex* detected in different host plants in the recently emerged outbreak in the region of Tuscany, Italy. *European Journal of Plant Pathology* 154(4): 1195–1200. https://doi.org/10.1007/s10658-019-01736-9

Schaad N.W., Postnikova E., Lacy G., Chang C.J., 2004. *Xylella fastidiosa* subspecies: *X. fastidiosa* subsp *piercei*, subsp. nov., *X. fastidiosa* subsp. *multiplex* subsp. nov., and *X. fastidiosa* subsp. *pauca* subsp. nov. *Systematic and Applied Microbiology* 27(3): 290-300.

Trkulja V., Tomić A., Iličić R., Nožinić M., Milovanović T.P., 2022. *Xylella Fastidiosa* in Europe: From the Introduction to the Current Status. *The Plant Pathology Journal* 38(6): 551–571. https://doi.org/10.5423/PPJ.RW.09.2022.0127.

Wells J.M., Raju B.C., Nyland G., Lowe S.K., 1981. Medium for Isolation and Growth of Bacteria Associated with Plum Leaf Scald and Phony Peach Diseases. *Applied and Environmental Microbiology* 42(2): 357–363. https://doi.org/10.1128/aem.42.2.357-363.1981

Wells J.M., Raju B.C., Hung H.Y., Weisburg W.G., Mandelco-Paul L., Brenner D.J., 1987. *Xylella fastidiosa* gen. nov., sp. nov: Gram-Negative, Xylem-Limited, Fastidious Plant Bacteria Related to *Xanthomonas* spp. *International Journal of Systematic and Evolutionary Microbiology* 37(2): 136–143. https://doi.org/10.1099/00207713-37-2-136

Yuan X., Morano L., Bromley R., Spring-Pearson S., Stouthamer R., Nunney L., 2010. Multilocus Sequence Typing of *Xylella fastidiosa* Causing Pierce's Disease and Oleander Leaf Scorch in the United States. *Phytopathology* 100(6): 601–611. https://doi.org/10.1094/PHYTO-100-6-0601

ORCID:
DP: 0009-0004-1844-7596
VG: 0000-0002-3155-6066
VP: 0000-0002-9401-7916
AS: 0000-0002-8630-2434
EC: 0000-0003-1382-0318
IP: 0000-0002-8802-7448

Research Papers

Pseudothecium development and ascospore discharge in *Venturia asperata* and *V. inaequalis*: relation to environmental triggers

Daniele PRODORUTTI[1,2,*], Valeria GUALANDRI[1,2], Vincent PHILION[3], Arne STENSVAND[4], Emanuela COLLER[1], Ilaria PERTOT[1,2]

[1] *Fondazione Edmund Mach, via Mach 1, 38098 San Michele all'Adige, TN, Italy*
[2] *Center Agriculture Food Environment, University of Trento, via Mach 1, 38098 San Michele all'Adige, TN, Italy*
[3] *Institut de Recherche et de Développement en Agroenvironnement, IRDA, Saint-Bruno-de-Montarville, Québec, Canada J3V 0G7*
[4] *Norwegian Institute of Bioeconomy Research (NIBIO), P.O. Box 115, NO-1431 Ås, Norway*
*Corresponding author. E-mail: daniele.prodorutti@fmach.it

Summary. *Venturia asperata* (*Ascomycetes*) was first described in 1975, as a saprotroph on overwintered apple leaf litter, and then, in 2007, as the cause of atypical apple scab symptoms on scab-resistant apple cultivars in southern France, and later in northern Italy and China. Information on *V. asperata* is limited. This study expanded knowledge by comparing development of pseudothecia and ascospore discharge in *V. asperata* and *V. inaequalis*. Leaf litters with pseudothecia of *V. asperata* or *V. inaequalis* were prepared, and a spore trap was placed above each litter. Over the 2-year study, pseudothecia of the two pathogens developed differently: *V. asperata* had delayed pseudothecium maturation and emptying in relation to degree day accumulation, compared to *V. inaequalis*. The ascospore release for *V. asperata* was also delayed, commencing and ending later than *V. inaequalis*. The delayed spore ejection and pseudothecium development of *V. asperata* compared to *V. inaequalis* may partly explain the late onset of symptoms in orchards during each growing season. These results have implications for plant protection strategies on scab-resistant apple cultivars, in particular under warm climates that occur in the Mediterranean region.

Keywords. Apple scab, disease management, epidemiology, light, resistant cultivars.

INTRODUCTION

Use of apple cultivars resistant to scab, caused by *Venturia inaequalis* (Cke.) Wint., is increasing worldwide, with clear advantage in reductions in use of fungicides with potential negative impacts on human health and the environment (Didelot *et al.*, 2016). However, reduced fungicide applications could create favourable conditions for other diseases, including fruit rots, sooty blotch, or Marssonina blotch, which all thrive in the absence of regular fungicide applications (Ellis *et al.*, 1998; Boutry *et al.*, 2023).

The main source of resistance to scab in apple cultivars for more than 50 years has been the *Rvi6* (=*Vf*) gene (Caffier *et al*., 2012, Gessler and Pertot, 2012; Didelot *et al*., 2016). An important drawback of monogenic host resistance is that it may be overcome, and virulent, resistance breaking strains of *V. inaequalis* have become dominant in several countries in Europe (Parisi *et al*., 1993, 2004; Gessler and Pertot, 2012; Patocchi *et al*., 2020). In 2007, atypical apple scab symptoms were observed for the first time in southern France, on fruit of cultivars carrying the resistance gene *Rvi6*. Initially, these symptoms were reported on the cultivar Ariane/Les Naturianes®, and in the following years on the cultivars Co-op 38/GoldRush® and Prima. Morphological and molecular analyses and pathogenicity tests showed that the causal agent of the scab-like symptoms in France was not *V. inaequalis* but was *Venturia asperata* Samuels & Sivan. (Caffier *et al*., 2012).

Venturia asperata (*Ascomycetes*) was first described in New Zealand by Samuels and Sivanesan (1975), and was later reported in Canada by Cortlett (1985). In both locations, *V. asperata* was reported as a saprotroph, growing on overwintered apple leaves on the ground, with no symptoms observed on fruit and leaves in growing seasons. In 2012, atypical apple scab symptoms were recorded in Italy (Cesena, Emilia-Romagna Region), on the fruit of cultivar CIVG198/Modì®, a resistant cultivar carrying the *Rvi6* gene (Turan *et al*., 2019). Symptoms were more severe at fruit harvest, and became established in the following years. Morphological and molecular analyses of isolates from conidia and ascospores confirmed that *V. asperata* was the causal agent of these atypical scab symptoms (Turan *et al*., 2019). In 2018, *V. asperata* was reported on the *Rvi6* gene resistant cultivar in a commercial orchard in the province of Trento, Italy (Gualandri *et al*., 2021; Prodorutti *et al.,* 2023). *Venturia asperata* was also reported in the nearby province South-Tyrol in 2019 (Öttl, 2021), and in other regions of northern Italy (Piemonte, Veneto, Friuli Venezia Giulia; Erschbamer, 2024). In 2018, *V. asperata* was reported from the Heilongjiang Province in China (Zhou *et al*., 2021).

Venturia spp. are hemibiotrophic fungal pathogens. They overwinter as saprophytes in host plant leaf litter on orchard soil, where pseudothecia mature in late winter and spring, producing ascospores that cause primary infections. Subcuticular mycelia develop in fruit and leaves, producing conidiophores and conidia that emerge through the cuticles. During this parasitic stage, *Venturia* spp. can only infect particular hosts, and *V. inaequalis* and *V. asperata* are the only *Venturia* spp. known to cause scab symptoms on apple (Caffier *et al*., 2012; Turan *et al*., 2019). Conidia and ascospores of *V. inae-*

qualis and *V. asperata* differ in shape and size and can be distinguished morphologically (Samuels and Sivanesan, 1975, Caffier *et al*., 2012; Turan *et al*., 2019).

Little information is available on the epidemiology of *V. asperata*. Caffier *et al*. (2012) carried out a single season trial comparing release of ascospores from *V. asperata* and *V. inaequalis*. The first ascospores of both fungi *V. inaequalis* and *V. asperata* were detected in March, but those of *V. inaequalis* were detected at the beginning of that month, and those of *V. asperata* at the end. However, both species had coincident peak release and depletion of ascospores. Pathogenicity tests in France and Italy revealed difficulties in reproducing symptoms on apple leaves and fruit following artificial inoculations of conidia of *V. asperata* (Caffier *et al*., 2012; Turan *et al*., 2019). The symptoms were weak and appeared later than those caused by *V. inaequalis*, and few or no conidia were recovered from lesions developed on fruit and leaves. This suggests that climatic conditions for infection and sporulation of *V. asperata* differ from those for *V. inaequalis* (Caffier *et al.,* 2012), or that *V. asperata* may be a weaker parasite than *V. inaequalis*.

Daylight has been shown to affect ascospore discharge of *V. inaequalis* (Brook, 1969, 1975; MacHardy and Gadoury, 1986; Gadoury *et al*., 1998; Rossi *et al.,* 2001; Stensvand *et al*., 2009), but no information is available for light effects on *V. asperata*. If rain started during night-time, and there was continuous leaf wetness for the next 24 hours, most ascospores of *V. inaequalis* (98%) were discharged between 7:00 and 18:00 (MacHardy and Gadoury, 1986). The peak of ascospore numbers was reached between 11:00 and noon, with a noticeable increase in ascospore discharge beginning at approx. 7:00, i.e., 2-3 hours after sunrise (MacHardy and Gadoury, 1986). Similar results were reported by Rossi *et al*. (2001) in northern Italy, where 93% of the ascospores of *V. inaequalis* were ejected during daylight, with most became airborne within the first two hours after sunrise.

Venturia asperata should be considered an emerging pathogen of apples, spreading in key apple-growing regions of Europe, with symptoms appearing on cultivars carrying the *Rvi6* gene. For this reason, there is a need for epidemiology on this pathogen, particularly to determine whether the conditions and timing for infections align with, or differ from, those of *V. inaequalis*. Increasing knowledge on the epidemiology of *V. asperata* also has practical implications for management of apple scab, because this may influence the timing of fungicide treatments for disease control. Future breeding programmes and selection of scab-resistant cultivars should also consider host susceptibility to *V. asperata*, alongside *V. inaequalis*.

The present study aimed to fill knowledge on the epidemiology of *V. asperata*, by comparing the development of pseudothecia and ascospore discharge with those of *V. inaequalis*. The objectives were to characterize: i) development of pseudothecia, and ii) ascospore discharge in relation to rainfall and degree-day accumulation; and iii) assess effects of daylight on ascospore discharge.

MATERIALS AND METHODS

Apple fruit and leaves with suspected symptoms of *V. asperata* infections were collected on 3 September 2018 from an organic commercial orchard of cultivar Modì, located in Romagnano municipality (Trento Province, Italy; coordinates 45.995053°N, 11.118136°E). Symptoms and fungal propagules on the host samples were described, and compared with those caused by *V. inaequalis,* on fruit and leaves collected from an organic commercial orchard of 'Golden Delicious' in the same general location (46.010059°N, 11.112870°E). The samples from fruit and leaves were then processed for molecular and morphological identification of the putative causal agent. To obtain monosporic isolates, fruit skin was cut from the margins of brownish suberose patches on fruit, or small pieces were cut from dusty patches on leaves, for these sample sources resembling symptoms and signs of *V. asperata*, and a drop of water was put on each host lesion. The drop was then transferred to, and plated on, potato dextrose agar (PDA; Oxoid) containing chloramphenicol (100 mg mL^{-1}; Sigma), and then incubated at 18°C. After 24 h, individually germinated conidia were picked up under stereomicroscope observation, and transferred to PDA + chloramphenicol, and incubated at 18°C.

After development of isolates, two monosporic cultures obtained from fruit and two from leaves were used in molecular analyses. Total genomic DNA was extracted from mycelia using Nucleospin Plant II (Macherey-Nagel), and the ITS region was amplified using the primer Vasp (5'-GTCTGAGAAACAAGTAATAG-3') , specific for *V. asperata* (Stehmann *et al.*, 2001), in combination with ITS4 (White *et al.*, 1990). After sequencing of the PCR products of the two isolates from fruit, a BLAST search was carried out in the NCBI database.

To confirm presence of *V. asperata* in the field, fruit and leaves from the same 'Modì' orchard were sampled in 2019 and 2020, from August to October each year, and assessed for molecular identification of this fungus.

To assess evolution of disease incidence, the 'Modì' apple orchard was monitored at the end of each growing season in 2019, 2020 and 2021. The proportions of diseased fruit and shoots were calculated by randomly checking symptoms on 500 fruit immediately before harvest, and on 50 shoots before start of leaf fall. Just before leaf fall, on 31 October 2019 and 5 November 2020, apple leaves with symptoms of *V. asperata* were collected in the 'Modì' orchard, from trees where no fungicides had been applied during the growing seasons. At the same time, apple leaves with symptoms of *V. inaequalis* were collected from untreated trees in the 'Golden Delicious' orchard.

Leaves from the two cultivars were immediately placed on the ground in two separated plots (each plot containing leaves of one cultivar), in San Michele all'Adige (Trento Province, Italy; 46.189922°N, 11.135227°E). A sample of the collected leaves from each sampled orchard ('Modì' or 'Golden Delicious') was observed under a light microscope to confirm presence of infections of, respectively, *V. asperata* or *V. inaequalis*, by assessing morphological characteristics of conidia and conidiophores (Figure 2). At an experimental site in San Michele all'Adige, the collected leaves were placed in two plots in a grass meadow. The plots each measured 2 × 2 m, and were 100 m apart from each other and at least 100 m away from any apple trees, to avoid cross-contamination (MacHardy, 1996). Additionally, a plot (2 × 1 m) of leaf litter was placed adjacent to each of the 2 × 2 m plots, and was used for monitoring of pseudothecia. To confirm that *V. asperata* pseudothecia developed in the leaf litter of 'Modì', in 2020 maturing pseudothecia were collected from leaves overwintered in the leaf litter, and were directly subjected to PCR with specific primers for *V. asperata*, using the methods described above.

The plots were prepared as described in Prodorutti *et al.* (2024). Grass was removed by light soil tillage, and a layer of leaves was placed on the soil above a white non-woven fabric (permeable polypropylene, Ortoclima, Tenax s.p.a.), which prevented earthworms from degrading the leaves. Each plot was then covered with a wire mesh (1 × 1 cm) to keep the leaves in place. The leaves (approx. 150 m^{-2}) were placed in a single layer, avoiding overlapping.

Development of pseudothecia of *V. asperata* and *V. inaequalis* was evaluated weekly, in 2020 and 2021, from the first week of March to mid-July, in order to cover the complete primary season for ascospore maturation and release. Each week, ten leaves were randomly selected from the leaf litter from each cultivar (Modì or Golden Delicious), and 60 pseudothecia were randomly harvested and observed under a light microscope. Pseudothecia were harvested from leaves previously soaked in water for 10 min, and were then crushed on glass microscope slides and classified in three groups ("immature",

"mature", or "empty") according to their stages of development. The immature pseudothecia included stages from pseudothecium initials to pseudothecia with most asci containing non-pigmented (immature) ascospores. For the "mature" group, most asci contained septate and pigmented (mature) ascospores. Pseudothecia were classified as empty if most of the asci were empty or aborted (Prodorutti *et al*., 2024). The percentages of immature, mature, or empty pesudothecia (out of 60) were calculated for each assessment.

On 27 February 2020 and 24 February 2021, a volumetric spore trap (Myco-trap, Paul Illi Mech.) was placed above each leaf litter, in the middle of each plot. During the entire primary season for ascospore maturation and release, ascospores of the two *Venturia* spp. (Figure 2) captured by the spore traps were counted on each rainy day (≥ 0.2 mm rain d^{-1}). A microscope tape was mounted on a 7-d rotating clock cylinder in each spore trap. The microscope tapes were cut in pieces representing single days, placed on glass slides, and ascospores were counted using a light microscope (200 × magnification). Ascospore counting on the tapes was carried out by assessing along three parallel horizontal lines of each glass slide (Mandrioli, 2000). The daily total number of counted ascospores (sum of the three horizontal lines per slide) for each spore trap was calculated, and was used to compute total seasonal ascospore ejection and percentage of the total numbers of ascospores trapped during each season.

To study the effect of daylight on the ascospore release of *V. asperata*, hourly counting of spores was carried out in the days when rain started before sunrise (https://www.timeanddate.com/sun/) and continued after sunrise. In these days, ascospore counting on each tape (at 400 × magnification) was carried out by assessing 24 vertical lines of the slide, corresponding to each hour of the day.

Weather data were recorded by a weather station (model TMF 500, Nesa s.r.l.), located at the San Michele all'Adige experiment site. Tree budbreak of the two cultivars (Modì or Golden Delicious) was assessed in the 2020 and 2021. Because budbreak of 'Modì' (27 February, 2020; 24 February, 2021) was earlier than for 'Golden Delicious' (3 March, 2020; 1 March, 2021), summation of degree days (DDs, base 0°C) from budbreak of cultivar 'Modì' to the last day of ascospore ejection and to the emptying of pseudothecia was used to compare data of the two *Venturia* species. Hours and related hourly data reported here refer to solar hour (Central European Time, CET). A leaf wetness (LW, min h^{-1}) sensor (Vantage Pro, Davis Instruments Corporation) was placed on the ground to assess hourly wetting of the leaf

litter. Total solar irradiation (TSI, MJ m^{-2}) was recorded each hour, at 2 m above the ground.

'Tidyverse' packages (Wickham *et al*., 2019) of R language (version 4.4.1; R Core Team 2024) were used to handle data and generate plots. Cumulative proportions of empty pseudothecia of the two *Venturia* spp. were modeled as a function of scaled accumulated DDs since 'Modì' budbreak, using binomial regression. A mixed effect model (glmer, package lme4) was used, with sampling date as random effect. Different link functions were compared using the Akaike information criterion (AIC). The contribution of additional fixed effects (*Venturia* species, year, and their interactions) were assessed using likelihood ratio tests (LRTs). Scaled DDs were back transformed for interpretation.

The probability of observing ascospores on any given hour was modeled as a function of presence of light (TSI above zero) and LW at the ground level, using binomial regression. Similarly, hourly ascospore ejection intensity was modelled with count regression models using TSI. In all cases, the mixed effect model (glmer, package lme4) was used with sampling date as random effect.

RESULTS

Symptoms and signs on apple fruit were atypical apple scab spots, being less intense compared to scab lesions caused by *V. inaequalis* (Figure 1). The lesions on fruit developed first as small slightly grey spots, that slowly enlarged and then evolved into necrotic suberose spots, each surrounded with a light and smooth ring. Spots on fruit usually had less clear edges and were lighter (brownish) in appearance compared to those caused by *V. inaequalis* (grey to black; Figure 1). Leaf lesions caused by *V. asperata* were less distinct and more irregular compared to leaf lesions caused by *V. inaequalis*. Leaf lesions caused by *V. asperata* appeared only on abaxial leaf surfaces as velvety-grey spots, in contrast to those caused by *V. inaequalis* which were present on both surfaces of infected leaves (Figure 1). Observations with a light microscope showed that conidiophores and conidia, and pseudothecia and ascospores, collected from infected fruit and leaves in Romagnano, matched well with previous descriptions of *V. asperata* (Samuels and Sivanesan, 1975; Caffier *et al.,* 2012; Turan *et al*., 2019; Shen *et al*., 2020), that these structures differed from those of *V. inaequalis* (Figure 2). Conidiophores and conidia of *V. asperata* emerging on fruit or leaf epidermides were observed using stereo and light microscopes, developing from the margins of necrotic suber-

Figure 1. Fruit and leaves of apple cultivar Modì (top row) with (from left to right) sporulating lesions of *Venturia asperata* and leaf lesion detail, and of cultivar Golden Delicious (bottom row) with (left to right) sporulating lesions of *V. inaequalis* and leaf lesion detail.

ose spots on fruit or from spots on leaves (Figure 2). PCR with species-specific primers for *V. asperata* from monospore isolates obtained from fruit and leaves each gave the expected 450 bp product, and BLAST analyses of the sequences of the two isolates from fruit were 100% identical to the published sequence of *V. asperata* (KX156341). Consensus sequences of the two isolates were submitted and deposited in GenBank nucleotide database (accession nos. MT459450 and MT459451). The PCR analysis of pseudothecia collected on overwintered leaves of 'Modì' showed DNA amplification at 450 bp, and the PCR from symptomatic fruit and leaves samples collected in 2019 and 2020 confirmed establishment of *V. asperata* in the 'Modì' orchard.

Symptoms of *V. asperata* on apple fruit and leaves appeared later in the growing seasons than those caused by *V. inaequalis*. Symptoms caused by *V. asperata* on fruit occurred from the end of July to early August, and on leaves from September to October. The first symptoms of *V. inaequalis* infections on leaves appeared in April, and on fruit in May–June.

Monitoring of symptoms of *V. asperata* in the orchard showed increases in percentage of infected fruit at harvest (early September), from 1.2 to 9.4%, from 2019 to 2021 (Table 1). On 'Modì', only one to two spots per infected fruit were typically observed, and three to four or more spots were found on approx. 20% of symp-

Table 1. Incidence of *Venturia asperata* symptoms on apple fruit and shoots during 2019, 2020 and 2021 in an orchard of cultivar Modì located in Romagnano (Italy).

Year	Day/month	Symptomatic fruit (%)[a]	Day/month	Symptomatic shoots (%)[b]
2019	06/09	1.2	23/10	40.0
2020	04/09	5.6	06/11	100.0
2021	03/09	9.4	22/10	100.0

[a] 500 fruit assessed.
[b] 50 shoots assessed.

tomatic fruit. At the end of the growing seasons (late October to early November), high proportions of shoots were symptomatic (i.e., at least one leaf with scab per shoot), resulting in disease incidence of 40% in 2019, and 100% in 2020 and 2021 (Table 1). In the three years of monitoring, all fruit and shoots in the untreated trees of 'Golden Delicious' showed symptoms of *V. inaequalis* (100% incidence).

Pseudothecia of the two *Venturia* spp. developed differently in the 2-year trial. Pseudothecia of *V. asperata* had delayed maturation and emptying of ascospores compared to pseudothecia of *V. inaequalis* (Figure 3, C and D). The periods of detection of mature *V. inaequalis* pseudothecia were similar in the 2 years (13 March to
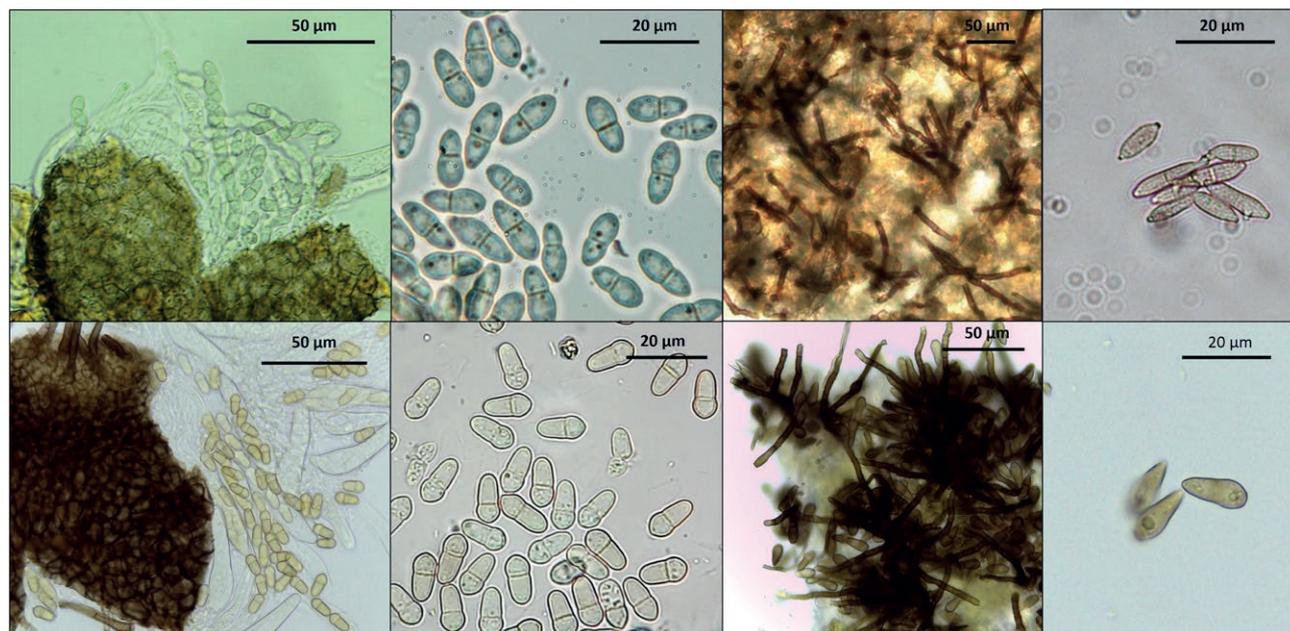
Figure 2. Pseudothecium with asci, ascospores, conidiophores, and conidia (left to right) of *Venturia asperata* (top) and *Venturia inaequalis* (bottom).

Table 2. Development of pseudothecia of *Venturia inaequalis* and *V. asperata* in San Michele all'Adige (Italy) in 2020 and 2021.

Year	Period with mature pseudothecia (day/month)		Peak of maturation (day/month)		DDs of 95% empty pseudothecia[a]	
	V. inaequalis	*V. asperata*	*V. inaequalis*	*V. asperata*	*V. inaequalis*	*V. asperata*
2020	13/03 to 29/05	08/05 to 26/06	24/04	22/05	1,181	1,744
2021	10/03 to 26/05	27/04 to 08/07	27/04	03/06	1,009	1,941

[a] Degree days (DDs, base temperature 0°C) from budbreak of cultivar Modì to 95% of the pseudothecia empty (data predicted by the probit model).

29 May in 2020; 10 March to 26 May in 2021). Mature pseudothecia of *V. asperata* were present from 8 May to 26 June in 2020, and from 27 April to 8 July in 2021 (Table 2). The peaks of proportions of mature pseudothecia of *V. inaequalis* were observed on 24 April (37% of mature pseudothecia) in 2020, and 27 April (32%) in 2021. *Venturia asperata* had greatest proportions of mature pseudothecia on 22 May (23%) in 2020, and on 3 June (15%) in 2021 (Table 2). These dates were approx. 1 month after equivalent dates for *V. inaequalis*.

The probit model gave overall better fits for pseudothecium emptying rate than logistic regression, and the probit model better represented data for *V. inaequalis* than for *V. asperata* (Figure 3, C and D). The triple interaction *Venturia* species × year × cumulative DDs was statistically significant (LRT = 9.7, df = 1, P = 0.0019), indicating that both the onset and rate of pseudothecium emptying were different for the two species for the two years. In both years, onset of emptying and the time of 95% empty pseudothecia predicted by the probit model were reached later for *V. asperata* than *V. inaequalis* (563 DDs later in 2020, 932 DDs later in 2021; Table 2). The difference in accumulated DDs between the two species when pseudothecia started emptying was similar in 2020 and 2021 (z = 0.8, P = 0.85). Rates of pseudothecium emptying were also similar for the two species in 2020 (z = 0.7, P = 0.5), but yearly variations in the rates of pseudothecium emptying were detected for *V. asperata* (z = 3.4, P = 0.0008), as the rate for *V. asperata* was slower in 2021, while a similar emptying rate was observed for *V. inaequalis* in 2020 and 2021 (z = 1.7, P = 0.09).

The periods of ascospore release were different for the two *Venturia* species, and were later for *V. asperata* than for *V. inaequalis* (Table 3; Figure 3, A and B). The
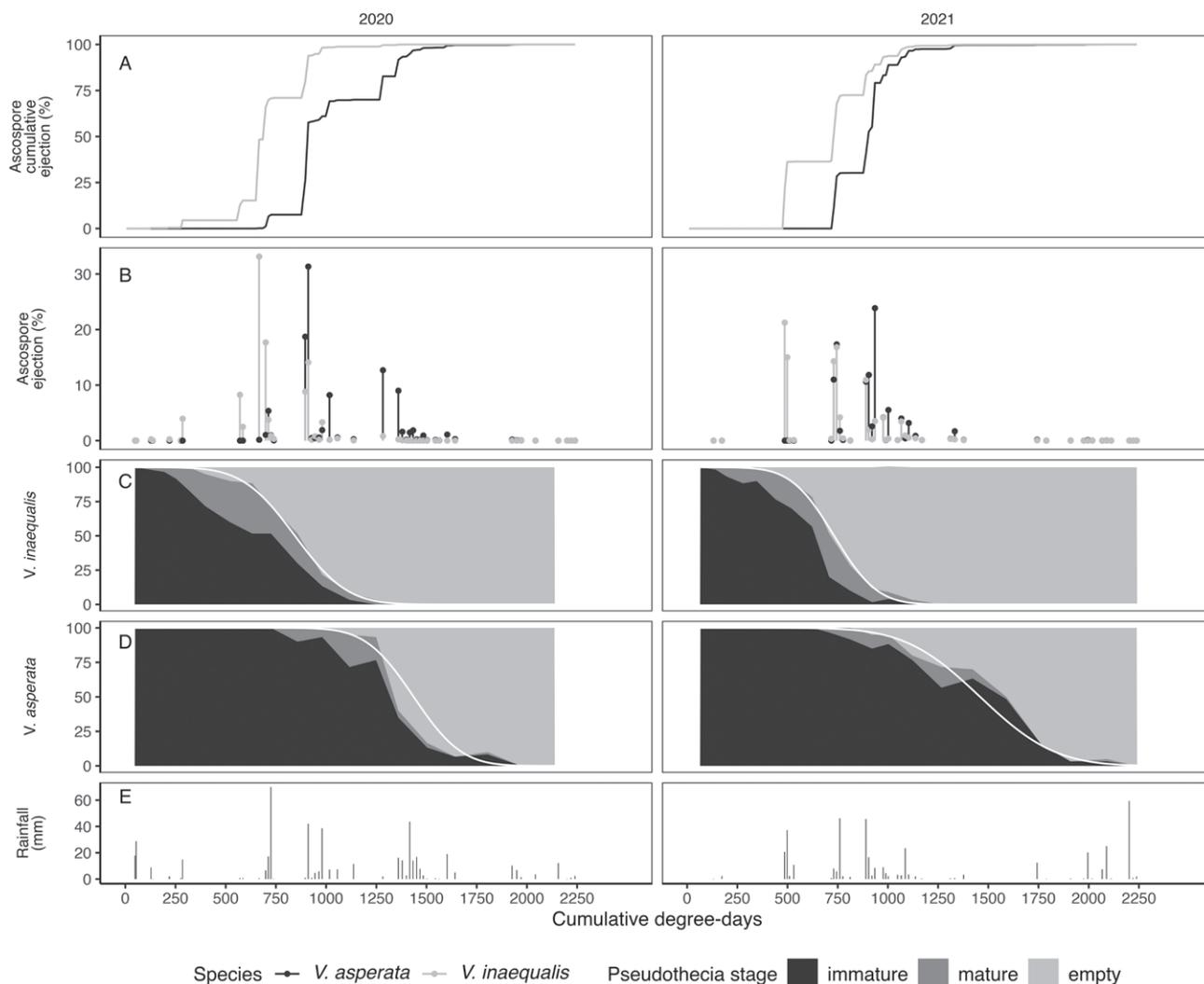
Figure 3. Degree-day accumulation (base temperature 0°C) since budbreak of apple cultivar Modì in 2020 and 2021 (San Michele all'Adige, Italy), in relation to the following. A, percentage of cumulated seasonal trapping of ascospores of *Venturia asperata* (black line) and *V. inaequalis* (grey line). B, percentages of the seasonal ascospores of *V. asperata* (black bars) and *V. inaequalis* (grey bars) released per day on days with rain (≥ 0.2 mm). C and D, percentages of immature, mature, and empty pseudothecia during the season for ascospore release of *V. inaequalis* (C) and *V. asperata* (D). Weekly assessments of 60 pseudothecia per species were evaluated in each year. Pseudothecia emptying was modelled using the probit model, represented by the white line. E, Daily rainfall (mm).

first ascospores of *V. asperata* were trapped at the end of April in both years, and continued until early July. Ascospore discharge of *V. inaequalis* commenced in mid-March and ended in early June in 2020, and commenced in early April and ended in the second half of June in 2021 (Table 3). Total numbers of ascospores released during entire seasons were greater in both years for *V. asperata* than for *V. inaequalis*. The difference was most noticeable in 2021, with *V. asperata* releasing almost three times the number of ascospores compared to *V. inaequalis* (Table 3). The peaks of ascospore ejection occurred later for *V. asperata*. In 2020, this was

reached 26 April (at 667 DDs) for *V. inaequalis* and 11 May (at 911 DDs) for *V. asperata*, corresponding to 33.1% of the seasonal ascospore amount for *V. inaequalis* and 31.3% for *V. asperata* (Figure 3 B). In 2021, the peak of ascospore release for *V. inaequalis* was reached on 11 April (21% of the seasonal ascospores were trapped; 486 DDs), and that for *V. asperata* was on 15 May (24% of the seasonal ascospores were trapped, 935 DDs) (Figure 3 B). The time of 95% of trapped ascospores was reached earlier in *V. inaequalis* (435 DDs earlier in 2020 and 56 DDs earlier in 2021) than the equivalent periods for *V. asperata* (Figure 3 A; Table 3). The 95% DD accumula-

Table 3. Rainfall data, numbers of ascospores of *Venturia inaequalis* and *V. asperata* trapped, and degree days recorded, in San Michele all'Adige (Italy) in 2020 and 2021.

Year	Total rainfall (mm)[a]	Total numbers of ascospores[b]		Period of ascospore release (day/month)		DDs for 95% ascospore release[c]	
		V. inaequalis	*V. asperata*	*V. inaequalis*	*V. asperata*	*V. inaequalis*	*V. asperata*
2020	452.2	5,474	6,742	14/03 to 06/06	26/04 to 03/07	965	1,400
2021	333.2	9,823	28,350	11/04 to 23/06	28/04 to 08/07	1,048	1,104

[a] Rainfall was recorded from budbreak of cultivar Modì to the last day of ascospore ejection from *V. asperata*.
[b] Total number of ascospores collected by volumetric spore traps in the season.
[c] Degree days (DDs, base temperature 0°C) from budbreak of cultivar Modì to the time of 95% of seasonal ascospore trap count.
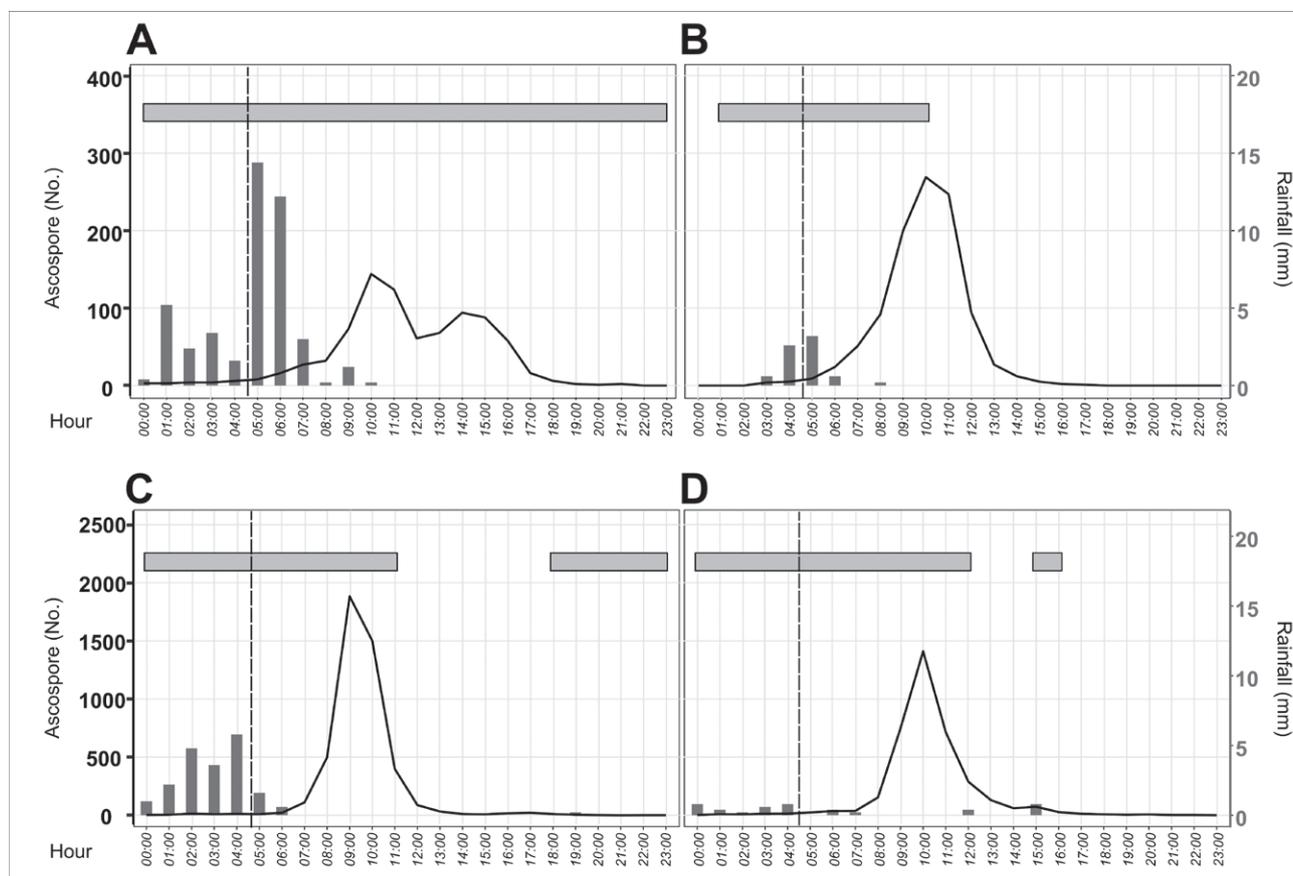
Figure 4. Hourly release of ascospores of *Venturia asperata* on four days when rainfall commenced before, and ended after sunrise. A) 15 May 2020, B) 17 May 2020, C) 12 May 2021, D) 25 May 2021. Sunrise occurred at 04:42 (Central European Time) on 15 May 2020, at 04:40 on 17 May 2020, at 04:46 on 12 May 2021 and at 04:32 on 25 May 2021. Vertical bars represent the hourly rainfall (mm), and horizontal bars indicate times when leaf wetness was recorded at ground surface. The solid line represents the hourly numbers of counted ascospores, and the vertical dashed lines indicate time of sunrise.

tions for empty pseudothecia and for ascospore ejection were similar in both years for *V. inaequalis,* and for *V. asperata* in 2020. However, in 2021 *V. asperata* reached 95% empty pseudothecia at 1,941 DDs compared to 1,104 DDs for 95% ascospore ejection (Table 2; Table 3). The last ascospores were trapped ca. 4 weeks later for *V.*

asperata than *V. inaequalis* in 2020 and ca. 2 weeks later in 2021 (Table 3).

The total rainfall measured during the primary season was greater in 2020 (452 mm) than in 2021 (333 mm; Table 3). The rainfall conditions necessary to observe the potential diurnal periodicity of ascospore

release of *V. asperata* (rain started before and continued after sunrise) were fulfilled during 4 d of substantial ascospore trapping, i.e., on 15 and 17 May 2020, and 12 and 25 May 2021 (Figure 4). Sunrise occurred at 4:42 and 4:40 on 15 and 17 May 2020, and at 4:46 and 4:32 am on 12 and 25 May 2021. The patterns of ascospore release were similar in the four days, but total numbers of ascospores counted in 2020 were less than those counted in 2021. Very few ascospores were trapped from midnight to 4:00 am each day, and ascospore trapping began to increase after sunrise (from 5:00 to 7:00 am). From 7:00 to 9:00-10:00 am each day numbers of trapped ascospores rapidly increased, with exponential trends. Greatest numbers were detected at 10:00 am on 15 May and 17 May 2020, and 25 May 2021, and at 9:00 am on 12 May 2021. After these times, there were rapid declines in ascospore numbers, with values close to zero after 5:00-6:00 pm each day (Figure 4). In each of the four days, the TSI was above zero from 6:00 am to 8:00 pm. In these time intervals, the proportions of ascospores counted per 24 h ranged from 96.4% on 15 May 2020 to 98.9% on 25 May 2021.

Similar rainfall conditions were recorded in the four days when hourly counting of ascospores were carried out. Rain started during the night and continued until early-mid morning. Small rainfall amounts (0.2 – 0.8 mm h^{-1}), as occurred on 25 April 2021, induced relevant ascospore ejection. The LW measured at soil surface was recorded continuously through 24 h on 15 May 2020. In the other three events, LW was recorded for 2 to 5 h after rainfall ceased (Figure 4).

Both LW at the soil surface (LRT = 6.2, P = 0.01) and light (LRT = 14.4, P < 0.001) significantly increased probability of detecting ascospores in the spore traps. The odds ratio (OR) of observing ascospores during light hours, as opposed to dark hours, was 37 (z = 2.624, P = 0.009), while the OR for wet hours compared to dry hours was 16 (z = 2, P = 0.045). Hourly ascospore ejection intensity was over-dispersed, and was adequately modelled using a negative binomial distribution. Light had an exponential effect on the numbers of ascospores ejected, with an Incidence Rate Ratio (IRR) indicating that ejection was 38 times more intense during light hours compared to dark hours (z = 12, P < 0.001), and seven times more intense during wet hours compared to dry hours (z = 5.5, P < 0.001). Within the limited dataset, ascospore release intensity was better modelled as a function of light intensity, increasing linearly with the log of TSI (LRT = 38, df = 0). This relationship can be expressed as: Ejection intensity = $28 \times (TSI + 0.01)^{0.82}$, for TSI values ranging from 0 to 3.03 MJ m^{-2} during dry hours. For wet hours, ascospore release intensity

was eight times greater than for dry hours. There was no interaction between the effect of TSI and wetness on ascospore release (P = 0.96).

DISCUSSION

In the present study, symptoms of *V. asperata* infections on apple fruit, and timing of their appearance, were similar to those previously described in France (Caffier *et al.*, 2012), and in Italy (Turan *et al.*, 2019). However, these symptoms were observed for the first time on leaves in a commercial orchard of the apple cultivar Modì. Caffier *et al.* (2012) were able to induce sporulating lesions of the pathogen on leaves of the apple cultivar Ariane, in controlled conditions and after artificial inoculations with conidia of *V. asperata*, and the symptoms they observed were weak and difficult to detect. In the present study, late appearance of leaf symptoms (September-October) was observed, with symptom intensity increasing towards leaf fall. Symptoms were confined to abaxial leaf surfaces and resembled late secondary infections of *V. inaequalis*, although lighter in appearance than for *V. inaequalis*. Because the symptoms of *V. asperata* on leaves are weak and often difficult to detect, confirmation through microscopic morphological analyses or molecular identifications are essential. The weak symptoms caused by *V. asperata*, observed both on fruit and leaves, could be due to fewer hyphae and conidia growing in each lesion, compared to *V. inaequalis* (Caffier *et al.*, 2012; Turan *et al.*, 2019).

Over the three years of observations, increases in incidence of symptoms and signs of *V. asperata* was observed in the monitored 'Modì' orchard, reaching almost 10% on the fruit in 2021. This increase over the 3 years may be partly due to gradual build-up of overwintering inoculum in infected leaf litter. The greater numbers of ascospores captured in 2021 compared to 2020, and the increasing incidence of disease, indicated increased overwintering of inoculum of the pathogen. High incidences of lesions caused by *V. asperata* on fruit of apple cultivars with *Rvi6* gene resistance to *V. inaequalis* were observed in southern France (up to 60%; Caffier *et al.*, 2012), and South Tyrol in Italy (up to 17.5% in 2023; Erschbamer, 2024). *Venturia asperata* has predominantly been reported in apple cultivars containing the *Rvi6* gene, mostly under organic management regimes. The limited use of fungicides, often only applied early in each growing season, probably facilitated outbreaks of *V. asperata* in the organic orchards with scab resistant cultivars. Little and unclear information is available about the presence of *V. asperata* on scab-sus-

ceptible (non-resistant to *V. inaequalis*) apple cultivars. Strict management of apple scab and greater competition of *V. inaequalis* in an orchard may lead to underestimation of the presence and spread of the less competitive *V. asperata* on these cultivars.

Pseudothecia of *V. asperata* had delayed maturation and ascospore emptying compared to *V. inaequalis*. The first mature pseudothecia were observed over a month and a half later than those of *V. inaequalis*, and the peak of maturation occurred about one month later for *V. asperata* than for *V. inaequalis*. The earlier onset of ascospore ejection for *V. inaequalis* in both years, and the slower rate of pseudothecium emptying for *V. asperata* in 2021, suggest that the two *Venturia* spp. have inherently different ejection patterns. As it was observed for the effect of irrigation on pseudothecium development (Prodorutti *et al.*, 2024), probit regression gave a better fit for pseudothecium emptying rates, and better represented *V. inaequalis* than *V. asperata*, which is another indication that the two species have differences in seasonal development of their pseudothecia and ascospores.

In both years, the ascospore release for *V. asperata* was delayed compared to *V. inaequalis*, with initiation and peak of ascospore release occurring later in *V. asperata* than in *V. inaequalis*. In 2021, the first ascospores of *V. inaequalis* were detected almost a month later than in 2020, likely due to the prolonged dry period in March and early April of 2021. Extended dry periods delay pseudothecium maturation and extend ascospore release seasons of *V. inaequalis* (Stensvand *et al.*, 2005), and this is also likely to be the case for *V. asperata*.

The less prominent difference in cease of ascospore release between the two fungi in 2021 than in 2020 may have been partly due to a more rapid breakdown of leaf litter of 'Modì' than 'Golden Delicious', although no records of leaf degradation were made in the present study.

Caffier *et al.* (2012) reported that the first ascospores of *V. asperata* were trapped approx. 20 d later than those of *V. inaequalis*, but that the peaks in ascospore release and end of ejection were observed at the same time for both species. The discrepancies between the present study results and those obtained in France may be due to the different methods used for leaf litter preparation. Caffier *et al.* (2012) placed leaves on ground covered by grass, so the leaves may have degraded more rapidly than in the present study experiments. Weekly development of pseudothecia of *V. asperata* had not been previously studied, and it was here shown that the periods of pseudothecium maturation and ascospore release overlapped.

Light triggered ascospore discharge of *V. asperata* in a manner similar reported for *V. inaequalis* (Brook,

1969; 1975; MacHardy and Gadoury, 1986; MacHardy, 1996; Gadoury *et al.,* 1998; Rossi *et al.*, 2001; Stensvand *et al.*, 2009). As for *V. inaequalis*, increases in *V. asperata* ascospore discharge were observed during the first 2 to 3 h after sunrise, and even small amounts of rain (0.2 mm h^{-1}) were sufficient to induce substantial ascospore ejection. Similar to previous reports for *V. inaequalis* (MacHardy and Gadoury, 1986; Rossi *et al.*, 2001), on average approx. 98% of the ascospores were released during daylight hours between 6:00 am to 8:00 pm. However, in the three days when LW was recorded until 10:00 to 12:00 am (2 to 5 h after the rain stopped), more rapid decreases in ascospore numbers were detected compared to 15 May 2020, when LW was recorded continuously for 24 h.

The OR and IRR values for ascospore ejection of *V. asperata* were both high and were similar, indicating the importance of light in triggering ascospore release. This suggests that the observed inhibition of release during dark conditions may have been proportional to numbers of ascospores primed for ejection, indicating a light-dependent regulatory mechanism of ascospore release, similar to that observed for *V. inaequalis*. The observations that ejection intensity was well-represented by the log of light intensity, and that no residual pattern was observed, indicate that the light effect rapidly saturates above a certain intensity. The substantial difference between the OR and IRR for the effect of wetness indicates that while ascospore ejection is much more likely during wet than dry periods, the total number of ejected ascospores is less influenced by wetness than by light. This implies that wet conditions are a primary trigger for ascospore release, but do not significantly increase the intensity of ejection. Again, this is similar to what has been observed for *V. inaequalis*.

CONCLUSIONS

Delayed pseudothecium development and ascospore ejection in *V. asperata* compared to *V. inaequalis*, may partly explain the late appearance of symptoms caused by *V. asperata* in apple orchards during the growing seasons. Further research is necessary to identify the optimal weather conditions for primary and secondary infections by *V. asperata* in susceptible apple tissues, and to define the latency period for this pathogen. The efficacy of fungicides commonly used for management of *V. inaequalis* should also be assessed for control of disease caused by *V. asperata*.

Future apple breeding programmes should consider resistance to emerging pathogens such as *V. asperata*,

and specific control strategies should be developed to address the delayed primary infections and late symptom onset caused by this pathogen. In Europe, *V. asperata* has been reported in northern Italy and southern France, areas with temperate climates. *Venturia asperata* probably has higher requirements of DD accumulation for maturation of pseudothecia compared to *V. inaequalis*. As climate change raises average temperatures, this could favour the spread and virulence of *V. asperata* in fruit-growing regions in Mediterranean areas and other areas across Europe and elsewhere, emphasizing that close monitoring of this pathogen in apple orchards is important.

AUTHOR CONTRIBUTIONS

ACKNOWLEDGEMENTS

LITERATURE CITED

Boutry C., Bohr A., Buchleither S., Ludwig M., Oberhänsli T., … Flury P., 2023. Monitoring spore dispersal and early infections of *Diplocarpon coronariae* causing apple blotch using spore traps and a new qPCR method. *Phytopathology* 113: 470–483. https://doi.org/10.1094/PHYTO-05-22-0183-R

Brook P.J., 1969. Stimulation of ascospore release in *Venturia inaequalis* by far red light. *Nature* 222: 390–392.

Brook P.J., 1975. Effect of light on ascospore discharge by five fungi with bitunicate asci. *New Phytologist* 74: 85–92.

Caffier V., Le Cam B., Expert P., Tellier M., Devaux M., … Chevalier M., 2012. A new scab-like disease on apple caused by the formerly saprotrophic fungus *Venturia asperata*. *Plant Pathology* 61: 915–924. https://doi.org/10.1111/j.1365-3059.2011.02583.x

Corlett M., 1985. *Venturia asperata*. In: *Fungi Canadenses* (M. Corlett, S.A. Redhead, G.P. White *et al.*, ed.), Biosystematics Research Institute, Ottawa, Canada, 291.

Didelot F., Caffier V., Orain G., Lemarquand A., Parisi L., 2016. Sustainable management of scab control through the integration of apple resistant cultivars in a low-fungicide input system. *Agriculture, Ecosystems and Environment* 217: 41–48. https://doi.org/10.1016/j.agee.2015.10.023

Ellis M.A., Ferree D.C., Funt R.C., Madden L.V., 1998. Effects of an apple scab-resistant cultivar on use patterns of inorganic and organic fungicides and economics of disease control. *Plant Disease* 82: 428–433. https://doi.org/10.1094/PDIS.1998.82.4.428

Erschbamer M., 2024. *Venturia asperata* – una nuova "ticchiolatura" si sta diffondendo. *Frutta e Vite* 48(2): 5–7.

Gadoury D.M., Stensvand A., Seem R.C., 1998. Influence of light, relative humidity, and maturity of populations on discharge of ascospores of *Venturia inaequalis*. *Phytopathology* 88: 902–909. https://doi.org/10.1094/PHYTO.1998.88.9.902

Gessler C., Pertot I., 2012. Vf scab resistance of *Malus*. *Trees* 26: 95–108. https://doi.org/10.1007/s00468-011-0618-y

Gualandri V., Prodorutti D., Delaiti L., Zaffoni M., Panizza C., … Angeli G., 2021. First report of *Venturia asperata* in Trentino Region (northern Italy). In: *Book of Abstracts 26° SIPaV Congress,* 15–17 September, 2021, virtual congress, 26.

MacHardy W.E., 1996. *Apple Scab: Biology, Epidemiology and Management*. The American Phytopathological Society, St. Paul, MN, USA, 545 pp.

MacHardy W.E., Gadoury D.M., 1986. Patterns of ascospore discharge by *Venturia inaequalis*. *Phytopathology* 76: 985–990.

Mandrioli P., 2000. *Metodo di campionamento e conteggio dei granuli pollinici e delle spore fungine aerodispersi*. Consiglio Nazionale delle Ricerche, Italy, 7 November 2000: 11 pp.

Öttl, S., 2021. *Venturia asperata* – prime evidenze della presenza in Alto Adige. *Frutta e Vite* 45(1): 35–36.

Parisi L., Lespinasse Y., Guillaumes J., Kruger J., 1993. A new race of *Venturia inaequalis* virulent to apples with resistance due to the *Vf* gene. *Phytopathology* 83: 533–537.

Parisi L., Fouillet V., Schouten H.J., Groenwold R., Laurens F., … Tsipouridis C., 2004. Variability of the pathogenicity of *Venturia inaequalis* in Europe. *Acta Horticulturae* 663: 107–113. https://doi.org/10.17660/ActaHortic.2004.663.13

Patocchi A., Wehrli A., Dubuis P.-H., Auwerkerken A., Leida C., … Bus V.G.M., 2020. Ten years of VINQUEST: first insight for breeding new apple cultivars with durable apple scab resistance. *Plant Disease* 104(8): 2074–2081. https://doi.org/10.1094/PDIS-11-19-2473-SR

Prodorutti D., Gualandri V., Bugiani R., Rimondi S., Delaiti L., … Pertot I., 2023. *Venturia asperata,* a new species causing apple scab in Italy. In: *Proceedings of 12th International IOBC/WPRS Workshop on Pome Fruit Diseases*, 13–16 June, 2022, Plovdiv, Bulgaria. IOBC-WPRS Bulletin 164, 26–27.

Prodorutti D., Bugiani R., Philion V., Stensvand A., Coller E., … Pertot, I., 2024. Irrigation targeted to provoke ejection of ascospores of *Venturia inaequalis* shortens the season for ascospore release and results in less apple scab. *Plant Disease* 108: 1353–1362. https://doi.org/10.1094/PDIS-07-23-1245-RE

R Core Team, 2024. R: A language and environment for statistical computing. *R Foundation for Statistical Computing,* Vienna, Austria. https://www.R-project.org/

Rossi V., Ponti I., Marinelli M., Giosuè S., Bugiani R., 2001. Environmental factors influencing the dispersal of *Venturia inaequalis* ascospores in the orchard air. *Journal of Phytopathology* 149: 11–19. https://doi.org/10.1046/j.1439-0434.2001.00551.x

Samuels G.J., Sivanesan A., 1975. *Venturia asperata* sp. nov. and its *Fusicladium* state on apple leaves. *New Zealand Journal of Botany* 13: 645–52.

Shen M., Zhang J.Q., Zhao L.L., Groenewald J.Z., Crous P.W., Zhang Y., 2020. *Venturiales. Studies in Mycology* 96: 185–308. https://doi.org/10.1016/j.simyco.2020.03.001

Stehmann C., Pennycook S., Plummer K.M., 2001. Molecular identification of a sexual interloper: the pear pathogen, *Venturia pirina*, has sex on apple. *Phytopathology* 91: 633–641. https://doi.org/10.1094/PHYTO.2001.91.7.633

Stensvand, A., Eikemo, H., Gadoury, D.M., Seem, R.C., 2005. Use of a rainfall frequency threshold to adjust a degree day model of ascospore maturity of *Venturia inaequalis*. *Plant Disease* 89: 198–202. https://doi.org/10.1094/PD-89-0198

Stensvand A., Eikemo H., Seem R.C., Gadoury D.M., 2009. Ascospore release by *Venturia inaequalis* during periods of extended daylight and low temperature at Nordic latitudes. *European Journal of Plant Pathology* 125: 173–178. https://doi.org/10.1007/s10658-009-9459-6

Turan C., Menghini M., Gazzetti K., Ceredi G., Mari M., Collina M., 2019. First identification of *Venturia asperata* from atypical scab-like symptoms in Italian apple orchards. *European Journal of Plant Pathology* 153: 1325–1331. https://doi.org/10.1007/s10658-018-01623-9

White T.J., Bruns T., Lee S., Taylor J., 1990. Amplification and direct sequencing of fungal ribosomal RNA genes for phylogenetics. In: *PCR Protocols: A guide to Methods and Applicatio*ns (M.A. Innis, D.H. Gelfand, J.J. Sninsky, T.J. White, ed.), Academic Press, San Diego, USA, 315–322.

Wickham H., Averick M., Bryan J., Chang W., McGowan L., … Yutani H., 2019. Welcome to the tidyverse. *Journal of Open Source Software* 4: 1686. https://doi.org/10.21105/joss.01686

Zhou Y., Bu H., Chaisiri C., Tan Q., Wang L., … Luo C., 2021. First report of atypical scab caused by *Venturia asperata* on apple in China. *Plant Disease* 105: 1858. https://doi.org/10.1094/PDIS-11-20-2431-PDN

ORCID:
AB: 0009-0005-6483-2222
OA: 0000-0002-8344-1113
AD: 0009-0004-1790-1320
NL: 0009-0006-6594-9411
BY: 0000-0003-0823-9860
ML: 0000-0001-7425-970X
NM: 0000-0001-5157-5099
AL: 0000-0001-6653-4425

Research Papers

Genetic diversity of GRSPaV-associated virus in Algeria

Adel BACHIR[1], Manel EL AIR[2], Oussama ALISAWI[5], Anfel DJENAOUI[1], Nourelhouda LAIDOUDI[4], Imane MAHDID[1], Bilal YAHIAOUI[4], Meriem LOUANCHI[1], Naima MAHFOUDHI[2,3], Arezki LEHAD[1,*]

[1] *Laboratoire de Phytopathologie et Biologie Moléculaire, Ecole Nationale Supérieure d'Agronomie, Rue Hacen Badi, Belfort, El Harrach, 16000 Alger, Algeria*
[2] *Laboratoire de Protection des Végétaux, Institut National de la Recherche Agronomique de Tunisie, Rue Hedi Karray, 1004 El Menzah, Tunis, Tunisia*
[3] *Université de Carthage, Avenue de la République, BP 77-1054 Amilcar, Tunisia*
[4] *Laboratoire de Microbiologie Appliquée, Faculté des Sciences de la Nature et de la Vie, Université Ferhat Abbas Sétif1, Algérie*
[5] *Department of Plant Protection, Faculty of Agriculture, University of Kufa, Najaf, Iraq*
*Corresponding author. E-mail: lehad.arezki@gmail.com

Summary. Grapevine rupestris stem pitting-associated virus (GRSPaV; *Foveavirus rupestris*, *Betaflexiviridae*) is the most widespread grapevine virus in most viticulture regions, and this virus has high genetic variability. Genetic diversity of GRSPaV in Algeria was examined, based on the complete capsid protein (CP) gene. Similarity proportions between the CP sequences varied from 76% to 99%. The complete coding sequence of Algerian GRSPaV isolate ALG99 (8,646 nt) was determined using high-throughput sequencing and bioinformatic analyses. Algerian GRSPaV isolates clustered into four groups, with most sequences in groups III and IV. This research is the first to determine the genetic variability of GRSPaV in Algeria.

Keywords. GRSPaV, high throughput sequencing, RT-PCR.

INTRODUCTION

Grapevine rupestris stem pitting-associated virus (GRSPaV; *Foveavirus rupestris*, *Betaflexiviridae*) (Martelli and Jelkmann, 1998; Petrovic *et al.*, 2003) is widespread in many wine-producing countries (Martelli *et al.*, 1997; Meng and Gonsalves, 2007; Morelli *et al.*, 2011). GRSPaV is known to be associated with rupestris stem pitting and vein necrosis in grapevine plants (Martelli, 2014), and the virus induces typical stem pitting symptoms on the indicator *Vitis rupestris* 'St. George' (Goszczynski and Jooste, 2003). However, definitive proof for the etiological role of this virus in stem pitting or vein necroses is lacking (Meng and Rowhani, 2017). No insect vectors have been related to the spread of GRSPaV, and its dissemination is explained by the exchange of infected material (Meng and Gonsalves, 2003).

GRSPaV particles are flexuous filaments particles of length approx. 723 nm. Each particle contains a positive-sense RNA molecule with a total of 8,725 nucleotides (nt) (Meng *et al.*, 1998; Zhang *et al.*, 1998; Petrovic *et al.*, 2003). The GRSPaV genome contains five open reading frames (ORFs), and is believed to be capped at the 5' end and have a polyA tail at the 3' end (Meng and Gonsalves, 2007). ORF1 encodes a polyprotein with domains including a methyl transferase, a helicase, and an RNA-dependent RNA polymerase (RdRP) (Meng *et al.*, 2013). ORF 2 encodes triple gene block protein 1 (TGBp1), ORF 3 triple gene block protein 2 (TGBp2), and ORF 4 encodes triple gene block protein 3 (TGBp3), which are involved in intra- and inter-cellular movement of the virus (Meng and Gonsalves, 2007; Rebelo *et al.*, 2008). The product of ORF5 is the coat protein (CP), which is essential for virion formation (Nolasco *et al.*, 2000; Minafra *et al.*, 2000; Haviv *et al.*, 2006; Meng *et al.*, 2006; Meng and Li, 2010).

Considerable knowledge has been developed on this virus in the past two decades. There is compelling evidence that GRSPaV consists of a range of genetic variants that differ in their genome sequences. To date, the genomes of 15 isolates have been completely of partially sequenced, and eight clusters of viral variants have been identified through phylogenetic analyses (Meng and Rowhani, 2017). A comparison of the full-length genome sequences of four Slovakian GRSPaV isolates and 14 sequences retrieved from GenBank showed four main phylogenetic lineages within populations of the virus. Additionally, genetic recombination and mutations may have shaped GRSPaV evolutionary history contributing to its genetic diversity (Glasa *et al.*, 2017).

No genetic diversity study of GRSPaV has been conducted in Algeria. Therefore, main objective of the present study was to examine the variability of GRSPaV in this country.

MATERIALS AND METHODS

Plant material

Ten infected grapevine accessions, including eight of table grape cultivars and two cultivars of wine grapes, were selected for this study (Table 1).

Nucleic acid extractions

Total nucleic acids (TNA) were extracted from phloem tissues of the different grapevine accessions, and were purified using the procedure of Foissac *et al.* (2001). Selected samples were tested by reverse transcrip-

Table 1. List and identifiers of GRSPaV strains sequenced and analysed in the present study.

Cultivar type	Accession number	Strain	Grapevine Cultivar
Table grape	OU862947.1	DZ-GRSPaV-N9	Dattier
	OU862948.1	DZ-GRSPaV -N10	Cardinal
	OU862949.1	DZ- GRSPaV -N11	Cardinal
	OU862950.1	DZ-GRSPaV -N13	Cardinal
	OU862951.1	DZ-GRSPaV-N14	Dattier
	OU862952.1	DZ-GRSPaV-N15	Gros noir
	OU862953.1	DZ-GRSPaV-N16	Dattier
	PP976048.1	ALG99	Local
Wine grape	OU862954.1	DZ-GRSPaV-N17	Valensi
	OU862955.1	DZ-GRSPaV-N18	Carignan

tion polymerase chain reaction (RT-PCR) for GRSPaV, using the specific primers RSP52 and PSR53 (Rowhani *et al.* 2000) to amplify approx. 905 nts of the entire CP genes as well as 62 bp of the upstream CP and 63 bp of the downstream CP.

Reverse transcription and amplification

TNA (10 μL) of each sample was mixed with 1 μL random primers (1 μg μL^{-1}) and 1.5 μL sterile water, and was then denatured at 95°C for 5 min. Reverse transcription was carried out for 1 h at 39°C in a solution of 8 U μL^{-1} Moloney murine leukaemia virus reverse transcriptase (M-MLV RT; Invitrogen), 5 μL RT buffer (1×), 8 mM DTT, and 200 μM dNTPs, in a final volume of 25 μL with sterile distilled water. A volume of of the synthesized cDNA (2.5 μL) was used for PCR amplification, using a mixture of 1× Taq DNA polymerase buffer, 2 mM MgCl$_2$, 200 μM dNTPs, 50 μM of each primer, and 0.05 U μL^{-1} of Taq DNA polymerase (Invitrogen Corporation), and adjusted to a final volume of 25 μL with sterile distilled water. PCRs each consisted of one cycle at 94°C for 5 min; followed by 35 cycles each of denaturation at 94°C for 35 s, annealing at 52°C for 45 s, and elongation at 72°C for 50 s; and a final extension step at 72°C for 7 min. The PCR products were analysed by electrophoresis in 1.2% agarose gel in 1× TBE buffer.

Sequencing and sequence analysis

The PCR products of ten GRSPaV isolates were purified using the ExoSAP-IT purification kit (Affym-

Table 2. Phylogenetic group GRSPaV reference sequences.

Accession number	Strain	Host plant	Origin	Phylogenetic group	Reference
KR054735.1	LSL	*Vitis vinifera* cv. Riesling	China	VII	(Hu *et al.*, 2015)
FJ943356.1	ORPN24b	*V. vinifera*	USA	VI	(Alabi *et al.*, 2010)
LT855243.1	AV99	Autochtones accession AV99	Tunisia	VIII	(Selmi *et al.*, 2020)
FR691076.1	MG	*V. vinifera* cv. Moscato Giallo	Italy	II	(Morelli *et al.*, 2011)
AY368590.1	Strain_Syrah	*V. vinifera* cv. Syrah	USA	IV	(Lima *et al.*, 2006)
AY881627.1	BS	Hybrid Bertille Seyve 5563	USA	III	(Meng *et al.*, 2005)
AF057136.1	CG1	*V. rupestris* cv. St. George	USA	I	(Meng *et al.*, 2006)
AY368172.2	PN	*V. vinifera* cv. Pinot noir	USA	V	(Lima *et al.* 2009)

etrix). Direct sequencing was carried out in both directions using the same primers as those used for RT-PCR (above), on a 3734xl automated analyzer sequencer (Applied Biosystems). The obtained sequences were submitted to the European Nucleotide Archive (ENA) (Table 1). Comparison of sequences of the CP gene of the Algerian GRSPaV isolates obtained in the present study with those of the different phylogenetic groups available in GenBank (Table 2) was conducted using MEGA X version 10.2.2 software.

Total RNA extraction and Illumina platform sequencing

The infected leaf sample ALG99 was placed in an Eppendorf tube and immersed in RNA, and the resulting solution was sent to DNA-link Company, Republic of Korea. The RNeasy® Plant Mini Kit (QIAGEN) was used to extract RNA from plant samples according to manufacturer's instructions. A TruSeq total RNA library prep kit for total RNA sequencing was used by QIAGEN to prepare an Illumina-NGS library. Total RNA sequences were generated using NovaSeq6000, 2x101PE, (Platform: Novaseq6000; Application: WTS/mRNA), after RNA quality was checked with an Agilent 2100 Expert Bioanalyzer. The raw reads were then trimmed using Trimmomatic-0.39 and BBduk v 37.22 in Geneious Prime® 2024.0.5 (Kearse *et al.*, 2012; http://www.geneious.com).

Map to reference

Geneious RNA was used to map the RNASeq data (Sensitivity: Medium-Low) to the reference sequence. The RNA clean reads were mapped against suspected

virus genomes using Geneious Prime® 2024.0.5 (Kearse *et al.*, 2012), and then consensus sequence was then extracted. All 5,040 plant virus sequences from GenBank were also concatenated into one representative sequence (76,145,671 nt), and this was mapped against the whole RNA reads. The outcomes were shown in a report that had a number of assembled reads, total used reads, coverage and pairwise similarity.

Phylogenetic analyses

To construct the phylogenetic tree, multiple alignments were constructed with sequences from retrieved from GenBank and originating from different world regions (www.cbi.nlm.nih.gov). Alignments of 662 nt for the CP gene were obtained using the Clustalw program implemented in MEGAX10 software (Kumar *et al.*, 2018). The nucleotide sequences of the GRSPaV strains were trimmed to obtain the best fits. Percent identity values were calculated using p-distance methods. A phylogenetic tree was constructed using the Neighbor Joining (NJ) method with 2-parameter Kimura (1,000 bootstrap).

RESULTS

Sequence analysis

The nucleotide-level comparison of the sequenced GRSPaV strains revealed sequence similarities ranging from 76 to 99%. Among the strains, DZ-GRSPaV-N18 had the highest similarity (99%) with the reference strain CG1. In contrast, the least similarity (76%), was observed between the reference sequences GRSPaV-

MG and GRSPaV-PN, and between GRSPaV-PN and GRSPaV-LSL.

The similarity proportions among the Algerian GRSPaV strains was considerable. Nucleotide comparison between the ten Algerian GRSPaV isolates showed similarities ranging from 79 to 97% (Table 1). Isolates DZ-GRSPaV-N9 and DZ-GRSPaV-N10 had the greatest similarity (97%), as did isolates DZ-GRSPaV-N13 and DZ-GRSPaV-N17. Isolates DZ-GRSPaV-N14 , DZ-GRSPaV-N16, DZ-GRSPaV-N18, and ALG99 showed similarities from 81 to 93%. Isolate ALG99 has 93% similarity with isolates DZ-GRSPaV-N15 and DZ-GRSPaV-N18, indicating genetic diversity among these isolates. Overall, these results highlight the considerable genetic diversity present among the ten Algerian GRSPaV strains.

The isolates DZ-GRSPaV-N14, DZ-GRSPaV-N9, DZ-GRSPaV-N15, and DZ-GRSPaV-N10 exhibited respective similarities of, respectively, 93, 94, 92, and 95% with the reference strain Syrah, suggesting low genetic variation and close phylogenetic relationship with each other. Compared with other reference strains, similarity percentages were 87 to 91% with GRSPaV-CG1, 81 to 82% with GRSPaV-MG, 79 to 81% with BS, 80 to 84% with GRSPaV-PN, and approx. 83 to 85% with ORPN24b, GRSPaV-LSL, and AV99. This indicates that although DZ-GRSPaV-N14, DZ-GRSPaV-N9, DZ-GRSPaV-N15, and DZ-GRSPaV-N10 has strong resemblance to Strain Syrah, they presented only moderate similarities with other reference strains, suggesting genetic diversity among these strains.

Isolates DZ-GRSPaV-N11, DZ-GRSPaV-N13 and DZ-GRSPaV-N17 showed similarities from 91 to 96%. Isolate DZ-GRSPaV-N17 and DZ-GRSPaV-N13 exhibited close similarity (96%) with the reference strain BS, indicating very low genetic variation. In contrast, DZ-GRSPaV-N11 had 91% similarity with BS, indicating strong resemblance but slightly greater variation. Compared to other reference strains, these strains had similarity identity percentages of 82 to 84% with GRSPaV-CG1, 84 to 86% with GRSPaV-MG, and 77 to 78% with Strain Syrah.

DZ-GRSPaV-N16 had 94% similarity with GRSPaV-MG, indicating a close relationship and low genetic variation between these two isolates. Compared to other reference strains, DZ-GRSPaV-N16 had 91% similarity with GRSPaV-CG1, 83% with BS, 85% with Strain Syrah, and approx. 83% with other strains (GRSPaV-PN, ORPN24b, GRSPaV-LSL, and AV99). These values suggest that DZ-GRSPaV-N16 shares a strong resemblance with GRSPaV-MG and GRSPaV-CG1, but moderate similarities with other strains, indicating genetic diversity from these other strains.

Isolate DZ-GRSPaV-N18 had close similarity (99%) with GRSPaV-CG1, indicating minimal genetic variation between these two strains. Compared to other reference strains, DZ-GRSPaV-N18 was similar to DZ-GRSPaV-N16, 91% similarity with GRSPaV-MG and approx. 83 to 84% for the other virus strains. This indicates that DZ-GRSPaV-N18 shared strong similarity with GRSPaV-CG1 and GRSPaV-MG, but moderate similarities with other strains, confirming genetic diversity among these strains.

The strain ALG99 had 93% similarity with DZ-GRSPaV-N11 and 94% with DZ-GRSPaV-N13, indicating strong genetic resemblance between these two strains. Compared to reference strains, ALG99 had 81% similarity with BS, 78% with GRSPaV-CG1, and 78% with GRSPaV-MG, indicating greater divergence from these strains. ALG99 was also 83% similar to GRSPaV-PN, 86% to ORPN24b, 77% to GRSPaV-LSL, and 83% similar to AV99. These results indicate that while ALG99 had moderate similarity with ORPN24b and AV99, and ALG99 had more pronounced genetic divergence from GRSPaV-PN and especially from GRSPaV-LSL. This suggests considerable genetic diversity among these virus strains.

Phylogenetic analyses

The phylogenetic analysis of the CP gene sequences of Algerian isolates of GRSPaV, compared to sequences from other countries, revealed nine distinct groups (Figure 1). Among these, four contained Algerian sequences: Group I with one sequence (DZ-GRSPaV-N18), Group II with one sequence (DZ-GRSPaV-N16), Group III with four sequences (DZ-GRSPaV-N17, DZ-GRSPaV-N13, DZ-GRSPaV-N11, and ALG99), and Group IV with four sequences (DZ-GRSPaV-N9, DZ-GRSPaV-N10, DZ-GRSPaV-N14, and DZ-GRSPaV-N15). This distribution showed that the Algerian sequences were primarily in Groups III and IV, which also exhibited intra-group diversity as well as varied genetic similarities with GRSPaV sequences from other countries.

The intra-group similarity proportions for the CP gene of the GRSPaV isolates indicated high genetic homogeneity within each group. The intra-group similarity was from 96 to 99%, while the inter-group proportions were from 81 to 90%.

The Groups I and VII isolates had the greatest intra-group similarity (99%), indicating low genetic variation within these groups. Group VI isolates had 97% similarity, also close intra-group relatedness. The isolates in Groups II, III, IV, and VIII had lower intra-group similarity percentages (95% for Group II, 94% for Groups III and IV, 96% for Group VIII). These results indicate moderate to
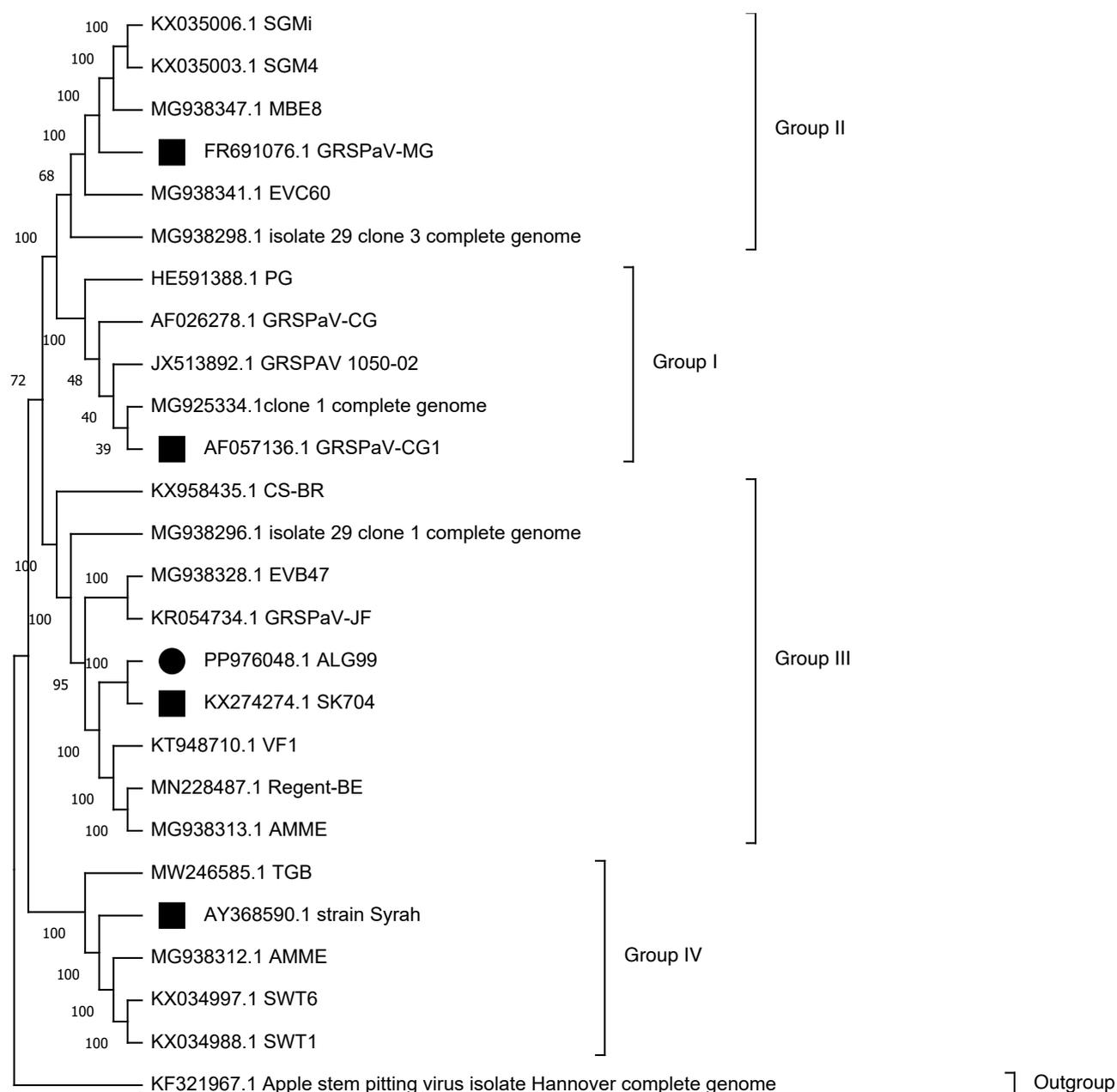
Figure 1. Phylogenetic tree of GRSPaV strains, constructed with sequences of a 662nt fragment of the viral capsid protein (CP) gene, obtained in this study and retrieved from GenBank, with percentage bootstrap support (≥50%) with 1,000 bootstrap replicates indicated on each tree branch. The CP gene of apple stem pitting virus strain KF321967.1 was used as the outgroup. ● indicates Algerian sequences, and ■ indicates the reference sequence for the group.

low genetic variation within these groups. These results indicate that some GRSPaV groups consisted of genetically similar strains, while others had greater genetic diversity.

The between group similarity analysis showed that the GRSPaV isolates in Groups I and II had 90.47% similarity, indicating close phylogenetic relationship. Similarly, Groups III and V, with 87.97% similarity, had strong resemblance. In contrast, most of the groups had moderate similarity proportions (80 to 85%) with other groups, such as Groups II and IV (84.52%), IV and VI (84.49%), III and VI (85.52%), and VII and IV (84.34%). Isolates in Group IX had similarities ranging from 41.53 to 43.00% with other Group isolates, indicating that the Group IX isolates were genetically distinct from the other groups.
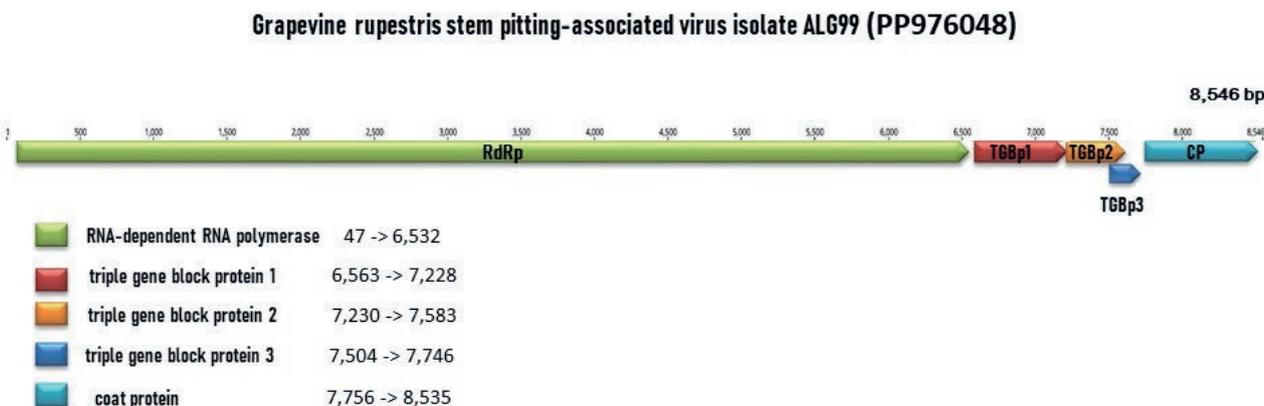
Figure 2. Genome organization of isolate ALG99 of grapevine rupestris stem pitting-associated virus. There are five open reading frames (ORFs) in the genome. ORF1 encodes RNA-dependent RNA polymerase protein (47 to 6,532 nt). ORF 2 represents triple gene block protein 1 (TGBp1) (6,563 to 7,228 nt). ORF3 encodes triple gene block protein 2 (TGBp2) (7,320 to 7,583 nt). ORF4 encodes triple gene block protein 3 (TGBp3) (7,504 to 7,746 nt). The last ORF represents the coat protein (7,756 to 8,535 nt).

Total RNAseq data generated by the Illumina platform included 47,034,642 short reads of 101 bases. In Geneious software, all RNA reads were paired and mapped against suspected virus and viroid genomes. The assembled reads were 8,484 against the sequence of GRSPaV and produced a consensus sequence of 8,546 bp. The coverage was 96.5% and the GC content was 43.2%. The sequence covering the whole coding regions was deposited in GenBank as accession number PP976048. The genome of GRSPaV isolate ALG99 had five open reading frames. ORF1 codes a RdRP with 6,486 nt and 2,161 residues. ORF2 represents triple gene block protein 1 (TGBp1), with 666 nt and 222 residues. ORF3 encodes triple gene block protein 2 (TGBp2), with 354 nt and 118 residues. ORF4 encodes triple gene block protein 3 (TGBp3), with 243 nt and 81 residues. The last ORF represents the coat protein gene, with 780 nt and 260 residues. The nucleotide alignment with the reference virus genome GRSPaV isolate 12G4102D (MZ484760) was 97.1%, while the amino acid alignments for each ORF were 98.4% for ORF1, 98.2% for ORF2, 99.1% for ORF3, 98.8% for ORF4 and 99.2% for the coat protein (Figure 2).

DISCUSSION

GRSPaV *is* the predominant grapevine virus reported in Algeria, with an infection rate of 57.92% (Bachir *et al.*, 2019). The prevalence of this virus in Algerian vineyards is not surprising, as it is a prevalent virus in many grapevine-producing countries (Martelli, 1993; Digiaro *et al.*, 1999; Meng and Gonsalves, 2007; Fiore *et al.*, 2016; Selmi *et al.*, 2017; Morelli *et al.*, 2011). The high

incidence in the vineyards can mainly be attributed to dissemination through grapevine propagation material. Natural transmission of GRSPaV has not been described, although the virus has been reported with high incidence from most regions where grapevines are cultivated, and in wild grapevines in the Mediterranean basin (Pacifico *et al.*, 2016; Selmi *et al.*, 2020).

Examination of nucleotide relationships between the GRSPaV isolates for CP genes showed that similarities were from 76 to 99%. The Algerian strain DZ-GRSPaV-N18 exhibited the greatest similarity (99%) with the CG1 strain. The analysis showed that some strains are strongly related. For example, strains DZ-GRSPaV-N09, DZ-GRSPaV-N10, DZ-GRSPaV-N14, and DZ-GRSPaV-N15 had high nucleotide similarity but were different from strains DZ-GRSPaV-N11, DZ-GRSPaV-N13, and DZ-GRSPaV-N17, which had 92 to 97% similarity. The two strains DZ-GRSPaV-N16 and DZ-GRSPaV-N18 had low similarity with each other and with other Algerian strains. These results are consistent with those reported elsewhere. Selmi *et al.* (2020) showed high CP gene variability of Tunisian strains, with nucleotide similarity ranging from 71 to 100%. Hu *et al.* (2015) reported high variability of Chinese strains, with nucleotide similarity from 82 to 98%. Alabi *et al.* (2010) reported significant genetic variability in strains in the United States of America, for CP and RdRP genes of GRSPaV, with nucleotide similarities from 79 to 100%.

A phylogenetic study of the CP gene was carried out for the strains sequenced and for strains downloaded from GenBank. The phylogenetic tree constructed confirmed the results obtained during the nucleotide comparisons of the Algerian strains, and reveals the presence of nine distinct groups. The Algerian GRSPaV sequences

obtained from wine and table grape varieties clustered into four groups: I, II, III, and IV, with the majority (eight) of the sequences clustered in groups III and IV. The Selmi *et al.* (2020) phylogenetic analysis showed that the Tunisian GRSPaV sequences clustered into four main groups: I, II, III, and IV, with group III containing mainly strains from commercial grapevines. However, Selmi *et al.* (2020) showed the presence of two new groups consisting of Tunisian strains from spontaneous and autochthonous cultivated grapevines. This suggests that confined natural habitats could be sources of virus diversity.

Several studies have examined the distribution of GRSPaV variants. Meng *et al.*, (2006) reported that phylogenetic analyses based on the CP gene for strains from table and wine grapes in the United States of America, Canada, and Italy were in Groups I, II, III, and IV. They reported that 68% of GRSPaV were Group I and II variants, and 24% were Group III variants, and only 8% were Group IV variants. Hooker (2017) also reported that more than 50% of the variants in the United States of America clustered in Group IV, and 23% were in Group I.

These virus strain variations may be due to the broad commercialization of *Vitis* plant material infected with these variants. Further studies on the infection rates of autochthones and wild grapevine varieties are required to provide understanding of the distribution and evolution of GRSPaV in different regions of Algeria.

FUNDING

LITERATURE CITED

Alabi O.J., Martin R.R., Naidu R.A., 2010. Sequence diversity, population genetics and potential recombination events in grapevine rupestris stem pitting-associated virus in Pacific North-West vineyards. *Journal of General Virology* 91: 265–276. https://doi.org/10.1099/vir.0.014423-0

Bachir A., Selmi, I., Lehad A., Louanchi M., Mahfoudhi N., 2019. The occurrence of grapevine rugose wood disease in Algeria. *Acta Phytopathologica et Entomologica Hungarica* 54 (2): 221–227. https://doi.org/10.1556/038.54.2019.023

Digiaro M., Martelli G.P., Savino V., Symons R.H., 1999. Phloem-limited viruses of the grapevine in the Mediterranean and Near East. *Phytopathologia Mediterranea* 51 : 85–90.

Fiore N., Zamorano, A., Sánchez-Diana N., González X., Pallás V., Sanchez-Navarro J., 2016. First detection of Grapevine rupestris stem pitting-associated virus and Grapevine rupestris vein feathering virus, and new phylogenetic groups for Grapevine fleck virus and Hop stunt viroid isolates, revealed from grapevine field surveys in Spain. *Phytopathologia Mediterranea* 55(2): 225–238. https://doi.org/10.14601/Phytopathol_Mediterr-15875

Foissac X., Svanella-Dumas L., Gentit P., Dulucq M.J., C. T., 2001. Polyvalent detection of Tricho-, Capilloand *Foveavirus*es by nested RT-PCR using degenerated and inosine-containing primers. *Acta Horticulturae* 550: 37–43.

Glasa M., Predajňa L., Šoltys K., Sihelská N., Nagyová A., … Sabanadzovic S., 2017. Analysis of Grapevine rupestris stem pitting-associated virus in Slovakia reveals differences in intra-host population diversity and naturally occurring recombination events. The *Plant Pathology Journal* 33(1): 34–42. https://doi.org/10.5423/PPJ.OA.07.2016.0158

Goszczynski D.E., Jooste A.E.C., 2003. Identification of divergent variants of Grapevine virus A. *European Journal of Plant Pathology* 109: 397–403.

Haviv S., Galiakparov N., Goszczynski D.E., Batuman O., Czosnek H., Mawassi M., 2006. Engineering the genome of Grapevine virus A into a vector for expression of proteins in herbaceous plants. *Journal of Virological Methods* 132 (1–2): 227–231. https://doi.org/10.1016/j.jviromet.2005.10.020

Hooker J. 2017. Analysis of the genetic diversity of Grapevine rupestris stem pitting-associated virus in Ontarian vineyards and construction of a full-length infectious clone. M.Sc. Thesis. University of Guelph.

Hu G.J., Dong Y.F., Zhu H.J., Zhang Z.P., Fan X.D., … Zhou J., 2015. Molecular characterizations of two grapevine rupestris stem pitting-associated virus isolates from China. *Archives of Virology* 160(10): 2641–2645.

Kearse M., Moir R., Wilson A., Stones-Havas S., Cheung M., … Thierer T., 2012. Geneious Basic: an integrated and extendable desktop software platform for the organization and analysis of sequence data. *Bioinformatics* 28(12): 1647–1649.

Kumar S., Stecher G., Li, M., Knyaz C., Tamura K., 2018. MEGA X: Molecular evolutionary genetics analysis across computing platforms. *Molecular Biology and Evolution* 35(6): 1547–1549.

Lima M., Alkowni R., Uyemoto J.K., Rowhani A., 2009. Genomic study and detection of a new variant of grapevine rupestris stem pitting associated virus in declining California Pinot Noir grapevines. *Journal of*

Plant Pathology 91(1): 155–162. http://www.jstor.org/stable/41998586

Lima M.F., Alkowni R., Uyemoto J.K., Golino D., Osman F., Rowhani A., 2006. Molecular analysis of a California strain of Rupestris stem pitting-associated virus isolated from declining Syrah grapevines. *Archives of Virology* 151(9): 1889–1894. https://doi.org/10.1007/s00705-006-0742-y

Martelli G.P. Jelkmann W., 1998. *Foveavirus*, a new plant virus genus. *Archives of Virology* 143: 1245–1249. https://doi.org/10.1007/s007050050372

Martelli G.P., 1993. Rugose wood complex. In: Martelli, G.P. (Ed.) *Grafttransmissible Diseases of Grapevines, Handbook for Detection and Diagnosis*. Rome, Italy: Food and Agriculture Organization of the United Nations, pp. 45–54.

Martelli G.P., 2014. Rugose wood complex. *Journal of Plant Pathology* 96: S73–S88.

Martelli G.P., Minafra A., Saldarelli P., 1997. Vitivirus, a new genus of plant viruses. *Archives of Virology* 142(9): 1929–1932.

Meng B. and Rowhani A., 2017. Grapevine rupestris stem pitting-associated virus. In: Meng, B., Martelli, G.P., Golino, D.A. and Fuchs, M. (Eds.) *Grapevine Viruses: Molecular Biology, Diagnostics and Management*. Cham, Switzerland: Springer International Publishing AG, pp. 257–287.

Meng B., Gonsalves D., 2003. Rupestris stem pitting-associated virus of grapevines: genome structure, genetic diversity, detection, and phylogenetic relationship to other plant viruses. *Current Topics in Virology* 3: 125–135.

Meng B., Gonsalves D., 2007. Grapevine rupestris stem pitting-associated virus: A decade of research and future perspectives. *Plant Viruses* 1: 52-62.

Meng B., Li C., 2010. The capsid protein of Grapevine rupestris stem pitting-associated virus contains a typical nuclear localization signal and targets to the nucleus. *Virus Research* 153(2): 212–217. https://doi.org/10.1016/j.virusres.2010.08.003

Meng B., Li C., Wang W., Goszczynski D., Gonsalves D., 2005. Complete genome sequences of two new variants of Grapevine rupestris stem pitting-associated virus and comparative analyses. *Journal of General Virology* 86(5): 1555–1560. https://doi.org/10.1099/vir.0.80815-0

Meng B., Pang S.Z., Forsline P.L., McFerson J.R., Gonsalves D., 1998. Nucleotide sequence and genome structure of grapevine rupestris stem pitting-associated virus-1 reveal similarities to apple stem pitting virus. *The Journal of General Virology* 79(8): 2059–2069. https://doi.org/10.1099/0022-1317-79-8-2059

Meng B., Rebelo A. R., Fisher H., 2006. Genetic diversity analyses of grapevine Rupestris stem pitting-associated virus reveal distinct population structures in scion versus rootstock varieties. *Journal of General Virology* 87(6), 1725–1733.

Meng, B., Venkataraman, S., Li, C., Wang, W., Dayan-Glick, C., Mawassi, M., 2013. Construction and biological activities of the first infectious cDNA clones of the genus *Foveavirus*. *Virology* 435(2): 453–462. https://doi.org/10.1016/j.virol.2012.09.045

Minafra A., Casati P., Elicio V., Rowhani A., Saldarelli P., … Martelli G. P., 2000. Serological detection of Grapevine rupestris stem pitting-associated virus (GRSPaV) by a polyclonal antiserum to recombinant virus coat protein. *Vitis* 39(3): 115–118.

Morelli M., Minafra A., Boscia, D., Martelli G. P., 2011. Complete nucleotide sequence of a new variant of grapevine rupestris stem pitting-associated virus from Southern Italy. *Archives of Virology* 156(3): 543–546. https://doi.org/10.1007/s00705-011-0936-9

Nolasco G., Mansinho A., Teixeira Santos M., Soares C., Sequeira Z., … Sequeira O. A., 2000. Large scale evaluation of primers for diagnosis of rupestris stem pitting associated virus-1. *European Journal of Plant Pathology* 106(4): 311–318. https://doi.org/10.1023/A:1008748924494

Pacifico D., Stigliano E., Sposito L., Spinelli P., Garfi G., ... Carimi F., 2016. Survey of viral infections in spontaneous grapevines from natural environments in Sicily. *European Journal of Plant Pathology* 145(1): 189–197. https://doi.org/10.1007/s10658-015-0785-6

Petrovic N., Meng B., Ravnikar M., Mavric I., G., 2003. First detection of rupestris stem pitting associated virus particles by antibody to a recombinant coat protein. *Plant Disease* 87(5): 510–514. https://doi.org/10.1094/PDIS.2003.87.5.510

Rebelo A. R., Niewiadomski S., Prosser S. W., Krell P., Meng B., 2008. Subcellular localization of the triple gene block proteins encoded by a *Foveavirus* infecting grapevines. *Virus Research* 138: 57–69. https://doi.org/10.1016/j.virusres.2008.08.011

Rowhani A., Zhang Y.P., Chin H., Minafra A., Golino D.A., Uyemoto J.K., 2000. Grapevine rupestris stem pitting associated virus: population diversity, titer in the host and possible transmission vector. In: *Extended Abstracts of the 13th Meeting of the International Council for the Study of Viruses and Virus-like Diseases of the Grapevine (ICVG), 2000*. Adelaide, Australia: University of Adelaide, p. 37.

Selmi I, Pacifico D., Carimi F., Mahfoudhi N., 2017. Prevalence of viruses associated with grapevine rugose wood disease in Tunisia. *Tunisian Journal of Plant Protection* 12(2): 149–158.

Selmi I., Pacifico D., Lehad A., Stigliano E., Crucitti D., ...
    Mahfoudhi N., 2020. Genetic diversity of Grapevine
    rupestris stem pitting-associated virus isolates from
    Tunisian grapevine germplasm. *Plant Pathology* 69:
    1051–1059. https://doi.org/10.1111/ppa.13183

Zhang Y. P., Uyemoto J. K., Golino D. A., Rowhani A.,
    1998. Nucleotide sequence and RT-PCR detection
    of a virus associated with grapevine rupestris stem-
    pitting disease. *Phytopathology* 88(11): 1231–1237.
    https://doi.org/10.1094/PHYTO.1998.88.11.1231

Review

Bibliometric and sequence analyses of the pathogenic *Helicotylenchus* nematodes

Alessio VOVLAS[1,A], Ebunoluwa Ijeoma AJOBIEWE[1,2,A], Elena FANELLI[1], Alberto TROCCOLI[1], Francesca DE LUCA[1,*]

[1] *Institute for Sustainable Plant Protection-CNR, Via Amendola 122/D, 70126 Bari, Italy*
[2] *Department of European and Mediterranean Cultures, University of Basilicata, Via Lanera, 10, 75100 Matera, Italy*
*Corresponding author. E-mail: francesca.deluca@ipsp.cnr.it
[a] Authors contributing equally

Summary. Publications between 2000 and 2024 on plant pathogenic species of *Helicotylenchus* nematodes were reviewed using bibliometric analyses with VOSviewer software. Sequences in GenBank for the same period were used to reconstruct phylogenetic relationships and correctly assign all the *Helicotylenchus* sequences in the database. The Scopus database was selected for its professional standards, international visibility, broad coverage, and controlled-vocabulary thesaurus available for indexing and retrieving documents. GenBank collects nucleotide sequences and relevant bibliographic and biological annotations for sequence analyses. This study highlighted research trends and specific complexities of working with *Helicotylenchus*, and the suitability of molecular markers used for identification of the main pathogenic species and confirmation of occurrence of species complexes or cryptic species.

Keywords. Nematodes, phylogeny, VOSviewer.

INTRODUCTION

Members of *Helicotylenchus* Steiner, 1945 are emerging concerns because of their broad host ranges and high numbers in soils (da Silva *et al.*, 2023). These nematodes are cosmopolitan with more than 230 species distributed around plant roots, occurring in most soil samples of cultivated and uncultivated soils. They are known as spiral nematodes, through their coiled *habitus mortis* (Firoza and Maqbool, 1994; Decraemer and Geraert, 2006; Uzma *et al.*, 2015). *Helicotylenchus* spp. are migratory ectoparasites that complete their life cycles in the soil, feeding on cortical parenchyma tissues of colonized roots. Several species are semi-endoparasites, penetrating plant tissues with their anterior body regions (Wouts and Yeates, 1994) attacking outer cortical tissues of host plant roots, reducing ability of roots to adsorb water and nutrients (Subbotin *et al.*, 2011; Crozzoli, 2014; Xia *et al.*, 2022). Infestations of *Helicotylenchus* spp. do not directly reduce crop yields, so their true impacts on agricultural production remain unclear.

Increasing numbers of papers report the wide distribution of *Helicotylenchus*, its wide host range, and association with other plant-parasitic nematodes. A few *Helicotylenchus* spp., including *H. digonicus* Perry, 1959, *H. dihystera* (Cobb, 1893) Sher, 1961; *H. indicus* Siddiqi, 1963, *H. multicinctus* (Cobb, 1893) Golden, 1956, *H. pseudorobustus* (Steiner, 1914) Golden, 1956, and *H. oleae* Inserra, Vovlas and Golden, 1979, are considered pathogenic, as they are abundant in soil and cause damage to agricultural crops and turfgrass (Subbotin *et al.*, 2015; Rybarczyk-Mydlowska *et al.*, 2019; Mwamula *et al.*, 2020; Mwamula and Lee, 2021; Mwamula *et al.*, 2024). Recently, *H. multicinctus, H. dihystera, H. varicaudatus* and *H. erythrinae* have been reported as important pathogens of banana (Riascos-Ortiz *et al.*, 2020), and *H. cavenessi, H. microcephalus* and *H. microlobus* are pathogens of agricultural crops and turfgrass (Subbotin *et al.*, 2011; Mwamula and Lee, 2021; Mwamula *et al.*, 2024).

Helicotylenchus consists in many species with conservative morphology but phenotypic plasticity, leading to potential species misidentification. Subbotin *et al.* (2011) demonstrated that *H. pseudorobustus* is a species complex exhibiting high intraspecific variability at the genetic level.

The present review aimed to explore trends and research activity in the scientific literature on *Helicotylenchus* spp., for the five well-characterized pathogenic species during the period 2000 to 2024. To achieve this, a bibliometric and sequence analyses in the Scopus database by using VOSviewer software (van Eck and Waltman, 2010) and in GenBank database, respectively, were carried out. The Scopus Database was selected for the large and multidisciplinary content, its professional standards, international visibility, broad coverage, and controlled-vocabulary thesaurus available for indexing and retrieving documents (Zong *et al.*, 2012; Alryalat *et al.*, 2019; Baas *et al.*, 2020). The GenBank database collects nucleotide sequences and relevant bibliographic and biological annotations for sequence analyses.

MATERIALS AND METHODS

The literature search was carried out from the Scopus database (*https://www.scopus.com/*), using the keyword "*Helicotylenchus*" in paper titles, abstracts, and keyword lists, and selecting studies published from 2000 to September 2024 in indexed journals (Figure 1). No language restriction was made. The titles of all identified
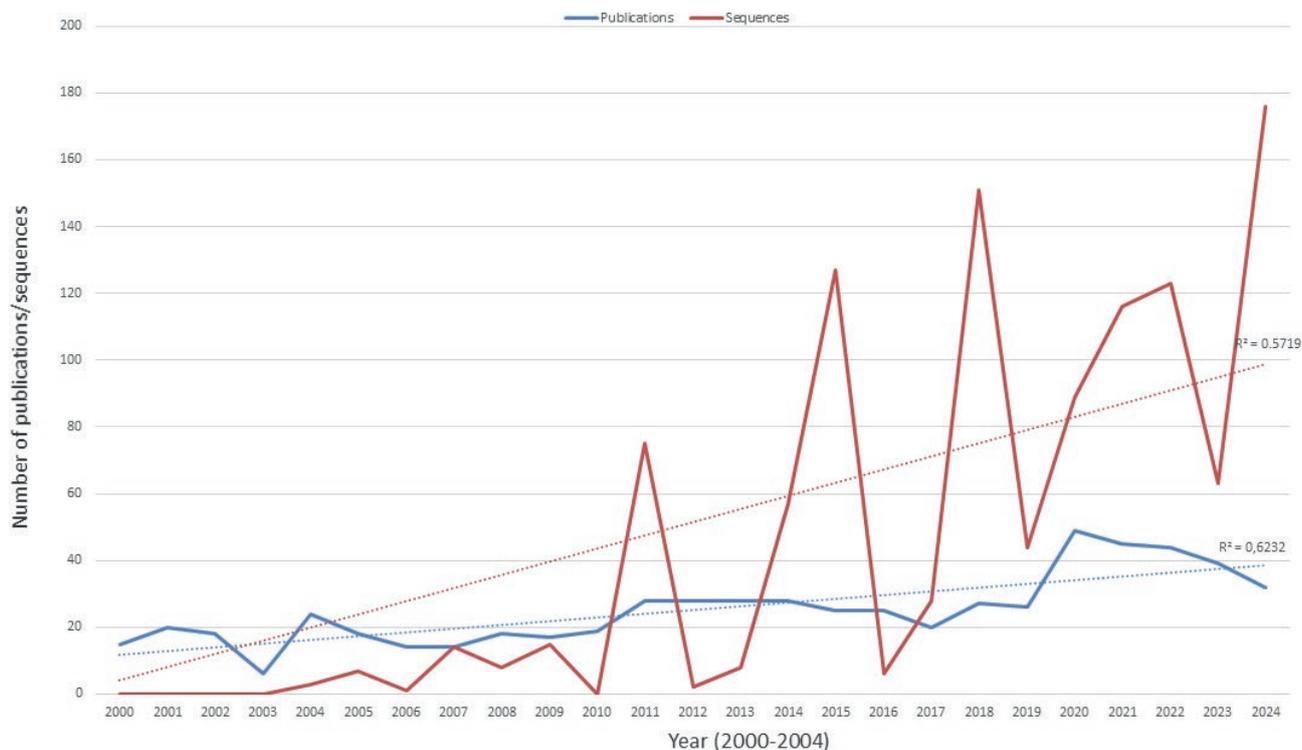
Figure 1. Publications and sequence trends relating to *Helicotylenchus* spp. between 2000 and 2024. The publications were retrieved from the SCOPUS database and sequences were from GenBank in the subject areas.

articles and their abstracts were also screened to ensure reliability of the search.

Bibliometric analysis

Bibliometric network analysis of *Helicotylenchus* literature was conducted using VOSviewer software (van Eck and Waltman, 2010), allowing creation of maps using bibliometric data. The output results consisted of maps showing several clusters, in different colours, and links based on keywords. Each cluster reflects groups of keywords that are strongly related. In the graphics, each node size is represented by a circle, the larger the circle at the node indicates greater the number of references on *Helicotylenchus* spp. The strongest relatedness between terms is also indicated by curved lines. Each network map can provide a temporal perspective on average publication per year, and a density visualization map was produced to indicate the most important areas of research. The time axis indicates research interest at the beginning of the study period (blue zone), while the yellow zone indicates the emerging direction in the research.

All selected papers were further analysed using the terms 'co-authorship countries network' and 'co-occurrence'. Co-authorship countries network used the terms "researchers" and "research institution" for each country, providing a map with several clusters, in different colours, linked to each other according to the number of papers that authors have jointly published. Co-occurrence of author keywords analysis, using the Boolean operators "*Helicotylenchus dihystera*" OR "*Helicotylenchus digonicus*" OR "*Helicotylenchus pseudorobustus*" OR "*Helicotylencus indicus*" OR "*Helicotylenchus multicinctus*" AND "plants", produced an overlay visualization map showing the number of papers in which the keywords were found, and distance between terms indicate relationships of the terms, while the lines connecting the nodes indicated how many times a specific *Helicotylenchus* sp. is present on a specific host plant. With

the requirement that a keyword occurs at least ten times, 4792 keywords met this threshold.

Sequence retrieval

Genbank at NCBI contains multiple types of nucleotide sequences from different sources and directly from authors, providing an interface for searching, visualization, and analysis of sequences.

Using "*Helicotylenchus*" as query in GenBank, 1113 sequences were found as submitted from 2000 to September 2024 (Figure 1). In addition to making use of search terms, a manual check was carried out on each resulting number of sequences per species and per molecular marker, to ensure accuracy. All sequences of *Helicotylenchus* were then re-analysed using the terms "ribosomal DNA", "mitochondrial COI gene", "mitochondrial COII gene" and "*hsp*90". This analysis also delivered 1113 sequences, 513 corresponding to D2-D3 expansion domains of the 28S rRNA gene, 291 to partial 18S rRNA gene, 211 to the ITS region, 86 to the mitochondrial COI gene, one to COII, and 11 sequences corresponding to the *hsp*90 gene.

The total number of *Helicotylenchus* sequences was then screened to obtain ribosomal and mitochondrial sequences belonging to the five major pathogenic species, *H. dihystera*, *H. pseudorobustus*, *H. digonicus*, *H. multicinctus* and *H. indicus* retrieved from 2000 to 2024 (Table 1).

Phylogenetic analysis

The retrieved sequences for D2-D3, ITS and COI were aligned by MAFFT version X and edited by using BioEdit software. For D2-D3 alignment, 99 sequences between lengths 600 and 700 bp were used, with *Hoplolaimus galeatus* (EU626787) used as the outgroup. For ITS alignment, 100 sequences between lengths 800

Table 1. *Helicotylenchus* sequences belonging to the five pathogenic *Helicotylenchus* species that have been released between 2000 and 2024.

Helicotylenchus species	Molecular markers						Total number of sequences
	ITS	18S	28S	COI	COII	hsp90	
H. dihystera	71	46	149	4	1	0	271
H. pseudorobustus	10	73	58	10	0	1	152
H. digonicus	9	11	25	3	0	1	49
H. multicinctus	9	5	25	0	0	0	39
H. indicus	2	7	2	0	0	0	11
Total	101	142	259	17	1	2	522

and 1000 bp long were used, with *Rotylenchus pumilus* (JX015436) used as the outgroup. COI, 47 sequences were used, with *Heterodera elachista* (MH144207) as the outgroup. Phylogenetic analyses of both sequence datasets were based on Bayesian inference (BI), using MrBayes 3.1.2 (Ronquist and Huelsenbeck, 2003). The best-fit model of DNA evolution was selected employing the Akaike Information Criterion (AIC), using JModel-Test V.2.1.10 (Darriba *et al.*, 2012) for all the datasets: a general time-reversible model with invariable sites and a gamma-shaped distribution (GTR + G + I) was used for COI, a general time-reversible model for ITS and a gamma-shaped distribution (GTR + G) distributed rates across sites for 28S. For this analysis, the best-fit models (including the base frequencies), the proportion of invariable sites, gamma distribution shape parameters, and the substitution rates derived from the AIC, were subsequently applied within Mr Bayes.

The Markov chain Monte Carlo search was carried out separately for each dataset, using four chains for 2×10^6 generations, sampled at intervals of 100 generations. Two runs were carried out for each analysis. Following the elimination of 25% of samples for the burn-in and evaluating convergence, the remaining samples were retained for in-depth analyses. The resulting topologies were used to generate a 50% majority-rule consensus tree, with posterior probabilities (PP) calculated for appropriate clades. The phylogenetic trees from all analyses were visualized, using iTOL (Letunic and Bork, 2021), and were edited with GIMP version 2.10.32 (available at *http://www.gimp.org*).

RESULTS

Bibliometric analysis

The literature search for *Helicotylenchus* spp. in Scopus identified 627 documents published between 2000 to September 2024 (Figure 1). These were of three types: 607 were scientific articles (96.8%), 12 reviews (1.9%), and eight edited book chapters (1.3%). This showed few papers at the beginning of the temporal period and increasing and then constant interest in *Helicotylenchus* during the period. The low number of publications is probably because most *Helicotylenchus* spp. do not directly lead to significant reductions in crop yields, and only a few species are considered as crop pathogens (Subbotin *et al.*, 2011; Brücher *et al.*, 2019). A total of 160 scientific journals published papers (at least 1 per year) on *Helicotylenchus*, but only five journals published large numbers of papers. These were *Nematropica* (55 papers), *Nematology* (47), *Journal of Nematology* (38), *Archives*

of Phytopathology and Plant Protection (22) and *Applied Soil Ecology* (21 papers). The main research topics of studies on *Helicotylenchus* spp. were soil nematode communities, molecular and morphological characterization, and control strategies.

Co-authorship countries network

Figure 2 shows the map of co-authorship analysis among countries. Reports on occurrence of *Helicotylenchus* spp. were from a total of 89 countries, but using a threshold of five publications per country, 42 countries were selected for the co-authorship network map. The most productive country was the United States of America (USA), with 114 papers, followed by India (64), Brazil (61), and China (53 papers). Figure 2 shows seven main clusters in different colours, highlighting high level of co-operation/collaboration. The USA had strong relationships with many of the countries with the greatest link strength. Belgium also had strong interactions with other countries. Of the 480 papers on *Helicotylenchus*, 221 reported the occurrence of *Helicotylenchus* spp. in association with nematode communities, and the remaining papers reported morphological, molecular and phylogenetic analyses, and nematode control strategies.

Co-occurrence author keywords

The overlay visualization map (Figure 3) provides the average publication year for keywords, summarizing the dynamics of old and emerging words. Each term is represented by a circle, and the size of each circle depends on the number of publications in which the term was found, and the distance between two terms indicates the relationships between them. The close relationships between terms are also highlight by curved lines, and the same colour identifies terms strongly related with each other. Figure 3 shows increasing use of the keywords *H. dihystera* and *H. multicinctus*, followed by banana, musa, maize, sugarcane, soybean, and cotton, during the period assessed. The density visualization map showed that grain and cereal crops (*Avena* spp., *Secale* spp., *Zea* spp., *Triticum* spp.) were the crops assessed early in the assessment period, and more recently assessed crops were peanut, coffee, cocoa, or tomato (brighter yellow colour). The density map also shows that *Helicotylenchus* spp. have been found on numerous woody plants, and that *H. multicinctus* and *H. digonicus* have been recently recorded as pests on date-palm (*Phoenix dactylifera*). Several papers have reported *H. digonicus* on pines, oaks, and in olive groves, and this
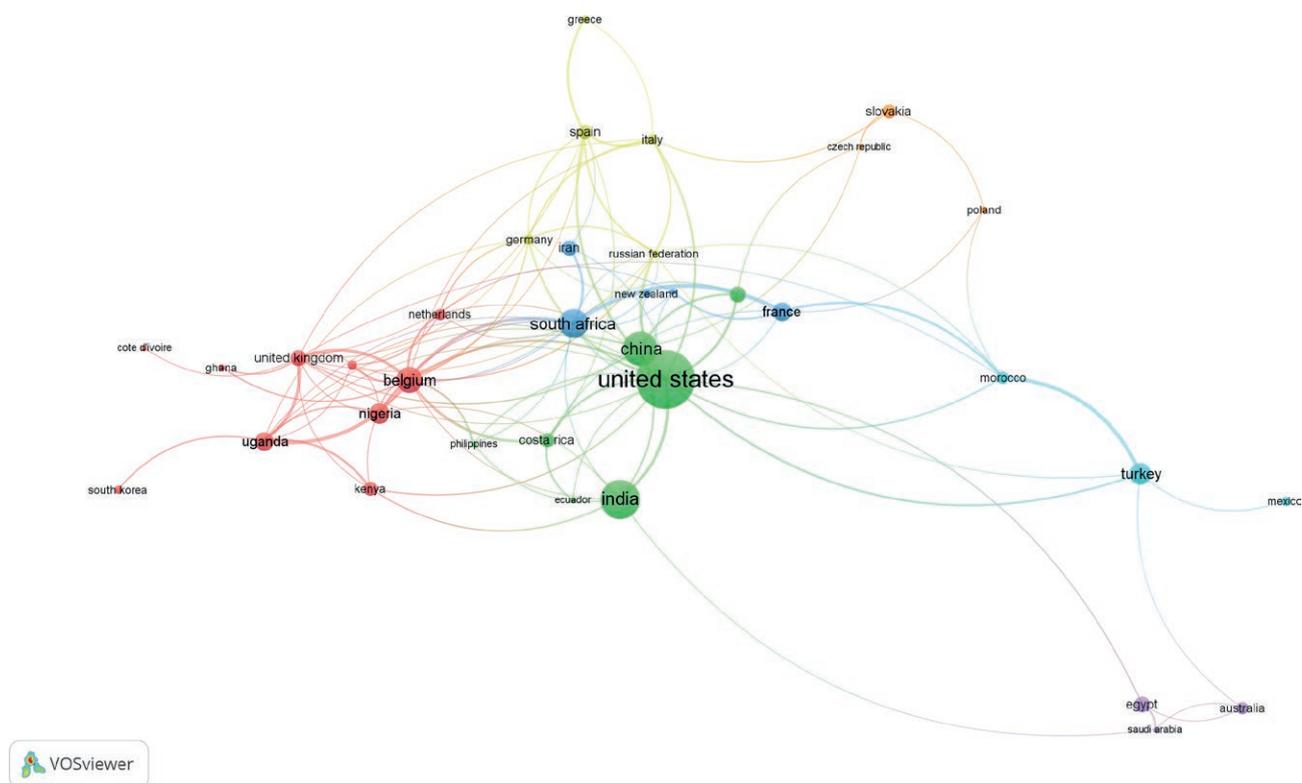
Figure 2. Co-authorship network map (developed with VOSviewer) showing countries where research on *Helicotylenchus* spp. has been carried out between 2000 and 2024. Each node number indicates the number of publications for each country, and the node size indicates occurrence of keywords.

nematode has been more recently detected on prunus, peach, and walnut. Research interest in *H. pseudorobustus* has increased, occurring in *Malus* sp. and *Prunus* sp. orchards.

Sequence analysis

A total of 1113 *Helicotylenchus* sequences were recorded in the GenBank database between 2000 and September 2024, corresponding to 513 sequences for D2-D3 expansion domains of the 28S rRNA gene, 291 for the 18S rRNA gene, 211 for ITS, 86 for COI, one for COII, and 11 for *hsp*90. Forty-seven percent (522) of the total sequences belonged to the five major known pathogenic *Helicotylenchus* species (Table 1), 259 corresponded with D2-D3 expansion domains of the 28S rRNA gene, 142 to the 18S rRNA gene, 101 to the ITS region, 85 to mitochondrial COI, one to COII, and two to the *hsp*90 gene. Table 1 emphasizes the increase of sequence numbers during the 2000 to September 2024 period.

Phylogenetic analyses were reconstructed, based on D2-D3 expansion domains, ITS, and partial mitochon-drial COI sequences of the major pathogenic *Helicotylenchus* spp. The topologies of the D2-D3 and ITS trees agree with those in research literature (Figures 4 and 5), confirming that several sequences in Genbank were misidentified and sometimes displayed sequencing mistakes, as has been elsewhere reported (Mwamula *et al.*, 2024).

Helicotylenchus pseudorobustus (type A), *H. microlobus* (type B), and *H. digonicus* (type A) were closely related to each other, and *H. dihystera* showed sister relationships with these three species types. *Helicotylenchus digonicus* (type B) grouped with *H. crassatus*. Presence along the tree of different sequence groups erroneously indicates presence and occurrence of species complexes.

DISCUSSION

The main objective of this study was to evaluate reported research on *Helicotylenchus*, with particular focus on the major pathogenic species, and spatio-temporal trends between 2000 and September 2024. The increasing trend in annual numbers of publications on *Helicotylenchus* spp. reflects increasing interest by the
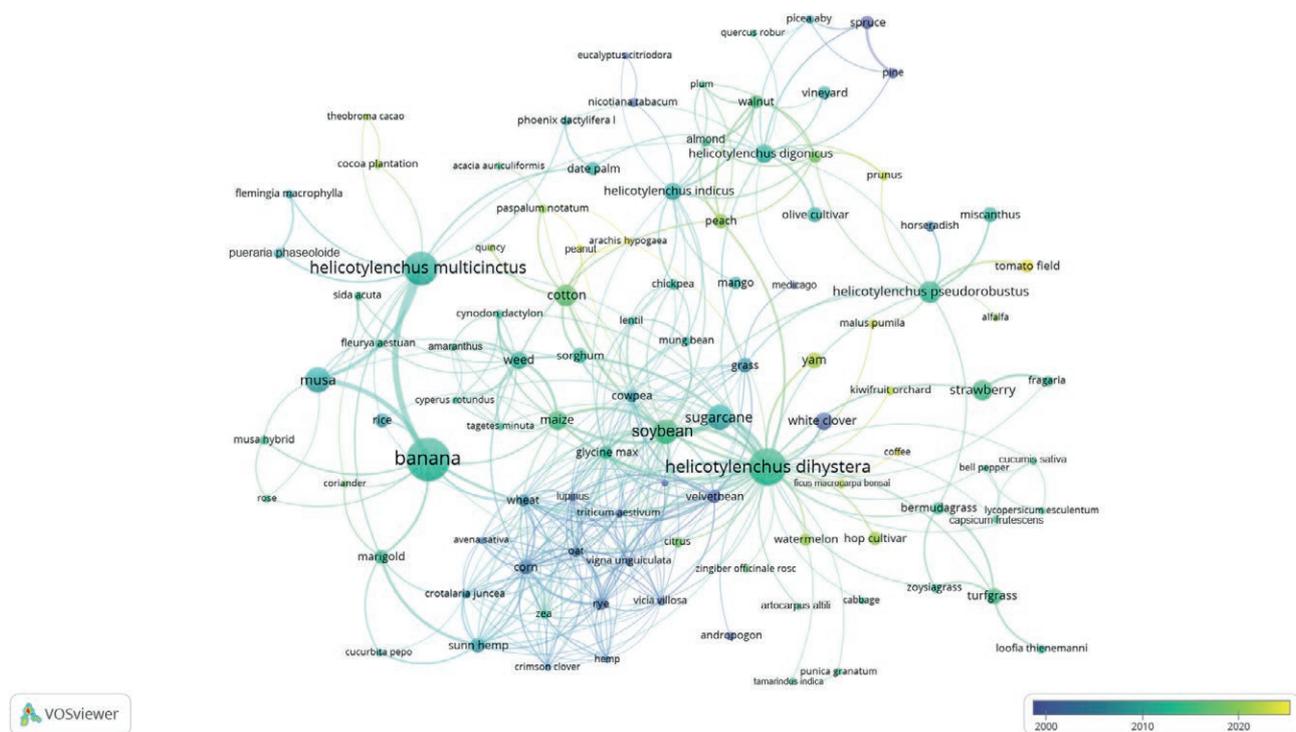
Figure 3. Cluster visualization of co-occurrence keywords for host plants and five plant pathogenic *Helicotylenchus* species. Each node number indicates the number of documents for the keywords, and the size of each node indicates the occurrence of the keywords. Different colours represent groups of terms that are strongly related to each other, and the curved lines indicate strong relationships between terms.

international nematologist community (Figure 1). The analysis of authorships and collaboration showed that researchers from the USA were the greatest contributors, followed by those from China, India, and Brazil (Figure 2), and that USA researchers have most collaborations with other countries. The keyword co-occurrence network map showed that the plant pathogenic *Helicotylenchus* species, particularly *H. dihystera* and *H. multicinctus* and their host plants are increasingly important research topics (Figure 3). The density visualization map showed that pathogenic *Helicotylenchus* species mainly attack banana, followed by musa, maize, sugarcane, soybean, and cotton, and this map also showed that grain and cereal crops (*Avena* spp., *Secale* spp., *Zea* spp, *Triticum* spp.) were the earliest studied in the review period, with other crops more recently attracting researcher attention. Pathogenic *Helicotylenchus* species have also been found on several woody plants in recent years. These observations indicate that climate changes may have increasingly act affected *Helicotylenchus* abundance, and new crops can be attacked and new pathogen species may evolve.

Helicotylenchus comprises more than 230 species, and most of these have conserved gross morphology, so molecular identification followed by sequencing

of molecular markers has been useful to discriminate among species. This has been confirmed by the increasing number of sequences in GenBank over the 2000 to 2014 period (Figure 1). Most sequences in GenBank belong to the most important plant pathogenic species of *Helicotylenchus* (Table 1). Several publications have reported incorrect sequences present in the public database, due to sequencing errors, misidentifications, and identification errors based on nematode morphology. In the present review, all D2-D3 and ITS sequences of the pathogenic *Helicotylenchus*, released in the database until September 2024, were used for phylogenetic analyses to correctly identify *Helicotylenchus* species by clusters. The phylogenetic trees illustrated in Figures 4 and 5 have identical topologies, showing that *H. pseudorobustus* sequences form three subgroupings (92% support), one containing the sequences of *H. pseudorobustus*, the second containing sequences identified as *H. digonicus* type B, and the third with sequences belonging to *H. microlobus*, as has been reported by Subbotin *et al.* (2015) and Mwamula *et al.* (2020). This confirms that *H. pseudorobustus* and *H. microlobus* are valid species, closely related but genetically distinct from each other. *Helicotylenchus digonicus* populations clustered in different groupings, types A and B, suggesting possible existence of spe-

Tree scale: 0.01

OK256085 Helicotylenchus pseudorobustus China
HM014279 Helicotylenchus pseudorobustus New Zealand
KM506817 Helicotylenchus pseudorobustus Switzerland
OK256091 Helicotylenchus pseudorobustus China
KM506819 Helicotylenchus pseudorobustus USA California
KM506820 Helicotylenchus pseudorobustus USA California
OK256093 Helicotylenchus pseudorobustus China
KM506821 Helicotylenchus pseudorobustus USA California
OK256096 Helicotylenchus pseudorobustus China
HM014280 Helicotylenchus pseudorobustus New Zealand
OK256090 Helicotylenchus pseudorobustus China
HM014278 Helicotylenchus pseudorobustus New Zealand
OK256089 Helicotylenchus pseudorobustus China
OK256094 Helicotylenchus pseudorobustus China
OK256095 Helicotylenchus pseudorobustus China
KM506807 Helicotylenchus pseudorobustus Russia
KM506808 Helicotylenchus pseudorobustus USA California
KM506809 Helicotylenchus pseudorobustus New Zealand
KM506810 Helicotylenchus pseudorobustus USA California
KM506811 Helicotylenchus pseudorobustus Switzerland
KM506812 Helicotylenchus pseudorobustus USA California
KM506813 Helicotylenchus pseudorobustus USA Washington
KM506814 Helicotylenchus pseudorobustus Germany
KM506815 Helicotylenchus pseudorobustus Switzerland
KM506816 Helicotylenchus pseudorobustus USA California
KM506818 Helicotylenchus pseudorobustus USA California
KM506822 Helicotylenchus pseudorobustus New Zealand
DQ328751 Helicotylenchus pseudorobustus Germany
MG653532 Helicotylenchus pseudorobustus Poland
MG653533 Helicotylenchus pseudorobustus Poland
MG653534 Helicotylenchus pseudorobustus Poland
MK481267 Helicotylenchus pseudorobustus Iran
KM506827 Helicotylenchus digonicus USA Kansas
KM506828 Helicotylenchus digonicus USA Kansas
OK256086 Helicotylenchus digonicus China
HM014274 Helicotylenchus digonicus USA Nebraska
OK256092 Helicotylenchus digonicus China
HM014267 Helicotylenchus digonicus USA Kansas
OK256088 Helicotylenchus digonicus China
HM014266 Helicotylenchus digonicus USA Kansas
HM014272 Helicotylenchus digonicus USA Nebraska
HM014271 Helicotylenchus digonicus USA Nebraska
KM506829 Helicotylenchus digonicus USA Kansas
OK256087 Helicotylenchus digonicus China
HM014270 Helicotylenchus digonicus
KM506830 Helicotylenchus digonicus USA Kansas
KM506831 Helicotylenchus digonicus USA Kansas
MN764326 Helicotylenchus microlobus
KM506799 Helicotylenchus microlobus
MG770480 Helicotylenchus microlobus
MG925220 Helicotylenchus microlobus USA
OK256081 Helicotylenchus microlobus China
HM014264 Helicotylenchus microlobus USA California
MK358143 Helicotylenchus microlobus USA
OK256083 Helicotylenchus microlobus China
MF996708 Helicotylenchus microlobus Iran
MN764324 Helicotylenchus microlobus
MN764323 Helicotylenchus microlobus
KM506793 Helicotylenchus microlobus
MG770482 Helicotylenchus microlobus
KM506800 Helicotylenchus microlobus
OK256082 Helicotylenchus microlobus China
MF996709 Helicotylenchus microlobus Iran
KU722387 Helicotylenchus microlobus Iran
MN764328 Helicotylenchus microlobus
MN764327 Helicotylenchus microlobus
MG770481 Helicotylenchus microlobus
FJ485649 Helicotylenchus microlobus USA Illinois
DQ328747 Helicotylenchus microlobus China
DQ328748 Helicotylenchus microlobus USA California
DQ328749 Helicotylenchus microlobus China
DQ328750 Helicotylenchus microlobus Italy
OK256084 Helicotylenchus microlobus China
HM014263 Helicotylenchus microlobus USA California
KM506805 Helicotylenchus microlobus
OL415766 Helicotylenchus dihystera Thailand
MT193469 Helicotylenchus dihystera China
MH156808 Helicotylenchus dihystera China
ON117414 Helicotylenchus dihystera China
MW674632 Helicotylenchus dihystera Kenya
MT321730 Helicotylenchus dihystera Colombia
MH087062 Helicotylenchus multicinctus India
MH087063 Helicotylenchus multicinctus India
MH084946 Helicotylenchus multicinctus India
MH087064 Helicotylenchus multicinctus India
MH087066 Helicotylenchus multicinctus India
MT321734 Helicotylenchus multicinctus Colombia
MT321733 Helicotylenchus multicinctus Colombia
MT321732 Helicotylenchus multicinctus Colombia
MF401446 Helicotylenchus multicinctus Greece
MN056344 Helicotylenchus multicinctus Nigeria
MT321731 Helicotylenchus multicinctus Colombia
MT239110 Helicotylenchus multicinctus Brazil
KF443214 Helicotylenchus multicinctus China
ON117537 Helicotylenchus indicus China
ON117538 Helicotylenchus indicus China
MN650241 Helicotylenchus sp. MN Nigeria
MN650242 Helicotylenchus sp. Nigeria
HM014241 Helicotylenchus sp. V South Africa
HM014240 Helicotylenchus sp. V South Africa
MN922339 Helicotylenchus sp. III USA Florida
OP297977 Helicotylenchus sp. III China
OK275497 Helicotylenchus sp. III Thailand
MF187651 Helicotylenchus oleae
MF187657 Helicotylenchus oleae
OR957396 Helicotylenchus crassatus
OR957399 Helicotylenchus crassatus
OR957397 Helicotylenchus crassatus
ON123552 Helicotylenchus digonicus
MT872099 Helicotylenchus digonicus
MT860283 Helicotylenchus digonicus
MH444651 Helicotylenchus digonicus
DQ328758 Helicotylenchus digonicus
EU626787 Hoplolaimus galeatus

Figure 4. Phylogenetic relationships among the five pathogenic *Helicotylenchus* species, as indicated using a Bayesian 50% majority rule consensus tree inferred from D2-D3 expansion domains of the 28S rRNA gene sequence alignment under a transversional with gamma-shaped distribution model (GTR + G). Posterior probabilities of greater than 0.50 are given for appropriate clades, and the scale bar indicates expected changes per site.

Figure 5. Phylogenetic relationships among the five pathogenic *Helicotylenchus* species, as indicated using a Bayesian 50% majority rule consensus tree inferred from ITS sequence alignment under a transversional with gamma-shaped distribution model (GTR+ G). Posterior probabilities of greater than 0.50 are given for appropriate clades, and the scale bar indicates expected changes per site.

Figure 6. Phylogenetic relationships among the five pathogenic *Helicotylenchus* species using Bayesian a 50% majority rule consensus tree as inferred from COI sequence alignment, under a transversional with correction for invariable sites and a gamma-shaped distribution model (GTR + I + G). Posterior probabilities of more than 0.50 are given for appropriate clades. The scale bar indicates expected changes per site.

cies complexes or cryptic species, and further study is required to elucidate this suggestion. The mMitochondrial COI phylogenetic tree (Figure 6) confirms that each species group are separated from the others. It is interesting to note that only *H. pseudorobustus* and *H. oleae* COI sequences contain stop codons, indicating genetic code

alterations or the occurrence of pseudogenes (Palomares-Rius *et al.*, 2018; Rybarczyk-Mydlowska *et al.*, 2019).

In conclusion, our observations reveal an increase of host plants infected by *Helicotylenchus* spp. and this could be explained by the species complexes of these nematodes. Identification of *Helicotylenchus* spp. therefore required polyphasic approaches, combining morphology, molecular and phylogenetic analyses, to correctly discriminate *Helicotylenchus* species, and through that knowledge, development of effective nematode management strategies. Bibliometric analysis is a method that can be useful for understanding past research, and development of new knowledge leading to worthwhile research advances.

ACKNOWLEDGEMENTS

AUTHOR CONTRIBUTIONS

AV and EIA equally contributed to bibliometric and sequence analyses; AV used VOSviewer and phylogenetic programs; EIA contributed to NCBI/GenBank sequence retrieval; AV and EIA contributed to writing, review and editing; EF and AT contributed to review and editing; FDL contributed to the study conception and design, writing original draft, review and editing. FDL contributed to fund acquisition. The first draft of the manuscript was commented by all authors and then they approved the final manuscript.

DATA AVAILABILITY

All sequences in this paper are freely available through GenBank database.

LITERATURE CITED

Alryalat S.A.S., Malkawi L.W., Momani S.M., 2019. Comparing bibliometric analysis using PubMed, Scopus, and Web of Science databases. *Journal of Visualized Experiments* 152, e58494. https://doi.org/10.3791/58494

Baas J., Schotten M., Plume A., Côté G., Karimi R., 2020. Scopus as a curated, high-quality bibliometric data source for academic research in quantitative science studies. *Quantitative Science Studies* 1(1): 377–386. https://doi.org/10.1162/qss_a_00019

Brücher E., Vuletic E.E., Guerra F.A., De Rossi R.L., Plazas M.C., … Doucet M.E., 2019. Characterization of a population of *Helicotylenchus dihystera* (Cobb, 1893) Sher, 1961, parasitizing maize roots, in southern Córdoba, Argentina. *Nematropica* 49(1): 49–58.

Crozzoli R, 2014. Nematodi Ectoparasiti. In: *Nematologia Agraria Generale e Applicata* (L. Ambrogioni, F.P. d'Errico, N. Greco, A. Marinari Palmisano, P.F. Roversi, ed.), Società Italiana di Nematologia, 279–300.

Darriba, D, Taboada G.L., Doallo R., Posada D., 2012. jModelTest 2: more models, new heuristics and high-performance computing. *Nature Methods* 9(8): 772. https://doi.org/10.1038/nmeth.2109

da Silva S.A., Cunha L.S., Pescim R.R., Machado A.C., 2023. Population dynamics of *Helicotylenchus dihystera* in cotton under greenhouse conditions. *Tropical Plant Pathology* 48: 90–96. https://doi.org/10.1007/s40858-022-00537-6

Decraemer W., Geraert E., 2006. Ectoparasitic nematodes. In: *Plant Nematology* (R.N. Perry, M. Moens, ed.), CABI, Wallingford, UK, 153–184.

Firoza K., Maqbool M.A., 1994. A diagnostic compendium of the genus *Helicotylenchus* Steiner, 1945 (Nematoda: Hoplolaimidae). *Pakistan Journal of Nematology* 12: 11–50.

Letunic I, Bork P., 2021. Interactive tree of life (iTOL) v5: an online tool for phylogenetic tree display and annotation. *Nucleic Acids Research* 49(W1): W293-W296. https://doi.org/10.1093/nar/gkab301

Mwamula A.O., Lee D.W., 2021. Occurrence of plant-parasitic nematodes of turfgrass in Korea. *The Plant Pathology Journal* 37(5): 446. https://doi.org/10.5423/PPJ.OA.04.2021.0059

Mwamula A.O., Na H., Kim Y.H., Kim Y.H., Han G., Lee D.W., 2020. Characterization of a new spiral nematode, *Helicotylenchus asiaticus* n. sp., and three known species from Korea; with comments on the validity of *Helicotylenchus microlobus* Perry in Perry, Darling & Thorne, 1959. *European Journal of Plant Pathology* 157(3): 565-581. https://doi.org/10.1007/s10658-020-02022-9

Mwamula A.O., Kwon O.G., Kwon C., Kim Y.S., Kim Y.H., Lee, D.W., 2024. A revision of the phylogeny of *Helicotylenchus* Steiner, 1945 (Tylenchida: Hoplolaimidae) as inferred from ribosomal and mitochondrial DNA. *The Plant Pathology Journal* 40(2): 171–191. https://doi.org/10.5423/PPJ.OA.01.2024.0013

Palomares-Rius J.E., Cantalapiedra-Navarrete C., Archidona-Yuste A., Vovlas N., Tzortzakakis E.A., Castillo P., 2018. Molecular and morphological characteri-

zation of the spiral nematode *Helicotylenchus oleae* Inserra, Vovlas & Golden, 1979 (Nematoda: Hoplolaimidae) in the Mediterranean Basin. *European Journal of Plant Pathology* 150: 881–891.

Riascos-Ortiz D., Mosquera-Espinosa A.T., De Agudelo F.V., de Oliveira C.M.G., Muñoz-Florez J.E., 2020. An integrative approach to the study of *Helicotylenchus* (Nematoda: Hoplolaimidae) Colombian and Brazilian populations associated with *Musa* crops. *Journal of Nematology* 52: 1–19. https://doi.org/10.21307/JOFNEM-2020-054

Ronquist F., Huelsenbeck J.P., 2003. MrBayes 3: Bayesian phylogenetic inference under mixed models, *Bioinformatics* 19: 1572–1574. https://doi.org/10.1093/bioinformatics/btg180

Rybarczyk-Mydłowska K., Dmowska E., Kowalewska K., 2019. Phylogenetic studies on three *Helicotylenchus* species based on 28S rDNA and mtCOI sequence data. *Journal of Nematology* 51(1): 1–17. https://doi.org/10.21307/jofnem-2019-033

Subbotin S.A., Inserra R.N., Marais M., Mullin P., Powers T.O., … Baldwin J.G., 2011. Diversity and phylogenetic relationships within the spiral nematodes of *Helicotylenchus* Steiner, 1945 (Tylenchida: Hoplolaimidae) as inferred from analysis of the D2-D3 expansion segments of 28S rRNA gene sequences. *Nematology* 13(3): 333–345. https://doi.org/10.1163/138855410X520936

Subbotin S.A., Vovlas N., Yeates G.W., Hallmann J., Kiewnick S., … Castillo P., 2015. Morphological and molecular characterisation of *Helicotylenchus pseudorobustus* (Steiner, 1914) Golden, 1956 and related species (Tylenchida: Hoplolaimidae) with a phylogeny of the genus. *Nematology* 17(1): 27–52. https://doi.org/10.1163/15685411-00002850

Uzma I., Nasira K., Firoza K., Shahina F., 2015. Review of the genus *Helicotylenchus* Steiner, 1945 (Nematoda: Hoplolaimidae) with updated diagnostic compendium. *Pakistan Journal of Nematology* 33(2): 115–160.

van Eck N.J., Waltman L., 2010. Software survey: VOSviewer, a computer program for bibliometric mapping. *Scientometrics* 84 (2): 523–538. https://doi.org/10.1007/s11192-009-0146-3

Wouts W.M., Yeates G.W., 1994. *Helicotylenchus* species (Nematoda: Tylenchida) from native vegetation and undisturbed soils in New Zealand. *New Zealand Journal of Zoology* 21(2): 213–224.

Xia Y., Li J., Hao P., Wang K., Lei B., … Li Y.U., 2022. Discovery of root-lesion nematode (*Pratylenchus scribneri*) on corn in Hainan Province of China. *Plant Disease*, 106(7), 1999. https://doi.org/10.1094/PDIS-09-21-1960-PDN

Zong Q.J., Shen H.Z., Yuan Q.J., Hu X.W., Hou Z.P., Deng S.G., 2013. Doctoral dissertations of Library and Information Science in China: A co-word analysis. *Scientometrics* 94: 781–799. https://doi.org/10.1007/s11192-012-0799-1

ORCID:
JKN: 0009-0000-4385-2447
JF: 0000-0002-5420-1559
ZB: 0000-0002-4608-775X
JÁ: 0000-0002-1088-4271
DD: 0000-0003-4425-6684
LP: 0000-0002-1850-6750
LK: 0000-0001-9769-8297
AK: 0000-0002-3473-1181
IS: 0009-0007-9353-3920

Research Papers

First report of *Rhodococcus fascians* causing leafy gall on *Iberis sempervirens* in Hungary

Judit KOLOZSVÁRINÉ NAGY[1], József FODOR[1], Zoltán BOZSÓ[1], János ÁGOSTON[2,*], Dénes DLAUCHY[3], László PALKOVICS[2,4,5], Lóránt KIRÁLY[1], András KÜNSTLER[1], Ildikó SCHWARCZINGER[1]

[1] *HUN-REN Centre for Agricultural Research, Plant Protection Institute, Budapest, Hungary*
[2] *HUN-REN-SZE PhatoPlant-Lab, Széchenyi István University, Mosonmagyaróvár, Hungary*
[3] *National Collection of Agricultural and Industrial Microorganisms, Institute of Food Science and Technology, Hungarian University of Agriculture and Life Sciences, Budapest, Hungary*
[4] *Department of Plant Sciences, Albert Kázmér Faculty of Mosonmagyaróvár, Széchenyi István University, Mosonmagyaróvár, Hungary*
[5] *Agricultural and Food Research Centre, Albert Kázmér Faculty of Mosonmagyaróvár, Széchenyi István University, Mosonmagyaróvár, Hungary*
*Corresponding author. E-mail: agoston.janos123@gmail.com

Summary. In spring of 2023, leafy gall symptoms were detected on plants of evergreen candytuft (*Iberis sempervirens* 'Pink Ice') in Hungary. Bacteria isolated from gall-like tissues of short, stunted shoots, and showing a characteristic appearance on selective culture media were investigated using bacteriological and molecular methods, and phylogenetic analysis. Nucleotide sequences of the 16S rRNA gene, *fasD* and *vicA* genes were determined. Pathogenicity of selected isolates was confirmed on garden pea (*Pisum sativum* 'Tristar'). Characterization of the investigated isolates indicated the presence of *Rhodococcus fascians* in *I. sempervirens*. This is the first report identifying the causal agent of leafy gall from this plant in Hungary.

Keywords. Bacterial plant disease, evergreen candytuft, fasciation.

INTRODUCTION

Evergreen candytuft (*Iberis sempervirens* L., *Brassicaceae*) is a popular ornamental subshrub plant which is native to the Mediterranean basin (POWO, 2024). One of its bacterial pathogens (Putnam and Miller, 2007) is the Gram-positive *Rhodococcus fascians* (Tilford 1936) Goodfellow 1984 [syn. *Rhodococcoides fascians* (Tilford 1936) Val-Calvo and Vázquez-Boland 2023], the only known phytopathogenic *Rhodococcus* species. This pathogen impairs development and growth of a wide range of host plants, including developmental abnormalities, many of which can be mimicked by application of the plant hormone cytokinin (Jameson *et al.,* 2019). These

growth disorders include hyperplasia, stunting and formation of leafy galls, which are masses of differentiated tissues compacted into small spaces (Cornelis *et al.,* 2001; Putnam and Miller, 2007; Stes *et al.,* 2013). These galls can reduce host plant vigour and make affected plants unmarketable. *Rhodococcus fascians* infections are often not obvious due to the bacterium's ability to be latent or to induce mild symptoms, which may lead to rapid spread by vegetative host propagation material (Putnam and Miller, 2007). To avoid severe economic losses, sanitation and prevention are the primary means of disease management, because the pathogen can spread in plant sap and on cultivation tools (Gordon *et al.,* 2024).

Leafy gall was first reported nearly 100 years ago from the United States of America on sweet peas (*Lathyrus odoratus* L.) (Brown, 1927). The disease is now widely distributed (CABI, 2022), and *R. fascians* is a regulated non-quarantine pest based on Regulation 2019/2072 of the European Union concerning *Rubus* plants, with a 0% threshold for the planting material (EU, 2019). Accordingly, a policy in the Netherlands requires abnormal *Lilium* bulbs to be destroyed during flower bulb production (de Best *et al.,* 2000). During regular visual assessments of Hungarian perennial plant nurseries in 2023, unusual, leafy gall-like symptoms were observed on some *Iberis* plants in container production.

MATERIALS AND METHODS

Sources of plant material, visual assessments and isolation of the potential pathogen

In spring of 2023, a general visual assessment of several *Iberis sempervirens* cultivars was carried out at four major Hungarian perennial plant nurseries, which produce approx. 50% of the total perennial plant output of the country. At each nursery, all potted plants were separated from the soil by a drainage layer and weed barrier cloth. The *Iberis* cuttings had originated from Germany and the Netherlands in autumn 2022. During spring of 2023 plants of *I. sempervirens* 'Pink Ice', a popular *Iberis* cultivar with narrow leaves and racemes of pale pink flowers, showed characteristic symptoms of leafy gall in two nurseries. The symptomatic plants had leafy galls, which developed primarily at the plant bases (Figure 1). Based on these symptoms, plant material was collected and tested for the presence of *R. fascians*.

Symptomatic stems and leaves of the collected plant samples were homogenized without surface disinfection using mortar and pestle in phosphate buffered saline (PBS) pH 7.4, prior to dilution plating onto cycloheximide-amended (100 ppm) D2 agar (Kado and Heskett, 1970) plates. This medium favours growth of *Rhodococcus* spp. (syn. *Corynebacterium* spp.). Inoculated plates were incubated in the dark at 27°C (Klement *et al.,* 1990) for 4 days, after which small, circular, convex, mucoid

Figure 1. Symptoms of leafy gall detected on *Iberis sempervirens* 'Pink Ice' plants. A: Dense clusters of deformed leafy shoots (red arrows), compared to symptomless *I. sempervirens* 'Fischbeck' plants (B and C).

and glistening orange shade colonies were selected for purification and organism identification.

Characterization of pathogenic isolates

Phenotypic characterization of selected isolates was carried out according to standard methods (Klement *et al.,* 1990; Schaad *et al.,* 2001) using the *R. fascians* strain NCAIM B.01614 isolated by W.J. Dowson from chrysanthemum as a reference strain.

Genomic DNA was extracted from 23 colonies by suspending them in 50 µL sterile nuclease-free water, then boiling (10 min at 99°C) and centrifuging (10 min at 4°C, 16700 *g*) each bacterial suspension separately. Supernatants were used as templates for PCR-amplification of the partial 16S rRNA gene using universal primers 27F/1492R (Lane, 1991), while the *fasD* (encoding isopentenyltransferase) gene fragment amplified with fasD-F/FasD-R primer pair, and the *vicA* (encoding malate synthase) gene fragment amplified with the vicA44-F/vicA737-R primer pair were used according to Park *et al.* (2021) (Table 1).

DNA sequencing of the PCR amplified products of the three loci were carried out for species identification of the bacterial isolates. The isolated bacteria were identified mainly on the basis of 16S rRNA and the virulence gene *fasD* sequence analyses, while *vicA* was used to compare the relationships among the *Rhodococcus* strains.

Amplified DNA products of two isolates (IsHu1 and IsHu2) and the strain NCAIM B.01614 were selected for sequence analysis and were purified using a high pure PCR product purification kit (Roche) according to the manufacturer's protocol. The sequences obtained (Macrogen Europe BV, Amsterdam, The Netherlands) were compared with publicly available sequences of plant-associated *Rhodococcus* strains derived from NCBI databases by BLAST (https://blast.ncbi.nlm.nih.gov/Blast.cgi), and were used to construct a phylogenetic tree of 26 *Rhodococcus* isolates and a *Streptomyces* strain as the outgroup. Phylogenetic analysis was carried out using MEGA software version 11 (Tamura *et al.,* 2021) after multiple alignments of sequence data were achieved using the ClustalW algorithm. The amplified 16S rRNA, *fasD*, and *vicA* gene regions were concatenated into a single data set of 2406 sites, and were incorporated into a single phylogenetic tree using the Maximum Likelihood method and Tamura-Nei model (Tamura and Nei, 1993).

Pathogenicity tests

Pathogenicity tests were carried out according to Dhaouadi *et al.* (2021), with modifications. Germinated seeds of garden pea (*Pisum sativum* L. 'Tristar') were inoculated with 19 bacterial isolates carrying the *fasD* gene. Following surface disinfection, the pea seeds were placed between moistened sterile blotting papers in 9 cm Petri dishes in the dark at constant 20°C for 4 days. The germinated seeds were then inoculated by shaking in bacterial suspensions (10^8 CFU mL^{-1}) for 2 h at 125 rpm at room temperature. Treatment with PBS served as a negative control. Three seeds inoculated with each isolate were then sown into autoclaved soil-peat mixture (1:1), and were incubated in a growth chamber at 25°C/20°C 16 h/8 h light/dark cycles for 14 days. Re-isolations of *R. fascians* from symptomatic seedlings inoculated with isolates IsHu1 or IsHu2, or from a PBS-treated negative control plant, were carried out following the isolation procedure described above, and pathogen identity was assessed by colony PCR using *fasD*-specific primers.

Table 1. Oligonucleotide primers and PCR conditions applied in the present study.

Primer	Nucleotid sequence (5' → 3')	Target gene	Amplicon length (bp)	Cycling conditions denaturation (initial and repeated), annealing, extension, cycle number, final extension	Reference
27F	AGAGTTTGATCMTGGCTCAG	16S rRNA	1517	95°C / 5 min, 95°C / 30 s, 59°C / 30 s, 72°C / 90 s, 35, 72°C / 5 min	Lane, 1991
1492R	GGTTACCTTGTTACGACTT				
fasD-F	ATTGTTGTTGCCGACCGTATC	*fasD*	573	95°C / 3 min, 95°C / 20 s, 55°C / 30 s, 72°C / 60 s, 40, 72°C / 10 min	Park *et al.,* 2021
fasD-R	AAGGACGCCGTGCTCGACATAC				
vicA44-F	TCCTATTCGATTTCGTCGAGAAG	*vicA*	694		
vicA737-R	GGGTCGATCTGGATCTCGAA				

A further pathogenicity test was carried out with the three selected isolates (IsHu1, IsHu2, and IsHu3), which had caused characteristic symptoms. The strain NCAIM B.01614 was used as a positive control and PBS was used as the negative control.

The numbers and lengths of plant shoots grown from ten treated seeds per isolate were measured at 14 days post-inoculation. Means and standard deviations for these data were calculated and statistical analysis was performed using the Kruskal-Wallis test with Statistica software (StatSoft, Inc.).

RESULTS

During surveys conducted in 2023 in nurseries in Hungary, abnormal growth of *Iberis sempervirens* plants was observed at two different locations (Table 2).

Table 2 shows marked susceptibility of the cultivar 'Pink Ice', as compared to other cultivars assessed. During the 2023 growing season, the symptomatic plants became severely weakened and they were unable to overwinter.

Following isolations of bacteria from symptomatic plant samples, colonies typical of *R. fascians* formed on D2 agar, nutrient-broth yeast extract agar (NBY), and 1% glucose nutrient agar (GNA). The isolated bacteria were Gram-positive, aerobic, non-motile, with urease activity, were unable to grow at 36°C, and did not tolerate 7% sodium chloride, in line with data outlined by Klement *et al.* (1990) and Schaad *et al.* (2001).

Nineteen isolates tested were positive by PCR for the plasmid-associated virulence gene *fasD*, which is present in the fasciation (fas) operon in *R. fascians*, while the chromosomal malate synthase gene *vicA* was found in all 23 isolates. Sequence analyses showed that isolates IsHu1 and IsHu2 had 100% sequence identity within 16S rRNA, *fasD* and *vicA* gene fragments. Comparison with sequences available in GenBank indicated that isolate IsHu1 belonged to *R. fascians*. The sequences of IsHu1 and NCAIM B.01614 were deposited in NCBI GenBank under accession numbers PP125720 and PP125739 for the partial 16S rRNA gene, PP130585 and PP130586 for *fasD*, and PP130584 and PP130587 for *vicA*.

Rhodococcus isolates used for sequence analyses and construction of a phylogenetic tree are shown in Table 3.

The 16S rRNA gene sequence comparisons in NCBI GenBank revealed 100% identity between isolate IsHu1 and the plant-associated *R. fascians* strains D188, 15-508-1b and YWS4-1 (Table 4). The *fasD* gene sequence obtained from isolate IsHu1 showed 100% identity with the type strain *R. fascians* D188, and with several other *Rhodococcus* isolates (Table 4). The sequence of the *vicA* gene of isolate IsHu1 shared >99% identity with *R. fascians* strains NBRC 12155 = LMG 3623 (99.83%), YWS8-2 (99.66%), A78 (99.49%) and YWS3-1 (99.49%) (Table 4).

Sequences of 16S rRNA, *fasD* and *vicA* genes were concatenated into one combined alignment, which was used for Maximum Likelihood tree inference. IsHu1 was closely related to strains D188 and 15-508-1b in the phylogenetic tree (Figure 2). The strain NCAIM B.01614, which served as a positive control in the artificial inoculation experiments, clustered in the same clade as IsHu1,

Table 2. Leafy gall incidence (assessed visually) for different *Iberis* cultivars at different nurseries in Hungary in 2023.

Location	Assessment date	Cultivar	Disease incidence (%)	Total number of plants assessed
Northwest Great Plain	April 17	Appen-Etz	0	1200
		Fischbeck	0	1200
		Golden Candy	0	520
		Nevina	0	1200
Western Transdanubia	April 21	Appen-Etz	0	1600
		Fischbeck	0	3200
		Pink Ice	100	408
		Schneeflocke	0	1680
Northwest-Transdanubia	April 24	Absolutely Amethyst	0	520
		Appen-Ezt	0	1040
		Snowsurfer Compact	0	1040
Southeastern Great Plain	May 5	Appen-Etz	0	9360
		Golden Candy	0	1560
		Pink Ice	10.22	74880

Table 3. *Rhodococcus* isolates used for sequence analyses and construction of a phylogenetic tree.

Strain	Accession number (NCBI GenBank)			Host/Source	Pathogen	Reference
	16S rRNA	vicA	fasD			
Rhodococcus fascians IsHu1	PP125720	PP130584	PP130585	*Iberis sempervirens* 'Pink Ice', Hungary, 2023	+	present study
R. fascians D188	CP015235	CP015235	CP015236	*Chrysanthemum* × *morifolium*, UK, 1946	+	Desomer *et al.*, 1988
R. fascians 15-508-1b	NPFO01000033	NPFO01000016	NPFO01000019	*Petunia* 'Flash Mob Pinkceptional', USA, 2015	nt	Savory *et al.*, 2017
R. fascians YWS4-1	MW394218	MW394214	MW394222	*Lilium* sp., South Korea, 2020	+	Park *et al.*, 2021
R. sp. 05-2221-1B	NOZL01000044	NOZL01000021	NOZL01000042	*Verbascum* 'Sierra Sunset', USA, 2005	nt	Savory *et al.*, 2017
R. sp. 14-2496-1d	NPFV01000050	NPFV01000029	NPFV01000030	*Scabiosa* sp., USA, 2014	nt	Savory *et al.*, 2017
R. fascians A76	JMEV01000015	JMEV01000004	JMEV01000021	*Veronica spicata* 'Royal Candles', USA, 2002	+	Creason *et al.*, 2014a
R. fascians A21d2	CP049748	CP049748	None	*Oenothera speciosa*, 'Siskiyou', USA, 2002	+	Serdani *et al.*, 2013
R. sp. 14-2483-1-1	NPFX01000030	NPFX01000022	NPFX01000024	*Geranium* sp., USA, 2014	nt	Savory *et al.*, 2017
R. fascians NCAIM B.01614	PP125739	PP130587	PP130586	*Chrysanthemum* sp., UK	+	present study
R. fascians A78	JMEU01000039	JMEU01000016	JMEU01000002	*Leucanthemum* × *superbum*, 'Becky', USA, 2002	+	Creason *et al.*, 2014a
R. fascians YWS8-2	MW394219	MW394215	MW394223	*Lilium* sp., South Korea, 2020	+	Park *et al.*, 2021
R. fascians YWS1-1	MW394216	MW394212	MW394220	*Lilium* sp., South Korea, 2020	+	Park *et al.*, 2021
R. fascians A3b	JMEY01000022	JMEY01000029	JMEY01000009	*Heliopsis helianthoides* 'Loraine Sunshine', USA, 2005	+	Creason *et al.*, 2014a
R. fascians NBRC 12155 = LMG 3623	JMEN01000010	JMEN01000030	JMEN01000005	*Lathyrus odoratus*, USA, Ohio, 1936	+	Tilford, 1936
R. fascians YWS3-1	MW394217	MW394213	MW394221	*Lilium* sp., South Korea, 2020	+	Park *et al.*, 2021
R. sp. 05-2254-3	NOZI01000017	NOZI01000027	NOZI01000005	*Veronica* 'Sunny Border Blue', USA, 2005	nt	Savory *et al.*, 2017
R. fascians A25f	CP049744	CP049744	CP049745	*Nemesia* 'Natalie', USA, 2002	+	Creason *et al.*, 2014a
R. fascians 05-339-2	NOYW01000001	JMFC01000021	NOYW01000019	*Hosta* 'Blue Umbrellas', USA, 2005	+	Creason *et al.*, 2014a
R. fascians A73a	JMEW01000018	JMEW01000014	JMEW01000015	*Aster amellus* 'Violet Queen', USA, 2003	+	Creason *et al.*, 2014a
R. fascians 02-815	JMFF01000017	JMFF01000006	JMFF01000005	*Campanula* 'Sarastro', USA, 2002	+	Creason *et al.*, 2014a
R. fascians A44A	JMEX01000006	JMEX01000005	JMEX01000009	*Veronica spicata* 'Minuet', USA, 2002	+	Creason *et al.*, 2014a
R. sp. 06-156-4	NPGB01000004	NPGB01000015	NPGB01000038	*Campanula* sp., USA, 2006	nt	Savory *et al.*, 2017
R. sp. 15-1189-1-1a	NPFQ01000064	NPFQ01000035	NPFQ01000039	*Leucanthemum* sp., South America, 2015	+	Savory *et al.*, 2017
R. kyotonensis DS472	AB269261	FZOW01000009	None	soil, Japan	nt	Li *et al.*, 2007
R. corynebacterioides DSM 20151	LPZL01000057	LPZL01000030	None	air contaminant	nt	Yassin and Schaal, 2005
Streptomyces sp. NEAU-BLH26	JBFBOR010000023	JBFBOR010000006	JBFBOR010000010	*Adonis amurensis* 'Regel', China, 2021	nt	unpublished

Abbreviation: nt, not tested.

Table 4. Sequence identities (%) for the 16S rRNA, *fasD* and *vicA* genes between *Rhodococcus fascians* IsHu1 and other isolates used for construction of the phylogenetic tree.

Isolate	Homology (%)		
	16S rRNA	*fasD*	*vicA*
R. fascians D188	100.00	100.00	98.62
R. fascians 15-508-1b	100.00	100.00	98.97
R. fascians YWS4-1	100.00	100.00	97.04
R. sp. 05-2221-1B	99.76	100.00	87.19
R. sp. 14-2496-1d	99.76	100.00	87.39
R. fascians A76	99.76	100.00	88.40
R. fascians A21d2	99.76	None	87.39
R. sp. 14-2483-1-1	99.76	100.00	87.59
R. fascians NCAIM B.01614	99.44	100.00	98.62
R. fascians A78	99.36	100.00	99.49
R. fascians YWS8-2	99.36	100.00	99.66
R. fascians YWS1-1	99.36	100.00	97.92
R. fascians A3b	99.36	100.00	98.97
R. fascians NBRC 12155=LMG 3623	99.36	100.00	99.83
R. fascians YWS3-1	99.36	100.00	99.49
R. sp. 05-2254-3	99.20	100.00	88.59
R. fascians A25f	99.12	97.05	86.38
R. sp. 05-339-2	99.04	100.00	86.99
R. fascians A73a	98.08	100.00	75.14
R. fascians 02-815	98.08	100.00	77.02
R. fascians A44A	98.08	100.00	75.38
R. sp. 06-156-4	98.08	100.00	77.02
R. sp. 15-1189-1-1a	98.01	100.00	76.08
R. kyotonensis DS472	97.93	None	75.85
R. corynebacterioides DSM 20151	96.33	None	70.73
Streptomyces sp. NEAU-BLH26	89.71	45.76	45.39

Figure 2. Evolutionary analysis of homologous sequences of concatenated 16S rRNA, *fasD* and *vicA* genes in *Rhodococcus* spp., which was conducted with the Maximum Likelihood algorithm in MEGA 11 using the bootstrap method and the Tamura-Nei model. The percentages of replicate trees in which the associated taxa clustered together in the bootstrap test (1000 replicates) are shown next to the branches; only values >50% are shown at branch points. *Rhodococcus fascians* IsHu1 is shown in bold type. The scale bar represents the number of substitutions per site.

along with YWS strains isolated from symptomatic lilies, as well as strains A3b, A78, and LMG 3623 (Figure 2).

During the pathogenicity test with 19 bacterial isolates, all of the inoculated plants showed characteristic symptoms of shoot proliferation, stunting, and hypertrophy, as compared to the control plants, that grew normally (Figure 3). There were no differences among severity of disease symptoms caused by these 19 isolates. Therefore, two groups of plants displaying characteristic symptoms (inoculated respectively with IsHu1 or IsHu2) were selected for re-isolation to assess fulfilment of Koch's postulates. *Rhodococcus fascians* was re-isolated from symptomatic seedlings that had been artificially inoculated with isolates IsHu1 or IsHu2, and its identity was confirmed through colony PCR using the *fasD*-specific primers. The bacterium was not present in PBS-treated control plants.

Inoculations of pea plants with the selected bacterial isolates IsHu1, IsHu2, and IsHu3 increased the numbers of shoots by 5.6- to 7.1-fold, and reduced shoot lengths by 72 to 79%, as compared to the untreated controls. The Kruskal-Wallis non-parametric test revealed no differences ($P < 0.05$) among mean numbers and lengths of shoots 2 weeks after inoculation with different isolates, including the positive control inoculation with strain NCAIM B.01614 (Table 5).

Table 5. Mean shoot lengths and numbers for pea plants inoculated 14 days previously with different *Rhodococcus fascians* isolates.

Inoculation treatments	Mean shoot lengths (mm) (± SE)	Mean numbers of shoots (± SE)
IsHu1	27.4 ± 5.6 b	5.6 ± 0.6 a
IsHu2	26.8 ± 4.5 b	5.7 ± 0.6 a
IsHu3	19.8 ± 2.9 b	7.1 ± 0.5 a
NCAIM B.01614	25.7 ± 4.5 b	6.0 ± 0.8 a
PBS control	96.5 ± 8.8 a	1.0 ± 0.0 b
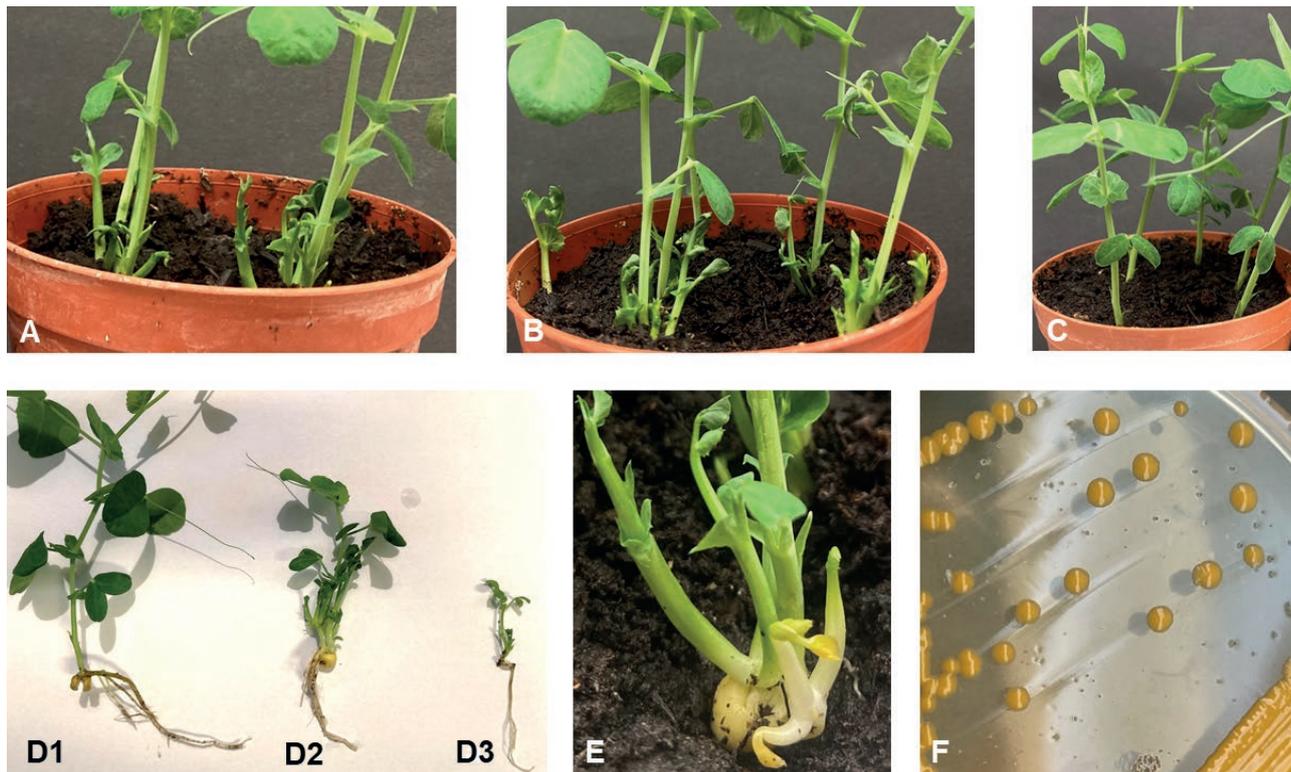
Figure 3. Pathogenicity assessments for *Rhodococcus fascians* isolate IsHu1. Typically small, distorted shoots developed from artificially inoculated *Pisum sativum* 'Tristar' seeds (photos A, D2, D3, and E), and similarly after inoculation with isolate NCAIM B.01614 used as a positive control (B). The negative control plants (C, and D1) developing from seeds treated with PBS showed normal growth. These photos were taken at 14 days post-inoculation. Typical orange *R. fascians* colonies formed on D2 agar plates (F).

Inoculations were carried out with three selected *R. fascians* isolates (IsHu1, IsHu2, IsHu3) and strain NCAIM B.01614 on pea (*Pisum sativum* 'Tristar') seedlings raised from ten seeds per isolate. The number and lengths of shoots were recorded 2 weeks after inoculation. Means and standard errors (SE) were calculated from ten replicates. Statistical analyses were carried out using the Kruskal-Wallis test and Statistica software (StatSoft Inc.). Different lowercase letters in each column indicate differences ($P < 0.05$) between means.

DISCUSSION

Of the *Iberis sempervirens* cultivars assessed in the nurseries, only 'Pink Ice' plants had leafy gall symptoms. Each nursery growing this cultivar had symptomatic plants at the time of the visual assessment. The affected plants were unmarketable and had to be destroyed to prevent further spread of the infections.

The present study showed that the severe leafy gall symptoms on *I. sempervirens* 'Pink Ice' in 2023 in Hun-gary were caused by *R. fascians*. Phylogenetic analysis of the pathogen was employed on the aligned 16S rRNA, *fasD* and *vicA* gene sequences. The virulence gene *fasD* is usually present in pathogenic *R. fascians* isolates (Savory *et al.*, 2020). Pathogenicity of *R. fascians* requires a cluster of three loci present on a linear plasmid, of which the fasciation (*fas*) operon plays a core role in virulence (Creason *et al.*, 2014b) through local and persistent secretion of an array of synergistically operating cytokinins which bring about continuous tissue proliferation (Pertry *et al.*, 2009; 2010). The *fasD*-coded isopentenyltransferase protein is a pivotal factor in symptom initiation (Pertry *et al.*, 2010). On the other hand, *vicA* is a chromosomal gene encoding malate synthase G of the glyoxylate shunt of the Krebs cycle. Although this gene is not associated with the pathogenic phenotype, it is a suitable marker for phylogenetic reconstructions in *Rhodococcus* (Savory *et al.*, 2017), as it exhibits greater sequence variation than the 16S rRNA gene, allowing for better discrimination among bacterial strains.

The present study results showed that the nucleotide sequences of *R. fascians* isolate IsHu1 obtained had high

overall similarity with those of *R. fascians* 15-508-1b and the well-characterized virulent *R. fascians* model strain D188, based on sequence homology of 16S rRNA, *fasD* and *vicA* gene fragments.

To date in Hungary *R. fascians* has been identified only from geranium (*Pelargonium × hortorum* L. H. Bailey) (Süle, 1976). This bacterium is known for its ability to infect a variety of plant hosts (Dhaouadi *et al.,* 2020), including two species of *Iberis* (*I. gibraltarica* L. and *I. sempervirens* L.) (Putnam and Miller, 2007). However, the present study is the first to report *R. fascians* from a cultivar of *I. sempervirens*, but also from this plant in Hungary.

The severe outbreak of *R. fascians* reported here may imply that the propagation material used could have been contaminated with the pathogen. Putnam and Miller (2007) suggest that non-pathogen-free propagating material was probably the primary means by which *R. fascians* can be introduced into non-infested areas. The present report may contribute towards further research on the control of *R. fascians*, which is still based on pathogen prevention.

LITERATURE CITED

Brown N.A., 1927. Sweet pea fasciation, a form of crown gall. *Phytopathology* 17: 29–39.

CABI, 2022. *Rhodococcus fascians* (fasciation: leafy gall). PlantwisePlus Knowledge Bank. Technical factsheet. Available at: https://doi.org/10.1079/pwkb.species.15332

Cornelis K., Ritsema T., Nijsse J., Holsters M., Goethals K., Jaziri M., 2001. The plant pathogen *Rhodococcus fascians* colonizes the exterior and interior of the aerial parts of plants. *Molecular Plant-Microbe Interaction* 14: 599–608. https://doi.org/10.1094/MPMI.2001.14.5.599

Creason A.L., Davis E.W., Putnam M.L., Vandeputte O.M., Chang J.H., 2014a. Use of whole genome sequences to develop a molecular phylogenetic framework for *Rhodococcus fascians* and the *Rhodococcus* genus. *Frontiers in Plant Science* 5: 406. https://doi.org/10.3389/fpls.2014.00406

Creason A.L., Vandeputte O.M., Savory E.A., Davis E.W., Putnam M.L., … Chang J.H., 2014b. Analysis of genome sequences from plant pathogenic *Rhodococcus* reveals genetic novelties in virulence loci. *PLoS One* 9:e101996. https://doi.org/10.1371/journal.pone.0101996

de Best A.L.I.C., Zwart M.J., van Aartrijk J., van den Ende J.E., Peeters J.M.M., 2000. *Ziekten en afwijkingen bij bolgewassen: Liliaceae* (Vols. 1–2, Vol. 1). Lisse: Laboratorium voor Bloembollenonderzoek.

Desomer J., Dhaese P., van Montagu M., 1988. Conjugative transfer of cadmium resistance plasmids in *Rhodococcus fascians* strains. *Journal of Bacteriology* 170(5): 2401–2405. https://doi.org/10.1128/jb.170.5.2401-2405.1988

Dhaouadi S., Mougou A.H., Rhouma A., 2020. The plant pathogen *Rhodococcus fascians*. History, disease symptomatology, host range, pathogenesis and plant–pathogen interaction. *Annals of Applied Biology* 177(1): 4–15. https://doi.org/10.1111/aab.12600

Dhaouadi S., Mougou A.H., Rhouma A., 2021. Isolation and characterization of *Rhodococcus* spp. from pistachio and almond rootstocks and trees in Tunisia. *Agronomy* 11(2): 355. https://doi.org/10.3390/agronomy11020355

European Union (2019). Commission Implementing Regulation (EU) 2019/2072 establishing uniform conditions for the implementation of Regulation (EU) 2016/2031 of the European Parliament and the Council, as regards protective measures against pests of plants, and repealing Commission Regulation (EC) No. 690/2008 and amending Commission Implementing Regulation (EU) 2018/2019. *Official Journal of the European Union* L 319: 1–279. Available at: https://eur-lex.europa.eu/homepage.html

Goodfellow M., 1984. Reclassification of *Corynebacterium fascians* (Tilford) Dowson in the genus *Rhodococcus*, as *Rhodococcus fascians* comb. nov. *Systematic and Applied Microbiology* 5(2): 225–229. https://doi.org/10.1016/S0723-2020(84)80023-5

Gordon M.I., Thomas W.J., Putnam M.L., 2024. Transmission and management of pathogenic *Agrobacterium tumefaciens* and *Rhodococcus fascians* in select ornamentals. *Plant Disease* 108(1): 50–61. https://doi.org/10.1094/PDIS-11-22-2557-RE

Jameson P.E., Dhandapani P., Song J., Zatloukal M., Strnad M., … Novák O., 2019. The cytokinin complex associated with *Rhodococcus fascians*: Which compounds are critical for virulence? *Frontiers in Plant Science* 10: 674. https://doi.org/10.3389/fpls.2019.00674

Kado C.I., Heskett M.G., 1970. Selective media for *Agrobacterium*, *Corynebacterium*, *Erwinia*, *Pseudomonas*, and *Xanthomonas*. *Phytopathology* 60(6): 969–976. https://doi.org/10.1094/phyto-60-969

Klement Z., Rudolph K., Sands D.C. (eds.), 1990. *Methods in phytobacteriology*. Akadémia Kiadó, Budapest, Hungary, 568 pp.

Lane D.J., 1991. 16S/23S rRNA sequencing. In *Nucleic acid techniques in bacterial systematics* (E. Stackebrandt, M. Goodfellow, eds.), John Wiley and Sons, New York, United States of America, 115–176.

Li B., Furihata K., Ding L.X., Yokota A., 2007. *Rhodococcus kyotonensis* sp. nov., a novel actinomycete isolated from soil. *International Journal of Systematic and Evolutionary Microbiology* 57(9): 1956-1959. https://doi.org/10.1099/ijs.0.64770-0

Park J.M., Koo J., Kang S.W., Jo S.H., Park J.M., 2021. Detection of *Rhodococcus fascians*, the causative agent of lily fasciation in South Korea. *Pathogens* 10(2): 241. https://doi.org/10.3390/pathogens10020241

Pertry I., Václavíková K., Depuydt S., Galuszka P., Spíchal L., … Vereecke D., 2009. Identification of *Rhodococcus fascians* cytokinins and their modus operandi to reshape the plant. *PNAS* 106(3): 929–934. https://doi.org/10.1073/pnas.0811683106

Pertry I., Václavíková K., Gemrotová M., Spíchal L., Galuszka P., … Vereecke D., 2010. *Rhodococcus fascians* impacts plant development through the dynamic fas-mediated production of a cytokinin mix. *Molecular Plant-Microbe Interaction* 23(9): 1164–1174. https://doi.org/10.1094/MPMI-23-9-1164

POWO, 2024. Plants of the World Online. Facilitated by the Royal Botanic Gardens, Kew. Published on the Internet. Available at: https://powo.science.kew.org/taxon/urn:lsid:ipni.org:names:324670-2

Putnam M.L., Miller M.L., 2007. *Rhodococcus fascians* in herbaceous perennials. *Plant Disease* 91(9): 1064–1076. https://doi.org/10.1094/PDIS-91-9-1064

Savory E.A., Fuller S.L., Weisberg A.J., Thomas W.J., Gordon M.I., … Chang J.H., 2017. Evolutionary transitions between beneficial and phytopathogenic *Rhodococcus* challenge disease management. *eLife* 6: e30925. https://doi.org/10.7554/eLife.30925

Savory E.A., Weisberg A.J., Stevens D.M., Creason, A.L., Fuller S.L., … Chang, J. H., 2020. Phytopathogenic *Rhodococcus* have diverse plasmids with few conserved virulence functions. *Frontiers in Microbiology* 11: 1022. https://doi.org/10.3389/fmicb.2020.01022

Schaad N.W., Jones J.B., Chun W. (eds.), 2001. *Laboratory guide for identification of plant pathogenic bacteria*. 3rd ed. APS Press, St. Paul, MN, United States of America, 373 pp.

Serdani M., Curtis M., Miller M.L., Kraus J., Putnam M.L., 2013. Loop-mediated isothermal amplification and polymerase chain reaction methods for specific and rapid detection of *Rhodococcus fascians*. *Plant Disease* 97(4): 517–529. https://doi.org/10.1094/PDIS-02-12-0214-RE

Süle S., 1976. Bacterial fasciation of *Pelargonium hortorum* in Hungary. *Acta Phytopathologica Academiae Scientiarum Hungaricae* 11(3–4): 223–230.

Stes E., Francis I., Pertry I., Dolzblasz A., Depuydt S., Vereecke D., 2013. The leafy gall syndrome induced by *Rhodococcus fascians*. *FEMS Microbiology Letters* 342(2): 187–194. https://doi.org/10.1111/1574-6968.12119.

Tamura K., Nei M., 1993. Estimation of the number of nucleotide substitutions in the control region of mitochondrial DNA in humans and chimpanzees. *Molecular Biology and Evolution* 10(3): 512–526. https://doi.org/10.1093/oxfordjournals.molbev.a040023

Tamura K., Stecher G., Kumar S., 2021. MEGA11: Molecular Evolutionary Genetics Analysis Version 11, *Molecular Biology and Evolution* 38(7): 3022–3027. https://doi.org/10.1093/molbev/msab120

Tilford P.E., 1936. Fasciation of sweet peas caused by *Phytomonas fascians* n. sp. *Journal of Agricultural Research* 53(5): 383–394.

Val-Calvo J., Vázquez-Boland J.A. 2023. Mycobacteriales taxonomy using network analysis-aided, context-uniform phylogenomic approach for non-subjective genus demarcation. *mBio* 14: e02207-23. https://doi.org/10.1128/mbio.02207-23

Yassin A.F., Schaal K.P., 2005. Reclassification of *Nocardia corynebacterioides* Serrano et al. 1972 (Approved Lists 1980) as *Rhodococcus corynebacterioides* comb. nov. *International Journal of Systematic and Evolutionary Microbiology* 55(3): 1345-1348. https://doi.org/10.1099/ijs.0.63529-0

ORCID:
EM: 0000-0003-4927-9367
DO: 0000-0002-8542-9089
AN: 0000-0001-5484-7088
EM-N: 0000-0001-7973-0345
SB: 0000-0002-2929-6410
MPV-A: 0000-0001-7176-0435
CO-G: 0009-0004-6511-2633
BBL: 0000-0002-9511-3731

Short Notes

Outbreak of *Xylella fastidiosa* subsp. *pauca* ST53 affecting wild and cultivated olive trees on the island of Mallorca, Spain

Eduardo MORALEJO[1,*], Bàrbara QUETGLAS[1], Marina MONTESINOS[1], Francisco ADROVER[2], Diego OLMO[2], Alicia NIETO[2], Ana PEDROSA[2], Marta LÓPEZ[3], Andreu JUAN[3], Ester MARCO-NOALES[4], Inmaculada NAVARRO-HERRERO[4], Silvia BARBÉ[4], María Pilar VELASCO-AMO[5], Concepción OLIVARES-GARCÍA[5], Blanca B. LANDA[5]

[1] Tragsa, Empresa de Transformación Agraria, Delegación de Baleares, 07005 Palma de Mallorca, Spain
[2] Institut de Recerca i Formació Agroalimentària i Pesquera de les Illes Balears, 07009 Palma de Mallorca, Spain
[3] Servicio de Agricultura, Conselleria de Medi Ambient, Agricultura i Pesca, 07006 Palma de Mallorca, Spain
[4] Centro de Protección Vegetal y Biotecnología, Instituto Valenciano de Investigaciones Agrarias (IVIA), CV-315 km 10.7, 46113 Moncada, Spain
[5] Institute for Sustainable Agriculture, Consejo Superior de Investigaciones Científicas (IAS-CSIC), 14004 Córdoba, Spain
*Corresponding author: E-mail: emoralejor@gmail.com

Summary. The Balearic Islands have emerged as a hotspot for the invasive plant pathogen *Xylella fastidiosa* (*Xf*). Since 2016, the *Xf* subsp. *fastidiosa* and *multiplex* have been detected causing almond leaf scorch and Pierce's disease on the island of Mallorca, Spain, and a new sequence type (ST), ST80, of subsp. *pauca* is infecting wild and cultivated olive trees on the island of Ibiza. In addition, *Xf* subsp. *multiplex* ST81 is widespread in scrublands, and causes mild, sub-lethal dieback of wild olive trees in Menorca and Mallorca. A new outbreak is here reported of the *Xf* subsp. *pauca* in the municipality of Sencelles in the centre of Mallorca island. In early 2024, dying patches were observed in wild olive trees (*Olea europaea* var. *europaea* subsp. *sylvestris*). Samples from these trees were *Xf*-positive in different qPCR tests, and the pathogen was subsequently identified as belonging to ST53 of subsp. *pauca*, the same genetic variant responsible for olive quick decline syndrome in Apulia, Italy. More than 184 plants of eight hosts have tested positive for subsp. *pauca* within a demarcation zone of approx. 1 km radius. The identified host species include 124 wild olive trees, 40 cultivated olive trees, nine *Rhamnus alaternus*, six *Nerium oleander*, two *Lavandula angustifolia*, one *Laurus nobilis*, one *Lavandula dentata* and one *Polygala myrtifolia*. Of particular concern is detection of co-infections by *Xf* subsp. subsp. *pauca* and *multiplex* on plants from natural settings (wild olives, *L. dentata* and *R. alaternus*), posing potential risk of genetic recombinations. Intensive surveys are being carried out to contain the spread of ST53, and infected plants have been destroyed in the demarcated zone.

Keywords. Genetic diversity, olive quick decline syndrome, invasive pathogens, Multi-Locus Sequence Typing (MLST), disease outbreak.

INTRODUCTION

The vector-borne plant pathogenic bacterium *Xylella fastidiosa* (*Xf*) has recently emerged as a threat to agriculture in southern Europe. Following its first detection in Apulia (Italy) in 2013, associated with the rapid decline syndrome of olive trees (Saponari *et al.*, 2013), the European Union (EU) took decisive action with mandatory surveys to contain possible spread of the pathogen within the EU (Reg. EU 2016/2031). The three main subspecies of *Xf* have since then been detected, and their establishment confirmed, in several southern European countries, including the island of Corsica and the Balearic Islands (Saponari *et al.*, 2013; Denance *et al.*, 2017; Landa *et al.*, 2020; Olmo *et al.*, 2017; Carvalho-Luis *et al.*, 2022).

The Balearic Islands have become a hotspot for establishment of genetic diversity of this pathogen, which originated from North, Central and South America. Since 2016, the three main subspecies of *Xf*, *fastidiosa*, *multiplex,* and *pauca*, have been detected, along with unique genotypes such as the sequence type (ST) 81 (from subsp. *multiplex*) on the islands of Mallorca and Menorca, and the ST80 (from subsp. *pauca*) on the island of Ibiza (Olmo *et al.*, 2021). Subspecies *fastidiosa,* and in particular ST1, is only known on Mallorca island, where it caused severe outbreaks of Pierce's disease of grapevines and leaf scorch of almond (Moralejo *et al.*, 2019; Moralejo *et al.*, 2020). Some evidences suggest that the genotypes responsible for Pierce's disease (ST1) and almond leaf scorch (ST1 and ST81) in Mallorca were likely a single introduction via infected plant material from California, in approx. 1993 (Moralejo *et al.*, 2020; Velasco-Amo *et al.*, 2022).

METHODS

Early in 2024, plant health inspectors in the Balearic Islands noticed an unusually severe decline in a stand of wild olive trees (*Olea europaea* subsp. *europaea* var. *sylvestris*) (Figure 1). Samples from different tree branches were collected, were pooled, and then sent to the Balearic Islands Official Plant Health Laboratory (LOSVIB) for analyses. Sample extracts were prepared by homogenizing 0.5 g of leaf petioles in an extraction bag (BIOREBA®) and grinding them in 5 mL (1:10 weight:volume) of phoshate buffered saline (PBS) using a semi-automated homogenizer (Homex 7; BIOREBA®).

Total DNA extraction was carried out using 200 µL of each sample extract, and the EZNA HP Plant Mini kit (Omega-Biotek), which employs a CTAB-based method,

Figure 1. A group of wild olive trees with severe symptoms of quick decline syndrome. This photograph was taken at focus 0 near the municipality of Sencelles, Mallorca Island, Spain, where *Xylella fastidiosa* subsp. *pauca* ST53 was found for the first time in January 2024.

as described in the EPPO protocol (EPPO, 2023). The DNA extracts were subsequently tested for the presence of *Xf* by quantitative real-time PCR (qPCR), according to Harper *et al.* (2010). Aliquots of DNA from the *Xf* positive samples from the wild olive tree were sent to the Institute for Sustainable Agriculture (IAS-CSIC), Córdoba, Spain, for ST determination, which was carried out by conventional MultiLocus Sequence Typing (MLST) analysis (Yuan *et al.*, 2010). A nested-MLST (Cesbron *et al.*, 2020) analysis was used when not enough amplification product for direct sequencing was obtained when using the conventional MLST approach.

RESULTS AND DISCUSSION

MLST analyses identified the presence of alleles *leu*A-7, *pet*C-6, *mal*F-16, *cys*G-24, *hol*C-10, *nuo*L-16 and *glt*T-14 associated with *Xf* subsp. *pauca* ST53 in the affected wild olive tree. Additionally, the qPCR protocol of Dupas *et al.* (2019) validated the diagnosis as *Xf* subsp. *pauca*.

After confirming the diagnosis and recognizing the potential devastating impact if this subspecies were to spread, the phytosanitary authority of the Balearic Government implemented a targeted action plan. This included increasing surveys and intensive sampling in the area of the new outbreak. Additional measures were also established to those already in place from the current Regulation (EU) 2016/2031. These included analyses to determine the subspecies present in all the *Xf*-positive samples, in collaboration with the Valencian Institute of Agricultural Research (IVIA), using the qPCR protocols developed by Dupas *et al.* (2019) and Hodgetts *et al.* (2021).

Since the first detection in January 2024 and up to December 2024, a total of 1,328 samples from within the disease outbreak area have been analyzed. This has shown that 184 plants were infected by *Xf* subsp. *pauca*,

Table 1. Host plant species, numbers of plants analysed, and numbers infected by different subspecies *Xylella fastidiosa* (*Xf*), in single or in mixed infections, in the outbreak of subspecies *pauca* around the locality of Sencelles (Mallorca island, Spain)

Hosts	Total analyzed	*Xf* positive[a]	%	*Xylella fastidiosa* subspecies[b]					
				pauca	*mutliplex*	*fastidiosa*	*pauca/ multiplex*	*pauca/ fastidiosa*	*multiplex/ fastidiosa*
Laurus nobilis	6	2	33	1	1				
Lavandula angustifolia	8	8	100	2	6				
Lavandula dentata	6	5	83		4		1		
Nerium oleander	22	6	27	6					
Olea europaea var. *europaea* subsp. *europaea*	57	41	72	37	1		3		
Olea europaea var. *europaea* subsp. *sylvestris*	929	155	17	106	29	2	18		
Polygala myrtifolia	1	1	100				1		
Prunus dulcis	8	1	13		1				
Rhamnus alaternus	190	26	14	5	8	6	3	1	2
Salvia rosmarinus	23	19	83		19				
Thirteen other plant species	78	-							
Totals	1328	264	19.88	157	69	8	26	1	2

[a] Diagnoses performed using the qPCR test of Harper *et al.* (2010).
[b] Subspecies assignation based on the qPCR tests as described by Dupas *et al.* (2019) and Hodgetts *et al.* (2021).

and eight different hosts tested positive for *Xf* subsp. *pauca*, from within a demarcated zone (approx. 1 km radius) around the first disease detection. The infected host species include 124 wild olive trees, 40 cultivated olive trees, nine *Rhamnus alaternus* plants, six of *Nerium oleander*, two of *Lavandula angustifolia*, and one each of *Laurus nobilis*, *Lavandula dentata* and *Polygala myrtifolia* (Table 1).

Despite the numerous cases of *Xf* subsp. *pauca* infections detected (Table 1), all cases analyzed by MLST, up to present, and within the initial focus of the outbreak belong to the ST53 (Figure 2). However, given that *Xf* subsp. *fastidiosa* and *Xf* subsp. *multiplex* were already established in the area, it was not surprising to find some mixed infections by these two subspecies in some individual plants. Eleven percent of *Xf*-positive samples were of mixed infections, with 26 cases of subspp. *pauca/multiplex*, one of subspp. *pauca/fastidiosa* and two of subspp. *multiplex/fastidiosa* (Table 1). The multiple infections probably may increase risk of genetic recombinations in the pathogen and the formation of new sequence types with different virulence and/or host ranges (Potnis *et al.*, 2019).

Although it is premature to draw definitive conclusions, the ST53 strain identified in Mallorca exhibited a level of virulence comparable to that associated with the olive quick decline syndrome observed in Apulia, based on the observed higher severity of symptoms in both wild and cultivated olive trees, compared to those induced by *Xf* subsp. *multiplex* ST81. Efforts are current-

ly underway (December 2024) to isolate the bacterium, to enable complete genome sequencing and carry out comparative analysis of the pathogen's compete genome with those of ST53 strains from Apulia.

A new procedure has been established based on targeted sequence capture enrichment of *Xf* in combination with high-throughput sequencing using the Illumina platform. This is being implemented to provide additional genomic information (Velasco-Amo *et al.*, 2021). Initial results based on approx. 126 genes have shown close genetic relatedness of the ST53 strain infecting the wild olive in Mallorca with all other ST53 strains isolated from Costa Rica and Italy (M.P. Velasco-Amo and B.B. Landa; *unpublished results*).

A complicating factor in containment of ST53 strains is the large population of wild olive trees throughout Mallorca, which may facilitate transmission of the pathogen to cultivated olive trees. Tight wild olive tree population networks can be dense reservoirs of *Xf*, and provide effective dispersal pathways to commercial olive plantations. It is also unclear whether previous infections of wild olive trees by ST81 of *Xf*. subsp. *multiplex* will have influence subsequent infections by ST53. It is estimated that more than 50% of wild olive trees are infected with ST81 (Olmo *et al.*, 2021), so any interaction between ST53 and ST81 in co-infections, regardless of its intensity, could have important epidemiological implications (Jeger and Bragard, 2019).

Epidemiological models have shown that the most effective strategy for preventing spread of *Xf* is to decel-
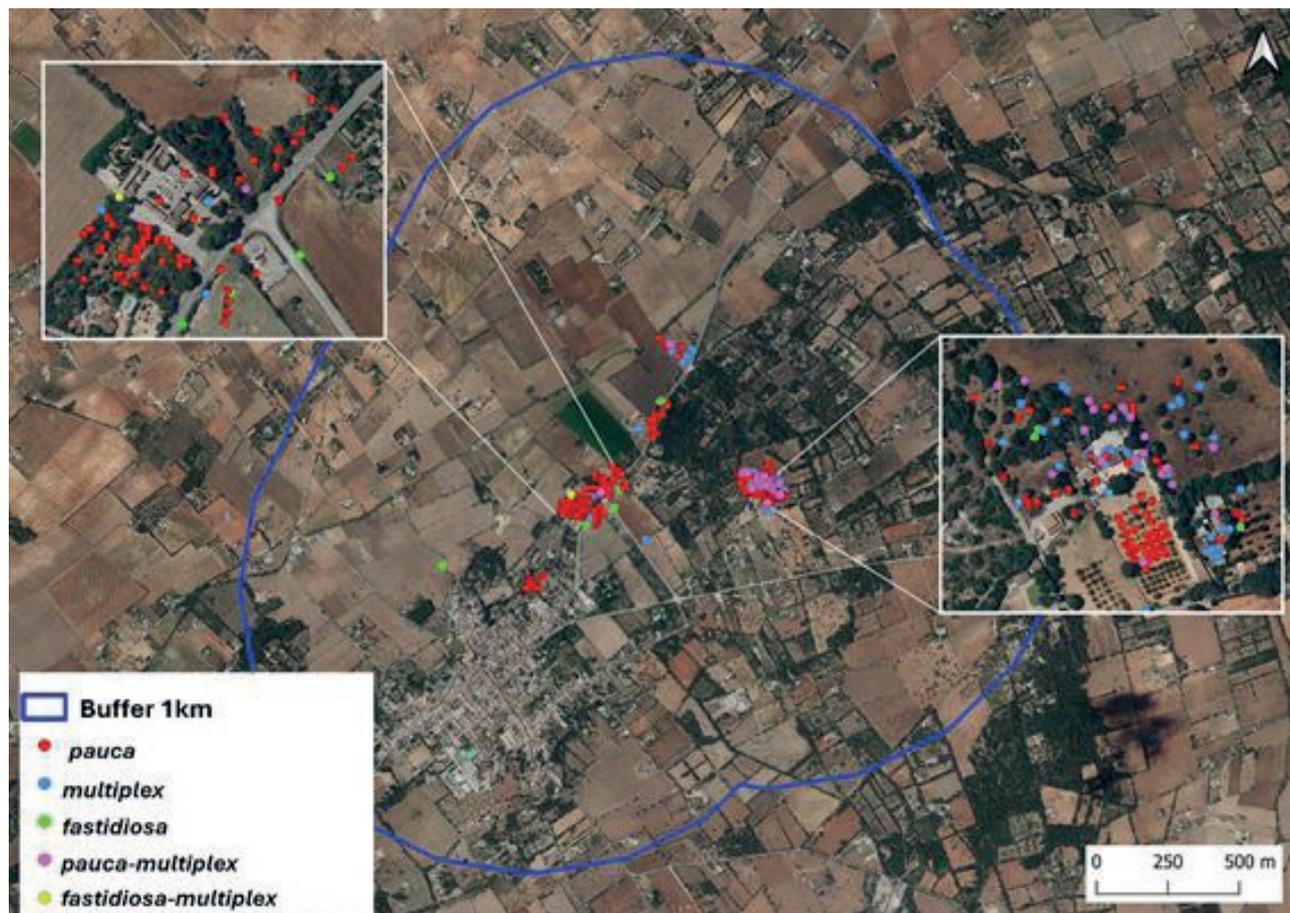
Figure 2. Map of the outbreak focus of *Xylella fastidiosa* subsp. *pauca* ST53 in the municipality of Sencelles, near the centre of Mallorca Island, Spain. The *Xf pauca*-positive plants were found within a radius of < 1 km. Both squares with amplified views show *Xf*-positive plants within the natural vegetation, formed mainly by wild olive trees near farms where other *Xf* subsp. *pauca* ST53 positive plants were found within olive orchards. The positive samples of *Xf* subsp. *pauca* ST53 plants were mixed with other infected with subsp. *multiplex*, and to a lesser extent with subsp. *fastidiosa*. In a few cases, co-infections by *Xf* subsp. *pauca* ST53 and subsp. *multiplex* were found in the same plant (Table 1).

erate transmission chains (White *et al.*, 2020; Giménez-Romero *et al.*, 2023). Accordingly, in Mallorca, the decision has been taken to eradicate infected plants wherever feasible. Although this is a difficult and arguably unattainable objective, the attempt can have significant long-term impacts. It is anticipated that populations of the principal insect vector of *Xf*, *Philaenus spumarius*, will progressively decline in Mallorca in response to rising temperatures associated with climate change (Giménez-Romero *et al.*, 2024). Unsuitable conditions for the vector may become significant in a period of approx. 15 to 20 years. Climate change could be beneficial for containing the outbreak, provided that exponential infection rates can be reduced. Appropriate implementation of these actions will alleviate the economic consequences of *Xf* for the Mallorcan olive production sector in the medium term.

LITERATURE CITED

Carvalho-Luis C., Rodrigues J.M., Martins L.M., 2022. Dispersion of the bacterium *Xylella fastidiosa* in Portugal. *Journal of Agricultural Science and Technology. A* 12(1): 35–41. https://doi.org/10.17265/2161-6256/2022.01.005

Cesbron S., Dupas E., Beaurepère Q., Briand M., Montes-Borrego M., Velasco-Amo MdP., Landa B.B., Jacques M-A., 2020. Development of a nested-MultiLocus Sequence Typing approach for a highly sensitive and specific identification of *Xylella fastidiosa* subspecies directly from plant samples. *Agronomy* 10(8): 1099. https://doi.org/10.3390/agronomy10081099

Denancé N., Legendre B., Briand M., Olivier V., de Boisseson C., … Jacques M.A., 2017. Several subspecies and sequence types are associated with the emergence of *Xylella Fastidiosa* in natural settings in France. *Plant Pathology* 66(7): 1054–1064. https://doi.org/10.1111/ppa.12695

Dupas E., Briand M., Jacques M.A., Cesbron S., 2019. Novel tetraplex quantitative PCR assays for simultaneous detection and identification of *Xylella fastidiosa* subspecies in plant tissues. *Frontiers in Plant Science* 10: 1732. https://doi.org/10.3389/fpls.2019.01732

EPPO (European Plant Protection Organization), 2023. PM 7/24 (5) *Xylella fastidiosa*. *EPPO/OEPP Bulletin* 53(2): 205–276. https://doi.org/10.1111/epp.12923

European Commission, 2016. Regulation (EU) 2016/2031 of the European Parliament of the Council of 26 October 2016 on protective measures against pests of plants, amending Regulations (EU) No 228/2013, (EU) No 652/2014 and (EU) No 1143/2014 of the European Parliament and of the Council and repealing Council Directives 69/464/EEC, 74/647/EEC, 93/85/EEC, 98/57/EC, 2000/29/EC, 2006/91/EC and 2007/33/EC. *Official Journal of the European Union L* 317: 4–104. http://data.europa.eu/eli/reg/2016/2031/oj/eng

Giménez-Romero À., Moralejo E., Matías M.A., 2023. A compartmental model for *Xylella fastidiosa* diseases with explicit vector seasonal dynamics. *Phytopathology* 113(9): 1686–1696. https://doi.org/10.1094/PHYTO-11-22-0428-V

Giménez-Romero À., Iturbide M., Moralejo E., 2024. Global warming significantly increases the risk of Pierce's disease epidemics in European vineyards. *Scientific Reports* 14: 9648. https://doi.org/10.1038/s41598-024-59947-y

Harper S.J., Ward L.I., Clover G.R.G., 2010. Development of LAMP and real-Time PCR methods for the rapid detection of *Xylella fastidiosa* for quarantine and field Applications. *Phytopathology* 100(12): 1282–1288. https://doi.org/10.1094/PHYTO-06-10-0168

Hodgetts J., Glover R., Cole J., Hall J., Boonham N., 2021. Genomics informed design of a suite of real-time PCR assays for the specific detection of each *Xylella fastidiosa* subspecies. *Journal of Applied Microbiology* 131(2): 855–872. https://doi.org/10.1111/jam.14903

Jeger M., Bragard C., 2019. The epidemiology of *Xylella fastidiosa*; A perspective on current knowledge and framework to investigate plant host–vector–pathogen interactions. *Phytopathology* 109: 200–209. https://doi.org/10.1094/PHYTO-07-18-0239-FI

Landa B.B., Castillo A.I., Giampetruzzi A., Kahn A., Román-Écija M, …Almeida R-P.P., 2020. Emergence of a plant pathogen in Europe associated with multiple intercontinental introductions. *Applied and Environmental Microbiology* 86: e01521-19. https://doi.org/10.1128/AEM.01521-19

Moralejo E., Borràs D., Gomila M., Montesinos M., Adrover F., … Landa B. B., 2019. Insights into the epidemiology of Pierce's disease in vineyards of Mallorca, Spain. *Plant Pathololgy* 68: 1458–1471. https://doi.org/10.1111/ppa.13076

Moralejo E., Gomila M., Montesinos M., Borràs D., Pascual A., … Olmo D., 2020. Phylogenetic inference enables reconstruction of a long-overlooked outbreak of almond leaf scorch disease (*Xylella fastidiosa*) in Europe. *Communications Biology* 3: 560. https://doi.org/10.1038/s42003-020-01284-7

Olmo D., Nieto A., Adrover F., Urbano A., Beidas O., … Landa B.B., 2017. First detection of *Xylella fastidiosa* infecting cherry (*Prunus avium*) and *Polygala myrtifolia* plants, in Mallorca Island, Spain. *Plant Disease* 101(10): 1820–1820. https://doi.org/10.1094/PDIS-04-17-0590-PDN

Olmo D., Nieto A., Borràs D., Montesinos M., Adrover F., … Landa B.B., 2021. Landscape epidemiology of *Xylella fastidiosa* in the Balearic Islands. *Agronomy* 11(3): 473. https://doi.org/10.3390/agronomy11030473

Potnis N., Kandel P.P., Merfa M.V., Retchless A.C., Parker J.K., … De La Fuente L., 2019. Patterns of inter- and intrasubspecific homologous recombination inform eco-evolutionary dynamics of *Xylella fastidiosa*. *The ISME journal* 13(9): 2319–2333. https://doi.org/10.1038/s41396-019-0423-y

Saponari M., Boscia D., Nigro F., Martelli G.P., 2013. Identification of DNA sequences related to *Xylella fastidiosa* in oleander, almond and olive trees exhibiting leaf scorch symptoms in Apulia (southern Italy). *Journal of Plant Pathology* 95(3): 668. https://doi.org/10.4454/JPP.V95I3.035

Velasco-Amo M.P., Arias-Giraldo L.F., Marín Sanz J.A., Fernández Soria V.M., Imperial J., Landa B.B., 2021. Assessing genome-wide diversity in *Xylella fastidiosa* through target enrichment via hybridization-based capture from natural host plant and insect samples. In: *Book of Abstracts of the 3rd European conference on* Xylella fastidiosa *and XF-ACTORS final meeting*, 61, April 26-30, On-line event, 2021.

Velasco-Amo M.P., Arias-Giraldo L.F., Olivares-García C., Denancé N., Jacques M.-A., Landa, B.B., 2022. Use of *tra*C Gene to type the incidence and distribution of pXFAS_5235 plasmid-bearing strains of *Xylella fastidiosa* subsp. *fastidiosa* ST1 in Spain. *Plants* (Basel) 11(12):1562. https://www.mdpi.com/2223-7747/11/12/1562. Erratum in: *Plants* (Basel). 2024. 13(2): 200. https://doi.org/10.3390/plants13020200.

White S.M., Navas-Cortés J.A., Bullock J.M., Boscia D., Chapman D.S., 2020. Estimating the epidemiology of emerging *Xylella fastidiosa* outbreaks in olives. *Plant Pathology* 69(8): 1403–1413. https://doi.org/10.1111/ppa.13238

Yuan X., Morano L., Bromley R., Spring-Pearson S., Stouthamer R., Nunney, L., 2010. Multilocus Sequence Typing of *Xylella fastidiosa* causing Pierce's disease and oleander leaf scorch in the United States. *Phytopathology* 100(6): 601–611. https://doi.org/10.1094/PHYTO-100-6-0601

ORCID:
MC: 0009-0002-2238-8395
MCL: 0000-0002-6547-7702
PB: 0000-0003-1287-1711

Short Notes

"AFLA-peanut", a mechanistic prototype model to predict aflatoxin B1 contamination

Matteo CROSTA, Marco CAMARDO LEGGIERI*, Paola BATTILANI

Department of Sustainable Crop Production, Università Cattolica del Sacro Cuore, Via Emilia Parmense 84, Piacenza, Italy
*Corresponding author. E-mail: marco.camardoleggieri@unicatt.it

Summary. Italian production of peanuts has recently increased. Aflatoxin B1 (AFB1) contamination of peanuts is currently not in Italy, but changing climatic conditions of the Mediterranean region may increase risks posed by this mycotoxin. A mechanistic weather-driven prototype model to predict AFB1 contamination in peanuts was developed by adapting the mechanistic AFLA-maize model for the *Aspergillus flavus*-peanut pathosystem. The peanut growth stages were examined to develop a phenology model based on growing degree days (GDD), which was linked to an *A. flavus* infection cycle model, and exploited to develop the "AFLA-peanut" prototype model. Starting from sowing, 686 GDD were required to reach flowering (as the critical growth stage for *A. flavus* infection), and 1925 GDD were required to reach harvesting, in a short season peanut variety. Variability of the AFB1 index, across years and locations, highlighted the capacity of AFLA-peanuts to account for weather data inputs in predicting AFB1 contamination risks. Although model validation will be mandatory to assess AFLA-peanut performance, this study has provided the first evidence that the prototype model could become an important tool for aflatoxin risk management.

Keywords. *Aspergillus flavus*, model transfer, weather, phenology, mycotoxin, climate change.

INTRODUCTION

Peanut (*Arachis hypogaea* L., *Fabaceae*), also known as groundnut, is an annual herbaceous plant, which is native to Central and South America, and is characterized by fruit development beneath soil surfaces. Peanut crop production now occurs in many countries thanks to its beneficial nutritional properties (Mingrou *et al.*, 2022). Annual world peanut production has grown by over 54 million tons per year, with China as the main producer, followed by India, Nigeria, and the United States of America (FAOSTAT, 2024). In the Mediterranean region, peanut production is widespread, especially in Turkey and Egypt, and limited production occurs in Spain and Greece (Sannino *et al.*, 2020; Özkaya *et al.*, 2024). Italian peanut production is increasing, from 22 tons per year in 2017 to 712 tons per year in 2024 (Istat, 2024).

Aspergillus flavus infects and colonizes several crops, and among these, peanut is one of the most susceptible (Horn, 2005; Amaike and Keller, 2011; Payne, 2014). Aflatoxins (AFs) are toxic and cancerogenic substances. Consumption of food and feed contaminated by these compounds can cause several harmful effects, including genotoxicity, hepatotoxicity, carcinogenicity, and nephrotoxicity, and have mutagenic, teratogenic, cytotoxic, and immunosuppressive effects (Shephard, 2008; Aristil *et al.*, 2020, Singh *et al.*, 2021). Contamination can occur or increase throughout the peanut supply chain, from the field, during crop growth, natural drying after digging, harvesting, storage and product delivery, and to eventual processing (Torres *et al.*, 2014; Cervini *et al.*, 2022).

Italy is considered at low risk for AFs contamination in peanuts, and this is an added value for the crop in this country. However, the spread of *A. flavus* in Mediterranean countries, including Italy, due to climate changes, may increase the risk of AF contamination in Italian peanuts, as has occurred in maize from 2003 (Piva *et al.*, 2006; Giorni *et al.*, 2007; Kos *et al.*, 2013; Battilani *et al.*, 2016; Moretti *et al.*, 2019). Applying suitable management practices along the peanut value chain is likely to reduce the risk of AF contamination (Chulze *et al.*, 2024).

Mechanistic models that consider interactions between *A. flavus*, host plants, and the environment to predict the risk of AF contamination are important tools in Integrated Pest Management (IPM) for sustainable agriculture. In particular, exploiting these models for sustainable agriculture promotes enhancement of agricultural practices, refinement of harvest strategies, and implementation of post-harvest measures, that aim to reduce potential risks for consumer exposure to AFs.

Some studies have aimed to predict AF contamination using crop growth simulation models. In Mali, Boken *et al.* (2008), through the CSM-CROPGRO-Peanut model, which is based on crop genetics, agricultural practices, soil data, and meteorological data, estimated peanut reproductive stages and crop yields. With this information Boken *et al.* (2008) performed regression analysis to correlate AF contamination measured post-harvest with weather conditions during the reproductive stages. Craufurd *et al.* (2006) carried out a similar study in Niger, using the CROPGRO-Peanut model to simulate crop growth and yield. Aflatoxin contamination at harvest was correlated with the fraction of extractable soil water (FESW) in the crop rhizosphere during the reproductive phase. Chauhan *et al.* (2010) in Australia also developed a predictive model based on the crop simulation model APSIM (Agricultural Production Systems Simulator). This model uses the APSIM's peanut module to simulate crop growth. It calculates an aflatoxin temperature factor (ATF) during the last 40% of growth when soil water availability is below 0.20 (range 0-1), and the accumulated ATF generates an AF risk index (ARI). All of these models are empirical, and require recalibration for use outside their original geographic contexts, for example for use in the Mediterranean basin.

The present study aimed to develop a mechanistic model, as a flexible tool usable across different geographic regions without requirement for adjustments (Battilani and Camardo Leggieri, 2015). The mechanistic model AFLA-maize was adapted for the *A. flavus*-peanut pathosystem, following the successful application to AFLA-pistachio nuts (Battilani *et al.*, 2013; Kaminiaris *et al.*, 2020). The first step was to study peanut growth stages, and then build a phenological model based on growing degree days (GDD). The model was then integrated with the model for the *A. flavus* infection cycle model, and was exploited to produce the prototype AFLA-peanut predictive model.

MATERIALS AND METHODS

Location of field studied

Between 2021 and 2023, meteorological data were collected from a total of 14 locations across Northern Italy provinces (Figure 1), including Ferrara (one location in 2021, six in 2022, two in 2023), Modena (one location in 2022), Cuneo (one in 2022), Verona (two in 2023), and Pordenone (one in 2023). The meteorological data from the 2022 and 2023 in the respective loca-
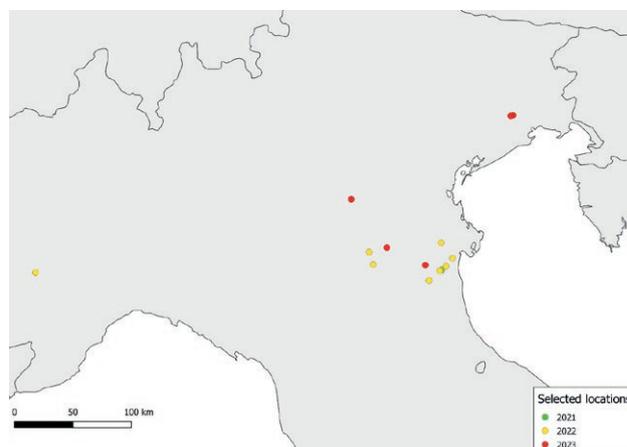
Figure 1. Geographical distribution of selected fields in Northern Italy across years (2021, 2022 and 2023).

tions were used as input to run the AFLA-peanut model. Among these production areas, four fields in the province of Ferrara (2021 and 2022), and one field in Pordenone (2023), were specifically selected to observe peanut growth stages for the peanut variety Lotos.

Lotos is commonly cultivated in Italy, and is characterised by early maturity and a crop cycle length of 120 to 130 d. Peanut season length is classified as "early" to 130 days, "medium" 133 to 139 d, "medium-late" 140 to 145 d, and "late-maturing" 146 to 155 d (Carter *et al.*, 2016; GRDC, 2018).

Meteorological data

Hourly data of air temperature (T, °C), relative humidity (RH, %), and rainfall (R, mm) were collected from the agro-meteorological network in Emilia Romagna region, from 1 January to 31 October during 2021, 2022 and 2023 (Table 1s, supplementary material). The Emilia Romagna region is virtually shared by a grid of squares, each of 5 km², with meteorological data delivered for each square (Arpae, 2024). These data come from all available sources, including meteorological stations and radar (Bottarelli and Zinoni, 2002). The proper squares were selected based on the locations of the monitored peanut fields. For the sampling points in other regions, meteorological data were provided by "Agrometeo Service" Image Line® and AgroNotizie®.

The meteorological data were used: i) to develop the peanut phenological sub-model included in the AFLA-peanut model, and ii) as input to run AFLA-peanut.

Growth stages

Crop phenology descriptions were based on field observations carried out every 2 weeks, from crop emergence to harvesting, during the complete peanut growth period (May to October). The growth stages were defined according to the BBCH scale (Meier, 2001), and after analysis of existing literature, the crucial peanut growth stages most susceptible for *A. flavus* infection were then indicated (Cole *et al.*, 1986; Pitt *et al.*, 1991; Horn, 2005).

The GDDs were calculated, starting from sowing date, for each observed peanut growth stage (Mcmaster and Wilhelm, 1997), using the following equation:

$$GDD_i = [(T_{max,i}-T_{min,i})/2] - T_{base},$$

where T_{max} is the hourly maximum temperature, T_{min} is the hourly minimum temperature, and T_{base} is the base temperature of 10°C.

T_{base} was set as the low threshold for peanut growth (Ketring and Wheless, 1989; Canavar and Kaynak, 2010; Kingra and Kaur, 2012). Collected data were assessed with literature sources (Banterng *et al.*, 2003; Canavar and Kaynak, 2010), leading to development of a crop phenology model for peanuts based on GDD (Canavar and Kaynak, 2010).

Predictive model

Commencing from the existing relational diagrams of AFLA-maize and AFLA-pistachio (Battilani *et al.*, 2013; Kaminiaris *et al.*, 2020), a new diagram was developed following the principle of "system analysis" (Leffelaar, 1993). The diagram was composed of different state variables linked in a coherent mathematical framework, which operates in a predictive model to generate a cumulative index for aflatoxin B1 (AFB1) contamination (AFB1-I). The predictive model, named "AFLA-peanut", is a weather-driven model that predicts crop phenology and *A. flavus* behaviour based, on meteorological data (T, RH, and R).

RESULTS

Meteorological data

Data from selected locations are shown in Table 1s (supplementary materials). Temperatures in 2023 were characterised by high variability between locations. Nevertheless, during the first part of the year (January to April), and in September, temperatures were high (location daily thermal sum mean = 1012.9 °C, and 648.8 °C, respectively), compared to the same periods of 2021 (904.9 and 615.5 °C) and 2022 (888.5 and 595.8 °C). Nevertheless, Cavallermaggiore, in 2022, was the warmest location, compared to the other locations and years, from January to April (daily thermal sum = 949.7 °C). The opposite was recorded from May to July 2022, as daily thermal sum means were higher than in 2023 and 2021. For precipitation, high variability was observed between locations over the 3 years. However, drier periods occurred in 2022 and 2021 than in 2023, from May to July and during October. The exception was in Ostellato, in July of 2021 and in June of 2022. Similarly, in September of 2023, Bondeno and Cordovado had similar rainfall and were comparable to some of the other locations of 2022. In particular, during this month, the greatest amounts of precipitation were recorded in 2021. In 2023, Bondeno and Cordovado were the rainiest locations.

Peanut growth stages

GDD were computed for the main growth stages of peanuts, based on field observations conducted in 2021, 2022, and 2023 (Figure 2). The data collected were comparable to data reported previously for the early variety Florispan, with the same season length as Lotos, considered in the present study (Table 2s). For available data for late maturing varieties, required GDD increase from the beginning of flowering until harvest is approx. +20%.

Results of the relationships between GDD and BBCH are shown in Figure 2. Crop phenology can be split between vegetative and reproductive growth stages. The vegetative stages, from sowing (BBCH 0) to the beginning of flowering (BBCH 61), lasted for about 5 weeks, requiring approx. 425 GDD. The reproductive stage, which extends from flowering (BBCH 65) to harvest (BBCH 99), requires an additional 1239 GDD to be completed. Flowering was identified as the critical stage for *A. flavus* infection.

Predictive model

The infection cycle of *A. flavus* on peanuts is illustrated in the relational diagram in Figure 3. Inoculum source, which is not quantified in the model, represents the starting point of the cycle, considering that suitable environmental conditions influence the sporulation rate of the *A. flavus* (SpoR), promoting the production of spores. Subsequently, the spores produced on inoculum sources (SoI) are then dispersed according to a dispersal rate (DispR) and reach the peanut plants (DSoP). When the peanut crop is at a critical growth stage (GS) for *A. flavus* infection, from flowering, and the environmental conditions are suitable, the spores germinate, and the fungus grows on pegs and pods (GoPP), leading to infection of peanut seeds (IPS). These stages are regulated by the spore germination and growth rates, which are influenced by T, RH, and R. Once the seeds are infected,

the fungus may produce AFB1 (AFB1-I) according to an AFB1 production rate (AFB1R).

AFB1-I was computed daily, using hourly data collected in all the available meteorological data sources. Cumulative AFB1-I, from peanut flowering to harvesting, is the final output of the AFLA-peanut model. The AFB1-I index showed high variability across the 3 years and the locations considered in the present study (Table 1).

DISCUSSION AND CONCLUSIONS

Peanut production in Italy has increased in recent years, although AFB1 contamination has been only very rarely detected, and then only as traces (Crosta *et al.*, in preparation). However, increasing climate variability, with extreme events such as heat waves and droughts, attributed to climate change in the Mediterranean basin, underscore the need for a robust, weather driven-mechanistic model to predict AFB1 contamination risks (Battilani and Camardo Leggieri, 2015; Battilani *et al.*, 2016). Meteorological data collected in the present research has revealed distinct patterns across the years and locations studied, confirming the impacts of climate on weather dynamics at regional scale (Leggieri *et al.*, 2020). While drought conditions were more marked in 2021 and 2022, 2023 had more favourable precipitation for peanut growth. The locations selected for this had considerable rainfall differences and distribution throughout the growing seasons. AFB1-I, provided as output by AFLA-peanut, was characterized by high variability across years and locations, indicating the influence of meteorological data used as input, with temperature playing an important role, as has been previously observed for AFLA-maize and AFLA-pistachio (Battilani *et al.*, 2013; Kaminiaris *et al.*, 2020). In the present study, the model was transferred from the maize pathosystem to that for peanut, without modifying the fungal component, as was previously done for pistachio. Sensitivity analysis was therefore not applied because the results were con-

BBCH	0	9	24	61	62	65	66	73	79	85	89	99
Growth stage	Sowing	Emergence	4th lateral shoot visible	Beginning of flowering	Peg formation	Flowering	Pegs penetrate the soil	Beginning of pods filling	Complete pods development	50% of pods are ripe	Complete maturity	Harvesting
GDD	0	92*	297	425	560	686	718	907	1304	1500	1759	1925

Figure 2. Crop phenology (described by the BBCH scale), mean GDD calculated for each growth stage, of the early peanut variety Lotos, observed in the fields of Ferrara and Pordenone from 2021 to 2023. T_{base}= 10°C was considered to calculate GDD.
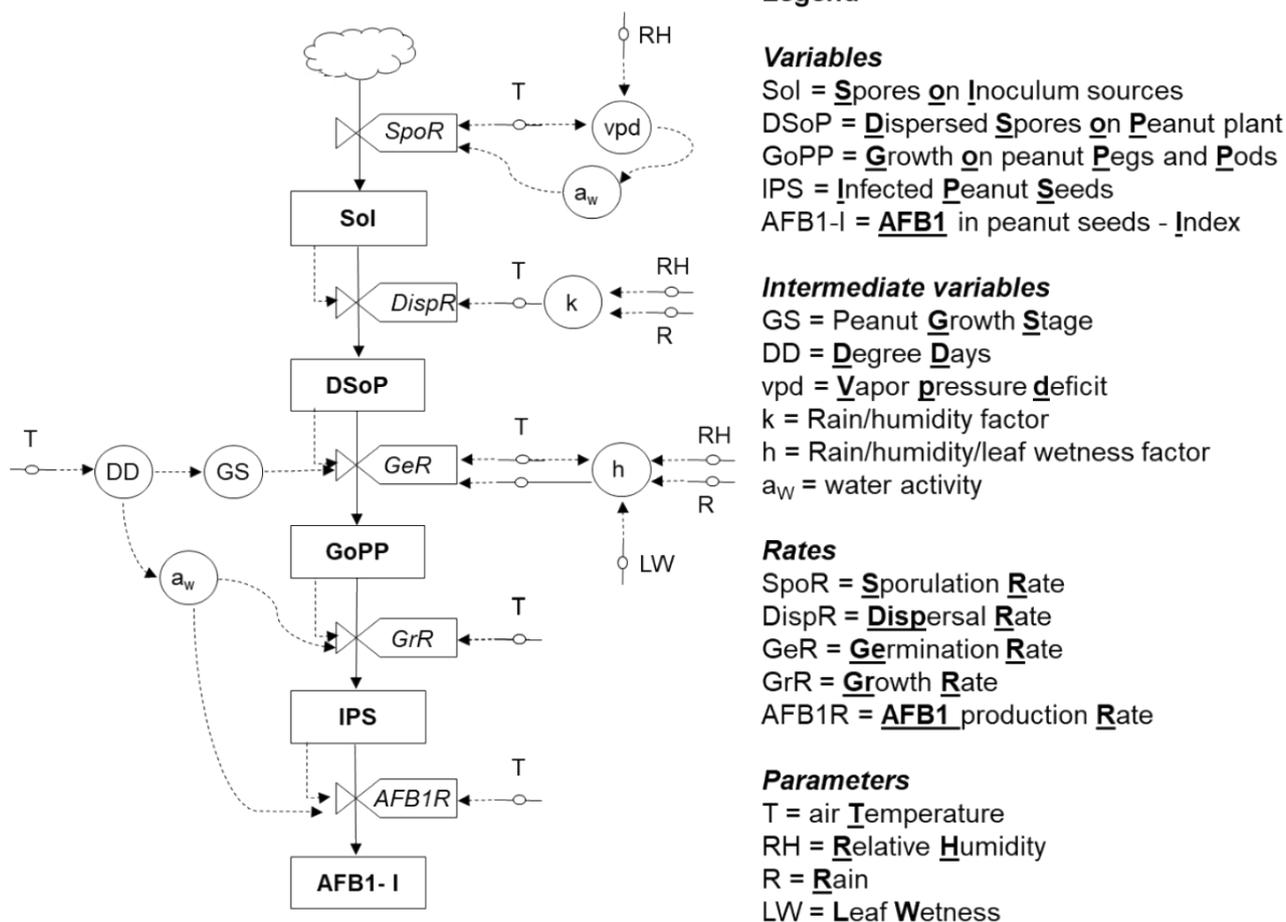
Figure 3. Relational diagram for the *Aspergillus flavus* infection cycle and aflatoxin production on peanuts.

sistent with those reported by Battilani *et al.* (2013) and Battilani *et al.* (2016).

Despite the differences in meteorological conditions between the three growing areas, GDDs from different sources and related to peanut growth stages agreed. This indicated that the peanut phenology model developed in the present study is reasonably robust (Banterng *et al.*, 2003; Canavar and Kaynak, 2010). For early season peanut varieties, 686 GDD were related to flowering (the critical stage for *A. flavus* infection), and 1925 GDD were related to peanut harvest.

The model presented here for AF contamination risk prediction is an improvement compared with existing empirical models, such as those by Craufurd *et al.* (2006), Boken *et al.* (2008), and Chauhan *et al.* (2010). The mechanistic approach of AFLA-peanut can adapt to diverse climatic profiles without the need for significant adjustments, positioning AFLA-peanut as a valuable tool

for both regional and international contexts (Battilani and Camardo Leggieri, 2015). The model's flexibility and adaptability to environmental conditions are especially relevant for the Mediterranean environment, where climate affects traditional agricultural practices, and can threaten crop quality and safety (Battilani and Camardo Leggieri, 2015; Chulze *et al.*, 2024).

Results from the present study emphasize the need for thorough validation of the AFLA-peanut model. Georeferenced data on weather and AFB1 contamination from diverse peanut production regions, and additional data on peanut cropping systems, are important for achieving this aim. Such validation will provide important insights into the model's prediction accuracy, and will strengthen its applicability in a broad range of environments.

The AFLA-peanut model's ability to incorporate weather variability offers a strategic advantage for proactively managing AFs risks, which are increasingly chal-

Table 1. Summary data related to selected field locations in northern Italy in 2022 and 2023, with geographical coordinates, dates of sowing and complete maturity, and AFB1-I, the AFs cumulative indices generated as output by the prototype AFLA-peanut model.

Year	Location	Province[a]	Long	Lat	Sowing	Complete maturity	AFB1-I
2021	Ostellato	FE	12.063674	44.699471	10/05	30/09	7454
2022	Ostellato	FE	12.046193	44.695327	10/05	13/09	6018
	Lagosanto	FE	12.188809	44.788623	10/05	07/09	4552
	Volania	FE	12.116027	44.728864	10/05	10/09	6209
	Dosso	FE	11.328936	44.759730	10/05	04/10	852
	Argenta	FE	11.926363	44.623563	11/05	22/09	2290
	Mezzogoro	FE	12.071466	44.911498	09/05	16/09	3707
	Finale Emilia	MO	11.287771	44.856394	19/05	29/09	828
	Cavellermaggiore	CN	7.681548	44.715500	07/05	28/09	532
2023	Bondeno	FE	11.481934	44.887692	30/05	29/09	5465
	Ostellato	FE	11.891678	44.743345	27/05	21/09	8188
	Bovolone	VR	11.109327	45.270235	14/06	03/10	1708
	Bovolone	VR	11.111219	45.268570	14/06	03/10	1708
	Cordovado	PN	12.914613	45.870081	27/05	03/10	3408

[a] FE = Ferrara, MO = Modena, CN = Cuneo, VR = Verona, and PN = Pordenone

lenging under the Mediterranean region's shifting climate conditions. As climate change accelerates, extreme weather events are expected to intensify, directly affecting crop health and AF contamination (Battilani *et al.*, 2016; Chulze *et al.*, 2024). These climate changes pose threats to food safety, and to the economic stability of agricultural sectors and to food security. *Aspergillus flavus* outbreaks reduce crop yields and restrict market access for affected produce (Moretti *et al.*, 2019) in areas where peanuts contribute significantly to farmer income.

AFLA-peanut could be an important tool for safeguarding peanut supply chains and consumer health, by providing early risk alerts, once its robustness is confirmed through validation. This has already been demonstrated for AFLA-maize and AFLA-pistachio (Battilani *et al.*, 2013; Kaminiaris *et al.*, 2020). By anticipating contamination risks, these models help mitigate adverse health effects and economic losses associated with the disposal of unsafe product batches. Implementation of costly interventions could be justified in cases of high AF contamination risk.

Future research should focus on validating the AFLA-peanut model using diverse datasets with a broad range of AFB1 contamination to further assess the model's predictive performance. In subsequent developments, the model output could be a foundation for a comprehensive Decision Support System (DSS). This would integrate additional variables, such as peanut genetic, agricultural, and soil factors, to enhance AF risk prediction and support improved peanut safety management within the framework of sustainable agriculture.

LITERATURE CITED

Amaike S., Keller N.P., 2011. *Aspergillus flavus. Annual Review of Phytopathology* 49: 107–133. https://doi.org/10.1146/annurev-phyto-072910-095221

Aristil J., Venturini G., Maddalena G., Toffolatti S.L., Spada A., 2020. Fungal contamination and aflatoxin content of maize, moringa and peanut foods from rural subsistence farms in South Haiti. *Journal of Stored Products Research* 85: 101550. https://doi.org/10.1016/j.jspr.2019.101550

Arpae, 2024. Hourly meteorological open data. Available at: https://www.arpae.it/it/temi-ambientali/clima/dati-e-indicatori/open-data-meteo-clima/dataset-meteo-climatici

Banterng P., Patanothai A., Pannangpetch K., Jogloy S., Hoogenboom G., 2003. Seasonal variation in the dynamic growth and development traits of peanut lines. *Journal of Agricultural Science* 141(1): 51–62. https://doi.org/10.1017/S0021859603003435

Battilani P., Camardo Leggieri M., Rossi V., Giorni P., 2013. AFLA-maize, a mechanistic model for *Aspergillus flavus* infection and aflatoxin B1 contamination in maize. *Computers and Electronics in Agriculture* 94: 38–46. https://doi.org/10.1016/j.compag.2013.03.005

Battilani P., Camardo Leggieri M., 2015. Predictive modelling of aflatoxin contamination to support maize chain management. *World Mycotoxin Journal* 8(2): 161–170. https://doi.org/10.3920/WMJ2014.1740

Battilani P., Toscano P., Van Der Fels-Klerx H.J., Moretti A., Camardo Leggieri M., … Robinson T., 2016. Aflatoxin B1 contamination in maize in Europe increases due to climate change. *Scientific Reports* 6: 1–7. https://doi.org/10.1038/srep24328

Boken V. K., Hoogenboom G., Williams J. H., Diarra B., Dione S., Easson G. L., 2008. Monitoring peanut contamination in Mali (Africa) using AVHRR satellite data and a crop simulation model. *International Journal of Remote Sensing* 29(1): 117–129. https://doi.org/10.1080/01431160701264250

Bottarelli L., Zinoni F., 2002. La rete meteorologica regionale. *Il Divulgatore* 5: 13–17.

Canavar Ö., Kaynak M. A., 2010. Growing degree day and sunshine radiation effects on peanut pod yield and growth. *African Journal of Biotechnology* 9(15): 2234–2241. https://doi.org/10.5897/AJB10.1432

Carter E.T., Troy P., Rowland D.L., Tillman B.L., Wynne K.W., … Mulvaney, M., 2016. Methods to evaluate peanut maturity for optimal seed quality and yield. *Edis 2016* (7). https://doi.org/10.32473/edis-ag411-2016

Cervini C., Verheecke-Vaessen C., He T., Mohammed A., Magan N., Medina A., 2022. Improvements within the peanut production chain to minimize aflatoxins contamination: an Ethiopian case study. *Food Control* 136: 108622. https://doi.org/10.1016/j.foodcont.2021.108622

Chauhan Y.S., Wright G.C., Rachaputi R.C.N., Holzworth D., Broome A., … Robertson M.J., 2010. Application of a model to assess aflatoxin risk in peanuts. *Journal of Agricultural Science* 148(3): 341–351. https://doi.org/10.1017/S002185961000002X

Chulze S.N., Alaniz Zanon M.S., Taniwaki M.H., Tsitsigiannis D., Olsen M., … Battilani, P., 2024. Aflatoxins in the nut chains: strategies to reduce their impact on consumer's health and economic losses. *World Mycotoxin Journal* 17(1): 33–56. https://doi.org/10.1163/18750796-bja10003

Cole R.J., Hill R.A., Blankenship P.D., Sanders T.H., 1986. Color mutants of *Aspergillus flavus* and *Aspergillus parasiticus* in a study of preharvest invasion of peanuts. *Applied and Environmental Microbiology* 52(5): 1128–1131. https://doi.org/10.1128/aem.52.5.1128-1131.1986

Craufurd P.Q., Prasad P.V.V., Waliyar F., Taheri, A., 2006. Drought, pod yield, pre-harvest *Aspergillus* infection and aflatoxin contamination on peanut in Niger. *Field Crops Research* 98(1): 20–29. https://doi.org/10.1016/j.fcr.2005.12.001

FAOSTAT, 2024. Food and Agriculture Organization of the United Nations. Available at: https://www.fao.org/faostat/en/#data/QCL/visualize. Accessed October 02, 2024.

Giorni P., Magan N., Pietri A., Bertuzzi T., Battilani, P., 2007. Studies on *Aspergillus* section *Flavi* isolated from maize in northern Italy. *International Journal of Food Microbiology* 113(3): 330–338. https://doi.org/10.1016/j.ijfoodmicro.2006.09.007

GRDC, 2018. *Peanuts Northern Region - GrowNotes*. Available at: https://grdc.com.au/resources-and-publications/grownotes/crop-agronomy/peanutgrownotes

Horn B.W., 2005. Colonization of wounded peanut seeds by soil fungi: selectivity for species from *Aspergillus* section *Flavi*. *Mycologia* 97(1): 202–217. https://doi.org/10.1080/15572536.2006.11832854

Istat, 2024. *Istat: coltivazioni*. Available at: https://www.istat.it/statistiche-per-temi/economia/agricoltura/#Microdati. Accessed October 02, 2024.

Kaminiaris M.D., Leggieri M.C., Tsitsigiannis D.I., Battilani P., 2020. AFLA-PISTACHIO: Development of a mechanistic model to predict the aflatoxin contamination of pistachio nuts. *Toxins* 12(7): 445. https://doi.org/10.3390/toxins12070445

Ketring D.L., Wheless T. G., 1989. Thermal time requirements for phenological development of peanut. *Agronomy Journal* 81(6): 910–917. https://doi.org/10.2134/agronj1989.00021962008100060013x

Kingra P.K., Kaur P., 2012. Effect of dates of sowing on thermal utilisation and heat use efficiency of groundnut cultivars in Central Punjab. *Journal of Agricultural Physics,* 12(1): 54–62.

Kos J., Mastilović J., Hajnal E.J., Šarić B., 2013. Natural occurrence of aflatoxins in maize harvested in Serbia during 2009-2012. *Food Control* 34(1): 31–34. https://doi.org/10.1016/j.foodcont.2013.04.004

Leffelaar P.A., 1993. Basic elements of dynamic simulation. In: *On System Analysis and Simulation of Ecological Processes with Examples in CSMP and FORTAN* (Leffelaar P.A., ed), Springer Netherlands, Dordrecht, Netherlands, 11–27. https://doi.org/10.1007/978-94-011-2086-9_2

Leggieri M.C., Lanubile A., Dall'Asta C., Pietri A., Battilani, P., 2020. The impact of seasonal weather variation on mycotoxins: Maize crop in 2014 in northern Italy as a case study. *World Mycotoxin Journal* 13(1): 25–36. https://doi.org/10.3920/WMJ2019.2475

Mcmaster G.S., Wilhelm W.W., 1997. Growing degree-days: one equation, two interpretations. *Agricultural and Forest Meteorology* 87(1): 300.

Meier U., 2001. *Growth stages of mono-and dicotyledonous plants: BBCH Monograph*. 2nd ed. Federal Biological Research Centre for Agriculture and Forestry, Bonn, Germany.

Mingrou L., Guo S., Ho C.T., Bai, N., 2022. Review on chemical compositions and biological activities of peanut (*Arachis hypogaea* L.). *Journal of Food Biochemistry* 46(7): 1–16. https://doi.org/10.1111/jfbc.14119

Moretti A., Pascale M., Logrieco A.F., 2019. Mycotoxin risks under a climate change scenario in Europe. *Trends in Food Science and Technology* 84: 38–40. https://doi.org/10.1016/j.tifs.2018.03.008

Özkaya S., Soylu S., Kara M., Gümüş Y., Soylu E.M., … Lavkor I., 2024. Disease prevalence, incidence, morphological and molecular characterisation of Lasiodiplodia pseudotheobromae causing collar rot disease on peanut plants in Turkey. *Journal of Plant Diseases and Protection* 131(5): 1639-1651. https://doi.org/10.1007/s41348-024-00933-x

Payne G., Yu J., 2010. Ecology, development and gene regulation in *Aspergillus flavus*. In: *Aspergillus: Molecular Biology and Genomics* (M. Masayuki, G. Katsuya, ed.), Caister Academic Press, Norfolk, United Kingdom, 157-171.

Pitt J.I., Dyer S.K., McCammon S., 1991. Systemic invasion of developing peanut plants by *Aspergillus flavus*. *Letters in Applied Microbiology* 13(1): 16–20. https://doi.org/10.1111/j.1472-765X.1991.tb00558.x

Piva G., Battilani P., Pietri A., 2006. Emerging issues in southern Europe: Aflatoxins in Italy. In *The Mycotoxin Factbook: Food and Feed Topics* (D. Barug, D. Bhatnagar, H. P. van Egmond, J. W. van der Kamp, W. A. van Osenbruggen, A. Visconti, ed.), Wageningen Academic Publishers, Wageningen, Netherlands. https://doi.org/10.3920/978-90-8686-587-1

Sannino M., Piscopo R., Assirelli A., Serrapica F., Caracciolo G., … Faugno, S. 2020. Evaluation of *Arachis hypogaea* as new multipurpose crop for central-sud Italy. In: *European Biomass Conference and Exhibition Proceedings*, On-line, 6-9 July 2020, 155–159.

Shephard G.S., 2008. Impact of mycotoxins on human health in developing countries. *Food Additives and Contaminants - Part A Chemistry, Analysis, Control, Exposure and Risk Assessment* 25(2): 146–151. https://doi.org/10.1080/02652030701567442

Singh U., Gupta S., Gupta M., 2021. A review study on biological ill effects and health hazards of aflatoxins. *Asian Journal of Advances in Medical Science* 3(1): 1–8. https://mbimph.com/index.php/AJOAIMS/article/view/1834

Torres A.M., Barros G.G., Palacios S.A., Chulze S.N., Battilani, P., 2014. Review on pre- and post-harvest management of peanuts to minimize aflatoxin contamination. *Food Research International* 62: 11–19. https://doi.org/10.1016/j.foodres.2014.02.023

Adaskaveg James, Riverside, California, USA
Aglietti Chiara, Florence, Italy
Agustí-Brisach Carlos, Córdoba, Spain
Alaniz Sandra, Montevideo, Uruguay
Alkowni Raed, Nablus, Palestine
Almeida Rodrigo, Berkeley, California, USA
Altomare Claudio, Bari, Italy
Alves Artur, Aveiro, Portugal
Angelini Elisa, Conegliano (TV), Italy
Armengol Forti Josep, Valencia, Spain
Arzanlou Mahdi, Tabriz, Iran
Baaijens Regina, Adelaide, Australia
Bahar Ofir, Rishon LeZion, Israel
Balestra Giorgio, Viterbo, Italy
Baránek Miroslav, Brno, Czech Republic
Baroncelli Riccardo, Bologna, Italy
Barrès Benoit, Maisons-Alfort, France
Marek Barta, Bratislava, Slovakia
Berbegal Mónica, Valencia, Spain
Blumenstein Kathrin, Freiburg, Germany
Bolton Melvin, Fargo, North Dakota, USA
Bonaterra Carreras Anna, Girona, Spain
Burbank Lindsey, Washington, D.C., USA
Camardo Leggieri Marco, Milan, Italy
Candresse Thierry, Bordeaux, France
Carillo Petronia, Caserta, Italy
Carlucci Antonia, Foggia, Italy
Chammem Hamza, Elvas, Portugal
Chiumenti Michela, Bari, Italy
Cirilli Marco, Milan, Italy
Cobos Rebeca, León, Spain
Cohen Daniel, Auckland, New Zealand
Congdon Benjamin, South Perth, Australia
Contaldo Nicoletta, Bologna, Italy
Corsi de Filippi Marta Cristina, Santo Antônio de Goiás, Brazil
Coutts Brenda, Perth WA, Australia
Crous Pedro, Utrecht, Netherlands
Dardani Greta, Torino, Italy
Davino Salvatore, Palermo, Italy
De Abreu Lucas Magalhães, Viçosa, Brazil
De Cal Antonieta, Madrid, Spain
de la Fuente Leonardo, Auburn, Alabama, USA
Dehnen-Schmutz Katharina, Coventry, England
Del Frari Giovanni, Lisbon, Portugal
Delić Duška, Banja Luka, Bosnia and Herzegovina
Di Marco Stefano, Bologna, Italy
Dissanayake Asha, Chengdu, China
Dreo Tanja, Ljubljana, Slovenia

Druzhina Irina, London, England
Elbeaino Toufic, Bari, Italy
Eskalen Akif, Davis, California, USA
Fetch Tom, Ottawa, Canada
Fontaine Florence, Reims, France
Foster Gary, Bristol, UK
Fowkes Aimee, York, UK
Frejlichova Lucie, Brno, Czech Republic
Fuchs Marc, New York, New York, USA
Gálvez Patón Laura, Madrid, Spain
González María Teresa, Madrid, Spain
Gonzalez-Dominguez Elisa, Piacenza, Italy
Gramaje David, Logroño, Spain
Guarnaccia Vladimiro, Torino, Italy
Gusella Giorgio, Catania, Italy
Habili Nuredin, Adelaide, Australia
Halleen Francois, Stellenbosch, South Africa
Harteveld Dalphy, Wageningen, Netherlands
Hassan Mohamed M., Ta'if, Kingdom of Saudi Arabia
Hausladen Hans, Munich, Germany
HAY Frank, Geneva, New York, USA
Hernandez-Martinez Rufina, Ensenada, Mexico
Hubbard Michelle, Ottawa, Ontario, Canada
Iacomi Beatrice, Bucharest, Romania
Infantino Alessandro, Rome, Italy
Ippolito Antonio, Bari ,italy
Isakeit Thomas, College Station, Texas, USA
Jones Eirian, Lincoln, New Zealand
Khan Iqra Haider, Punjab, Pakistan
Kil Eui-Joon, Andong, South Korea
Kreuze Jan F, Lima, Peru
Krugner Rodrigo, Parlier, California, USA
Lacomme Christophe, Edinburgh, UK
Landa del Castillo Blanca, Cordoba, Spain
Dung Le Tien, Ho Chi Minh City, Vietnam
Le Floch Gaetan, Brest, France
Le May Christophe, Le Rheu Cedex, France
Leal Catarina, Logroño, Spain
Leyronas Christel, Avignon, France
Linaldeddu Benedetto, Padova, Italy
Lindberk Kurt, Wagga Wagga, Australia
Locatelli Gabriel, Recife, Pernambuco, Brazil
Loconsole Giuliana, Bari, Italy
Logrieco Antonio, Bari, Italy
Loi Martina, Bari, Italy
Lolas Mauricio, Talca, Chile
Longa Claudia, San Michele all'Adige (TN), Italy
Loreti Stefania, Rome, Italy
Luo Chao-xi, Wuhan, P.R. China

Luque Jordi, Cabrils, Spain
Maclot Francois, East Lansing, Michigan, USA
Mahillon Mathieu, Gent, Belgium
Malandrakis Anastasios, Athens, Greece
Maruthi Gowda, Kent, United Kingdom
Mascia Tiziana, Bari, Italy
Masiello Mario, Bari, Italy
May De Mio Louise Larissa, Curitiba, Paranà, Brazil
Michereff Sami Jorge, Juazeiro do Norte, Brazil
Mondello Vincenzo, Reims, France
Moragrega Concepcio, Girona, Spain
Moral Juan, Cordoba, Spain
Moretti Chiaraluce, Perugia, Italy
Mostert Lizel, Stellenbosch, South Africa
Munir Shahzad, Kunming, China
Nakashima Chiharu, Tsu, Japan
Nancarrow Narelle, Melbourne, Australia
Nicolia Alessandro, Salerno, Campania, Italia
Obradovic Aleksa, Belgrade, Serbia
Onaga Geoffrey, Cotonou, Benin, Africa
Pasche Julie, Fargo, North Dakota, USA
Pastor-Corrales Talo, Beltsville, Maryland, USA
Pavan Stefano, Bari, Italy
Pečenka Jakub, Brno, Czech Republic
Pensec Flora, Brest, France
Peres Natalia A., Florida, USA
Pethybridge Sarah, Ithaca, New York, USA
Philion Vincent, Québec, Canada
Phillips Alan J.L., Lisbon, Portugal
Pollastro Stefania, Bari, Italy
Potnis Neha, Auburn, Alabama, USA
Quaglino Fabio, Milan, Italy
Quilot-Turion Bénédicte, Paris, France
Reis Pedro Augusto Braga, Viçosa, Brazil
Risoli Samuele, Pavia, Italy
Rolshausen Philippe E., Riverside, California, USA
Romanazzi Gianfranco, Ancona, Italy
Romero Joaquín, Córdoba, Spain
Roper M. Caroline, Riverside, California, USA
Rubiales Diego, Cordoba, Spain
Saldarelli Pasquale, Torino, Italy
Sándor Erzsébet, Debrecen, Hungary
Sarrocco Sabrina, Pisa, Italy
Schiavi Daniele, Viterbo, Italy
Schnabel Guido, Clemson, South Carolina, USA
Schumpp Olivier, Nyon, Switzerland
Sharma Kalpana, Gainesville, Florida, USA
Shiskoff Nina, Fort Detrick, MD, USA
Siddiquee Shafiquzzaman, Sabah, Malaysia
Skoric Dijana, Zagreb, Croatia
Somma Stefania, Bari, Italy
Sosnowski Mark, Canberra, Australia

Spadaro Davide, Turin, Italy
Špetík Milan, Brno, Czech Republic
Stensvand Arne, Ås, Norway
Štůsková, Kateřina, Brno, Czech Republic
Surico Giuseppe, Florence, Italy
Talhinhas Pedro, Lisboa, Portugal
Tarquini Giulia, Udine, Italy
Taylor Paul, Melbourne, Australia
Testempasis Stefanos, Thessaloníki, Greece
Tjamos Sotirios, Athens, Greece
Turina Massimo, Turin, Italy
Tzima Aliki, Athens, Greece
Urbez-Torres Jose, Summerland, Canada
Uysal Aysun, Antakya, Turkey
Vannacci Giovanni, Pisa, Italy
Vargas Joseph, East Lansing, Michigan, USA
Vaz Patto Carlota, Lisbon, Portugal
Veerakone Stella, Auckland, New Zealand
Vergine Marzia, Lecce, Italy
Vicent Antonio, Moncada, Valencia, Spain
Walker Nathan, Stillwater, Oklahoma, USA
Ziebell Heiko, Quedlinburg, Germany

Mediterranean Phytopathological Union

Founded by Antonio Ciccarone
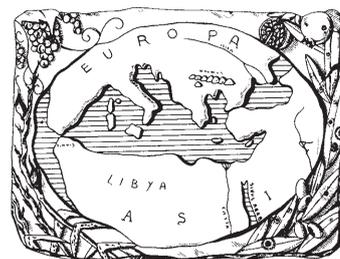
The Mediterranean Phytopathological Union (MPU) is a non-profit society open to organizations and individuals involved in plant pathology with a specific interest in the aspects related to the Mediterranean area considered as an ecological region.

The MPU was created with the aim of stimulating contacts among plant pathologists and facilitating the spread of information, news and scientific material on plant diseases occurring in the area. MPU also intends to facilitate and promote studies and research on diseases of Mediterranean crops and their control.

The MPU is affiliated to the International Society for Plant Pathology.

MPU Governing Board

President
Dimitrios Tsitsigiannis, Agricultural University of Athens, Greece
E-mail: dimtsi@aua.gr

Immediate Past President
Antonio F. Logrieco, National Research Council, Bari, Italy
E-mail: antonio.logrieco@ispa.cnr.it

Board members
Blanca B. Landa, Institute for Sustainable Agriculture-CSIC, Córdoba, Spain
E-mail: blanca.landa@csic.es
Anna Maria D' Onghia, CIHEAM/Mediterranean Agronomic Institute of Bari, Valenzano, Bari, Italy – E-mail: donghia@iamb.it
Dimitris Tsaltas, Cyprus University of Technology, Lemesos, Cyprus
E-mail: dimitris.tsaltas@cut.ac.cy

Honorary President - Treasurer
Giuseppe Surico, DAGRI, University of Florence, Firenze, Italy
E-mail: giuseppe.surico@unifi.it

Secretary
Anna Maria D' Onghia, CIHEAM-Mediterranean Agronomic Institute of Bari, Valenzano, Bari, Italy – E-mail: donghia@iamb.it

Treasurer
Laura Mugnai, DAGRI, University of Florence, Firenze, Italy
E-mail: laura.mugnai@unifi.it

MPU National Society Members

Croatian Plant Protection Society, https://hdbz.hr/
Egyptian Phytopathological Society
French Society of Plant Pathology, http://www.sfp-asso.org/
Hellenic Phytopathological Society, http://efe.aua.gr/
Israeli Phytopathological Society, http://www.phytopathology.org.il/
Italian Association for Plant Protection, https://aipp.it/
Italian Phytopathological Society, http://www.sipav.org/
Moroccan Society of Plant Protection, http://www.amppmaroc.org/
Palestinian Plant Production and Protection Society
Plant Protection Society in Bosnia and Herzegovina
Plant Protection Society of Serbia, https://plantprs.org.rs/
Portuguese Phytopathological Society, https://spfitopatologia.pt/
Spanish Phytopathological Society, https://sef.es/en
Turkish Phytopathological Society, https://www.fitopatoloji.org.tr/

MPU Affiliated Members

Arab Society for Plant Protection (ASPP), http://www.asplantprotection.org/
CIHEAM-Mediterranean Agronomic Institute of Bari, https://www.iamb.it/

2025 Information for authors of the Open Access journal *Phytopathologia Mediterranea*

Only MPU members are eligible to publish according to MPU membership categories (see https://oajournals.fupress.net/index.php/pm/about):

– All authors belonging to an MPU National Society Member (see list above) or to an MPU Affiliated Member (international organizations or networks), that signed a Memorandum of Understanding with MPU, are entitled to publish with a contribution to publication cost (https://oajournals.fupress.net/index.php/pm/about)

– All Individual Members (not in the above categories), including members of profit or non-profit entities, and physical person.

To become an Individual Member see www.mpunion.org or contact phymed@unifi.it

To receive the paper version of the journal please contact phymed@unifi.it

For information visit the MPU web site:
www.mpunion.org
or contact us at: Phone +39 39 055 2755861/862 – E-mail: phymed@unifi.it

Phytopathologia Mediterranea

Volume 63, December, 2024

Contents